TECHNISCHE UNIVERSITÄT MÜNCHEN

Fachgebiet für Waldinventur und nachhaltige Nutzung

Investigations into the potentials of hyperspectral and multi-seasonal /

multispectral satellites data for forest parameter determination.

Alata Elatawneh

Vollständiger Abdruck der von der Fakultät Wissenschaftszentrum Weihenstephan für Ernährung, Landnutzung und Umwelt der Technischen Universität München zur Erlangung des akademischen Grades eines

Doktors der Naturwissenschaften

genehmigten Dissertation.

Vorsitzender: Univ.-Prof. Dr. R. Mosandl

Prüfer der Dissertation:

       1. Univ.-Prof. Dr. Th. Knoke
       2. Priv.-Doz. Dr. X. Zhu

Die Dissertation wurde am 08.04.2015 bei der Technischen Universität München eingereicht und durch die Fakultät für Wissenschaftszentrum Weihenstephan für Ernährung, Land-nutzung und Umwelt am 08.06.2015 angenommen.

لجميع أولئك الأبرياء الذين يسعون جاهدين لأجل السلام ... فليكن عليكم من الله السلام

Für alle unschuldig Verfolgten, die nach Frieden streben … Möge der Friede mit euch sein

Preface

This work was prepared alongside the project "Method development for the use of parameters extracted from satellite data in the context of forest management planning and forest disaster management development (Methodenentwicklung zur Nutzung von Parametern aus Satellitendaten im Rahmen der forstlichen Betriebsplanung und des forstlichen Katastrophenmanagements)", funded by the Space Directorate of the German Aerospace Agency (Raumfahrtmanagement des Deutschen Zentrums für Luft- und Raumfahrt, DLR) under Number 50 EE 0919. The project was developed in response to the Announcement of Opportunity to the call for "Innovative information products by synergistic usage of RapidEye and TerraSAR-X satellite data (Innovative Informationsprodukte durch synergetische Nutzung von RapidEye und TerraSAR-X Satellitendaten)".

The work investigates options for deriving information relevant to forest management from high resolution satellite data. Two approaches offered through leading optical remote sensing satellite technologies are investigated. The first is the hyperspectral approach, using the first operating system developed, the experimental Hyperion sensor. The second is the multispectral / multi-seasonal approach utilizing the operational, commercially available RapidEye system. The intent of the investigation into the Hyperion data and the RapidEye data was to reveal the potential held by the planned next generation satellites for their application in forest management. The planned mission that will enhance spectral properties is the German Environmental Mapping and Analysis Program (EnMap). Sentinels satellites are the planned missions aiming to enhance the revisit capability, and these will increase the opportunity of acquiring multi-seasonal data.

Table of contents

List of Figures

List of Tables

List of abbreviations

AI	Area Index, a new developed index within this thesis
ALI	Advanced Land Imager
ANN	Artificial Neural Network
ATM	Airborne Thematic Mapper
BFNP	Bavarian Forest National Park
DBH	Diameter at Breast Height
DEM	Digital Elevation Model
DLR	Deutsches Zentrum für Luft- und Raumfahrt: German space research institutes
DLT	Direct Linear Transformation
DSS	Decision Support System
DWD	Deutscher Wetterdienst: German Meteorological Service
EnMap	Environmental Mapping and Analysis Program
EO	Earth Observation
ESA	European Space Agency
ETM+	Enhanced Thematic Mapper plus
GIS	Geographic Information System
Ha	Hectare
HSR	High Spatial Resolution
Km	Kilometer
LAI	Leaf Area Index
LU / LC	Land Use / Land Cover
LVG	Landesamt für Vermessung und Geoinformation Bayern: Bavarian State Office for Survey and Geoinformation
m	Meter
m²	Square meter
MD	Minimum Distance
MhD	Mahalanobis Distance
ML	Maximum Likelihood
MNF	Minimum Noise Fraction
NDVI	Normalized Difference Vegetation Index
NIR	Near-Infrared
nm	Nanometer
NN	Nearest Neighbor
OBIA	Object-Based Image Analysis

RE	Red edge, refers to the red edge band in RapidEye satellite
RESA	RapidEye Science Archive
RF	Random Forest
SAM	Spectral Angel Mapper
SNR	Signal to Noise Ratio
SVM	Support Vector Machine
SWIR	Short-wavelength infrared
USGS	United State Geological Survey
VI	Vegetation Index
VIS	Visible Spectrum
WB	Wuchsbezirk: Growth region

Summary

Forest management planning plays an important role in maintaining the long-term health of forests, one of the most economically important natural resources. Management planning is typically based on information obtained from terrestrial forest inventories, which are time-consuming, cost-intensive and conducted over a span of at least ten years. In light of these challenges, decision makers at the strategic / tactical levels in the forestry field have become increasingly interested in obtaining forest information from remote sensing data. This information, referred to as forest parameters, can be obtained at the forest stands level, and should be sufficient to contribute to the decision support system (DSS) for forest enterprises. Based on the judgment of forest experts, the most important forest parameters related to forest management planning, to be delivered by remote sensing means, were identified. These parameters include: forest cover, forest types, forest changes and the forest tree species - the parameter that presents the greatest challenge to remote sensing.

The focus of this work is to offer an operational solution, using the high spatial resolution (HSR) satellite data, to inform the strategic / tactical decision making process. Of the various optical satellite systems available, the HSR satellite data (5-30 m) are regarded as adequate for forest mapping at the stand level. Also, HSR data are cost effective, and offer an operational solution for forest enterprises to make strategic / tactical decisions. While the multispectral data from HSR satellite systems are well investigated, the enhancements of such data in terms of spectral and temporal resolutions have yet to be researched, due to the limited number of systems providing these data. The improvement of the data spectral and temporal resolution is at the forefront of HSR sensors development. The high spectral resolution data available for this study was the hyperspectral Hyperion data (about 200 spectral bands and 30 m spatial resolution). To date, the only system offering high temporal resolution (multi-seasonal) data is the RapidEye system (5 spectral bands and 6.5 m spatial resolution), a system employed here.

One shortcoming in research relating to HSR satellite data is a disagreement over forest definitions and functions among different stakeholders in forestry, and in the remote sensing community. In forest management, it is essential to establish proper definitions of all forest parameters, based on the requirements of the end users. Regarding the current state of knowledge, it is clear that further research is required for both the hyperspectral and the multi-seasonal approaches for operational forest inventory. In terms of the hyperspectral approach, research has been focused applying the Hyperion system only on the technical potentials and limitations of the

system. Another common issue is that research on multi-temporal optical data, offering operational means for forest monitoring, faces problems with clouds. Applying data of higher temporal resolution (multi-seasonal) to address this issue has yet to be investigated. Finally, for mapping the tree species parameter, neither the hyperspectral nor the active systems offer an operational solution, due to the cost constraints and limited coverage. Thus, the multi-seasonal approach remains as the only promising path towards offering an operational solution. This can be achieved by applying the ''phenological fingerprint'' concept, which uses the variation in phenology of the tree species. While a small number of studies have investigated this concept for tree species identification, key economic issues must also be addressed. Such issues include: the number of datasets that should be used, the appropriate seasons for data collection, and the influence of additional bands on mapping.

The aim of this thesis was to investigate the potential of two approaches, provided by these two HSR systems for offering operational means, to extract the above listed parameters. The first is the mono-temporal hyperspectral approach, using the Hyperion system in the Mediterranean forest. The second is the multi-seasonal multispectral approach, using the RapidEye system in three Bavarian forests representing different growth regions. The outcomes of both approaches will inform which approach should be considered the most suitable for individual parameter extraction. Results should further contribute to the next generation hyperspectral satellite EnMap, as well as multi-seasonal satellites like the Sentinel missions.

The investigations into the Hyperion data were carried out by applying a variety of classification methods including: pixel-based, spectral unmixing and object-based, to extract forest cover, types, and tree species. For the pixel-based method, Spectral Angel Mapper (SAM) classifier was applied, for the spectral unmixing Artificial Neural Network (ANN) was implemented, and for the object-based the eCognition software was utilized. Conversely, investigations into the multi-seasonal RapidEye data were carried through with pixel-based and object-based methods. For the extraction of forest cover, type and forest changes, the object-based technique was used. The developed methods were found to be precise, timely computational efficient, and transferable to other test sites. For the forest change detection, additionally, a method was developed using the multi-seasonal data available to solve the problem of the cloud cover. Finally, for extraction of the tree species parameter, the ''Phenological fingerprint'' concept was investigated. A strategy to classify combinations of multi-seasonal RapidEye data was developed in order to address the aforementioned aspects of key economic importance.

Results show that data provided by both systems were generally successful in extracting forest parameters. However, the multi-seasonal RapidEye data showed a greater potential than the hyperspectral Hyperion data for operational application. For the extracted parameters forest cover and type, the higher spatial resolution of RapidEye tended to be more important than the high spectral resolution of Hyperion. However, where the forest was highly structured and more diverse, a form expected of future forests, RapidEye data achieved a lower accuracy for detecting forest types. The multi-seasonal data were essential for detecting forest change, while the high frequency of the multi-seasonal data offered an operational approach to solving the problem of cloud cover. The tree species results show that the ''phenological fingerprint'' concept is essential for their identification. Multi-seasonal RapidEye data picked up many aspects of the phenological development over time, and had a high potential to separate tree species. In this study, we dealt with seven different species. The new red edge band in the RapidEye data was found to slightly increase the accuracy for tree species identification. Meanwhile, a mono-temporal Hyperion dataset catching one aspect of the "phenological fingerprint" had the ability to identify only two coniferous species, which happened to have high variation in spectral reflectance during the acquisition time.

The multi-seasonal multispectral approach offered lower spectral resolution but higher spatial and temporal resolution than that of the mono-temporal hyperspectral approach. However, the RapidEye approach (either mono- or multi-seasonal) remains better suited for extracting the parameters forest cover, type, changes and tree species. The cost of the multi-seasonal multispectral approach will remain more affordable than the hyperspectral approach, taking into consideration the limited coverage of the hyperspectral systems. This trend is expected to continue with next generation hyperspectral EnMap satellite, as well as the multi-seasonal Sentinel satellites. To achieve greater success in forest inventory from the next generation satellites, a slight improvement in the spatial resolution is recommended, in order to meet the challenges presented by the highly structured forests of the future. Additionally, the multi-seasonal capability should remain key in development plans, in order to map the most challenging parameter, tree species. While the high quality spectral data from the hyperspectral approach can restrict the multi-seasonal capability, adding a few additional bands to the upcoming multispectral satellite can be of benefit for tree species identification.

Zusammenfassung

Forstmanagement spielt eine wichtige Rolle bei der langfristigen Erhaltung der Vitalität von Wäldern, eine der ökonomisch wichtigsten natürlichen Ressourcen. Managementplanung baut typischerweise auf Informationen auf, die aus terrestrischer Waldinventur stammen, die zeit- und kostenintensiv sind und über eine Zeitpanne von mindestens 10 Jahren durchgeführt werden müssen. Im Hinblick auf diese Herausforderung interessieren sich Entscheidungsträger der strategischen / taktischen Ebene des Forstbetriebs verstärkt dafür, Waldinformationen durch Fernerkundung zu erlangen. Diese Waldparameter können auf der Waldbestandsebene gesammelt werden und sollten genügend zum Entscheidungs-Unterstützung-System (EUS) der Forstbetriebe beitragen. Basierend auf der Beurteilung von Forstexperten wurden die für Forstmanagement und -planung wichtigsten Forstparameter, die die Fernerkundung beitragen kann, identifiziert. Diese Parameter umfassen: Fläche, Typ und Veränderung des Waldes, sowie der Parameter, der die größte Herausforderung für die Fernerkundung darstellt, die Forstbaumarten.

Der Schwerpunkt dieser Arbeit ist es, durch die Anwendung der Satellitensysteme von der hoch räumlichen Auflösungskategorien (HSR) operationelle Lösungen anzubieten, die für den EUS von Nutzen sind. Von den vielfältigen optischen Satellitensystemen, die verfügbar sind, werden die HSR-Satellitensysteme (5-30 m) als geeignet angesehen, den Forst auf der Bestandesebene zu erfassen. Des Weiteren sind HSR-Daten kosteneffizient und bieten eine operationelle Lösung bei der strategischen / taktischen Entscheidungsfindung in Forstbetriebenen. Während die Multispektraldaten von HSR-Satellitensystemen gut untersucht sind, müssen die in Bezug auf spektrale und zeitliche Auflösung weiterentwickelten Daten noch untersucht werden, da es wenige Systeme gibt, die diese Daten produzieren. Die Verbesserung der spektralen und zeitlichen Auflösung ist das Hauptanliegen der HSR-Sensorenentwicklung. Die Hochspektraldaten, die dieser Studie zur Verfügung standen, waren die hyperspektralen Hyperion-Daten (ca. 200 Spektralbänder und 30 m räumliche Auflösung). Bis heute ist das RapidEye-System das einzige System, das zeitliche Hochauflösung anbietet. Dieses System wurde hier angewendet.

Eine Unzulänglichkeit in der Forschung in Bezug auf HSR-Satellitendaten ist, dass es keine einheitlichen Forstdefinitionen und –funktionen zwischen verschiedenen Akteuren in den Forstwissenschaften und in der Fernerkundung gibt. Im Forstmanagement ist es grundlegend, geeignete Definitionen für alle Forstparameter zu etablieren, die auf den Anforderungen des Endnutzers basieren. Ausgehend von dem heutigen Wissensstand ist es klar, dass weitere Forschung notwendig ist sowohl für die hyperspektralen als auch die multisaisonalen

Anwendungen bei der operationellen Waldinventur. In Bezug auf die hyperspektrale Methode lag der Fokus der Forschung bezogen auf die Anwendung der Hyperiondaten lediglich auf den technischen Möglichkeiten und Grenzen des Systems. Ein weiteres allgemeines Problem ist, dass die Forschung an multitemporalen optischen Daten, die operationelle Mittel beim Forstmonitoring zur Verfügung stellen, Schwierigkeiten mit Wolken ausgesetzt ist. Um mit diesem Problem fertig zu werden, muss die Anwendung von Daten mit höherer zeitlicher Auflösung (multisaisonal) noch weitergehend untersucht werden. Letztendlich bieten weder die hyperspektralen noch die aktiven Systeme aufgrund von Kostenbeschränkungen und begrenzten Anwendungsmöglichkeiten eine operationelle Lösung zur Erfassung der Baumartenparameter. Daher verbleibt der multisaisonale Ansatz als die einzige Möglichkeit, eine operationelle Lösung anzubieten. Dies kann durch die Anwendung des Konzepts des ''Phänologischen Fingerabdrucks'' erreicht werden, welches die Variation in der Phänologie der Baumarten nutzt. Während eine kleine Anzahl an Studien dieses Konzept zur Identifizierung vom Baumarten untersucht hat, müssen auch entscheidende wirtschaftliche Aspekte berücksichtigt werden. Zu diesen Aspekten zählen: die Anzahl von Datensätze, die erhoben werden sollen, die richtige Jahreszeit für die Datenerhebung und der Einfluss von zusätzlichen Bändern auf die Identifizierung von Baumarten.

Das Ziel dieser Doktorarbeit war es, das Potential zweier Ansätze zu ermitteln, die auf den beiden HSR-System basieren, um die oben genannten Parameter zu extrahieren. Der erste Ansatz ist der monotemporale hyperspektrale Ansatz, bei dem das Hyperion System im mediterranen Wald benutzt wird. Der zweite ist der multisaisonale multispektrale Ansatz, bei dem das RapidEye-System, das in drei bayerischen Wäldern angewandt wird, die verschiedene Wachstumsregionen repräsentieren. Die Resultate beider Ansätze werden entscheiden, welcher von beiden als der am besten geeignete angesehen werden sollte bei der individuellen Parameterextraktion. Die Ergebnisse sollten darüber hinaus einen Beitrag leisten zu der nächsten Generation hyperspektraler Satelliten, wie z.B. EnMap und SPECTRA, sowie multisaisonaler Satelliten wie den Sentinel-Satelliten.

Die Untersuchungen zu den Hyperion Daten wurden unter Anwendung einer Vielzahl von Klassifikationsmethoden ausgeführt, welche umfassten: das pixelbasierte, das objektbasierte, und das spectral-unmixing-Verfahren zur Bestimmung der Waldfläche, der Typen und der Baumarten. Bei der pixelbasierte Methode wurde der Spectral Angel Mapper (SAM)-Algorithmus angewendet, bei dem spectral-unmixing-Verfahren wurde das Artificial Neural Network (ANN) verwendet, und für die objektbasierte Methode wurde die eCognition-Software benutzt. Im Falle der Untersuchungen zu den multisaisonalen RapidEye-Daten wurden pixel-und objektbasierte

Methoden durchgeführt. Bei der Ermittlung der Waldfläche, des Typs und der Waldveränderungen wurde die objektbasierte Technik benutzt. Die entwickelten Methoden stellten sich als präzise, schnell durchführbar und übertragbar auf andere Testgebiete heraus. Für die Erfassung der Waldveränderungen wurde eine zusätzliche Methode entwickelt, bei der die verfügbaren multisaisonalen Daten verwendet wurden, um das Problem mit der Wolkendecke zu lösen. Und schließlich wurde zur Extraktion der Baumartenparameter das ''Phänologischer Fingerabdruck''-Konzept untersucht. Eine Strategie zur Klassifizierung von Kombinationen von multisaisonalen RapidEye-Daten wurde entwickelt, um die zuvor genannten Wirtschaftsaspekte zu berücksichtigen.

Die Ergebnisse zeigen, dass beide Systeme im Allgemein erfolgreich waren bei der Extraktion von Forstparametern. Jedoch zeigten die multisaisonalen RapidEye-Daten ein größeres Potential als die monotemporalen hyperspektralen Hyperion-Daten für die operationelle Anwendung. Für die extrahierten Parameter Waldfläche und -typ war die höhere räumliche Auflösung von RapidEye tendenziell wichtiger als die hohe spektrale Auflösung von Hyperion. Allerdings erreichten die RapidEye-Daten eine geringere Genauigkeit bei der Erfassung des Waldtyps, wenn der Wald hoch strukturiert war und eine höhere Diversität aufwies, was von zukünftigen Wäldern verstärkt zu erwarten ist. Die multisaisonalen Daten waren essenziell, um Veränderungen im Wald zu detektieren, während die große Häufigkeit der multisaisonale Daten einen operationellen Ansatz lieferten, um das Problem der Wolkendecke zu lösen. Die Baumartenergebnisse zeigen, dass das ''Phänologische Fingerabdruck''-Konzept grundlegend ist für die Identifizierung der Baumarten. Multisaisonale RapidEye-Daten nahmen viele Aspekte der phänologischen Entwicklung über die Zeit hinweg auf und hatten ein hohes Potenzial, die Baumarten zu differenzieren. In dieser Studie befassten wir uns mit sieben verschiedenen Arten. Es zeigte sich, dass das neue ''red edge''-Band in den RapidEye-Daten die Genauigkeit der Baumartenidentifizierung leicht erhöhte. Im Gegensatz dazu war es mit dem monotemporalen Hyperion-Datensatz, der einen Aspekt des ''Phänologischen Fingerabdrucks'' erfasste, lediglich möglich, zwei Nadelbaumarten zu identifizieren, die zufällig eine hohe Variation in ihrer Spektralreflexion aufwiesen während des Aufnahmezeitpunkts.

Zusammenfassend lässt sich sagen, dass der multisaisonale Ansatz eine niedrigere Spektralauflösung bot, aber eine höhere räumliche und zeitliche Auflösung als der monotemporale hyperspektrale Ansatz. Allerdings eignet sich der multisaisonale RapidEye-Ansatz zur Extraktion der Parameter Walfläche, -typ und –veränderung sowie Baumarten. Die Kosten der multisaisonalen multispektralen Methode werden leichter zu decken sein als die der hyperspektralen Methode, wenn man die begrenzte Abdeckung des Hyperspektralsystems bedenkt. Es ist zu erwarten, dass

dieser Trend sich mit der nächsten Generation hyperspektraler Satelliten, EnMap und SPECTRA, sowie dem multisaisonalen Satelliten Sentinel, fortsetzen wird. Um größeren Erfolg bei der Waldinventur von der nächsten Generation Satelliten zu erreichen, wird eine leichte Verbesserung in der räumlichen Auflösung empfohlen, damit die Herausforderungen eines hoch strukturierten Waldes der nächsten Generation gemeistert werden können. Zusätzlich sollten die multisaisonalen Fähigkeiten im Fokus der Entwicklungspläne bleiben, damit der herausforderndste Parameter – Baumarten – erfasst werden kann. Während die qualitativ hochwertigen Spektraldaten des Hyperspektralansatzes als überflüssig angesehen werden können, könnte das Hinzufügen einiger zusätzlicher Bänder bei den zukünftigen Multispektralsatelliten bei der Identifizierung von Baumarten von Vorteil sein.

1 Introduction

1.1 General background

Forests are the most widely distributed vegetation ecosystem on the earth, accounting for approximately 31% of the global land cover (FAO, 2010), and serving as a significant store of CO_2. Forest management planning plays an important role in maintaining the long-term health of forests, one of the most important natural resources for economy (Franklin, 2001). Following the idea of sustainability (Carlowitz, 1713, reprint 2013), since the end of the eighteenth century, forest management planning has arisen in German-speaking countries in form of fundamental forest management textbooks, planning techniques and theoretical forest models, and sustainable forest management (Knoke et al., 2010). Recently, the economic and environmental importance of forest resources has prompted forest management planning to take into consideration the strategic, tactical and operational levels of planning, such that the highest feasible utility is yielded (Holmgren and Thuresson, 1998).

The forest management planning process defines the management goals and the measures to be taken for the next planning period, in Bavaria, Germany, usually being conducted over a span of at least ten years. Forest management planning is typically based on forest inventories (McRoberts and Tomppo, 2007). Forest inventory can be recorded using three categories of information including the spatial extent of forest cover, forest type, and biophysical and biochemical properties of the forest (Boyd and Danson, 2005). Traditional forest inventories are terrestrial observations relying on sample-based methods to collect up to 200 variables, including but not limited to: forest area, tree species, health conditions, growth, regeneration, removal, trends, forest height, and damages etc.. These terrestrial inventories are time-consuming and cost-intensive. Given these challenges, remote sensing has been presented as an alternative, or supplementary method to meet ongoing demands for forest resource information at extended spatial and temporal scales (Vohland et al., 2007).

The idea of applying remote sensing in forest management planning activities was first revealed in the newspaper "Berliner Tagesblatt" in 1886. Its integration in operational forest management began with the use of aerial photography in the first half of the twentieth century. Traditionally, and up until the present day, remote sensing practices have consisted of the interpretation and analysis of aerial photography in order to facilitate the creation of forest inventory and monitoring practices, and make these tasks more efficient (Boyd and Danson, 2005; Knoke, 2012; McRoberts

and Tomppo, 2007). The evaluation of aerial photography is typically accomplished through the use of visual interpretation, with the aim of direct decision making. Additionally, orthophotos are often used for orientation in the forest, or as maps for delineating forest stands or damages.

In the second half of the twentieth century, with the launch of the first Landsat satellite in 1972, space born remote sensing applications were revolutionized. Since then, numerous varieties of optical satellite systems have been launched into space. Optical satellite data have been routinely applied to forest management planning at different mapping scales, from local to global. There are many systems available for choosing the appropriated data type at the desired level of mapping, where selections are based on the system characteristic known as "the resolution". Four resolution types are defined according to their "technical" characteristics: the spatial, the spectral, the radiometric and the temporal resolution. Satellites can be categorized based on their spatial resolution and the scale of their achievable end mapping scale, as outlined in Table 1.

Table 1: Categories of the currently available optical remote sensing systems based on their spatial resolutions and the achievable mapping scale range, adapted after (Knoke, 2012)

Spatial resolution	Characteristic	System example	Mapping scale Better than
500 – 5,000 m	Global "Low resolution"	Meteosat, NOAA AVHRR, Vegetation, etc.	1 :1,000,000
50 – 500 m	Regional "Mid-resolution"	Landsat MSS, WIFS, MERIS, MODIS.	1:500,000
5 – 30 m	Regional "High resolution"	Landsat TM und 7, Spot, IRS, Rapid Eye, etc.	1:50,000
1 – 4 m	Stand level "Very high resolution"	Ikonos, Quick Bird, WorldView, etc.	1:10,000
< 1 m	Local "Extreme high resolution"	Digital Aerial images: VMS EXCEL© Cam, DMC, etc.	1:500

While the benefits of optical remote sensing systems are numerous, data costs (rule of thumb: the higher the resolution the higher the costs) and handling costs (down streaming, storage, computation time) serve as the limiting factors as to the chosen resolution for a given application. As space systems operated from satellites are usually designed for specific application profiles, a key emphasis is placed on the required resolution type.

This research is focused on informing decision makers of forest enterprise at the strategic / tactical level (see Figure 1) and finding operational solutions. At this level, high resolution (HSR) satellite data can provide information needed for forest management planning towards inventory and monitoring (Holmgren and Thuresson, 1998). Remote sensing requires simultaneous imaging of the entire area managed by an enterprise in order to keep the assessment conditions comparable and the information detail available, at least at stand level. Optical data of HSR (5 – 30 m) satellite

category are adequate for forest mapping down to the forest stand level (De Kok et al., 1999). Moreover, satellite data at the HSR level is more cost effective and offers an operational solution for forest enterprises. While the options offered by HSR multispectral satellite systems have been widely investigated for about three decades, the improvements made by increasing the **spectral** and especially the **temporal resolution** are still in question and are addressed in this thesis.
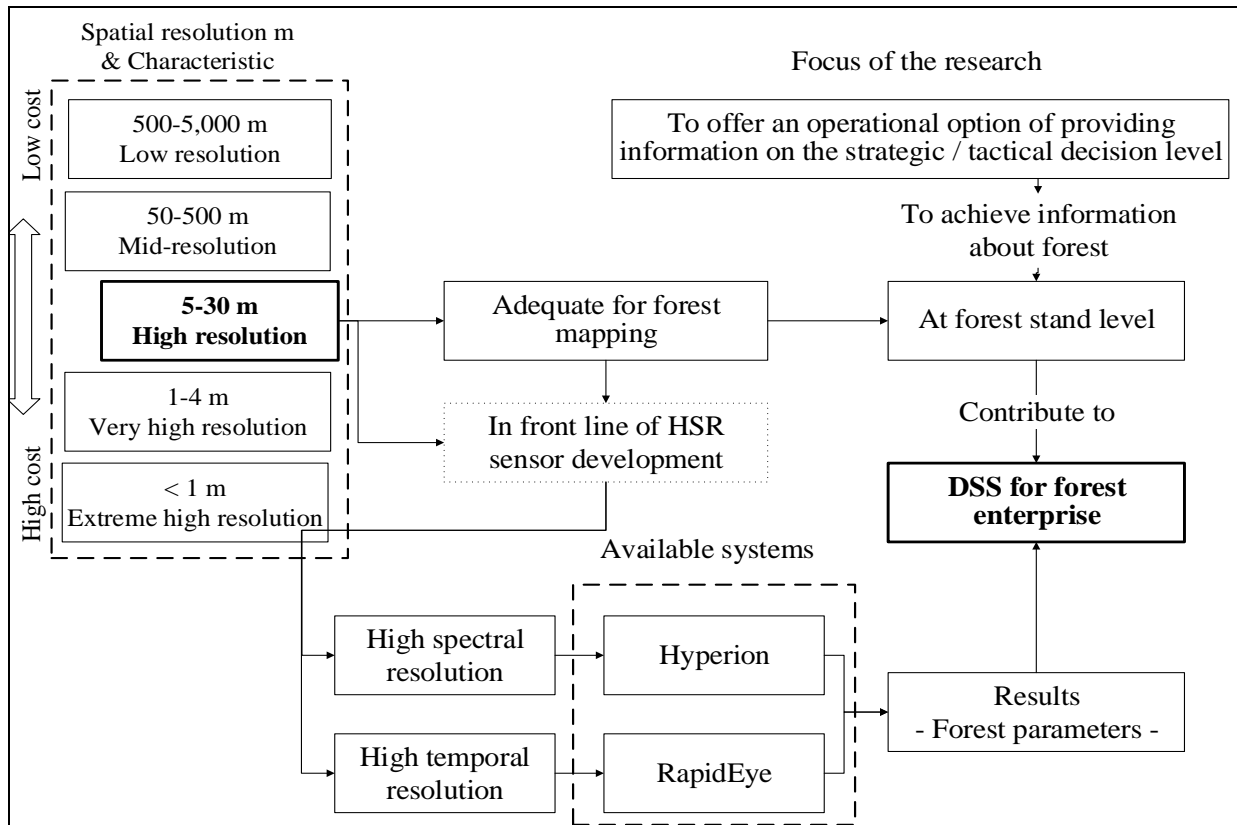
Figure 1: Conceptual framework of the research

The aforementioned HSR improvements are in the front line of optical satellite development. Therefore, research to enhance the **spectral resolution** or the **multi-date**[1] acquisition capabilities of current and next generation space-borne sensors remains ongoing. The hyperspectral Hyperion sensor is the space-borne sensor available for this work of the HSR family, which offers detailed spectral resolution data. Meanwhile, the only space-borne system of the HSR family offering high revisiting frequency so far is the RapidEye constellation system (status February 2015). The Hyperion sensor on board NASA Earth Observation 1 (EO-1) satellite was launched into space in the year 2000. The sensor covers both the visible near-infrared (VIS / NIR) and the shortwave-

---

[1] The term multi-date data can refer to multi-temporal or multi-seasonal data. In this work, the term of **multi-seasonal** data refers to a dataset from different growing seasons (phenological phases) from a single year, or multiple successive years. Meanwhile, the term of **multi-temporal** data refers to a dataset from different years but from similar growing seasons.

infrared (SWIR) spectrum (400-2500 nm) collected in about 200 spectral bands, at a ground spatial resolution of 30 m. Following this, the RapidEye constellation, consisting of 5 identical sensors, was launched into space in 2008. Each RapidEye sensor collects five spectral bands (VIS / NIR) and is capable of data acquisition every 2-3 days. The data collected has a pixel size of 6.5 m (resampled to 5 m) and a swath width of 75 km.

The spectral signature is considered to be the data characteristic with the highest information content for identification and status assessment of the Earth's surfaces. The attempt to increase the spectral resolution of optical systems is driven by the idea to redraw the spectral signature of Earth surfaces as accurately as possible, in order to make the entire spectral diagnostic option via satellite data available. For this reason, we are looking forward to the German EnMap hyperspectral system, which originally was to be launched in 2011, before technical challenges prompted a rescheduling to March 2018. Instead, the hyperspectral datasets of the experimental Hyperion system were analyzed in this work, which offer similar specifications of the spectral and spatial resolutions to the EnMap.

Many studies, investigating the spectral option, showed the limitations of spectral signatures in determining diagnostic characteristics of vegetation (Davranche et al., 2010; Eckert and Kneubühler, 2004; George et al., 2014; Mickelson et al., 1998; Pengra et al., 2007; Reese et al., 2002; Schriever and Congalton, 1995; Stoffels et al., 2012; Townsend and Walsh, 2001; Wolter et al., 1995). These studies indicated that imaging differing phenological stages may not only be a complementary solution, but also a precise indicator for the identification of tree species, at a minimum. For the first time, the RapidEye system, an operational system of the high resolution HSR category, allows for the investigation of the option of multi-seasonal image analysis (more details in section 3.2.1.2). Primarily seen as a system supporting precision agriculture, the EUS-FH project (Schneider, 2013) investigated the success of multi-seasonal RapidEye time series in forest species identification. Therefore, we are looking forward to the Sentinels satellites, the planned missions aiming to enhance the revisit capability, which will increase the opportunity of acquiring multi-seasonal data. There are seven Sentinel missions, each consisting of two satellites, and the first satellite of Sentinel-1 was launched on 3 April 2014.

Foresters conducting fieldwork expect remote sensing data to fulfill the needs of forest management planning in practice. In a study (Felbermeier et al., 2010) aimed at determining foresters' requirements of remote sensing application in forest management planning, the most important forest parameters were found to be tree species, forest area, forest boundary, and damages (changes) inflicted on forest. Forest cover and damages thereby appear as the most

essential parameters since they incorporate the forest area, boundary and gaps all together. Additionally, forest tree species has been, and continues to be, representing the frontline in forest related remote sensing research, and remains the most challenging task for the remote sensing community. Furthermore, tree species mapping has been identified as necessary in assisting remotely sensed data to achieve its full potential in forest inventory and monitoring. Moreover, tree species mapping are basic information necessary to control biotic pests, a major threat to forests caused by global warming which threatens tree species specifically.

However, research to date has been met with limitations in achieving these parameters. These limitations can be summarized in three main points:

First, a fixed definition for forest cover is yet to be assigned, despite having thirty years' experience in mapping and monitoring forest cover from satellite (Bennett, 2001). Similarly, there remains no unified definition of forest among all European countries (Pulla et al., 2013; Schneider et al., 2013). There still exists a disagreement as to the appropriate forest definition between the remote sensing community, who have been mapping wood land as a forest, and the foresters, who hold other expectations.

Second, although the detection of damages and changes in forests have been intensively investigated, the search for an operational solution is still underway. Typically, multi-date satellite optical data can offer an operational solution for forest change and damage detection, though clouds and haze challenge the optical systems (Nagendra et al., 2013). Given these challenges, one recommendation for further research is to collect data more frequently over time (multi-seasonal) in order to increase the likelihood of overcoming issues with clouds (Duveiller et al., 2008).

A third limitation remains as no operational solution has been determined for tree species identification to date. Many studies proposed that the increase of the spatial, spectral and the radiometric resolutions will be the key to achieving better tree species identification (Boyd and Danson, 2005; Salajanu D. and Olson C. E., 2001; van Ardet and Wynne, 2001). Using multi-seasonal data may increase the chance of better identifying forest species (Wolter et al., 1995). This is attributed to the spectral variations between the different classes in different seasons or phenological phases, referred to as the ''phenological fingerprint''. The search for the optimal operational method of tree species is still underway, with uncertainty over whether to use the hyperspectral or the multi-seasonal approach. Investigation into the ''phenological fingerprint'' concept is still very limited and many economically important questions need to be answered (see section 1.2; objective 4).

1.2 Aim and hypotheses of research

The aim of this thesis is to compare two approaches, offered by leading optical satellite sensor technologies, in order to deliver operational solution for forest parameters determination. The first is the hyperspectral mono-temporal approach using Hyperion data, and the second is the multispectral multi-seasonal approach using RapidEye data. According to the foresters' requirements for application in forest management planning (Felbermeier et al., 2010), the targeted parameters to be extracted are:

1- Forest cover and forest type

2- Forest changes (only applying the multi-seasonal approach)

3- Forest tree species.

Working with different sensor types in differing geographical regions, the comparison is conducted on behalf of the extraction success of parameters required by operational forest management at the strategic / tactical decision level of an enterprise. An overview about the workflow is given in Figure 2.

The investigation into the hyperspectral Hyperion approach is carried out in Anopoli, a forested region representative of the Mediterranean. Anopoli is located on the island of Crete in the Mediterranean Sea, and holds the most extensive remains of Crete's coniferous forest. In contrast, the investigation into the multispectral multi-seasonal RapidEye approach is carried out in three forest growth regions in Bavaria. The first of these sites is the Bavarian Forest National Park (BFNP), the first and one of the biggest national parks in Germany located in the growth region Innerer Bayerischer Wald, (Wuchsbezirk (WB) 11.3). The second is the Freising forest located in the growth region Oberbayerisches Tertiärhügelland (WB 12.8). The last site is Traunsteiner Stadtwald located in the growth region Östliche kalkalpine Jungmoräne (WB 14.4 / 3), which neighbors the Alps. To compensate for the lower radiometric resolution of the less technically advanced Hyperion (generation of the mid-1990s techniques, more details in section 3.2.1.1), Hyperion data from the Crete island in the Mediterranean were investigated, registered at better illumination conditions and less affected by aerosols than the compared RapidEye data from Bavaria.
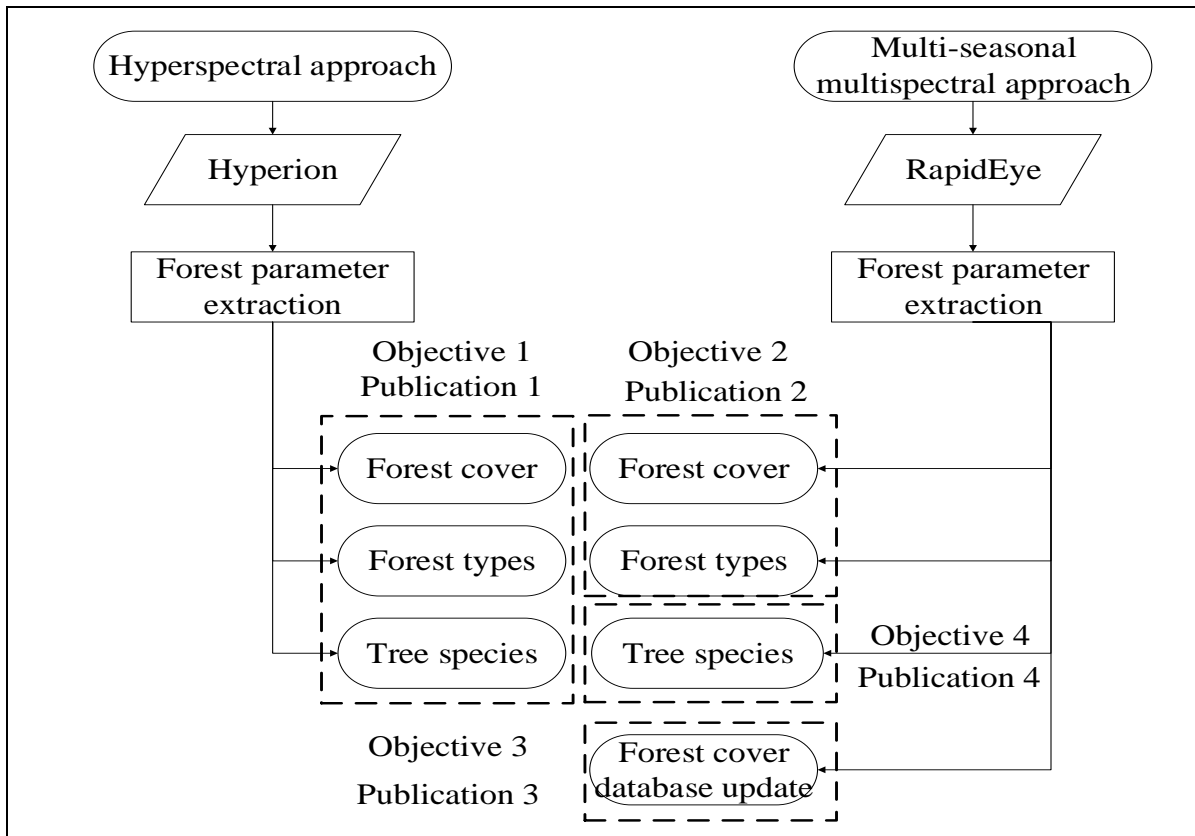
Figure 2: *The general direction, objectives and publications of the thesis*

The outcomes of both approaches will inform us as to which method should be considered as most suitable for each parameter extraction. In this pursuit, the following objectives were defined (see also Figure 2):

Objective 1: To investigate various analysis techniques applied to the single Hyperion data to extract the following parameters: forest cover, types and tree species. The results should contribute to further investigations regarding the multi-seasonal multispectral RapidEye data approach (section 4.3)

Objective 2: To investigate methods development using mono-temporal RapidEye data for forest type and cover mapping in the three Bavarian test sites. The necessary characteristics of this method include the delivery of precise results, quick implementation, and easy transferablility into any of the test sites (section 4.4)

Objective 3: To investigate an operational solution using multi-seasonal RapidEye data for forest database annual updates. The solution should overcome the issue of clouds and visibility

and be transferable to defferent test sites. Furthermore, the solution should offer the ability to quickly respond to sudden changes at a reasonable cost (section 4.5.1)

Objective 4: To investigate the success of multi-seasonal RapidEye data in applying the ''phenological fingerprint'' concept in order to determine forest tree species (section 4.5.2). The investigation should answer questions of key economic importance. These questions include:

- How many datasets from various phenological phases are needed to obtain the most accurate results?

- How does using additional bands or indices influence tree species identification?

- Is there a phenological phase with high potential for identifying a specific tree species?

- Which phenological phase is the most promising to identify all tree species?

Questions about the possible outcomes triggered three main hypotheses that will be tested in this research, and will be addressed in the general discussion. The main question raise here is, which approach could be used to achieve more information about these parameters? The hyperspectral approach utilizes Hyperion data which has very rich spectral information (200 bands), while the multi-seasonal multispectral approach utilizes RapidEye data which has poor spectral information (only 5 bands). Although RapidEye data are collected over a time span that includes variations in vegetation phenology, their spectral resolution is poor in comparison to the Hyperion data. Given these traits, the normative assumption is that the Hyperion data will surpass the RapidEye data, giving rise to the first hypothesis of this work:

H_1: Hyperspectral resolution outperforms multi-spectral high temporal resolution in determining forest parameters.

With a focus on identifying forest depletion arising from standard management practices and unexpected events such as storms, the forest cover database updates rely on aerial image surveys that take place once every three years covering all of Bavaria, and annually for the BFNP. Applying satellite optical data is still problematic due to the cloud cover problem, especially in Mid-Europe. This leads to the second hypothesis in this work:

H_2: The multi-seasonal RapidEye data evaluation approach does not meet the requirements for annual forest database updates.

Tree species is both the most important and the most challenging parameter to be extracted, and to date no sensor has been able to offer an operational solution for tree species mapping. Still, multi-seasonal multispectral RapidEye system offers data from various phenological phases, and could have the potential to increase the separability between the tree species. RapidEye data, however, have only five bands which may not contribute to the success of the ''phenological fingerprint'' principle. Accordingly, the third and most important Hypothesis to be tested here is:

H₃: Applying the ''phenological fingerprint'' concept using the multi-seasonal RapidEye data does not improve the identification success of forest tree species significantly.

1.3 Embedded original publications and author's contributions

This thesis includes four publications (Figure 2) and covers investigations into both hyperspectral and multi-seasonal approaches. The titles, short summaries and author's contributions of the publications are the following:

First publication: Elatawneh A., Kalaitzidis C., Petropoulos G. P., Schneider T. 2012. Evaluation of diverse classification approaches for land use / cover mapping in a Mediterranean region utilizing Hyperion data. International Journal of Digital Earth. doi 10.1080/17538947.2012.671378

This work investigates the extraction of the forest parameters in Anopoli using hyperspectral Hyperion data. Here, extraction of the forest parameters from remote sensing data is based on image classification. The techniques which classify each pixel in the remote sensing data as an individual unit are called pixel-based techniques, while those that classify groups of pixels as one unit are called object-based techniques. Moreover, the techniques which break the pixels down to define the surface material fractions are called spectral unmixing. The pixel-based, spectral unmixing, and object-based classification techniques are applied to the Hyperion data for extracting the required forest parameters.

Author contributions: This publication was written by Alata Elatawneh with a simultaneous contribution by George Petropoulos. All data collection, preparation and analysis were done by Alata Elatawneh under the supervision of Chariton Kalaitzidis. The research approach was developed by Alata Elatawneh and Thomas Schneider. The research coordination and revision of work structure was done by Thomas Schneider.

Second publication: Schneider T., Elatawneh A., Rahlf J., Kindu M., Rappl A., Thiele A., Boldt M., Hinz S. 2013 Parameter Determination by RapidEye and TerraSAR-X Data: A Step Toward a

Remote Sensing Based Inventory, Monitoring and Fast Reaction System on Forest Enterprise Level; In: Krisp JM, Meng L, Pail R, Stilla U, eds. 2013. Lecture Notes in Geoinformation and Cartography. Berlin, Heidelberg: Springer Berlin Heidelberg, S. 81-107

This publication investigates the extraction of the parameters forest cover, type, and gaps in the Bavarian test sites. The publication investigated the use of the multi-seasonal RapidEye data and the radar data from the active sensor Terra-SAR-X, although this accumulative thesis includes only the RapidEye data analysis section. The methods developed in this publication for the forest cover, types and gaps extraction will be further improved, as presented in section 4.3.

Author contributions: This publication was written by Thomas Schneider, Alata Elatawneh, Adelheid Rappl (now Wallner), and Antje Thiele with contribution by Johannes Ralf and Mengistie Kindu. RapidEye data analysis was done by Alata Elatawneh, and related geospatial data collection and preparation was conducted by Adelheid Rappl. TerraSAR-X data analysis were done by Antje Thiele and Markus Boldt. The research coordination and major revision of the work was done by Thomas Schneider and Stefan Hinz.

Third publication: Elatawneh A., Wallner A., Manakos I., Schneider T., Knoke T. 2014. Forest Cover Database Updates Using Multi-Seasonal RapidEye Data—Storm Event Assessment in the Bavarian Forest National Park. Forests. 5: 1284-1303.

This publication investigates the extraction of the forest changes parameter, or in other words, the continuous updating of forest cover database using multi-seasonal RapidEye data. The method is developed to be applicable in various areas and is designed to be easily applied. The intention behind using multi-seasonal RapidEye data is to detect changes caused by regular management and sudden events, such as storms, in Bavaria. It demonstrates the success of using multi-seasonal RapidEye data, and its benefits in comparison to the aerial images.

Author contributions: The paper was written by Alata Elatawneh with a contribution by Ioannis Manakos. Geospatial data collection and preparation was done by Adelheid Wallner. The research approach was developed by Alata Elatawneh and Thomas Schneider. The research coordination and significant contribution to the discussion was done by Thomas Knoke.

Fourth paper: Elatawneh A., Rappl A., Rehush N., Schneider T., Knoke T. 2013. Forest tree species identification using phenological stages and RapidEye data: a case study in the forest of Freising. In book: From the Basics to the Service, Editors: Erik Borg, Holger Daedelow, Ryan Johnson, Publisher: GITO Verlag, pp.21–38. ISBN: 978-3-95545-022-1

Here, the extraction of the most challenging forest parameter, tree species, is investigated using multi-seasonal RapidEye data. The method is developed and tested in the Freising test site, and RapidEye data from all seasons over three years are collected. The intention is to check the potential of using data from different growing seasons to increase the separability between the tree species.

Author contributions: The paper was written by Alata Elatawneh with contribution by Adelheid Rappl (now Wallner). Geospatial data collection and preparation was done by Adelheid Rappl (now Wallner). RapidEye data preprocessing was carried out by Natalia Rehush. The research approach was developed by Alata Elatawneh and Thomas Schneider. The research coordination and significant contribution to the discussion was done by Thomas Knoke.

2 Literature reviews

2.1 Hyperion data and forest mapping

Hyperspectral remote sensing is a rich source of spectral data that provides potential information on several vegetation variables relating to the biophysical, physiological or biochemical characteristics (Hansen and Schjoerring, 2003). The Hyperion hyperspectral sensor was launched in late 2000 as the first high spatial resolution hyperspectral sensor on board EO-1 satellite. This presented the opportunity to investigate the use of Hyperion data for applications related to work in land use / land cover classification and forest studies. This section will summarize the findings of the studies that compared Hyperion data with other hyperspectral data, or with multispectral satellite data. It will also summarize the potential benefits and challenges of using Hyperion data, in addition to highlighting the importance of the acquisition date.

Hyperion data has often been compared to multispectral Advanced Land Imager (ALI), the Enhanced Thematic Mapper plus (ETM+) data for land cover and forest studies, and in investigations intended to demonstrate the abilities of the so far unique Hyperion sensor. Xu and Gong (1984) compared Hyperion data with ALI data for land use / land cover mapping including forest cover. They conclude that Hyperion had no significant improvement on mapping level I (Anderson et al., 1976) relative to current study forest cover, while only slight improvement was achieved by Hyperion on mapping level II forest types. Conversely, list of studies reveal that Hyperion outperformed ALI, while ALI achieved better results than ETM+. Of this list is a study conducted in Canada (Goodenough et al., 2003), where Hyperion data provided better results than those of the ALI and ETM+ multispectral data for classification of land cover and forest tree species, as attributed to the great dimensionality of Hyperion spectra. Another study in the Himalayas (George et al., 2014) compared Hyperion data with Landsat ETM+ when mapping tree species, and concludes the outperformance of Hyperion was due to the narrow spectral bands, which increase the variations between the tree species. Additionally, Thenkabail et al., (2004) compared Hyperion data with the high spatial resolution IKONOS and high spatial resolution multispectral ALI, and ETM+ data for the classification of 9 forest classes in Cameroon. Here, results indicate that Hyperion outperformed other data because of its rich spectral information, even in comparison to the high quality spatial resolution data of IKONOS.

In general, all previously mentioned studies focused on the spectral capability of the Hyperion data. However, two specific studies (Goodenough et al., 2003; Thenkabail et al., 2004) pointed out

that spatial characteristics of the sensor should be investigated in the future. This recommendation was supported by a third study (Walsh et al., 2008) which utilized high spatial resolution QuickBird images to help analyze Hyperion data for invasive species mapping. The authors here proposed that data fusion between these two data type will increase mapping efficiency (Walsh et al., 2008).

In addition to high spectral resolution, the use of Hyperion data holds further potential with its broad scale of data coverage and the higher frequency of data acquisition, making it applicable to real world problems (Pengra et al., 2007; Petropoulos et al., 2012a). Furthermore, the low cost of Hyperion data in comparison to airborne hyperspectral data has been highlighted (Pignatti et al., 2009). Moreover, using Hyperion data showed a possibility for retrieving biophysical and biochemical variations as a result of variations in LAI (Eckert and Kneubühler, 2004).

Disadvantages of the Hyperion data have also been reported. The main issue with this technique is that space-borne hyperspectral sensors receive low reflected energy from the Earth surface even at 30 m spatial resolution. This decreases the variation in spectra between various surfaces (Pengra et al., 2007). As a result, the signal to noise ratio (SNR) is increased. Meanwhile, a relatively low spatial resolution combined with small pattern targeted classes (Eckert and Kneubühler, 2004) or low density of class cover (Walsh et al., 2008) often produces mixed pixels which increases the confusion between classes. It was also found that, mixed pixels used within training areas as samples for classification will decrease the accuracy of the samples and consequently decrease the achieved result accuracy (Carpenter et al., 1999; Pignatti et al., 2009; Walsh et al., 2008).

Finally, a very important point regarding the acquisition time of the Hyperion data selected for the analysis must be made. While all previously mentioned studies utilized Hyperion dataset for vegetation and forest analysis, only few highlight the importance of the acquisition date. George et al., (2014) stated that the data was intentionally selected in April because of higher phenological variations between tree species, and the high solar illumination achieved high SNR at that time. Pengra et al., (2007) selected the data in September, for the pronounced spectral variation between their targeted invasive species and other wetland classes, assisting them in their mapping efforts. Conversely Eckert and Kneubühler (2004) addressed the late phenological phase at the time of data acquisition, and the low observed spectral variation among the agricultural fields in the test areas as one of the reasons for obtaining low accuracy. However, collecting optical satellite data at any preferred time is made challenging due to many factors including but not limited to cloud free coverage, solar illumination, research area location, or time restrictions of field campaigns. These factors may significantly decrease the time span for data acquisition, perhaps explaining why other

studies were restricted to unsuitable acquisition dates, such as in December, for forest classification (Pignatti et al., 2009).

All in all, investigations into using Hyperion data for forest applications are very limited. Studies have focused primarily on comparing Hyperion with other multispectral sensors, as well as the potential benefits and limitations of the sensor characteristics. However, investigations into the Hyperion system's potential operational applications, such as extracting forest attributes, are limited. Goodenough et al., (2003) is the only study that states tree species identification with an accuracy over 80% would be considered operational. However, the study did not take into consideration all the limiting factors influencing the creation of an operational approach. However, the investigation into Hyperion's potential for operational applications in forestry should take into account a range of limiting factors including: spatial resolution, temporal resolution, the SNR, area coverage and cost.

2.2 Multi-seasonal data of forest mapping and monitoring

The evolution of space-borne remote sensing has produced numerous satellites providing ever-increasing quantities of multi-date data. The temporal component offered by such data has the potential to produce complex information that can be further used in applications such as environmental monitoring and land cover dynamics (Bruzzone et al., 2003). Since the launch of the Landsat satellite family in 1972, the use of multi-date data has been investigated for forest inventory recordings including forest cover mapping, monitoring, and tree species identification. As previously mentioned, multi-date data include multi-temporal and multi-seasonal data. Studies show that even single date data can be successful in mapping forest cover and types, however, mapping success can be increased using multi-seasonal data. Meanwhile, forest cover monitoring depends on multi-date images. Achieving forest tree species identification, a leading goal of forest related remote sensing research, has been and remains to be a challenging task. There have been no operational options offered in the literature, despite breakthroughs in active sensors (LIDAR, RADAR) and optical passive system (multispectral, hyperspectral). This is due to the cost and limited coverage of the active and hyperspectral sensors, leaving multi-seasonal data as the only promising approach towards offering operational tree species mapping. There have been few studies directed towards tree species mapping with a multi-seasonal approach, despite the fact that this topic relates to many key research questions of economic importance.

In general, remote sensing of forest mapping depends on land cover classification, in particular separating forest from non-forest cover (Boyd and Danson, 2005). In a review of multispectral data

applications, Holmgren and Thuresson (1998) showed that most studies followed the classification scheme for forest cover mapping proposed by Anderson et al., (1976). Anderson's classification scheme includes many levels, where forest cover belongs to Level I, forest types (coniferous, deciduous, and mixed forest) belong to Level II, and forest tree species belong to Level III.

Using high spatial resolution sensors (e.g. Landsat, SPOT), studies have successfully classified forest cover, ranging from regeneration forests to mature forests. Although results suggest that single data can map forest cover precisely, multi-date data proved to help in overcoming problems associated with clouds (Nagendra et al., 2013). Additionally, multi-seasonal data have the potential to increase the forest types mapping success, especially when using data collected in spring or autumn (Borry et al., 1993; Schriever and Congalton, 1995). Walsh (1980) showed that data from mid-autumn achieved better forest type results than summer data due to the phenological variation and the low sun angle, which help to detect gaps. Conversely, using data from early summer data has also been recommended because of the high sun angle (Holmgren and Thuresson, 1998). Others addressed the issues of rugged terrain and mixed forest as problems which decreased the quality of the achieved results (Dorren et al., 2003; Reese et al., 2002).

Vegetation applications, including detecting forest changes, have been developed and used in the last three decades (Chen et al., 2012; Coppin et al., 2004; Lu et al., 2004). Studies focusing on the high resolution sensors such as: Landsat and SPOT (Carvalho et al., 2001; Desclée et al., 2006; Duveiller et al., 2008; McDermid et al., 2003; McDermid et al., 2008; Willhauck et al., 2000), dealt with forest loss and disturbance monitoring (biotic and abiotic), and obtained appropriated results. None of the above studies overcame the problem with clouds, despite having identified this problem as the main obstacle with the use of optical data. In a study estimating the deforestation rate in central Africa, (Duveiller et al., 2008) concluded that the cloud problem is the only obstacle standing in the way of considering their method operational. As a solution, they recommended using more frequent multi-date data or using data from active sensors (Duveiller et al., 2008; Nagendra et al., 2013). While active sensors fusion with optical data showed the ability to detect changes (Rappl et al., 2012; Thiele et al., 2012), their high cost and small operating area restrict their present contributions at the operational level.

Forest tree species mapping using multi-seasonal remote sensing data has been investigated in many studies. The approach used most often for forest tree species mapping was typically based on the "phenological fingerprint" hypothesis, which assumes that phenological developments of different tree species shows distinct shifts in appearance, which can be explored for classification. Past research has investigated various topics such as: the influence of using datasets from different

seasons, and the most appropriate data collection seasons to achieve the best tree species separability. Limited research has been conducted to investigate the quality of tree species identification results through the increase of dataset numbers or the collection of datasets in different seasons.

Studies investigating the multi-seasonal data for tree species identification utilized mainly Landsat data (Mickelson et al., 1998; Reese et al., 2002; Schriever and Congalton, 1995; Townsend and Walsh, 2001; Wolter et al., 1995), SPOT data (Stoffels et al., 2012) and ASTER data (Davranche et al., 2010). A range of two to eight datasets has been used, and the results declared that combining all data together achieved higher accuracy than using a single dataset. However, none of these studies focused on the effects of an increased number of dataset combinations on the accuracy.

Two other studies using only very high spatial resolution airborne data investigated the effect of increasing the number of datasets on accuracy. First, Key et al., (2001) investigated nine aerial photos for tree species classification, and reported the highest accuracy by using all bands and five to six images, out of a possible nine. The second study by Hill et al., (2010) investigated all possible combinations of five multispectral airborne sensor ATM datasets (2 m spatial resolution). Their results reported that the highest accuracy was achieved when a combination of three datasets out of five were used. However, the authors reported that the quality of the data is far more important than quantity of data, in terms of capturing the highest variation in phenology between species.

Determination of the best season for data collection in pursuit of species separation was also researched, and different results were reported. Researchers consistently reported that autumn has a high potential as a successful season for data collection because of phenological conditions (Hill et al., 2010; Schriever and Congalton, 1995; Wolter et al., 1995). Others show that in addition to autumn, spring (Mickelson et al., 1998) or summer (Reese et al., 2002) show potential for species determination.

It is key to identify the season most suitable for data collection in order to potentially identify a specific tree species, and for this reason some studies have investigated this issue Table 2. Hill et al., (2010) noted that data from early spring, collected during times where deciduous trees were leafless, were helpful in detecting silver birch and European oak. This was due to the reflectance of the understory vegetation related to these species. However, their second data collection period was in late May when no phenological differences were captured. Therefore, they recommended the end of April as an ideal acquisition time when different timing of budburst and leaf unfolding between silver birch, European oak and elm is higher. The authors also revealed that data collected

at the end of September had a high potential to detect field maple as a result of the full autumn coloring of this species. Data collected at the end of October were shown to have little potential to separate European oak, but data collection in mid- or late November to detect oak were recommended, when autumn coloring is reached.

Table 2: Some studies that investigated the season most suitable for data collection in order to identify a specific tree species and their findings

Study reference, region	Date of acquisition	Species to be detected	Finding
Hill et al., (2010), Cambridgeshire, Estern England	Mid-March	Silver birch, European oak	Deciduous trees were leafless, understory vegetation had distinct spectra
	Late May	Silver birch, European oak	There were no phenological differences
	Recommended late April	Silver birch, European oak, elm	Time difference of budburst and leaf unfolding
	Late September	Field maple	Maple reached full autumn coloring
	Late October	European oak	Data had little potential to separate oak
	Recommended mid- or late November	European oak	Oak autumn coloring was reached
Schriever and Congalton (1995), Southeastern New Hampshire, USA	Late October	American beech, red oak, red maple	Data had high potential, because red maple trees lost their leaves prior to the other two species
Wolter et al., (1995), northwestern Wisconsin, USA	Mid-October	Red oak	Red oak was the only deciduous species still holding their leaves
	Mid-September	Black ash	Black ash was the only leafless deciduous species
	Mid-May	Trembling aspen	Data could catch trembling aspen leaves unfolding
	Late February	American larch	American larch was the only coniferous species without needles

Schriever and Congalton (1995) also found that data collected in October achieved the highest success for identification of American beech, red oak and red maple. However, they indicate that this success might have been due to the fact that maple trees lose their leaves prior to other species. Additionally, Wolter et al., (1995) point out the benefits of using Landsat data collected in mid-October to separate red oaks, because they were the only deciduous species still holding their leaves. For black ash separation, data collection appeared promising during mid-September given that these were the only leafless deciduous species at that time. Data collected in mid-May were found to highlight trembling aspen leaf flush. Finally, data collected at the end of February were used to separate American larch from other coniferous species, because it was identified as the only

coniferous species without needles. On the other hand, the authors pointed out that it is difficult to identify sugar maple using only one dataset collected either in autumn (September, October) or spring (May), because of the similarity in autumn leaf coloring timing with aspen. These studies demonstrate the suitability of a specific season for only few tree species and a limited number of phenological phases due to limitations in the amount of data collected.

Many other obstacles for analyzing multi-seasonal data to map tree species have been reported. Problems include phenological variations of the same tree species within the same area based on the aspect, altitude, or existence of water source, which can delay the autumn leaf coloring and fall. Also, the phenological phases are shifting from one year to another based on the weather conditions. Furthermore, data collected over a long time span may include changes attributed to reasons beyond phenological condition. Cloud cover is also often connected with active development of the phenological phase. An additional factor is the understory, which can be a good indicator for a tree species, but can be problematic by increasing the confusion between the tree species (Hill et al., 2010; Wolter et al., 1995). Additional problems associated with of multi-seasonal analysis techniques are presented in section 2.3.2.

2.3 Techniques for analyzing HSR optical data in forest applications

One of the most common applications of remote sensing for land cover and forest mapping is the preparation of thematic maps using digital image classification (Foody, 2002). Classification can be broken down into three main groups: pixel-based, sub-pixel-based, and object-based. These techniques have been applied to multispectral data analysis and to hyperspectral data analysis for forest mapping.

Pixel-based techniques can be unsupervised methods (i.e. ISODATA) or supervised methods (i.e. Maximum Likelihood - ML, Mahalanobis Distance - MhD, minimum distance - MD, Nearest Neighbor - NN, Support Vector Machines - SVM etc.). Unsupervised methods classify the pixels based on statistics only, without any pre-defined training classes, while supervised methods classify pixels based on pre-defined training classes. Unsupervised methods could be implemented with remote sensing data in order to better understand its spectral dimensionality and information content (Elatawneh et al., 2012; Walsh et al., 2008). Meanwhile, supervised methods are usually implemented to achieve final mapping of remote sensing data.

2.3.1 Techniques for analyzing Hyperion data

Hyperspectral data, offering high spectral resolution, have encouraged the adaptation of a series of techniques in order to exploit their rich spectral information. To apply the supervised methods used originally to analyze multispectral data for Hyperion data, spectral dimensionality reduction (selection) is usually carried out. Many notable reduction techniques have been applied to Hyperion data such as: minimum noise fraction (MNF), principal component analysis (PCA), and linear discriminant analysis (LDA) (Goodenough et al., 2003; Nelson, 1984; Thenkabail et al., 2004). The supervised algorithms ML, MhD, and MD have also been applied to Hyperion data for forest mapping and classification, leading to the claim that the MD achieves the best results in comparison to the others (Pignatti et al., 2009). Still, other studies have successfully applied ML (Goodenough et al., 2003) and MhD (Nelson, 1984) to Hyperion data for the purpose of forest mapping and LU / LC classification. Other techniques that can deal with the full spectral feature of hyperspectral data were developed, including Spectral Angle Mapper (SAM) (Kruse et al., 1993). SAM has often been used with Hyperion data to map forest cover and tree species. While some studies applying SAM to Hyperion data achieved better results in comparison to the other aforementioned classifiers, (Berrichi et al., 2012; Pignatti et al., 2009), others pointed out its limitations in comparison to support vector machine SVM (George et al., 2014) and object-based methods (Eckert and Kneubühler, 2004). Still, SAM classifier is highly insensitive to the illumination variation effect, because the algorithm uses only the direction of the vector and not its length in feature space.

Sub-pixel-based techniques are designed to determine the relative abundance of land features that are depicted in remote sensing data based on the features' spectral properties. Sub-pixel-based techniques can be divided into linear spectral mixing (Iordache et al., 2011) and non-linear spectral mixing (i.e. artificial neural network – ANN Heylen et al., 2014). Both linear and non-linear techniques have been applied to Hyperion data, yet studies reveal the non-linear technique consistently outperforms the linear technique (Pengra et al., 2007; Petropoulos et al., 2012a; Walsh et al., 2008).

Object-based techniques have recently become commonplace in the remote sensing community for the purpose of digital image analysis (Baatz and Schäpe, 2000). However, few studies have applied object-based techniques to Hyperion data for forest mapping. A study (Eckert, 2006) comparing object-based and SAM techniques showed that object-based achieved slightly better results. However, this study concluded that the inaccuracy of the results provided by the object-based technique was due to the low spatial resolution of the Hyperion data combined with the small

structured land pattern in the test site. Another study (Petropoulos et al., 2012b) compared object-based technique with SVM for land cover mapping, and also showed that object-based techniques achieved better results. The strength and limitations of both results were discussed, and leading to the finding that the main limitation of the SVM was the ''salt and pepper'' effect, resulting from the small structured landscape and the 30 m pixel size of the system. A study in China (Wang et al., 2010) applied object-based techniques to Hyperion data for land cover classification and investigated the effect of the object size on the result accuracy. Researchers here compared the results with the pixel-based technique, and concluded that the object-based technique outperformed the pixel-based technique.

All in all, object-based techniques show more flexibility over traditional pixel-based techniques, especially if the targeted class is of similar size or bigger than the pixel size of the analyzed data. In addition, object-based techniques have the capability to support transferability, easy GIS integration, and enhancement of the results through incorporation of additional features beyond spectral properties (Blaschke, 2010). The above findings increase the visual appeal of object-based approaches, making it a competitive paradigm for image analysis (Blaschke et al., 2014). Pixel-based techniques require more careful training data regarding small areas, making their transferability difficult. Also, concerning the spectral reflectance of the data, pixel-based approaches are very suitable for small pattern classes, but have limited success in achieving the desired results for large scale classes.

2.3.2 Techniques for analyzing multi-seasonal data

Many studies have used varieties of pixel-based techniques (unsupervised and supervised) to classify forest cover classes. Since early 2000, object-based image analysis technique has been applied to land cover and forest mapping research, and shows the potential to achieve more accurate results than that of the pixel-based (De Kok et al., 1999; Eckert, 2006; Gao et al., 2007; Zhou et al., 2008). Additionally, the results of OBIA were more realistic and represent current situations better than the results of pixel-based techniques (Dorren et al., 2003).

Forest change detection applications have been based on using many pixel-based methods in the last three decades (Coppin et al., 2004; Lu et al., 2004). Looking at the past decade, several methods using object-based image analysis techniques have been adapted and used for detecting forest cover changes (Carvalho et al., 2001; Duveiller et al., 2008; Eckert, 2006; Linke et al., 2009; McDermid et al., 2008; Willhauck et al., 2000; Wulder et al., 2008). Object-based change detection (OBCD) techniques have also shown advantages over pixel-based change detection techniques (Hussain et

al., 2013). Chen et al., (2012) arranged OBCD methods into four groups: image-object, class-object, multi-temporal-object and hybrid change detection. The implementation of these methods have been discussed in previous studies (Desclée et al., 2006; Duveiller et al., 2008; Willhauck et al., 2000), and hybrid methods performed better than others when detecting forest change. This can be attributed to the insensitivity of this method to geometric registration errors, atmospheric fluctuations, and differences in vegetation due to phenological stage (Carvalho et al., 2001). The basic concept of the hybrid method is to initially obtain results of changes using any of the pixel-based change detection algorithms, and then apply the object-based technique to enhance the results (Walter, 2004). This way, the calculation time can be reduced by avoiding segmentation of the whole image at the pixel level, while at the same time allowing for automation of the process. Given these benefits, a method with such characteristics has been used by the government of Minas Gerais in Brazil since 2003 (Chen et al., 2012).

Many methods have been developed for using multi-seasonal remotely sensed data in order to conduct forest tree species mapping, with Maximum Likelihood (ML) being most commonly used. The ML can be a powerful classifier, if the suitable reference data are available and the assumption of having a multivariate normal distribution of spectral values of a thematic class holds (Stoffels et al., 2012). The ML classifier has often been applied to forest studies and has proven to be preferable over other classifiers such as minimum distance (MD), spectral angle mapper (SAM) and artificial neural network (ANN) (Shafri et al., 2007; Thomasson et al., 1994). However, ML can be strongly biased for small samples, and leading to incorrect classification when the data are multi-modal or non-normally distributed (Wang et al., 2008). On the other hand, SAM has been successfully applied to remote sensing data of high spectral dimension such as hyperspectral data, and has the potential to perform well with the high spectral dimension of multi-seasonal data.

Many problems are typically associated with the analysis of the multi-date data because of the increased complexity of the information compared with single-date data (Bruzzone et al., 2003). Specifically, this includes the reduction of the geometric quality due to the geometric co-registration errors between the images (Key et al., 2001), and an increase in the amount of training data required to analyze the dataset (Key et al., 2001). Including further data from other seasons provides additional information, but also can contain noise which leads to a slight reduction in the result quality, referred to as the ''Hughes effect'' (Hughes, 1968). In addition, there may be differences in the illumination and observation of the canopy based on different sun angles during each data take. Issues with these shadow effects can be reduced by using solely the sunlit crown canopy, as reported in a series of studies (Immitzer et al., 2012; Waser et al., 2014). These studies

used very high spatial resolution (0.5 m) Worldveiw-2 data for tree species classification, and showed that choosing training data within the sunlit crown of the trees will definitely improve the identification of single tree species.

3 Test sites and datasets

3.1 Test sites

Four test sites were selected to investigate which type of satellite data is more suitable for extracting the desired forest parameters. The first test site was Anopoli village in Crete, representing a Mediterranean forest environment, where hyperspectral Hyperion data were examined. The other three test sites were located in different growth regions within Bavaria as a central European forest environment. Here, multispectral multi-seasonal RapidEye data were examined. The Bavarian test sites were the Bavarian Forest National Park (BFNP) in a mountainous region, along with Freising and Traunsteiner Stadtwald forest in hillside growth regions. It would be preferable to have both data types acquired for the same test sites. However, this was not possible because of the lack of cloud-free or proper acquisition timing of Hyperion data in the Bavarian test sites, as well as the absence of free of charge RapidEye data in the Anopoli test site. Moreover, Hyperion data were collected in Anopoli, in order to compensate for the lower radiometric resolution of the Hyperion system as it was mentioned in section (1.2).

3.1.1 Anopoli

The test site of Anopoli is located on the southeastern Island of Crete in Greece (35°13'7"N, 24°5'5"E). The study site is located between the White Mountains (Lefka Ori) in the north, extending down to the Libyan Sea in the south. The altitudes range from 0 m in the south up to 2,200 m in the north. The climate typical for the Mediterranean is characterized by hot, dry summers and cool, wet winters, with a dry season starting in April and lasting until September. The landscape formation is greatly affected by lasting grazing processes, which is followed by deliberate fires and intensive tree-felling in the forest. The main vegetation cover types include a phryganic ecosystem, coniferous forests, cultivated fields of varied plantations and some alpine vegetation (junipers) at high altitudes.

The phrygana cover a relatively large area, located between sea level and moderate altitudes (800 m). The dominant forest species here are pine (*Pinus brutia*), cypress (*Cupressus sempervirens*), Cretan maple (*Acer sempervirens*) and Mediterranean oak (*Quercus coccifera*). The spatial distribution of these species follows a vertical structure. For example, pines form pure stands beginning at sea level and become much denser at altitudes of 400 m up to 700 m. Many pine trees are infected by the Pine Processionary pest (*Thaumatopoea pityocampa*), and are mostly found at the Anopoli plateau at an altitude of 700 m. Gradually, cypresses begin to appear, forming mixed

30

stands amongst the pines, up to an altitude of 1,100 m. At this level and beyond to 1,500m, cypresses are dominant, and in some areas form mixed stands with maple and oak. Many species are found under the pine forest canopy such as *Hypericum empetrifolia*, *Asparagus acutifolis* and *Osyris alba*. Meanwhile, at high altitudes, vegetation cover is scarcer and differs from low to moderate altitudes with the presence of species such as *Teucrium species*. and *Verbascum spinosum*.

3.1.2 Bavarian Forest National Park (BFNP)

The study site of the Bavarian Forest National Park (BFNP) is located in southeastern Germany (49°03'53''N, 13°21'57''E) along the Czech Republic border. This is a mountainous area with altitudes ranging between 600 and 1,450 m. The BFNP was founded in 1970 as Germany's first national park, and was extended in 1997 to hold a total area of 240 km^2. Only the northern part of the park was chosen for the investigation, containing an area of 104km^2, of which forest cover made up approximately 9,300 ha on 19 April 2011. The test site is located in the growth region called Innerer Bayerischer Wald (Wuchsbezirk (WB) 11.3). The landscape is divided into three ecological zones - highlands, hillsides and valleys. In each zone, different compositions of tree species are found. Based on the inventory results from 2002 to 2003 (Heurich and Neufanger, 2005), the tree species compositions in the dominant layer of the forest are distributed in each ecological zone as follows: in the highlands, 90% Norway spruce (*Picea abies*), 2% beech (*Fagus sylvatica*) and 8% other broadleaf trees; on hillsides, 58% Norway spruce, 3% fir (*Abies alba*), 34% beech and 5% other broadleaf trees; in the valleys, 83% Norway spruce, 5% fir, 6% beech and 6% other broadleaf trees.

Severe disturbance cycles of storms and bark beetle attacks began in the early 1990's, and about 17,000 m^3 of wood was affected (Heurich, 2001). However, according to the philosophy of the BFNP administration, no forest management activities are allowed in the core zone of the park. Bark beetle management is allowed only in a small strip at altitudes between 500-800m, along enclaves of the residential areas in the BFNP and its boundaries.

3.1.3 Freising forest

The Freising forest test site is located in the southern part of Bavaria, close to the city of Freising (48°24'45''N, 11°40'45''E). It has a total area of approximately 2,180 ha and is divided into the Kranzberger and Thalhausener Forests. Its growth zone is located in the Bavarian Tertiary Hills, which hold a great potential for holding a diverse variety of tree species. The Bavarian State

Forestry group is responsible for the forest management of the test site. The forest is found in the growth region of Oberbayerisches Tertiärhügelland (WB 12.8). The main tree species and their composition in the area are Norway spruce (*Picea abies*) 73%, European beech (*Fagus sylvatica*) 5%, European and Japanese Larch (*Larix decidua Mill.*, *Larix Kaempferi*) 5%, Scots pine (*Pinus sylvestris L.*) 4%, European oak (*Quercus petraea*) 3%, Douglas fir (*Pseudotsuga menziesii M.F.*) 2%, and Maple (*Acer pseudoplatanus*) 2%. The remaining 6% consist of various uncommon coniferous and deciduous tree species. According to the management strategies, the forest structure varies from even aged pure stands to uneven aged mixed stands.

3.1.4 Traunsteiner Stadtwald forest

The test site of Traunsteiner Stadtwald is situated on southeastern Bavaria within the municipality of Traunstein (47°51'42''N; 12°39'20''E). The altitude in this area ranges from 660 m to 700 m and consists of plateaus and valleys. The forest cover is roughly 243 ha, and it is owned by the city of Traunstein, but managed by the Chair for Forest Growth and Yield at the Technische Universität München. The forest belongs to the growth region Östliche kalkalpine Jungmoräne (WB 14.4 / 3). The main tree species in the area are Norway spruce (*Picea abies*), European beech (*Fagus sylvatica*) and European silver fir (*Abies alba*). The forest structure here varies from homogeneous (e.g. even aged pure stands) to inhomogeneous (e.g. uneven-aged mixed stands). The geology can be described as Swabian-Bavarian young moraine and molasse mountain spar.

3.2 Datasets

3.2.1 Satellite data

The two satellite data types that were investigated to achieve forest descriptors are the hyperspectral data from the Hyperion sensor, and the multispectral multi-seasonal data from the RapidEye satellite constellation.

3.2.1.1 Hyperion data

Hyperion satellite data over the test site of Anopoli were acquired on 23 May 2006, under a visibility of 40 km and sun elevation of 65 degrees. The data were received as a full long scene (185-km strip) and a swath width of 7 km. The data were of level 1R that includ radiometric at sensor correction but no geometric correction. The Hyperion data were collected at Nadir, with spatial resolution of 30 m and radiometric resolution of about 10 nanometers (nm). The data consisted of 242 bands, of which 44 were not calibrated, in the visible Near Infrared VIS / NIR and

Short-wavelength infrared SWIR. The VIS / NIR region has 70 bands (only 50 are calibrated); while the SWIR region has 172 bands (only 148 are calibrated). The Hyperion data were by provided the United State Geological Survey (USGS).

3.2.1.2 RapidEye data

The RapidEye is a constellation consisting of five satellites, and each satellite has on board one of the five identical Jena Space Scanner JSS 56 sensors. Each sensor provides data consisting of five channels: in the blue (440-510 nm), green (520-590 nm), red (630-680 nm), red edge (690-730 nm), and near infrared (760-880 nm) regions of spectrum.

Table 3: Number of the used RapidEye scenes of the level 3A (#), with the corresponding visibility in kilometer (vs. km) and sun elevation in degree (s.e.°) in each of the Bavarian test sites

	BFNP			Freising			Traunstein		
Date	#	vs. km	s.e. °	#	vs. km	s.e. °	#	vs. km	s.e. °
17.05.2009							1	26	61°
20.05.2009				1	60	62°			
27.07.2009				1	70	60°			
01.08.2009							1	16	60°
07.09.2009							1	40	48°
22.04.2010				1	30	54°			
11.05.2010							1	15	60°
08.06.2010				1	30	64°			
21.07.2010				1	30	62°			
15.08.2010				1	75	56°			
10.10.2010				1	30	35°			
22.03.2011				1	45	42°			
07.04.2011				1	75	47°			
19.04.2011	2	28	52°						
21.04.2011							1	19	54°
06.05.2011				1	25	58°			
10.05.2011							1	35	60°
04.06.2011				1	25	64°			
22.06.2011	1	35	64°				1	30	66°
28.06.2011				1	55	65°			
10.07.2011				1	40	64°			
12.07.2011	1	55	63°				1	24	64°
16.07.2011				1	45	63°			
22.08.2011	2	30	53°						
23.08.2011				1	30	53°	1	40	54°
03.09.2011				1	30	49°			
25.09.2011				1	26	41°			
01.10.2011	2	40	38°				1	27	39°
06.10.2011				1	35	36°			
22.10.2011				1	18	30°			
23.10.2011							1	23	31°
04.11.2011				1	8	26°			

Typically, data collection took place at Nadir, with a spatial resolution of 6.5 m (5 m resampled) and a swath width of 75 km. The data were ordered as level 3A products for all test sites. The RapidEye Ortho Product data of level 3A were provided with radiometric at sensor and geometric corrections. The level 3A products are provided as individual 25km × 25 km tiles. All data were provided by the RapidEye Science Archive (RESA) at the German Aerospace Center (DLR). Table 3 presents the acquisition dates and the RapidEye data values corresponding to visibility and sun elevation in each test site in Bavaria.

3.2.2 Ancillary data

Ancillary data were those additions that helped support classification, such as by helping to identify the end-members and in the preprocessing of the Satellite data including the Geometric and the Atmospheric corrections. Also, the ancillary data were indispensable for the verification of the results of the satellite data analysis.

3.2.2.1 QuickBird and aerial images

The QuickBird satellite image was acquired on 10.06.2003 over the test site of Anopoli. The image was mainly used to help in identifying the end members and the reference data. The image was of the "Ortho-Ready Standard Imagery" product (Standard2A), corrected geometrically and radiometrically at the sensor. It consists of four bands: one panchromatic with 0.6 m spatial resolution and three multispectral bands in the blue, green and red spectral region with 2.5 m spatial resolution.

Digital aerial images were acquired for all test sites in Bavaria, and were mainly used to help in defining the reference data. The acquisition dates for the test sites were as follows: BFNP on 22.08.2011, Freising on 29.07.2009 and Traunstein Stadtwald on 25.04.2009. All images were georectified, and have a spatial resolution of 0.2 m, and a radiometric resolution of 8 bit. The images have three bands in the visible spectral region in all test sites, except those in the BFNP, which have an additional band in the near infrared NIR. Each of the aerial images covers a ground area of 1km × 1km, and all were delivered from the Bavarian State Office for Survey and Geoinformation (Landesamt für Vermessung und Geoinformation Bayern - LVG).

3.2.2.2 Field spectra

The field spectra were collected in 2007 and 2008 using an ASD FieldSpec® pro FR spectroradiometer. Information about the instrument specification, field spectral data collection and preparation can be found in Elatawneh et al., (2012). Training samples of the common land cover classes in the area were collected and their spatial coordinates were determined using a GPS.

Additionally, about 40 measurements of pure spectra of the vegetation and trees species were also collected. The spectra were mainly used for the preprocessing of the Hyperion data, and specifically for the spectral polishing.

3.2.2.3 Forest inventory data

Forest inventory data consist of parameters that describe the forest stand characteristics such as tree species, Diameter at Breast Height (DBH), height, age and further management-related features. In Bavaria, inventory data are typically collected within plots which are systematically arranged in a 200×200 m (100×100 m in Traunsteiner Stadtwald) sample grid. Each plot consists of three concentric circles where various information about the trees within these circles are collected. The inner circle has an area of 31 m² (3.15 m radius) wherein all trees including those with a DBH smaller than 10 cm are measured. The intermediate circle has an area of 125 m² (6.31 m radius) in which all trees with a DBH ranging between 10 cm and 30 cm are recorded. The outer circle has an area of 500 m² (12.62 m radius) wherein all trees with a DBH greater than 30 cm are recorded. Forest inventory data were available for the Freising test sites from the last inventory taken in 2001, and for the Traunsteiner Stadtwald forest test site from the inventory of the Chair for Forest Growth and Yield at the Technische Universität München taken in 2008.

3.2.2.4 Digital Elevation Models (DEMs)

The Digital Elevation Model (DEM) for the Anopoli test site was originally produced for the Fireguard project (2004) initiated by the Joanneum Research Institute. The DEM had a spatial resolution of 20 m, and was used for the orthorectification and the topographic correction of the Hyperion data. The DEMs of the test sites in Bavaria were mainly produced by the LVG using airborne Laser scanning data. The DEMs had a spatial resolution of 5 m and were mainly used for the radiometric correction as described in section 4.2.

3.2.2.5 Forest tree species phenology

The data of the forest tree phenology were provided by the German weather service (Deutscher Wetterdienst DWD) from the Dürnast station in the Freising test site. The observations are collected annually and includ the following phenological phases: May shoot, beginning of leaf / needle unfolding, oak lammas growth, beginning of flowering, autumn coloring, and leaf / needle fall. The observation program started as early as 1964 and continues until today, however, not all of the phases have been recorded over the whole period. The observations are recorded by the Julian day (the day of the year) as seen in Table 4, with the statistics of the observation ordered by the day of

the occurrence. The tree species included in Table 4 are Norway spruce (*Picea abies L.*), Scots pine (*Pinus sylvestris L.*), European larch (*Larix decidua MILL.*), European beech (*Fagus sylvatica*), European oak (*Quercus robur Mattuschka*), and Norway maple (*Acer platanoides*). The details on the phases are observed and collected by volunteers in an observation area with a radius of 1.5 to 2 km far from the main station. However, because all the tree species included in the program found rarely all together within a small finite area, the radius can be extended to 5km, and the difference in the altitude between the observed trees and the central station should be no more than ± 50 m. In addition, the forest hollows, narrow valleys, and southern or northern hillsides should be excluded from the observation areas. After the observation stage, the collected data are routinely checked for their quality and plausibility. More details about the methodology of the observation and data correction can be found in Buttler et al., (1991).

*Table 4: The phenological phases from the Dürnast station in Freising show the different phenological phases of the main forest tree species ordered ascendingly based on the average of the Julian day. Data here show for each phenological phase the number of observations, the starting and ending year of collecting the observations in addition to statistics including average, first and third quartiles (Q1, Q3), minimum and maximum of the Julian day (see **Figure 20**)*

Phase	Count	Start year	End year	Average	Q1	Min.	Max.	Q3
Larch flowering begins	24	1965	1990	97	91	70	125	102
Larch needle unfolding begins	51	1964	2014	100	92	78	119	108
Maple flowering begins	51	1964	2014	102	96	85	119	109
Oak leaf unfolding begins	51	1964	2014	121	117	103	135	126
Beech leaf unfolding begins	51	1964	2014	122	118	103	135	128
Spruce May Shoot	51	1964	2014	127	123	112	140	131
Spruce flowering begins	5	1980	1990	132	127	125	145	137
Oak flowering begins	23	1965	1990	133	130	121	143	137
Pine May Shoot	48	1967	2014	134	130	120	148	138
Pine flowering begins	34	1980	2014	138	134	125	157	140
Oak lammas growth	20	1964	1986	173	167	153	199	178
Oak autumn coloring	50	1964	2013	284	281	270	299	288
Beech autumn coloring	50	1964	2013	287	284	276	299	289
Larch autumn coloring	23	1991	2013	296	295	283	304	299
Beech leaf fall	23	1991	2013	297	292	287	313	302
Oak leaf fall	23	1991	2013	298	292	284	324	302
Larch needle fall	23	1991	2013	310	307	298	322	314

4   Forest parameter extraction

Forest parameter extraction in the Anapoli test site was based on analysis of the single hyperspectral Hyperion data, and the following parameters were extracted: forest cover and forest types (including forest tree species). Forest parameter extraction in the Bavarian test sites were based on analysis of the multispectral RapidEye data and guided by a study outlining key requirements (Felbermeier et al., 2010). While the targeted parameters forest cover, forest gaps, and forest type were extracted from single RapidEye data, the parameters forest cover changes, and forest tree species were extracted from multi-seasonal RapidEye data.

The first step was to define the parameters extracted, especially forest cover, based on the accepted definition (section 4.1). Then, both satellite data, the Hyperion and the RapidEye, were prepared and preprocessed using a variety of techniques including the application of geometric and radiometric corrections (section 4.2). Next, the targeted forest parameters to be extracted from the single hyperspectral Hyperion data were derived based on land cover LC classification (section 4.3). The extraction of the targeted forest parameters using the RapidEye data is covered in three sections. Section (4.4) explains the extraction of the targeted parameters forest cover and types from the single RapidEye dataset. Section (4.5.1) goes on to show the development of an operational method used to detect old forest growth losses, and continues with an assessment of the method based on the fast respond, cost and transferability using the multi-seasonal RapidEye data. Finally, section (4.5.2) focuses on the extraction of forest tree species based on the phenological fingerprint concept using the multi-seasonal RapidEye data. This section also includes an analysis strategy that addresses the economically important research question mentioned in the introduction.

4.1   Forest parameter definitions

Forest cover definition varies depending on the country and the users who are interested in forests. While the hyperspectral Hyperion approach was investigated in Anopoli, the multi-seasonal RapidEye approach was applied in Bavaria. Given that this study has components nested in different countries, it is important to explicitly define the forest parameters in question. For this work, the targeted parameters were defined for each approach as follows:

Forest cover in Anopoli is defined as 10% crown cover, with a minimum height of 5 m, of an area of 0.5 ha or strips of 30 m width, and not used for other purposes other than wood production. Meanwhile, in Germany, forest cover is any area of ground covered by forest trees including forest

tracks, fire breaks, openings, clearings, and forest gaps (which can be used as timber yards or feeding ground for games), in addition to any further areas linked to serve the forest. As forest gaps are important units of the forest cover in Germany, it was decided that gaps ought to be classified within the forest cover. This was recommended by foresters in the remote sensing user workshop held on 14 February 2012 by the institute of forest management. The result of this workshop was a recommended minimum area of 0.5 ha for the forest as well as for the gaps.

Forest type parameter refers to the main groups of forest tree species present, being either coniferous or deciduous. In a managed forest where stand information is made available, forest type per stand typically includes coniferous stands, deciduous stands, and mixed stands. The forest stand is the minimum management unit, within which management planning is conducted. While in Anopoli there are no forest management planning practices and the forest stands have not been reported, in Bavaria, forest management planning is practiced routinely, at least in the state owned forests. Therefore, in the Anopoli test site, forest types were simply defined as coniferous and deciduous types. Forest types were also initially defined as coniferous and deciduous in Bavarian forests, however, where additional forest stand information was available, the forest stand types were further identified as coniferous stands, deciduous stands, and mixed stands. The forest type per stand is determined based on the dominant tree group, and a threshold of 80% was recommended by foresters in the remote sensing user workshop.

Forest change refers to the loss of trees within an area defined as forest based on the Bavarian definition. These changes can be induced by standard forest management practices or calamities such as bark beetle outbreaks or storms.

Finally, the tree species parameter includes the common, endemic or important forest tree species in the study site. In Anopoli, the targeted tree species were the abundant coniferous species such as pine and cypress, along with the deciduous species Mediterranean oak and, most importantly, the Cretan endemic maple. Similarly, in the Bavarian test sites the targeted species were among the abundant forest trees species, which are frequently found in the area of the terrestrial forest inventory. Usually, these species are of economic importance due to their timber value, or of management planning importance because they are suitable for adapting under climate change conditions.

4.2 Satellite data preprocessing

Before the information extraction, remote sensing data are processed for preliminary corrections. These corrections involve detecting and addressing any distortion, noise or degradation

that may have occurred during image acquisition. Preprocessing includes checking for internal errors, caused by sensor malfunctioning, which are systematic and predictable. Preprocessing also includes reviewing for external errors which can be incurred by satellite instability, or atmospheric and topographic conditions, which are unsystematic and dependent on time and location (Campbell, 1996; Jensen, 1996).

The Hyperion data were collected by an experimental sensor and usually require additional preprocessing beyond the standard for other satellite data. For this reason, essential preprocessing steps were applied to the Hyperion data as described in Figure 3. The first step was to perform a linear interpolation of all the sensor detectors, based on a common set of wavelengths, then the full width at half-maximum values were averaged for each band. The second step involved the elimination of non-calibrated and overlapping bands. Following this, the third step was to perform a vertical striping to account for the darker stripes which appeared because of malfunctioning detectors. Next, atmospheric correction was carried out by using FLAASH, implemented in the ENVI software package. Spectral polishing was then executed by applying a running average filter over nine adjacent channels, utilizing some of the field spectra, in order to smooth the spectral reflectance. The fifth step involved the orthorectification of the Hyperion data, which was based on the direct linear transformation (DLT) model implemented in ERDAS Imagine software package. After that, a minimum noise fraction (MNF) transformation was applied to deal with the visible-near infrared (VIS / NIR) and shortwave infrared (SWIR) data separately. As a final step, an inverse MNF was used to the transformed Hyperion bands in order to reduce the uncorrelated noise that was not reduced by the spectral polishing (Goodenough et al., 2003). The corrected Hyperion data consisted of 157 bands, in which 49 bands were in the realm of VIS / NIR, and 108 bands in the SWIR regions (Elatawneh et al., 2012).
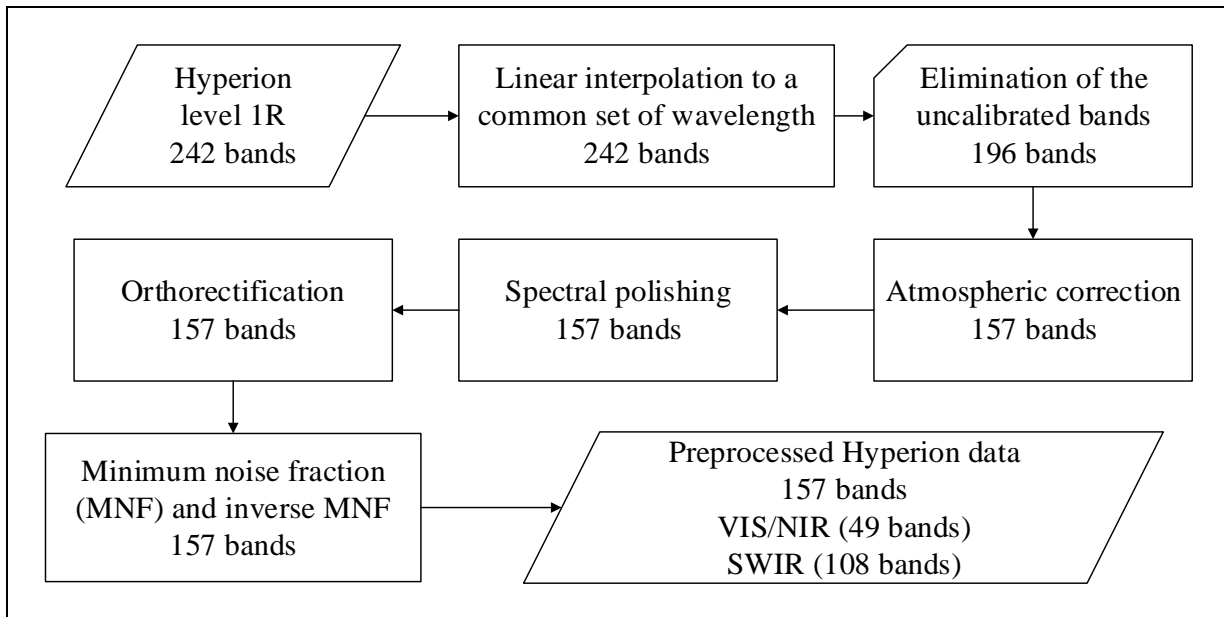
Figure 3*: The preprocessing analysis steps applied to the Hyperion data, and the resulted number of bands after each step*

The essential preprocessing steps for the multi-seasonal RapidEye data are geometric registration and atmospheric correction. The location uncertainty in RapidEye 3A level data could reach a maximum value of 50 m (RapidEye AG, 2012). Therefore, the accuracy of level 3A data was examined and, when necessary, improved by implementing co-registration with the reference geo-database. The RapidEye data of level 1B were orthorectified by using a rational polynomial function implemented in the PCI Geomatics software package. After geometric registration and correction were applied to the data, an atmospheric correction was performed using the ATCOR 3 algorithm implemented in PCI Geomatics. The algorithm used the DEM and visibility to compensate for topographic and atmospheric effects.

4.3 Parameter extraction from single hyperspectral Hyperion data

4.3.1 Methods

Forest parameter extraction in the Anopoli site, using the hyperspectral Hyperion data, was mainly based on land cover classification (Elatawneh et al., 2012, Publication 1 in Appendix). A successful classification is highly dependent on the classification scheme (Jensen, 1996). The classification scheme was developed based on the CORINE land cover, vegetation cover of the area, and the Hyperion data's ability to separate the land cover classes. After that, the Hyperion data were classified using the pixel-based, sub-pixel-based and object-based techniques. Subsequently, land cover results of forest related classes, the parameters forest cover, forest types, and tree species were identified based on their definitions.

The methodology of the Hyperion data analysis is described in Figure 4. First off, the classification scheme was defined based on the land cover map of the test site and the spectral separability of the Hyperion data. To achieve that, the unsupervised IsoData classifier was applied to the Hyperion data, and the result was intersected with the available vegetation thematic maps and QuickBird image in the area, in order to define the classes. The classification scheme was subsequently aligned to the CORINE land cover system proposed by the European Union for the Mediterranean region (European Environmental Agency, 1995). However, the broadleaved trees including Cretan maple and Mediterranean oak could not be separated into two single classes.
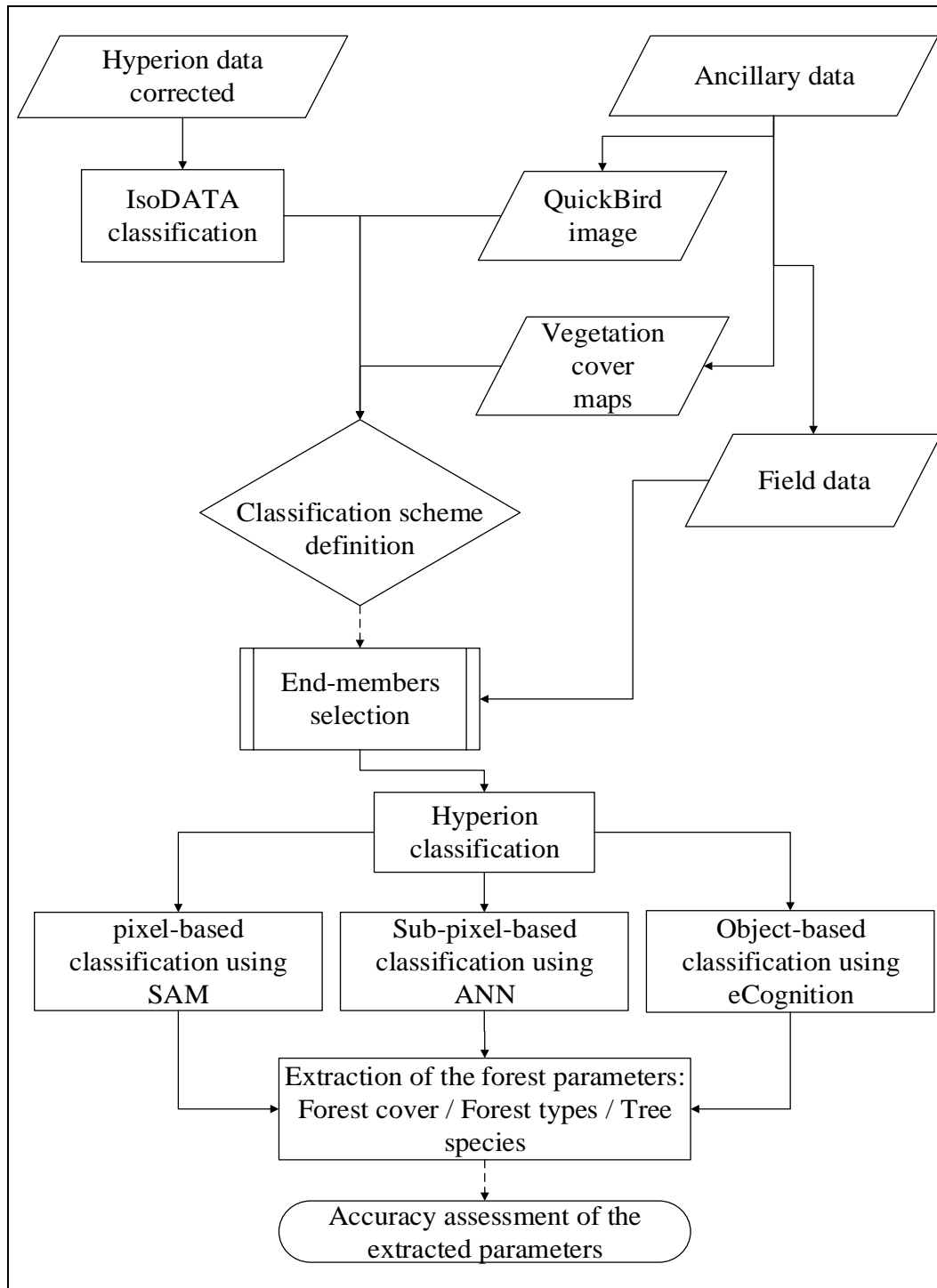
Figure 4: *The workflow followed for the Hyperion data classification in Anopoli test site*

After the classification scheme in Table 5 was defined, end-members representing the different classes were collected from the Hyperion data, based on the field training site and with the assistance of QuickBird image. The selection of the end-members was carefully decided and restricted to homogenous areas of consistent land cover. In total 550 samples, which represent the classes in Table 5, were assigned as end-members and used for the classification.

Next, pixel-based analysis was performed using SAM to classify the Hyperion data. The SAM technique (Kruse et al., 1993) classifies the pixels based on the similarity of their spectra to the reference spectra. The technique considers the reference and pixels spectra as vectors in multidimensional space, where the dimension of the vectors is equal to the number of the spectral bands. The similarity between the spectra of reference and data is based on the angle between their vectors, where small angles are more similar in spectra. Each pixel is then classified as that reference point of the most similar spectrum. SAM was applied to the corrected Hyperion image (consists of 157 bands) using the training set of approximately 50 spectra per class, to achieve the classification.

Table 5: Classification scheme was developed in Anopoli test site, adapted after (Elatawneh et al., 2012)

		Class name	Class description
Forest	**Coniferous**	Cypress trees	*Pinus brutia*
		Pine trees	*Cupressus sempervirens*
	Deciduous	Broadleaved trees	Cretan maple *(Acer sempervirens)* Mediterranean oak *(Quercus coccifera)*
Non-forest		Cultivated fields	Mainly vineyards
		Olive groves	Olive plantations in Anopoli village
		Rocks	Large areas of rocks exist mainly at high altitude and at the coastline
		Bare soil	Bare soil, some stones exist occasionally
		Alpine vegetation	Juniper trees at high altitude
		Sparse vegetation	Rarely coniferous trees distributed over bare soil mainly south of the village and near by the sea
		Phrygana	Low vegetation, mainly *Sarcopoterium spinosum, Phlomis fruticosa, Asphodelus albus, Urginea maritime, Coridothymus capitatus*
		Snow	Present at high altitudes

Next, the sub-pixel-based application was performed by using ANN with the Hyperion data. The ANN (Carpenter et al., 1999) is a machine learning technique which uses the spectral properties of the data to perform nonlinear unmixing in order to determine the relative fractions of land cover depicted in each pixel. The ANN assumes that the reflectance of a pixel is a nonlinear combination of the reflectance of the land cover classes present in that pixel. The ANN (Figure 5) establishes linkages between the input data (spectral bands) and the output data (land cover classes) through a hidden layer consist of single or multiple nodes (hidden layers) (Lillesand and Kiefer,

2000). The learning is carried out by adjusting the weights in the hidden layers to minimize the difference between the inputs and outputs, and then the error is back-propagated through the linkages. Weight adjustments are conducted repeatedly. Two parametric coefficients control the learning process: the learning rate coefficient and the learning momentum coefficient. The learning rate coefficient controls the magnitude of the adjustment of the weights, where a high value should be avoided because this leads to an increase of the process speed, thus increasing the risk of oscillation in the results. Meanwhile, the learning momentum coefficient encourages the magnitude of the adjustment of the weights along a specific direction, and a high value allows a greater learning rate coefficient to be set without risk of oscillations.
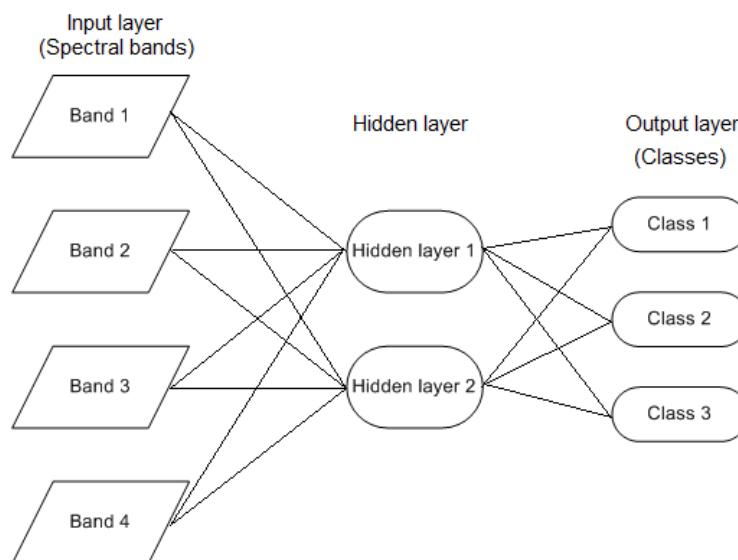
Figure 5*: Illustration of the Artificial Neural Network (ANN) of image analysis*

To apply the ANN to the Hyperion data, all corrected 157 bands were used as nodes in the input layer. Only one hidden layer was used, as this was found to be sufficient for many learning purposes (Carpenter et al., 1999). The learning rate and the learning momentum coefficient values were assigned as 0.3 and 0.7, respectively. The training threshold contribution value of 0.9 and training RMS error value of 0.1 were specified, and these values decided when the learning process should stop. All land cover classes were assigned as output layers, and the results will include 11 maps, each showing the percentage of specific land cover abundance.

The object-based analysis was applied to the Hyperion data using eCognition software (from Trimble). Object-based analysis (Blaschke, 2005) included two processing steps; the segmentation and the classification. The image segmentation process is able to automatically extract desired objects representing the real land cover features. This process allows the production of many object levels connected in a hierarchical manner, in which each object is aware of its adjacent objects,

lower objects and upper objects. Objects can be created using bottom-up or top-down segmentation approaches, and few parameters which should be defined, such as: scale, shape, compactness and bands weights. The scale parameter indirectly controls the average object size, where a high value produces big object, and vice versa. The shape criterion controls the influence of the data spectra or color on the segmentation process, while the compactness criterion controls the objects' geometry and the degree of their compactness or smoothness. The weights control the influence of each single band in the segmentation, where the higher the weight of a band, the more it influences on the objects formation. Subsequently, the classification process assigns each object to a certain class according to its spectral and geometric properties, such as: mean and standard deviation values of the bands and indices, texture, and hierarchal relations to the surrounding objects. Classification can also be based on supervised Nearest Neighbor (NN) classifier, in which few objects should be selected as samples to train the algorithm.

Before starting the object-based analysis of the Hyperion data, a variety of indices were first generated to aid in the segmentation and classification process. To create these indices, many combinations of the bands Blue (bands 11, 12, 13), Green (bands 18, 19, 20, 21), Red (bands 28, 29, 30), and NIR (bands 55, 56, 57, 58) were used. Here, the least noisy bands, and the best to assist in Land cover separation, were eventually selected for the formulation of indices (see Table 6).

Table 6: *Indices and weights were used for Hyperion data object segmentation*

Index	Index formulation	Weight
NIR-Red	band 56 $_{(913\,nm)}$ − band 29 $_{(638\,nm)}$	1
Blue-Green	band 12 $_{(465\,nm)}$ − band 20 $_{(546\,nm)}$	1
Red-Green	band 29 $_{(638\,nm)}$ − band 20 $_{(546\,nm)}$	1
B119-B133	band 119 $_{(1336\,nm)}$ − band 133 $_{(1477\,nm)}$	1
NIR / Red	band 56 $_{(913\,nm)}$ / band 29 $_{(638\,nm)}$	1
SAVI	(band 56 $_{(913\,nm)}$ − band 29 $_{(638\,nm)}$) / (band 56 $_{(913\,nm)}$ + band 29 $_{(638\,nm)}$ +0.8) × 1.8	1
NDVI	(band 56 $_{(913\,nm)}$ − band 29 $_{(638\,nm)}$) / (band 56 $_{(913\,nm)}$ + band 29 $_{(638\,nm)}$)	3
SWIR_VI	(band 119 $_{(1336\,nm)}$ − band 133 $_{(1477\,nm)}$) / (band 119 $_{(1336\,nm)}$ + band 133 $_{(1477\,nm)}$)	3
New_VI	(NDVI − SWIR_VI) / (NDVI + SWIR_VI)	3

The next step was to implement the segmentation and classification with the Hyperion, following the workflow of the analysis as presented in Figure 6. To perform the segmentation of the Hyperion data, parameter values were set as follows: scale parameter of 18, shape parameter of 0.1, and compactness of 0.6, based on try and error method. All Hyperion 157 corrected bands and indices were used in the segmentation, where the bands 11, 33, 56, 110, and 191, as well as the

indices NDVI, SWIR_VI, and New_VI were given each a weight of 3, while the rest of Hyperion bands and indices were given each a weight of 1. The weight values selection was based on the standard deviation values and the visual contrast of these bands.
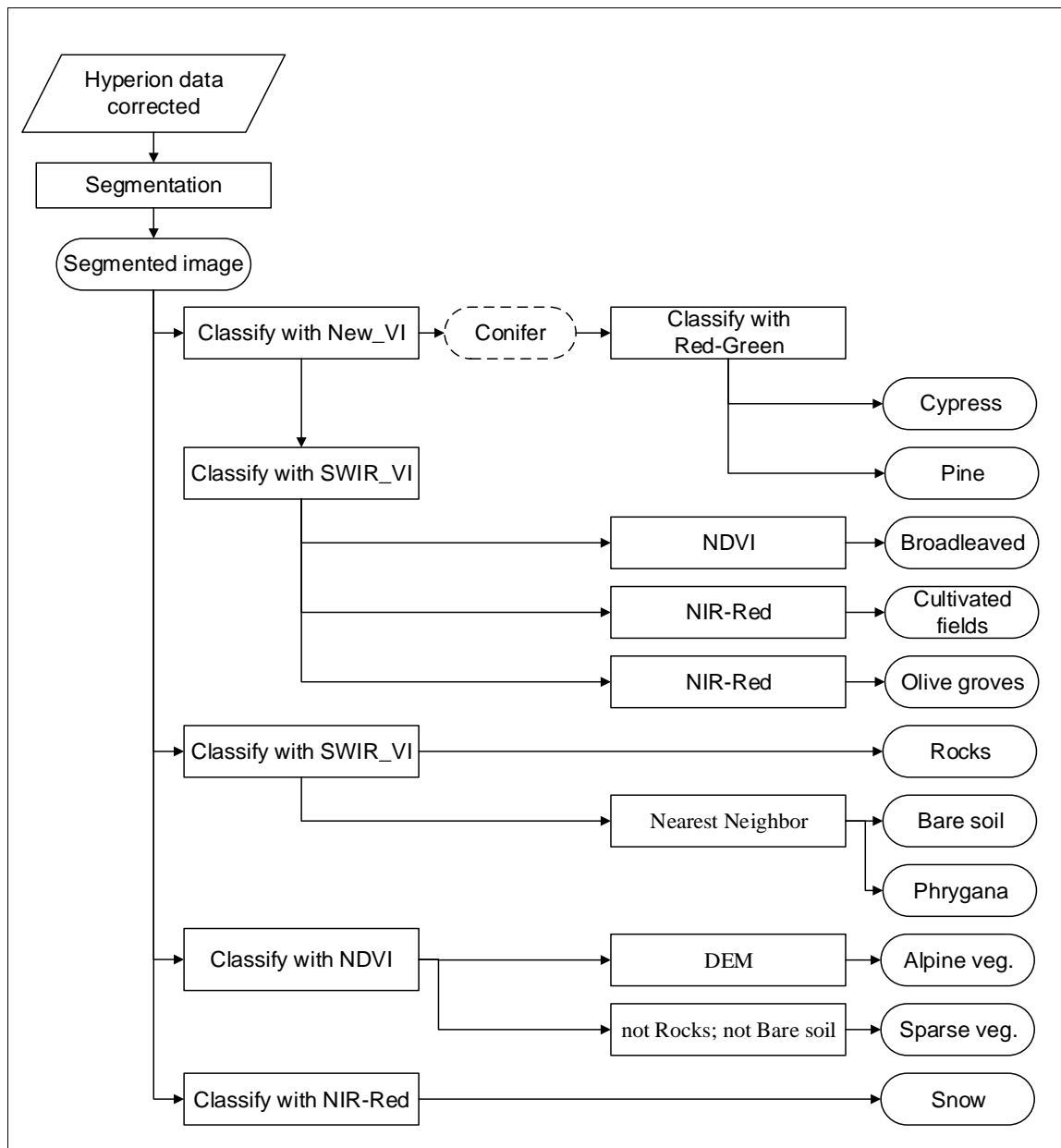
*Figure 6: The workflow followed for the Hyperion data object-based classification in Anopoli, (see **Table 7**)*

After the image segmentation, classification was performed based on membership functions and the 'NN' classifier. Table 7 includes the values of the indices and features that were used to create the membership functions. First, the conifer classes were successfully separated from other vegetated land cover by using the 'New_VI'. Then, to separate pine from cypresses, the index 'Red-Green' was used, where the value of the feature in the pine class was higher than that in the cypresses class.

Table 7: *Values of indices and features used for Hyperion data object-based classification in Anopoli, (see Figure 6)*

ID		Class name	Values of bands or indices used
Forest	**Coniferous**	Cypress trees	(0.121-0.123) New-VI and (0.117-0.119) Red-Green (0.129-0.132) Red-Green
		Pine trees	(0.124-0.126) New-VI and (0.129-0.132) Red-Green (0.140-0.150) Red-Green
	Deciduous	Broadleaved trees	(0.123-0.126) New-VI and (0.108-0.110) SWIR-VI and (0.130-0.150) NDVI
Non-forest		Cultivated fields	(0.123-0.126) New-VI and (0.108-0.110) SWIR-VI and (0.2-0.201) NIR-Red
		Olive groves	(0.123-0.125) New-VI and (0.104-0.11) SWIR-VI and (0.19-0.2) NIR-Red
		Rocks	(0.095-0.1) SWIR-VI
		Bare soil	(0.0965-0.101) SWIR-VI Nearest Neighbor
		Alpine vegetation	(0.119-0.121) NDVI and DEM
		Sparse vegetation	(0.119-0.121) NDVI and not Rocks and not Bare soil
		Phrygana	(0.097-0.115) SWIR-VI and Nearest Neighbor
		Snow	(-0.02- -0.01) NIR-Red

The classes broadleaved trees, cultivated field, and olive groves were also classified by using the 'New_VI' index. The 'broadleaved species' class was separated from the cultivated field and olive grove by using the 'NDVI' index. Conversely, the classes cultivated field and olive grove were distinguished by using 'NIR-Red' index. The classes rocks and bare soil were classified by using the 'SWIR_VI' feature, but since the bare soil class showed variable reflectance, the 'Nearest Neighbor' classifier was additionally used. Moreover, the classes alpine vegetation and sparse vegetation were classified by using the 'NDVI', while the 'DEM feature' was additionally applied in order to avoid the misclassification between the two classes. The features 'not Rocks' and 'not Bare soil' were used with the sparse vegetation class to avoid the misclassification with the soil and rocks land cover. The phrygana class was classified by using 'SWIR_VI', however, to prevent misclassification with the sparse vegetation and alpine vegetation classes, two samples were used

with the 'NN' classifier. Finally, the snow class was easily classified by using 'NIR-R' index, since its value was negative for snow class.

The parameters forest cover (usually easily extracted), forest type (whose extraction is more challenging), and the forest tree species (generally impossible to be extracted), were estimated from the various classification results. The forest cover parameter was defined as the sum of the cypress, pine, and broadleaved trees classes. Here, the 30 m spatial resolution of Hyperion data ensure that any detected forest cover is in alignment with the definition of forest cover in the area. The forest type parameter includes the coniferous type which is the sum of the cypress and pine classes, and the deciduous type which is the same class of broadleaved trees. Alternatively, the forest tree species parameter includes the single land cover classes of cypress and pine, in addition to the broadleaved trees.

Accuracy assessments were next applied to the parameter results, using a probability sampling design (Stehman and Czaplewski, 1998). The assessment was conducted via an error matrix based on point sampling units. About 170 samples were collected in the field during the data collection visits to the test site. In addition to that, 220 samples were obtained and their reference was determined based on the QuickBird image interpretation. In total, 390 samples were used as reference data to perform the accuracy assessment of each derived parameter.

4.3.2 Results

The parameters forest cover, forest type, and tree species were derived from the land cover classification by applying the classifiers SAM, ANN, and OBIA to the Hyperion data in Anopoli. However, determination of tree species was not fully achieved; only the coniferous species of pine and cypress were identified, while none of the classifiers succeeded in separating the Cretan maple and Mediterranean oak. The parameters were extracted with varying accuracy values. Forest cover achieved the highest accuracy, followed by the forest types, and finally the tree species achieved the lowest accuracy (Table 8). The results were also highly dependent on the implemented technique, for which OBIA outperformed ANN, except in the case of forest type parameter, where ANN surpassed SAM.

Table 8: *Overall accuracies of the extracted parameters in Anopoli*

Parameters Classifier	Forest cover %	Forest types %	Tree species %
SAM	84	80	73
ANN	90	92	80
OBIA	95	90	87

The results of forest cover classification were significantly different depending on the method used (Figure 7). The achieved accuracies in Table 8 show that OBIA outperformed the other methods. When SAM was applied, an overall accuracy of 84% was achieved. Here, the forest cover was mostly confused with cultivated fields, Phrygana, sparse vegetation, and the olive groves land cover. The ANN achieved an overall accuracy of 90%, due to the decrease in the confusion with cultivated fields, sparse vegetation and the olive groves, but the confusion with the Phrygana remained high. Applying the OBIA obtained an overall accuracy of 95%, and notably reduced the confusion between the forest cover and the other land cover classes. This shows that OBIA is the most suitable technique for mapping the forest cover.
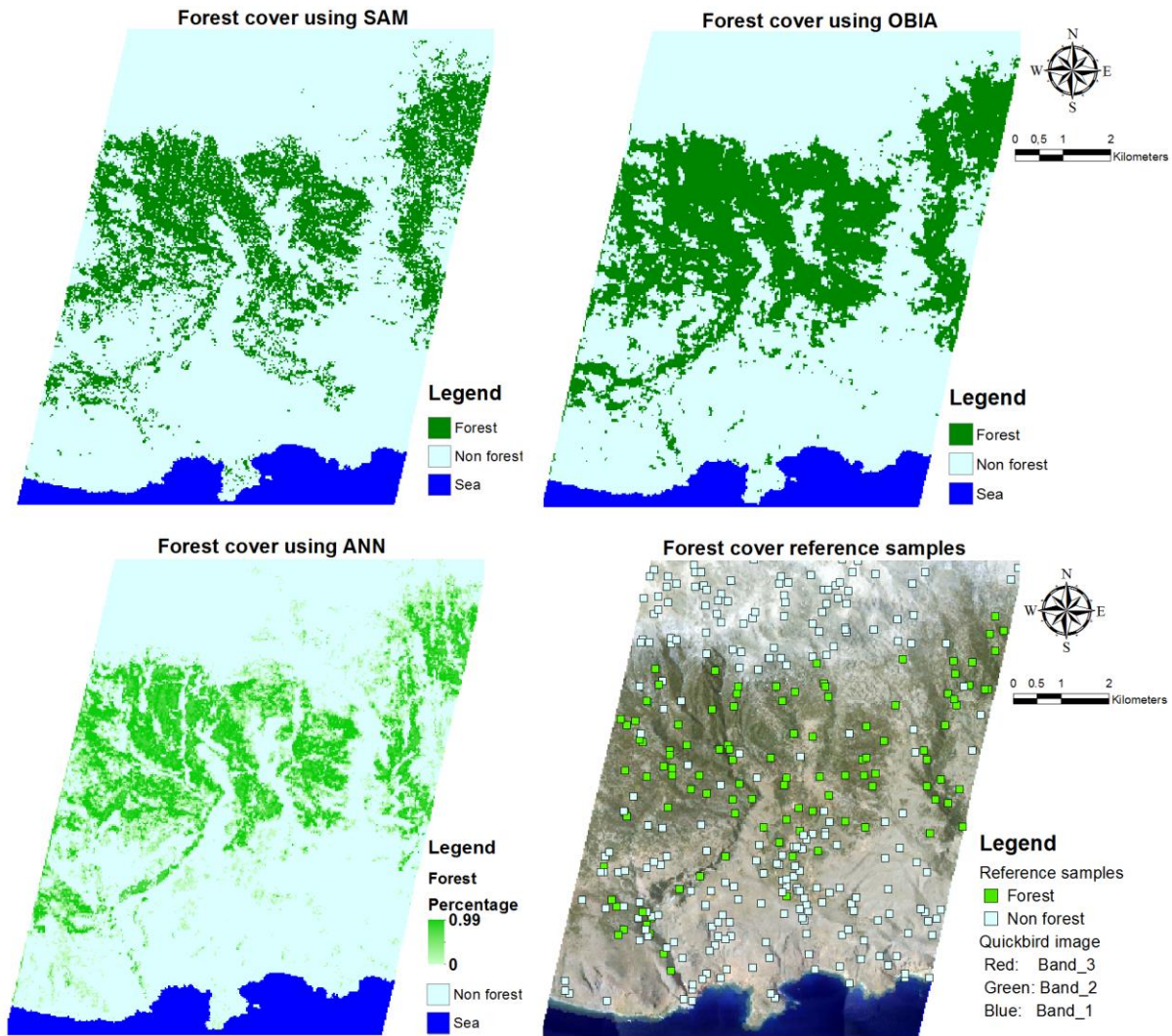
Figure 7: *Forest cover extracted using SAM, OBIA and ANN classification methods, and forest cover reference samples in Anopoli*

Forest type classifications showing the distribution of the coniferous and deciduous trees in the area are presented in Figure 8. For the forest type's distribution, SAM achieved the lowest overall accuracy with a value of 80%, where the coniferous and deciduous classes were often mistakenly interchanged. OBIA and ANN techniques obtained similar results, although ANN achieved the highest accuracy and best described the density and distribution of each forest type. However, results clearly demonstrate that the low spatial resolution of Hyperion lowered the accuracy score even more strongly than the selected technique. High confusion was observed between the coniferous and deciduous classes in areas of low forest density.
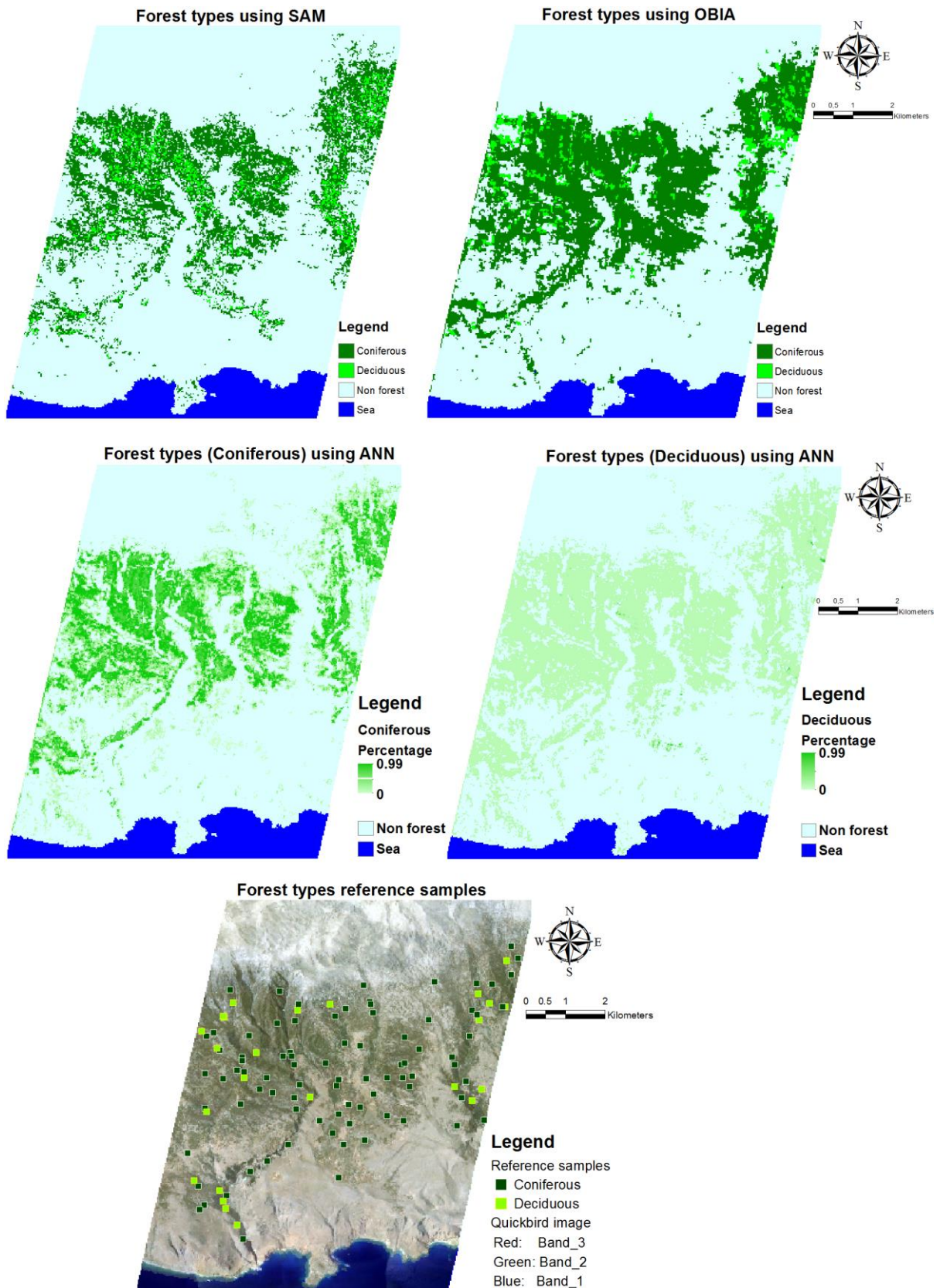
Figure 8: Extracted forest types using SAM, OBIA and ANN, and forest type's reference samples in Anopoli

The forest tree species parameter includes the mapping of the classes Cypress, Pine and broadleaved trees, since, as previously mentioned, maple and oak could not be separated (Figure

9). Overall accuracies illustrated in Table 8 show that OBIA outperformed ANN and SAM techniques. The user and producer accuracies of each single class, obtained by using the three techniques, are presented in Table 9.

Table 9: *Producer and user accuracies of the single tree species in Anopoli, adapted after (Elatawneh et al., 2012)*

Used technique	Accuracy	Cypress	Pine	Broadleaved
SAM	User %	35	94	53
	Producer %	40	58	52
ANN	User %	71	70	79
	Producer %	40	74	70
OBIA	User %	97	97	71
	Producer %	83	68	82

The cypress class, derived using SAM technique, achieved a low user accuracy of 35% because of the high confusion between cypress and the non-forest classes of cultivated fields, Phrygana and olive groves. On the other hand, the low producer accuracy of 40% for the cypress was also due to its confusion with non-forest classes such as Phrygana and sparse vegetation. When applying the ANN classifier, the confusion with the non-forest classes cultivated fields and olive groves was eliminated, improving the user accuracy of the cypress to 71%. When applying OBIA, the confusion between the cypresses with all other classes was minimized, and both its user and producer accuracies were drastically improved.

Regarding the pine class, when the SAM technique was implemented, little confusion between the pine and other classes occurred, and a very high user accuracy of 94% was achieved. As a result of the pine confusion with the broadleaved classes, its producer accuracy was only 58%. When the ANN was applied, the pine was slightly confused with the cypress and broadleaved classes, in addition to the non-forest class of olive groves. When OBIA was applied, the confusion of other classes with the pine dropped considerably, and a very high user accuracy of 97% was achieved. Meanwhile, the confusion of the pine with the broadleaved classes caused low producer accuracy to persist.
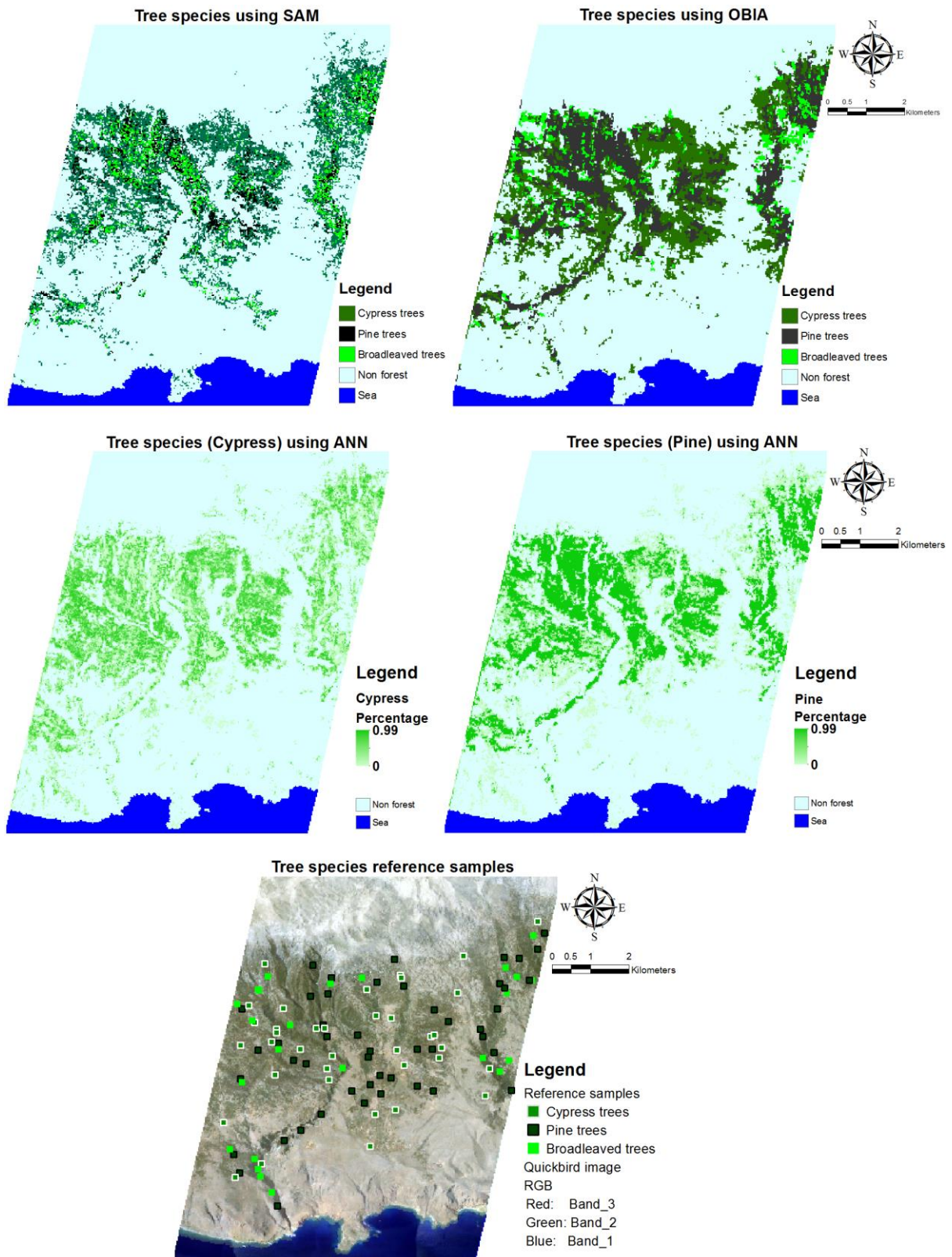
Figure 9: *Forest tree species parameter extracted using SAM, OBIA and ANN, and the tree species reference samples in Anopoli*

For the broadleaved class derived by the SAM classifier, low user and producer accuracies of 53% and 52%, respectively, were obtained, because of the confusion with the pine, cypress and the

olive groves classes. However, when ANN was implemented, the confusion with the cypress, pine and olive groves classes was reduced, and the accuracies of the broadleaved class were increased. When OBIA was implemented, the confusion between the broadleaved classes and the cultivated fields was increased, and the user accuracy again decreased to 71%. Confusion between the olive groves, pine and cypress classes was minimized and a user accuracy of 82% was achieved for the broadleaved class.

All in all, results show that forest cover was best mapped by applying the OBIA technique. While forest types (coniferous and deciduous) were best separated by either OBIA or ANN techniques, the low spatial resolution of the Hyperion data had its greatest effect on accuracy, especially at low forest tree density. Tree species mapping success using Hyperion data was limited since the deciduous oak and maple species could not be separated, regardless of the technique applied to the rich Hyperion spectral data. Finally, the results of forest types and forest tree species extracted by the pixel-based techniques (SAM and ANN) have slightly suffered from the so called ''salt and pepper'' effect. Meanwhile, when OBIA was implemented, the forest types and tree species results appeared not to be suffering from this effect.

4.3.3 Discussion

The results of the parameter extraction including forest cover, types and tree species, using the hyperspectral Hyperion data in Anopoli, was mainly based on land cover classification, as mentioned in section 4.3. The mapping and accuracy of the land cover classes, especially cypress, pine and broadleaved trees by implementing SAM, ANN, and OBIA classifiers will be discussed below.

Results show that SAM produced the lowest forest cover accuracy (84%) because of the confusion between the forest cover, cypress class, with the non-forest classes cultivated field, Phrygana, olive groves and sparse vegetation. One reason for this confusion was the similarity of the reflectance of the low density non-forest classes usually found in the transition zones between the cypress trees. Another reason was the combination of low density cypress trees with phryganic vegetative species of the understory. These reasons, combined with the relatively low spatial resolution of the Hyperion sensor (30 m), produced mixed pixels of similar reflectance to those of the Phrygana land cover. These results confirm the findings of a study applying the SAM classifier to Hyperion data in Switzerland (Eckert and Kneubühler, 2004). Additionally, the low accuracy of forest type (80%) was due to confusion between the cypresses with the broadleaved species, occurring within regions of low-density deciduous trees, or transition zones where cypress and

broadleaved trees overlapped. Furthermore, low overall accuracy of 73% was achieved for the tree species parameter, as a result of the confusion between cypress and pine existed largely in areas containing large cypresses, where these were confused with young pine trees given their similar reflectance. Additionally, the confusion between the pine and broadleaved trees occurred where the broadleaved trees are less dense or where the pine trees are very large as these trees also have similar reflectance. This similarity in reflectance is attributed to the low radiometric resolution of Hyperion (Pengra et al., 2007), which seems to be a challenge with any hyperspectral sensor on board a satellite platform.

Results demonstrated that applying ANN reduced the confusion between cypress trees and the classes cultivated field, olive groves and sparse vegetation. With this, forest cover accuracy was improved (90%), although high rates of confusion with the phrygana persisted. The reduction in the confusion is due to the ability of the ANN to extract the percentage of each land cover presented within each pixel (Walsh et al., 2008). However, the percentage of Phryganic species as a composite of the forest understory vegetation was often overestimated, leading to the misclassification. Conversely, the confusion between the cypress trees and the broadleaved trees was clearly reduced, which increased the accuracy of the forest type parameter (92%). The remaining confusion between these two classes was related to low density broadleaved trees.

The ANN technique calculated the exact fractions of each class within the pixels and improved the classification accuracy, however, OBIA achieved slightly better results than that of ANN. In fact, both implemented pixel-based analyses, SAM and ANN, suffered greatly from the relatively low spatial accuracy. This increased the confusion between the classes because of the similarity in the spectral reflectance of the mixed pixel (Petropoulos et al., 2012a). The low spatial accuracy also reduced the accuracy of the training sites, which led to the reduction of the accuracy. These results support the findings of previous studies (Carpenter et al., 1999; Pengra et al., 2007; Pignatti et al., 2009; Walsh et al., 2008), which applied SAM or ANN classifiers to Landsat and Hyperion data, where the low spatial accuracy affected the end members' accuracy. Applying SAM and ANN also resulted in the ''salt and pepper'' effect, which can in turn lower the accuracy (Petropoulos et al., 2012b).

Applying OBIA to the Hyperion data improved the extracted forest cover accuracy (95%) by reducing the confusion between the cypress and non-forest classes. This is attributed to the segmentation process occurring before the classification, which aggregates the pixels in objects and overcomes within-class spectral variation (Wang et al., 2010), thus reducing the "salt and pepper" effect. OBIA used additional features beyond the spectral properties of the Hyperion data

which had a tendency to improve the classification, as recommended by studies focusing only on spectral properties of Hyperion data (Goodenough et al., 2003; Thenkabail et al., 2004; Walsh et al., 2008).

Despite these improvements using OBIA, confusion between pine and broadleaved trees still occurred, which slightly decreased the forest type accuracy (90%) in comparison to ANN (92%). Slight confusions also remained between various classes such as broadleaved and cultivated fields. This occurred primarily in the transition zones, where many interspersed patches of various land cover types were segmented into objects belonging to other land covers. Generally, applying OBIA improved most of the individual classes' accuracies, and the confusion was minimized between the various land covers. This is because OBIA was not dependent upon the training sites exclusively, but also upon the membership functions. It was therefore influenced by a lesser degree by the accuracy of the training sites. However, at the periphery of the classes the results of OBIA were still suffering from the confusion between the classes, apparently due to the low spatial resolution. This shows that the overall success of OBIA in mapping single tree species, even using the Hyperion 30 m spatial resolution, is coming from successive distribution of the coniferous tree species in Anopoli.

In the end, none of the methods applied to the Hyperion data was able to separate the deciduous tree species (including the Cretan maple and oak). This was attributed to the mixed characteristics of the deciduous trees in the area, combined with the low spatial resolution of the Hyperion. In summary, the low signal to noise ratio (SNR) combined with the overall low energy of the Hyperion data. As well as, the acquisition date of 23 May 2006 (after the leaf unfolding phonological phase), all decreased the spectral variation between the deciduous classes. The results here demonstrate the importance of data acquisition during active phenological phases, confirming the findings of past studies implemented Hyperion data (George et al., 2014; Pengra et al., 2007). In general, deciduous tree species mapping is challenging, especially when using mono-temporal remote sensing data, as discussed in a previous study (Mickelson et al., 1998).

4.4 Parameter extraction from single multispectral RapidEye data

Methodology development led to the extraction of the parameters forest cover, forest gaps and forest types following guidelines to ensure precision, timely computational efficiency, and transferability to other test sites. The aim was to develop a method that can be applied to all test sites of interest with a minimal need for adjustment. These parameters were initially extracted based on the methods developed by Schneider et al., (2013) Publication 2 in Appendix). This method was further developed, as will be described in section 4.4.1. It was proven that mono-temporal RapidEye data can be sufficient to create a forest cover mask (Schneider et al., 2013). As such, a forest mask was created from the first available RapidEye data, which was then used as a reference for forest cover in subsequent analyses of forest types and gaps. Additionally, the reference forest cover was used as a basis for the calculation of the changes in the forest cover as will be described in section 4.5.1. The object-based image analysis implemented in eCognition from the company Trimble was utilized for the extraction of these parameters.

4.4.1 Methods

4.4.1.1 Forest cover extraction

To extract the forest cover, image analysis in eCognition applied both the iterative processes of segmentation and classification using the original band values, as well as additional indices. The assignment of a suitable segmentation parameter for the applied "multiresolution segmentation" based on many empirical trials. The weighting of the bands / indices considered was based on visual analysis of the image contrast of the two classes of forest / non-forest, as well as the standard deviation of the bands. The higher the contrast between forest and non-forest in a specific band, the higher the weight value of that band should be. The final proposed and applied parameters for the segmentation and classification processes are illustrated in Table 10.

After the image segmentation, a new index called Area index was developed and calculated based on the area of the polygon enclosed between the reflectance of the red, red edge, NIR bands and the value of the NDVI, which is depicted as the green area in Figure 10.

57
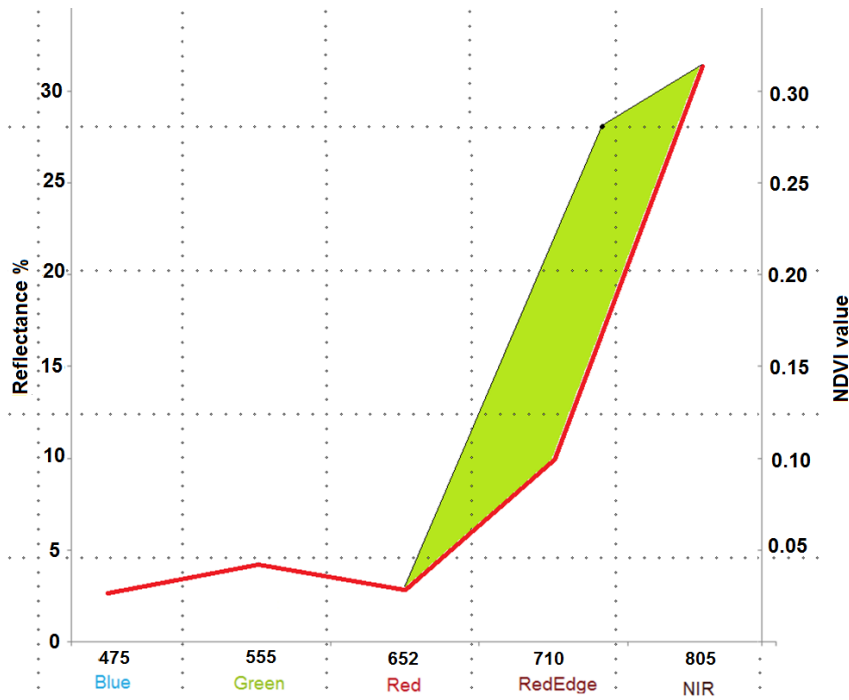
Figure 10: *Illustration shows the area encountered between the reflectance of the red, red edge, NIR and the NDVI (in green color) which was calculated as the Area index*

To calculate this area, the spectral reflectance was considered as a 2-dimensional plane, where the x-axis represents the center wavelength of these bands, and the y-axis represents the reflectance or value of these bands. Since the NDVI is an index calculated from the NIR and red bands:

$NDVI = (NIR - Red) / (NIR + Red)$, its assumed wavelength was calculated as the average of the red and NIR center wavelengths, specifically (652 nm + 805 nm) / 2 ≈ 728 nm. Then the area index (AI), or the area of the green polygon in Figure 10, was calculated based on its assigned coordinates based on the Shoelace formula as described in the following equation:

$$AI = \left| \frac{652 \times \rho \text{red edge} - 710 \times \rho \text{red} + 710 \times \rho \text{NIR} - 805 \times \rho \text{red edge} + 805 \times \rho \text{NDVI} - 728 \times \rho \text{NIR} + 728 \times \rho \text{red} - 652 \times \rho \text{NDVI}}{2} \right|,$$

where ρ represent the reflectance value of the related band.

The rule set was then developed to perform classifications separating forest from non-forest areas. In the first step, all classes belonging to the non-forest area such as water, urban areas and infrastructure were masked using the Blue band and the Area index.

Optimization of the remaining unclassified objects of the forest class using the Area index and the red edge band was next conducted. Following this, the classification of the classes forest and non-forest was enhanced by using variant functions as seen in Table 10. By applying the aforementioned steps, classification of more than 98% of the forest objects is automatically achieved.

Table 10: *The developed rule set for forest cover extraction*

Process	Class	Rule set Function	Values
Segmentation		Multiresolution segmentation	
		Parameters	Scale = 15 / Shape = 0.3 / Compactness = 0.2
		Layer weight	Blue = 1 / Green = 7 / Red = 1 / RE = 9 / NIR = 8 / NDVI = 5 / AI = 10
Classification	Non-forest	Classification (membership function)	Mean blue ⎰ 0.18 - 0.28
			AI ⎱ 75 - 85
	Forest	Classification (membership function)	AI ⎰ 80 - 85
			AI ⎱ 240 - 290
			RE ⎱ 13.5 –14.5%
Classification enhancement	Non-forest	Assign class (Threshold condition)	Mean green > 0.53%
	Forest	Assign class (Relations to neighbor objects)	Relative border to forest > 0.84
	Non-Forest	Assign class (Geometry)	Area (pixel) < 20 pixels
	forest	Assign class (Relations to neighbor objects)	Relative border to forest = 1
	Forest and Non-forest	Manual editing	Delete all the agricultural fields. Include all the forest objects
Border smoothing (Reshaping object)	Forest	Pixel-based object resizing	Grow into all where NIR > 16.1% and relative area of forest pixels in (3×3) > 0.5. Shrink using unclassified where relative area of non-forest pixels (3×3) < 0.5
	Non-forest	Pixel-based object resizing	Grow into all where NIR > 16.1% and relative area of forest pixels in (3×3) > 0.5. Shrink using unclassified where relative area of non-forest pixels (3×3) < 0.5
Enhancement	Forest	Merge region Remove objects	Area (pixel) < 200

However, classification enhancement is generally applied manually in order to reduce the confusion between the forest and non-forest classes. Next, the borders of the forest mask were smoothed using more spectral properties (NIR), and the forest mask was then unified. Due to the sensitivity of the methods used to detect forest trees, even very small patches of forest trees were detected and classified as forest. Therefore, all small objects which were less than 0.5 ha in area were excluded according to the forest definition mentioned in section 4.1.

4.4.1.2 Forest types and gaps extraction

The approach was undertaken to extract forest type and gaps without stand borders, and to again extract the forest types with stand borders. For the extraction of the forest types and gaps, eCognition software was used, and the segmentation parameters were defined according to the layers separability of the two classes, deciduous and coniferous. The final proposed and applied parameters for the segmentation and classification processes are illustrated in Table 11. For the forest type segmentation, a combination of two segmentation processes was used. The first was Quadtree based segmentation, and the second was multiresolution segmentation. Combining segmentation maintains desirable results while being faster than the exclusive use of multiresolution segmentation.

After segmentation, the objects were classified as forest or non-forest using the produced forest mask. The contrast split segmentation was then used to segment a second level, and classify the sub-object of forest into deciduous, coniferous and gaps. The contrast split segmentation was chosen because it combines aspects of both segmentation and classification, and it needs only two parameters to be defined by the user (step size, image layer). This segmentation method is therefore generally applicable to any test site or new dataset.

For the separate stand level classification, a new map (referred to as stand map) was produced from the main map. The Quadtree based segmentation was applied to level 2 using the stand borders to cut the classified objects of coniferous and deciduous areas into smaller fractions, in alignment with stand borders. After that, a segmentation of a new level called stand was established over level 2 by applying multiresolution segmentation and using thematic layer stands. The created object resembled perfectly the forest stands. Finally, the size of stand objects in the level stand were classified based on the relative area of each forest type in the lower level. The relative area threshold to classify stands into coniferous or deciduous was 80% or more. Thus stands with coniferous to deciduous ratios of less than 80% were classified as mix stands.

Table 11: *The developed rule set for forest types and gaps extraction*

Process	Class	Rule set Function	Values
Segmentation (Level 1)		Quadtree based segmentation	
		Parameters	Scale = 100
		Layer weights	Blue = yes / Green = yes / Red = yes / RE = yes / NIR = yes / NDVI = yes / AI = yes
		Multiresolution segmentation	At object level (merge only)
		Parameters	Scale = 60 / Shape = 0.3 / Compactness = 0.2
		Layer weights	Blue = 1 / Green = 7 / Red = 1 / Red edge = 9 / Nir = 8 / NDVI = 5 / AI = 10
Classification (Level 1)	Forest	Assign class	By thematic layer (Forest cover)
	Non-forest	Assign class	Unclassified as non-forest
	Forest and Non-forest	Merge region	
Segmentation and classification (Level 2)	Deciduous and Coniferous	Contrast split segmentation	Class filter: forest Step size: 100 Stepping type : add Image layer : red Edge Class for bright objects: deciduous Class for dark objects: coniferous
	Gaps and Deciduous	Contrast split segmentation	Class filter: deciduous Step size: 22 Stepping type : add Image layer : green Class for bright objects: gaps Class for dark objects: deciduous
Copy map (for forest type per stand)		Copy map	Copy map from main (Stands map)
Segmentation (level 2)		Quadtree based segmentation	Stands map
		Parameters	Scale = 3
		Layer weights Thematic layer weight	All layer = No Stands = Yes
Segmentation (Level stands)		Multiresolution segmentation	Create above
		Parameters	Scale = 50 / Shape = 0.1 / Compactness = 0.5
		Layer weights Thematic layer usage	All layers = 0 Stands = Yes
Classification (Level stands)	Stands	Assign class	By thematic layer (stands)
	Coniferous stand	Assign class	Relative area to sub-class coniferous >= 0.8
	Deciduous stand	Assign class	Relative area to sub-class deciduous >= 0.8
	Mixed stand	Assign class	Classified as stand

61

4.4.1.3 Accuracy assessment

Accuracy assessment of the extracted parameters was carried out for the three test sites in Bavaria. Sampling units were distributed systematically over grids in each test site. Based on the area of each test site, the number of units used for the assessment was 849 in the BFNP, 618 in Freising, and 320 in Traunsteiner Stadtwald test sites. The reference values of the samples were assigned based on visual interpretation of the digital aerial images and field trips. Eventually, the overall accuracies of the three forest covers in each test site were calculated (Congalton and Green, 1999). The overall accuracies of the forest types and gaps of each analyzed RapidEye data were also calculated in each test site, taking into consideration the forest cover losses which took place between 2009 and 2011.

4.4.2 Results

As previously mentioned (see section 4.4), for the determination of the forest cover even mono-temporal datasets provide satisfying results. Such RapidEye data from April were used to extract the forest cover in the Bavarian Forest National Park - BFNP test site, while, similar data from May were used to extract the forest cover in Freising and Traunsteiner Stadtwald test sites. The accuracy assessment of the forest cover parameters, extracted by using multispectral RapidEye data, achieved overall accuracies of 99.1%, 94.7% and 98.1% for the test sites BFNP, Freising and Traunstein, respectively. Also, the employed method succeeded in extracting the forest cover in various test sites within different Bavarian growth regions. However, confusion was noticed between the forest and non-forest land cover, primarily concerning fields in the Freising test site.

Overall accuracies of forest types and gaps extracted by each mono-temporal RapidEye dataset in the Bavarian test sites are shown in Table 12. The results of the forest types and gaps extracted for the three test sites are shown in Figure 11. Generally, the overall accuracies show that results vary decidedly based on the test site. The average of the achieved overall accuracies in the BFNP was the highest, followed by Freising, while the lowest values were found in the Traunsteiner Stadtwald. Within the same test site, the results vary in their accuracy based on the acquisition date of the analyzed image.

The results from most of the RapidEye data in the BFNP test site achieved overall accuracies between 87.5% (except the 80.2% from 19 April 2011) and 91.8%. The overall accuracies of the results in Freising were between 79.5% and 86.4%, and in Traunsteiner Stadtwald, overall accuracies were between 62% and 69.2%. Additionally, all results were achieved by applying the method developed here, which applied the same rule set with minimum adjustment.

Table 12: Overall accuracies of forest types and gap classification in the three Bavarian test sites

Number	Date	% BFNP	% Freising	% Traunstein
1	17.05.2009			67.0
2	20.05.2009		84.8	
3	27.07.2009		85.2	
4	01.08.2009			44.8
5	07.09.2009			67.1
6	22.04.2010		80.7	
7	11.05.2010			62.0
8	08.06.2010		86.2	
9	21.07.2010		86.4	
10	15.08.2010		84.9	
11	10.10.2010		82.5	
12	22.03.2011		81.5	
13	07.04.2011		83.0	
14	19.04.2011	80.2		
15	21.04.2011			68.1
16	06.05.2011		83.0	
17	10.05.2011			67.1
18	04.06.2011		82.2	
19	22.06.2011	91.8		65.6
20	28.06.2011		85.1	
21	10.07.2011		84.2	
22	12.07.2011	91.8		66.6
23	16.07.2011		79.8	
24	22.08.2011	88.9		
25	23.08.2011		82.6	67.0
26	03.09.2011		83.7	
27	25.09.2011		83.1	
28	01.10.2011	87.5		69.2
29	06.10.2011		83.3	
30	22.10.2011		81.4	
31	23.10.2011			66.4
32	04.11.2011		79.5	

Results of forest types per stand extracted for the three test sites are shown in Figure 12. The forest stand is the smallest management unit in forest applications, and offers a reference that allows further classification of the forest type into the third class, mixed forest. Results were delivered as required by foresters, and they give an excellent overview about the forest stands' tree group structures. Regardless of the accuracy, results at the stand level of each dataset were correctly classified.
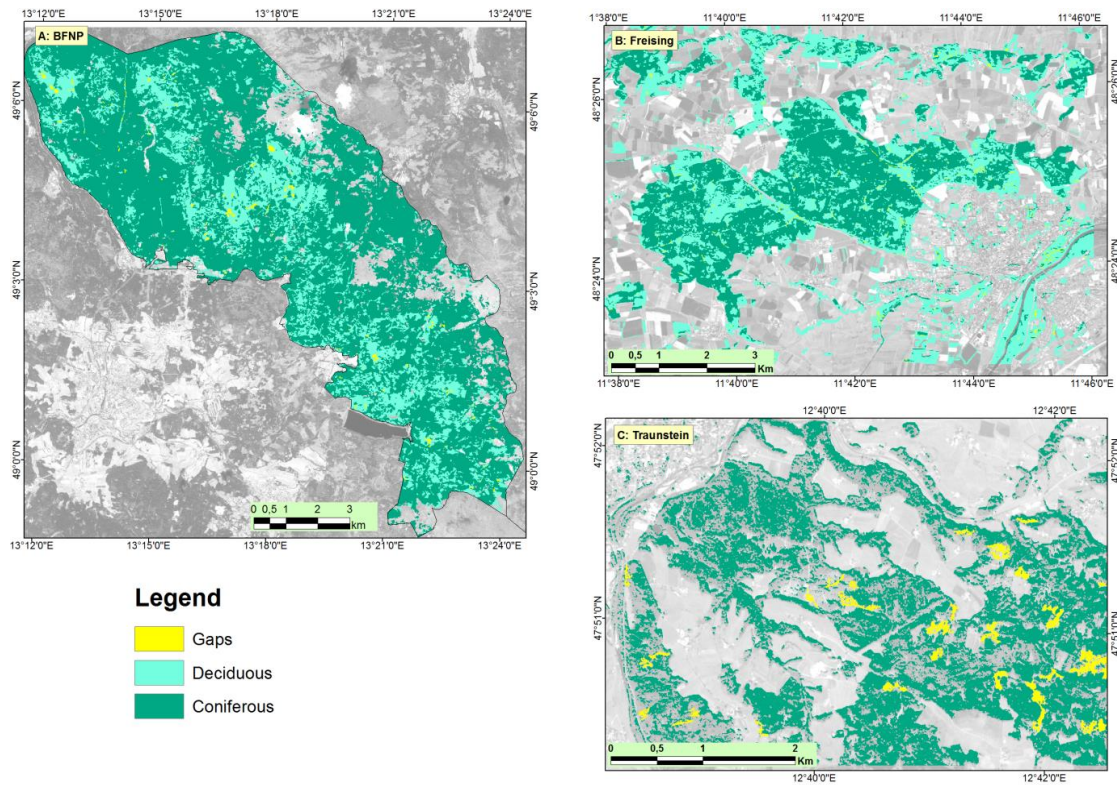
Figure 11*: Examples of the classification results of forest cover, types and gaps using RapidEye data in the Bavarian test sites*
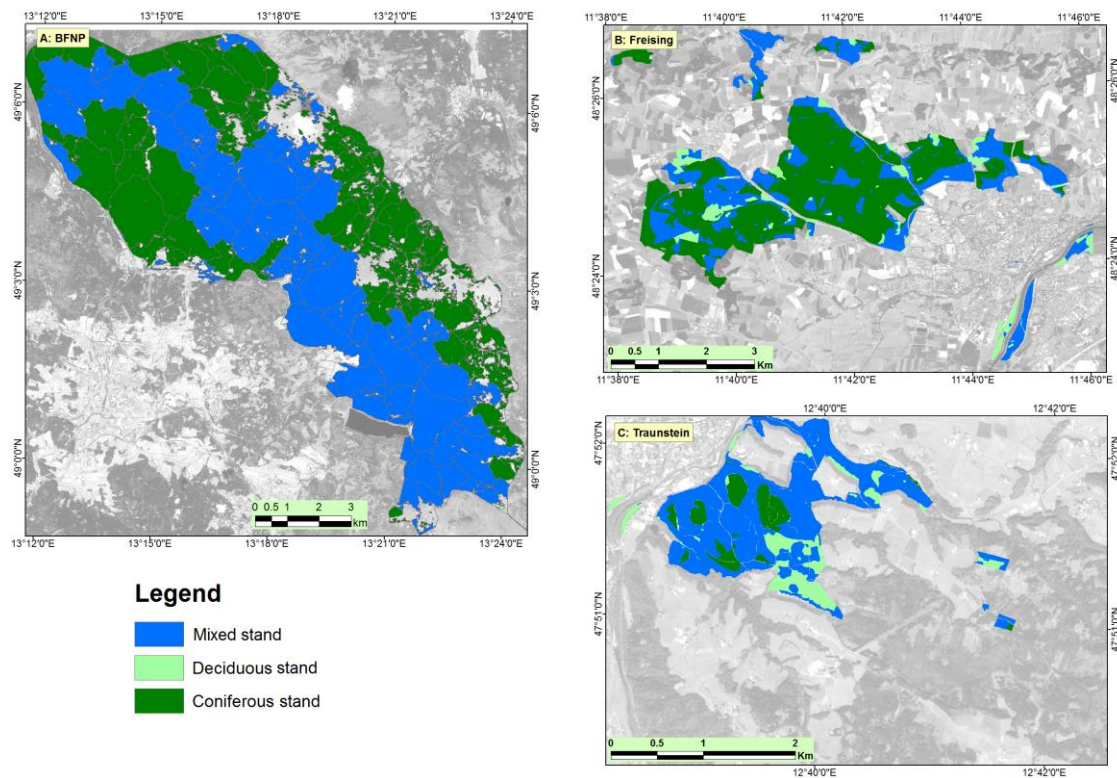
Figure 12*: Examples of the classification results of forest stand type (coniferous, deciduous, mixed) using RapidEye data in the Bavarian test sites*

4.4.3 Discussion

4.4.3.1 Forest cover parameter

The results of the extraction of forest cover parameter achieved by applying OBIA to multispectral RapidEye data in Bavaria produced similar or higher accuracies than those produced by applying OBIA to the hyperspectral Hyperion data. This demonstrates that the higher spatial resolution of the RapidEye data can often compensate for the higher spectral resolution of the Hyperion data concerning forest cover mapping. Furthermore, high accuracy results were achieved in various test sites of different conditions. This was because of the method design, which was intended to be transferable and able to identify the forest cover quickly and precisely. This was ensured by using only the blue band, red edge band, and the area index in analysis. Here, the area index helped with the precision of forest extraction, while using only a few bands makes the method fast applicable and easily transferable to other test site. Only slight confusion between the forest cover and non-forest land cover was noticed in the results. An important observation is that the implemented OBIA method applied to high spatial resolution RapidEye data can be successfully applied at the regional level. The potential of applying OBIA to SPOT data, similar to the RapidEye, in order to extract forest cover has been reported (De Kok et al., 1999). The challenge of applying optical HSR data to map forest cover at the regional level is due to the low frequency of the data, combined with the cloud coverage (Nagendra et al., 2013). The advantages of using RapidEye data, on the other hand, is that they can achieve the expected accurate mapping and overcome the problem of the cloud coverage.

4.4.3.2 Forest types and gaps

The forest type and gaps parameters extracted with the use of RapidEye data from different phenological phases in the three Bavarian test sites achieved overall accuracies ranging between 60% and 90%. Aggregated results of forest types per stand were in high agreement with the reality, while the accuracy of the results per stand were high enough to successfully classify each stand.

The variation in the accuracies appears to be based on the location of test sites within various growth regions, considering forest structure and the phenological phase of the vegetation. The average overall accuracies of the results was highest in the BFNP test site, where the dominant tree species in the forest is Norway spruce, and coniferous and deciduous forest types are typically not mixed. However, the result from 19 April 2011 in the BFNP was of the lowest accuracy, attributed to the low solar elevation that reduced the illumination and lowered the energy reached at the

RapidEye sensor during data acquisition. Another factor was the snow cover beneath the tree stands, especially at high altitudes, which disturbed the data reflectance. In the Freising test site, the average overall accuracy of all results from various datasets was less than that in the BFNP. This was due to the mixed forest structure in Freising, which is more diverse than that in the BFNP. This phenomenon was also identified by (Reese et al., 2002). The results in Freising varied minimally, with the lowest results being those collected in early spring or late autumn, and 16 July 2011 as an exception. The low accuracy of the result from November 2011 was achieved mainly because of the low solar elevation. Meanwhile, the low accuracy of the result from March 2011 was due to low solar elevation and snow cover. The lowest accuracies were achieved in Traunsteiner Stadtwald because of the complex forest structure, which is mixed and consists of multi-layer stands. Such forest structure approaches the model of ''forest of tomorrow'', which has been promoted by management policies of the Bavarian forest administration. Additionally, the area of Traunsteiner Stadtwald is more mountainous than the area of Freising, which subsequently reduced the accuracy of the results. Similar effects were reported in a study (Dorren et al., 2003) in the Austrian Alps, which applied pixel-based and OBIA to Landsat data for forest type mapping, and the quality of both results was reduced by the mountainous terrain. Additionally, accuracy was decreased by the low density of the forest type, which was likely attributable to the relatively low spatial resolution (30 m) of the Landsat data. Generally, the RapidEye sensors acquiring multi-seasonal data and covering an expansive area lay out the conditions in which one can define the reasons for results variation based on the date and the growth region (Borry et al., 1993; Schriever and Congalton, 1995). Results achieved in this study slightly outperformed the results that were reported in previous studies utilizing SPOT and Landsat multispectral sensors of similar characteristics to the RapidEye (Holmgren and Thuresson, 1998).

The primary success was the transferability of the applied method by applying OBIA to multi-seasonal RapidEye in various test sites. This was accomplished by maintaining the developed rule set in OBIA as simple as possible by limiting the number of parameters. It is of interest to mention that the method was originally developed in the Freising test site, and then was transferred to the BFNP and Traunsteiner Stadtwald sites. Achieving higher accuracy in the BFNP than in Freising demonstrates that applying the method to an area with less complex forest structures can provide realistic and consistent results. The BFNP region is a typical mountainous forest with a successive growing structure, predominated by spruce trees. The region encompassing the Freising test site is slightly more complicated and diverse than the BFNP, as Freising is located on flat terrain and still has many stands that are heterogeneous in tree species and age. Finally, the forest in the test site of

Traunsteiner Stadtwald is the most inhomogeneous and is highly mixed with many uneven-aged trees.

4.5 Parameter extraction from multi-seasonal multispectral RapidEye data

Applying the multi-seasonal multispectral approach with RapidEye data, the targeted parameters extracted in the Bavarian test sites, are forest changes and forest tree species. The object-based image analysis implemented in eCognition from the company Trimble was utilized for the extraction of forest changes parameter in section 4.5.1. Still, the forest tree species parameter in section 4.5.2 was extracted using pixel-based analysis.

4.5.1 Forest tree cover monitoring

4.5.1.1 Methods

A robust method was developed to monitor forest cover, defined for the test sites of Bavaria and using multi-seasonal RapidEye data (Elatawneh et al., 2014, Publication 3 in Appendix). The method aimed to monitor forest tree cover area losses by taking advantage of the high revisiting frequency of the RapidEye system, which nominally offers data uptake opportunities every 2 to 3 days. While the intention was to detect forest losses caused by standard management activities, special attention was given to sudden changes induced by bark beetle and storms. The high frequency of the RapidEye data plays a key role in overcoming any possible issues with cloud coverage, and contributes to the ''fast response'' capability in case of a storm or other calamities.

The development and assessment of this method was carried out in the BFNP test site over two time periods. The first period extended between 19 April and 22 June / 12 July 2011, and detected losses because of either bark beetle or regular management. The second period, between 22 June / 12 July and 22 August 2011, detected the losses caused by a storm that fell on 13 July. The success of this method in detecting sudden changes due to storm or other calamities was assessed by comparing the results to official storm damages survey of the BFNP administration. This survey was based on visual interpretation of the forest cover losses using stereoscopic digital aerial images also collected on 22 August 2011.

The strategy for mapping forest cover changes is based on using newly acquired RapidEye scenes to continuously update forest cover databases. The seasonally detected changes should contribute to the annual update of the forest cover database, which can serve as a basis to detect changes between two years. Based on the most recent available RapidEye data, the forest cover database was updated and assessed for the BFNP test site in the year 2011, as well as for the Freising and Traunstein study sites from 2009 to 2011.

4.5.1.1.1 Forest tree cover monitoring and cloud problem solving

The developed method applies hybrid approach change detection to multi-seasonal data (Figure 13). In the hybrid approach to change detection, the pixel-based extraction of initial changes is accomplished using an image-differencing technique (Singh, 1989).
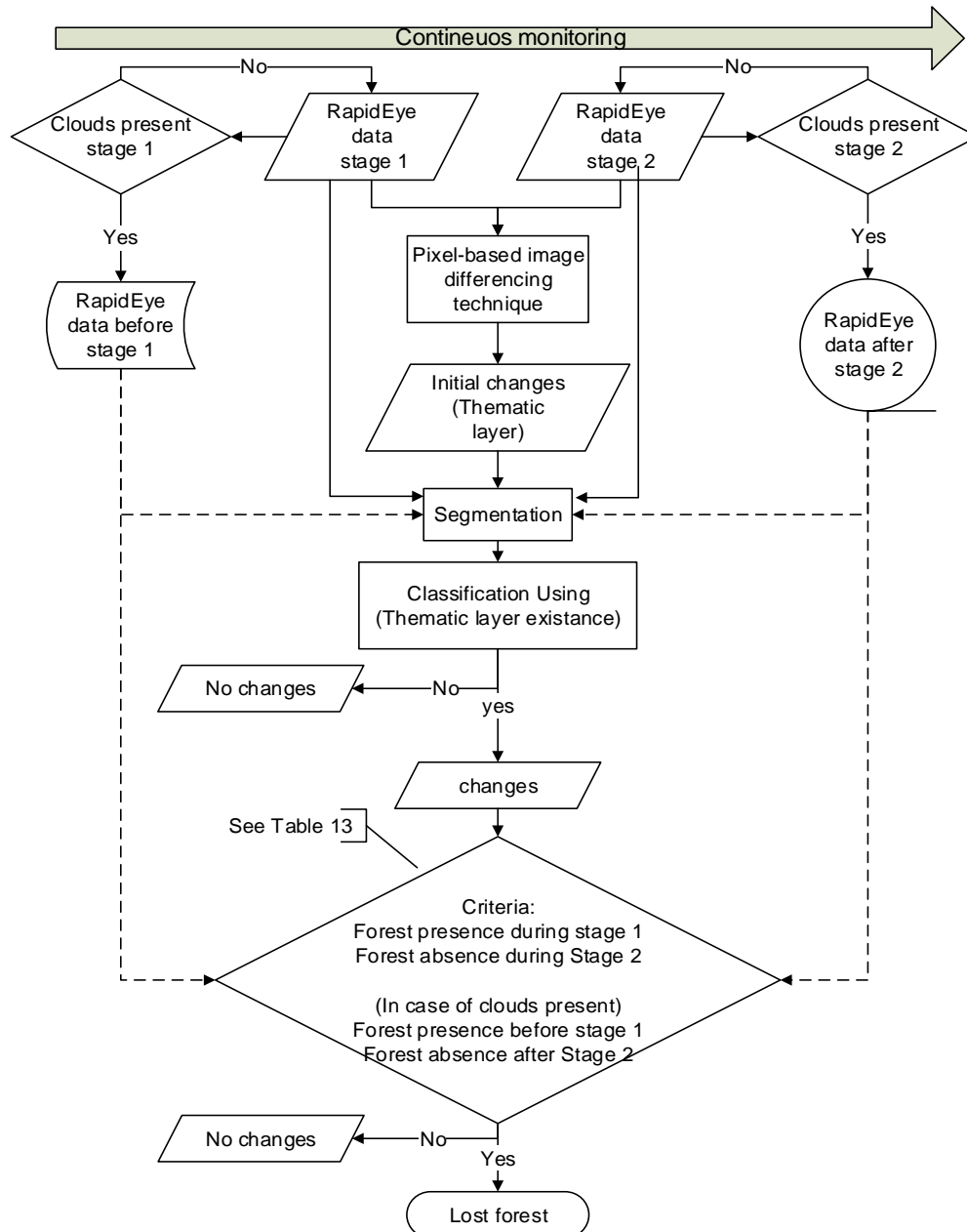
Figure 13: Methodology followed for the detection of loss in forest cover in the Bavarian test sites

One must be cautious with these initial changes, as many of the differences detected are not real changes in forest cover, but instead may be attributed to non-uniformly reflecting land cover types (e.g. water bodies); weather conditions, such as clouds or dense fog; or seasonal changes caused by plant phenology. These differences, which do not correspond to real forest changes, were excluded using the object-based technique.

In the object-based paradigm, the initial changes detected using pixel-based methods were used as a thematic layer on which a multiresolution image segmentation process was then performed. Following this, objects were initially classified as "change" based on the thematic layer representing initial changes. The results were then refined, based on the criteria outlined in Table 13, in order to identify the areas where forest cover was lost. Many spectral features (e.g. Blue / Green ratio, Brightness, NDVI) were calculated for each segment on each band for each of the multi-seasonal images separately, to refine the results using carefully selected criteria (see Table 13). More details about this method and the used parameters are made available in (Elatawneh et al., 2014, Publication 3 in Appendix).

Table 13: Criteria based on indices used for the extraction of forest cover loss in Bavaria

Criteria — Period	Stage 1– Stage 2
Forest present during stage 1	Blue / Green ratio (stage 1) Brightness (stage 1) NDVI (stage 1)
Forest absent during stage 2	Blue / Green ratio (stage 2) NDVI (stage 2)
(In case of cloud present during stage 1) Forest present before stage 1	Blue / Green ratio (before stage 1) Brightness (before stage 1) NDVI (before stage 1)
(In case of cloud present during stage 2) Forest absent after stage 2	Blue / Green ratio (after stage 2) NDVI (after stage 2)

The first criterion excluded the changes that occurred outside the forest area, such as relating to water bodies or agricultural fields. Criterion number two examined whether the areas where the initial changes occurred were in fact still forested in the second stage. If this was found to be the case, these changes were excluded from the forest change category and instead attributed to seasonal changes due to forest plant phenology.

Where clouds were present in either stage, criterion number three applied stored RapidEye data from before stage 1, while criterion number four used sequential RapidEye data from after stage 2 to compensate for the criterion number one and two, respectively. With this, the cloud problem was nearly overcome, except that the data from after stage 2 were still cloudy. In this case, the final decision regarding forest changes will be postponed until the next sequential data collections are made available.

4.5.1.1.2 Investigating the success of RapidEye data in the case of the storm in the BFNP

Investigation of the RapidEye approach success was based on comparison between the RapidEye data and the aerial images results, and included three aspects: the ''fast response'', the

precision to detect the lost forest tree cover, and the costs. First, the fast response comparison investigated the time needed after the storm to deliver mapping results about the forest tree area losses. Second, the mapping ability outlines and analyzes the similarities and the differences between the results from the RapidEye data analysis and the aerial images interpretation until 22 August 2011. Third, to compare costs associated with the two methods, three types of cost determinants were included in the calculation: the cost of the raw data, the cost of the data preprocessing and cost of data processing. To calculate the cost of the raw data, only data from the stage 2 were included, because it was assumed that reference data would already be available. Four RapidEye scenes are enough to cover the test site, while an additional four RapidEye tiles are necessary to overcome the problem of the clouds, the required total of eight RapidEye images were ordered at a cost of € 593 each (€ 4,744 in total). In comparison, one thousand aerial images are necessary to cover the same area, at a cost of € 18 per image (€ 18,000 in total). The calculation of the cost of data preprocessing and analysis was based on the cost per hour needed to accomplish these tasks. Data preprocessing consisted of Geometric corrections and the atmospheric correction of RapidEye data. The analysis of the data included the application of the developed method to the RapidEye data, and the manual delineation of the changes from the aerial images. The hourly rate was assigned to thirty five Euros / hour (€35 / h), according to the average wages outlined in the 2011 German payment scheme for workers with the relevant necessary skills.

4.5.1.1.3 Accuracy assessment

Assessment of the change detection performance was conducted via an error matrix in all Bavarian test sites. Sampling unit polygons were used instead of pixels, given that pixels tend to underestimate the accuracy of object-based results (Biging et al., 1998). Each polygon was of 60 m in diameter, and were distributed systematically over the test site. This size of the polygon was based on the average size of the objects formed during the change detection process. The reference values (change / no change) for these sampling units were assigned based on visual interpretation of the RapidEye data and the aerial images. If any changes were detected within the sampling unit polygon, it was assigned as change in the reference sample. The agreement between the results and the reference values were then assessed for each polygon. The polygons were distributed over the same grids used for the assessment of forest cover, type and gaps parameters (see section 4.4.1.3). In total, 849 polygons in the BFNP, 618 polygons in Freising, and 320 polygons in Traunstein test sites were used for the assessment. Out of this process yielded the users', producers', and overall accuracies, along with the kappa coefficient (Congalton and Green, 1999; Foody, 2002).

4.5.1.2 Results

As described in section 4.5.1.1, the strategy of monitoring changes in tree covered areas within the forest cover relies on the high revisiting frequency of the RapidEye system. The following sections present results gained with the developed workflow for forest cover monitoring (section 4.5.1.2.1) and by applying the method to overcome the problems with scattered clouds in such a monitoring context (section 4.5.1.2.2). The outcome of the workflow is a "change" layer for the respective year which has been proposed to be used for updating the forest databases. The success of a "fast response" case, here as the storm throw from 13 / 14 of July 2011 in the BFNP, is compared against the standard procedure of the BFNP administration. This standard procedure is based on digital aerial images that were taken after that event in order to map the damages and update the forest data base (section 4.5.1.2.3). The aforementioned examples are from the BFNP study site. Section 4.5.1.2.4 summarizes the results for all investigated three Bavarian test sites.

4.5.1.2.1 Forest trees cover monitoring

Results of the developed method for forest tree cover loss detection carried out in the BFNP during the first period - from 19 April to (22 June / 12 July) - are presented in Figure 14. The results of forest cover loss during the second period - from (22 June / 12 July) to 22 August - are presented in Figure 15. Results of lost forest cover are shown as polygons on top of the RapidEye images. As can be detected in Figure 14, the areas within the polygons appear brighter in the June / July image than they do in the April image due to the loss of forest tree cover. Similar results can be seen in Figure 15, as the areas within the polygons are brighter in the August image than in the June / July image. Both results depict accurate mapping of the losses during the first and second period. Analysis reveals that about 157 ha of forest cover were lost during the first period, most of which because of management against the bark beetle, as was made clear from the official results of the BFNP administration. During the second period, about 235 ha of forest cover were lost, which was attributed to the storm that occurred on 13 July.
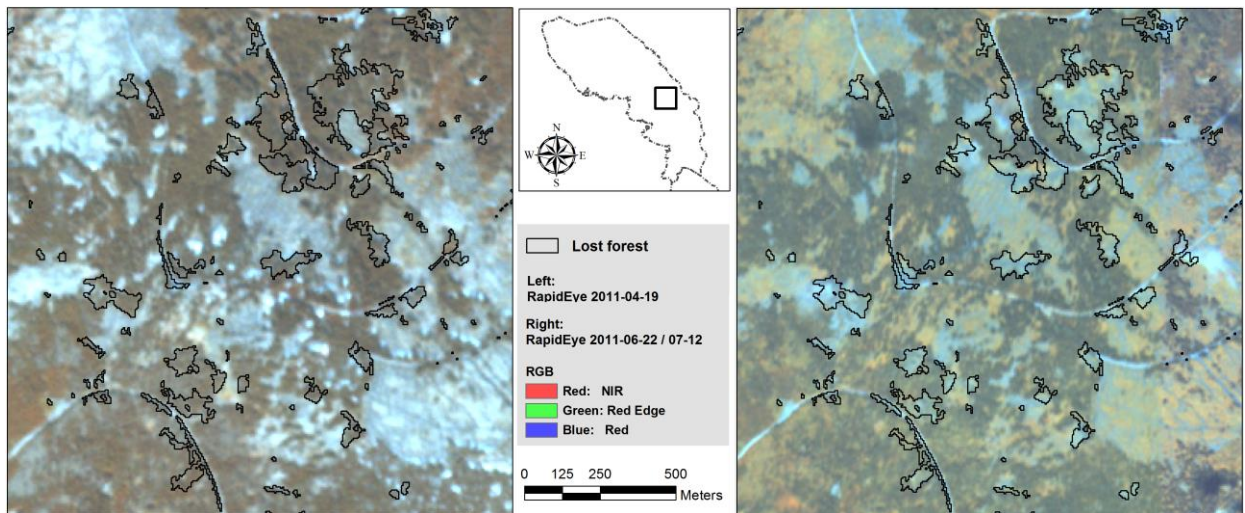
Figure 14: Example of some forest cover losses during the first period from 19 April to 22 June in the year 2011 in the BFNP (Elatawneh et al., 2014)
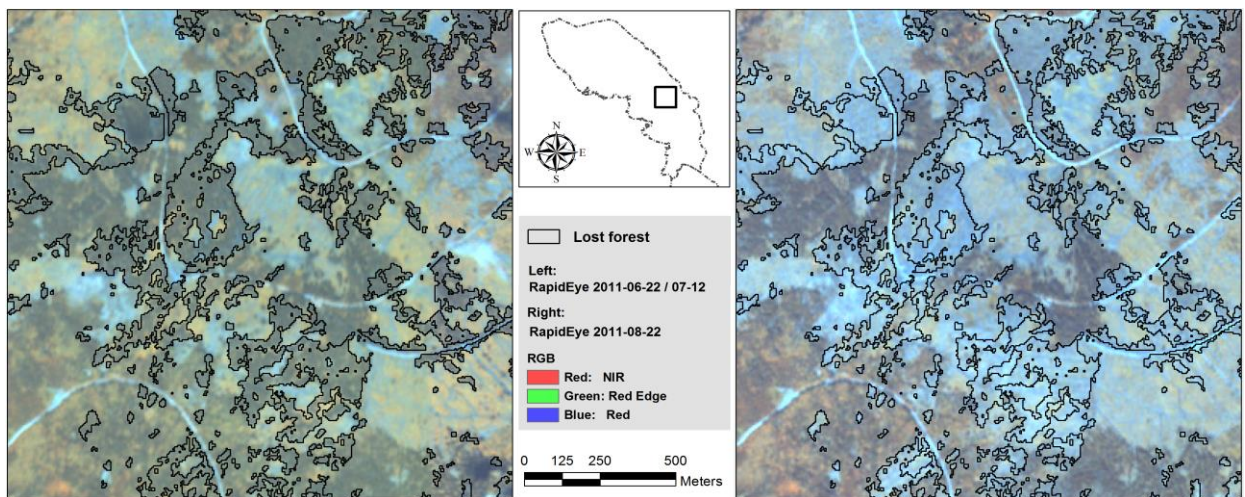
Figure 15: Example of some forest cover losses during the second period from 22 June to 22 August 2011 in the BFNP (Elatawneh et al., 2014)

Additionally, Figure 16 shows the results from the analysis of the last available RapidEye image from 01 October, which contributed to the final update in the year 2011. Similar to the previous results, the areas within these polygons, which represent the forest cover losses, become brighter in the 01 October image compared to those in the August image. The estimated forest cover loss during the period from 22 August to 01 October was about 16 ha. In total, about 408 ha of forest cover were lost within the BFNP test site during the year 2011.
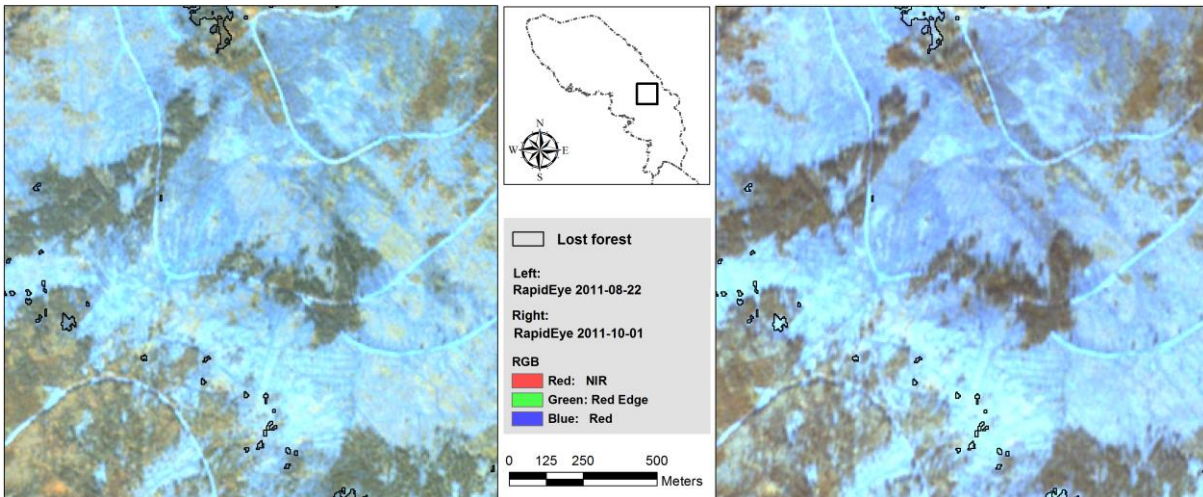
Figure 16: Example of forest cover loss during the third and last period from 22 August to 01 October 2011in the BFNP

4.5.1.2.2 Solving the problem of cloud cover

The problem of cloud presence, the most challenging problem when using optical remote sensing data for forest monitoring, was bypassed. Figure 17 shows an example from the BFNP illustrating how the developed method used subsequent RapidEye data to overcome the problem of scattered clouds.
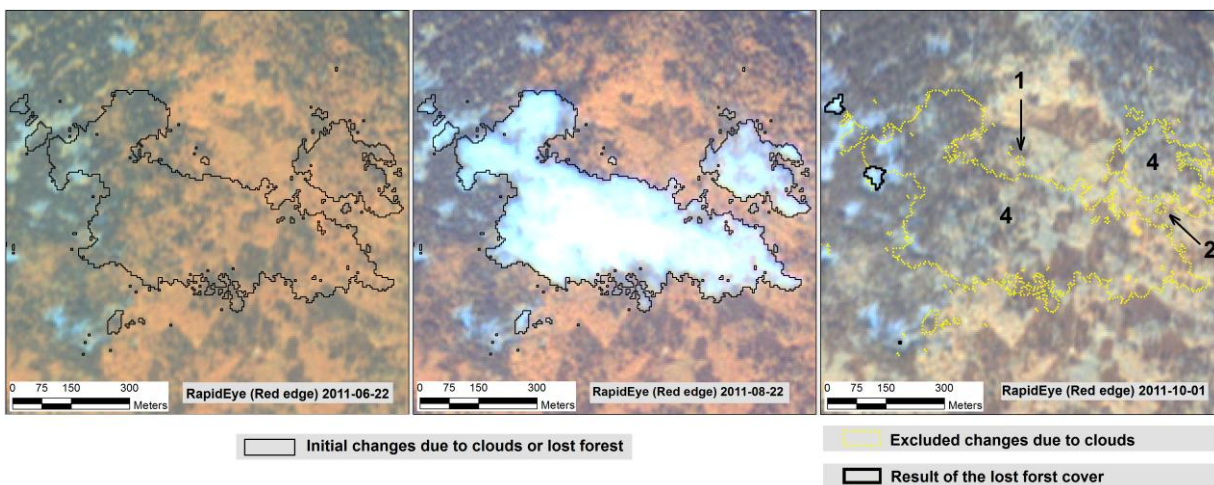
Figure 17: *The initial analysis of the changes between one image from 22 June / 12 July (Left) and a second image from 22 August (middle) show changes that were actually caused by either clouds or lost forest. Subsequent data from the image collected on 1 October (right) allowed for the exclusion of those changes due to clouds and kept the final results showing the actual losses in forest cover, by implementing the criteria described in Table 13. The numbers 1, 2, and 4 represent the areas excluded using the first, second and fourth criterion, respectively (Elatawneh et al., 2014)*

Figure 17 (left and middle) illustrates the initial changes detected in the period from 22 June 2011 / 12 July 12 to 22 August. Figure 17 (right) illustrates the final results of "forest loss" as well as the changes that were excluded after refinement by application of the criteria outlined in Table 13. During the refining of the initial changes, the first criterion excluded objects which were not identified as

forest on 22 June, while the second criterion excluded the objects which were still forest on 22 August. Because of cloud presence during the second period on 22 August, the fourth criterion used data from the images collected on 01 October to exclude objects which were still forest. Thus, only changes which represent actual loss of forest cover remained as illustrated in Figure 17 (right). Finally, the forest cover detected at the end of the vegetation period (01 October) contributed to the annual update of the forest database.

4.5.1.2.3 The success of the RapidEye approach in the BFNP

As described in section 4.5.1.1.2, comparisons between the RapidEye and aerial image results were based on three aspects: the ''fast response'', precision of forest tree loss detection, and the costs. Regarding the ''fast response'' aspect, after the storm event on 13 / 14 July 2011, the first opportunity to collect RapidEye data was on 22 August 2011 due to cloud coverage and weather conditions. Coincidently, the annual campaign of the aerial images also fell on 22 August 2011. Results of forest tree losses using the RapidEye data were delivered about two weeks later, at the beginning of September 2011, while the results obtained by interpreting aerial images were delivered about eleven weeks later, at the end of November 2011. In fact, the aerial images campaign including images acquisition, preprocessing and manual interpretation is typically a time-consuming process.

Regarding the detection of forest tree losses, the comparison of the results between RapidEye data analysis and aerial images interpretation, until 22 August, are presented in Figure 18. Based on the analysis, 361 ha of forest loss were mapped identically in both results, indicating very high agreement between both methods. However, there remain many differences between the two outcomes, especially at the edges and within the mapped lost forest. The differences between the two results were separated into two groups. First, the forest losses detected only using RapidEye (31 ha, or 8% of all losses), and second, forest losses detected only using aerial images (12 ha, or 3% of all losses). The exploration of the losses detected solely by RapidEye data show that these were actual losses in forest cover induced by either forest management or storm. On the other hand, some of the losses detected solely by aerial images were not actual forest cover losses, at least not during the period from 19 April to 22 August. Reasons and explanations of the differences of the losses are analyzed in section 4.5.1.3 of the discussion.

Finally, the cost comparison between applying RapidEye data and the manual interpretation of aerial images are presented in Table 14. The total cost of utilizing RapidEye data was about € 5,660, and the cost of the visual interpretation of the aerial images was about € 22,200. The cost of the

RapidEye data analysis was therefore only one fourth of the cost of the manual interpretation of the aerial images.
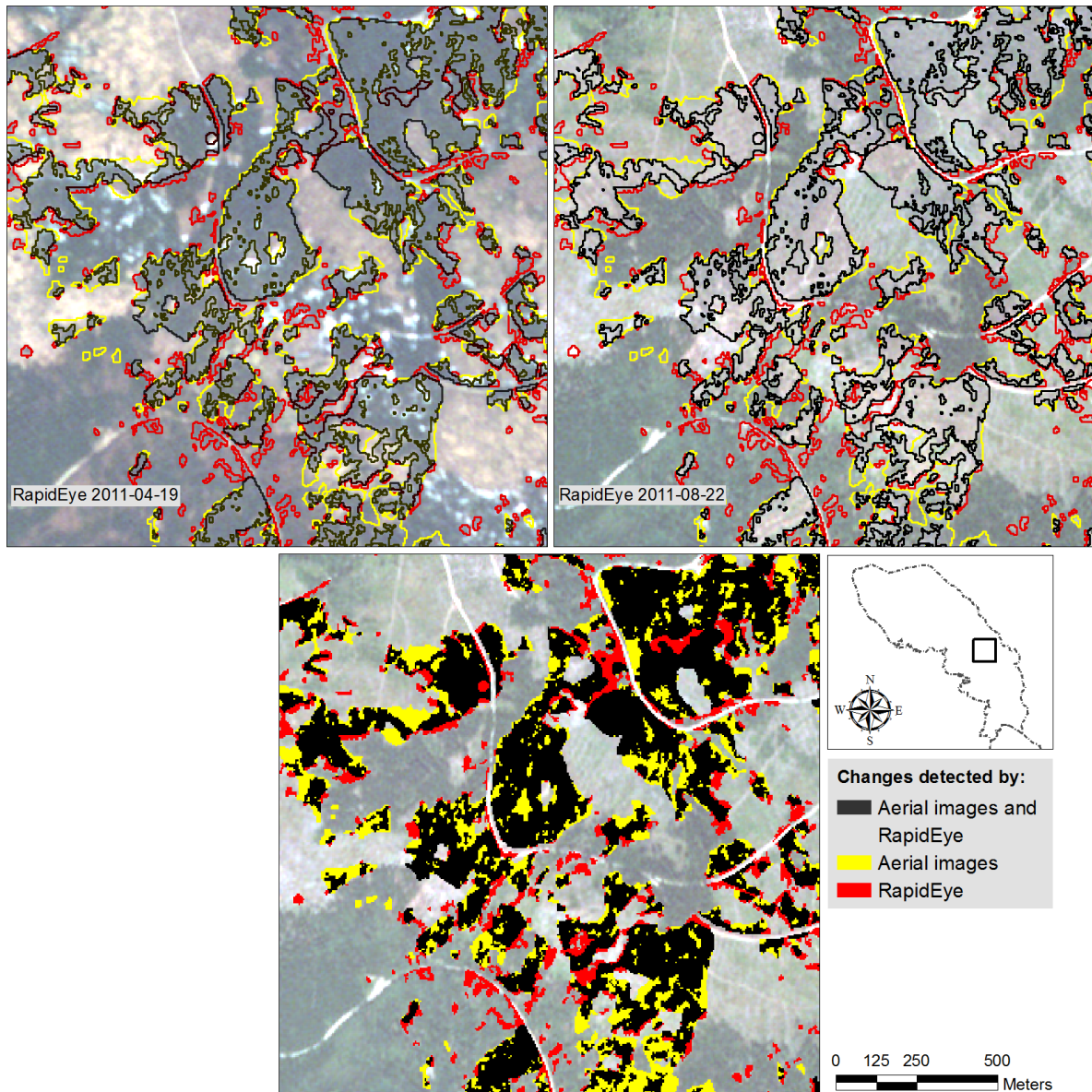
Figure 18*: Example comparing the results of forest covers loss, until 22 August, when RapidEye data was used with the official results of forest cover losses from aerial images interpretation. The upper two images show the results in hollow polygons, and the lower image shows the results in solid polygons*

Table 14*: Cost comparison of forest losses using RapidEye data analysis and aerial images interpretation in BFNP*

Category	RapidEye (Euros)	Aerial images (Euros)
Raw data	(8 images × €593) = 4,750	(1,000 images × €18) = 18,000
Preprocessing	(10 WH × €35) = 350	(40 WH × €35) = 1,400
Data analysis	(16 WH × €35) = 560	(80 WH × €35) = 2,800
Total	5,660	22,200

4.5.1.2.4 Accuracy assessment of forest monitoring in all Bavarian test sites

Results of forest cover lost during the year 2011 in the BFNP, and during the period from 2009 to 2011in the Freising and Traunstein test sites, are presented in Figure 19. The results in Table 15 present the area of the forest cover losses in hectare (ha) in these test sites. As can be seen, the losses of the forest cover during the year 2011 in the BFNP greatly exceeded those in Freising and Traunstein. About 4% of the forest cover in the BFNP test site were lost only during the year 2011, while about 0.8% and 1.2% of the forest cover in Freising and Traunsteiner Stadtwald test sites, respectively, were lost over three years (from 2009 to 2011).

No forest cover loss results were available in the BFNP before 2011 due to the lack of proper RapidEye data for the analysis. However, based on the official results from the BFNP administration, during the year 2010 (until 22 August) about 360 ha of forest cover were lost because of management against the bark beetle and the storm. The amount and the percentage of the forest cover losses in the BFNP were much higher than that in Freising and Traunsteiner Stadtwald. Still, annual results from Freising and Traunstein reveal continuous forest cover losses.

Table 15: *Calculated forest loss in hectare (ha) and as a percentage of the forested area, by data and method utilized, in the three Bavarian test sites*

Period	BFNP	Freising	Traunstein
2009	--	0.00	1.54
2009 – 2010	--	4.40	
2010	--	1.88	1.22
2010 – 2011	--	2.02	
2011	408	9.34	0.24
Total losses (ha)	**408**	**17.64**	**3**
Total losses (%)	**4%**	**0.8%**	**1.2%**
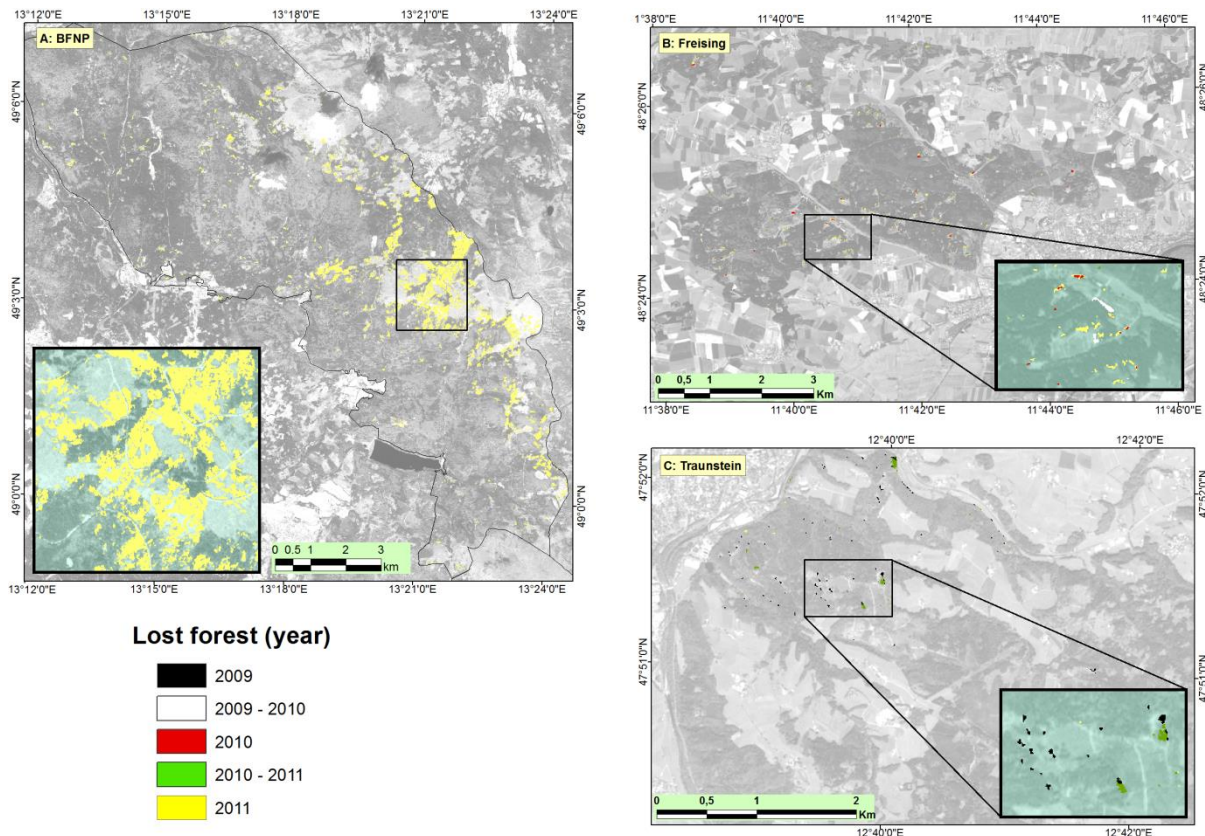
Figure 19*: Total forest cover losses during the period from 2009 to 2011 in the BFNP, Freising and Traunstein test sites based on the available RapidEye data*

The accuracy assessments of the forest cover loss results in the Bavarian test sites are presented in Table 16. Achieved overall accuracies were between 96.7% and 99.1%, which indicates that the RapidEye data and the method utilized here returned high accuracies for forest cover losses detection. In terms of the user and producer accuracies, similar patterns were observed in the three test sites.

Table 16*: Overall user and producer accuracies and kappa values of forest loss results in the Bavarian test sites*

Accuracies	BFNP	Freising	Traunstein
User %	87.4	89.3	81.8
Producer %	88.9	96.2	90.0
Overall %	96.7	98.7	99.1
Kappa	0.86	0.92	0.85

The user accuracies in the test sites ranged between 81.8% and 89.3%, while the producer accuracies ranged from 88.9% to 96.2%, indicating the overall success of the implemented method. Still, a few areas were mistakenly identified as losses when no actual loss had occurred, and some legitimate losses were not detected.

4.5.1.3 Discussion

Applying the developed method to multi-seasonal RapidEye data in order to detect forest cover losses in the Bavarian test sites achieved overall accuracies ranging between 96% and 99%. As seen in Table 15, the results included slight changes that took place between two sequential RapidEye data acquisitions, and succeeded in detecting changes that were caused by either sudden changes or standard management practices. The method contributed to the ''fast response'' strategy and also succeeded in overcoming the problem of clouds.

The fast response was the primary success derived by this method, which implemented the multi-seasonal RapidEye data within two weeks of the storm event, in comparison to the aerial image interpretation, which took place eleven weeks later. A fast response such as this contributes to the prevention of the following biotic calamities triggered by such a storm, and presents the possibility of more promptly introducing precautionary measures, which is often more important than the pure cost factor.

The developed method was transferred to various test sites of different topography and vegetation regions, and successfully updated the forest information layer with each successive RapidEye dataset. At the end of the year, the status of the forest database is updated, and, once implemented, can be used for analysis of the annual changes. At the Freising and Traunsteiner Stadtwald test sites, the continuous update process based on RapidEye data clearly reveals the continuous forest cover loss over the year. Most losses can be attributed to management activities including clearing following light storms, ice breaks, insect damages, etc. that took place from 2009 to 2011.

Results achieved here were generally consistent with the results of previous studies integrating object-based image analysis (OBIA) in approaches detecting changes in forest cover. Those studies applied OBIA to Landsat data (McDermid et al., 2003; McDermid et al., 2008), SPOT data (Desclée et al., 2006) and a combination of SPOT and aerial images (Willhauck et al., 2000) for forest change detection, reporting overall accuracies between 84% and 94%. However, these studies have neither focused on sudden changes nor dealt with the problems presented by clouds. To bypass the problem of cloud cover, these studies advocate collecting and analyzing optical data more frequently. Other studies demonstrated the use of data from the active satellite systems, e.g. TerraSAR-X, to overcome the problem of clouds (Rappl et al., 2012; Thiele et al., 2012). However, the high cost and the small coverage of the active systems limit their implementation in the operational forest loss detection. Here, the results of the multi-seasonal RapidEye data offered an

79

alternative and operational solution to overcome the problem of the clouds. Such a problem prevented the development of an operational method in a study in central Africa (Duveiller et al., 2008).

In addition to findings regarding faster response rates, a comparison between the results of the multi-seasonal RapidEye data analysis and the annual aerial images in the BFNP are also presented, though each method falls into different frame conditions. The method followed uses the RapidEye data analysis based on continuous forest observations, and the integration of each RapidEye dataset that is made available. Meanwhile, the method involving visual interpretation of the stereoscopic digital aerial images requires a special campaign which takes place once a year. The results from RapidEye data provided a continuous monitoring over three time periods in the year 2011. These detections were taken with increasing frequency as the forest change event approached, allowing for a better understanding of the factors that caused the changes in the forest cover. For example, during the first and third periods, about 157 ha and 16 ha, respectively, were lost within a period of about a month. These losses in the BFNP were caused solely by regular management against the bark beetles, which reveals the catastrophic sequences of the calamity. The concept of digital aerial image interpretation was developed by experts who estimate the cause of changes based either on the fallen trees or by comparison with the results from previous years. However, annual digital aerial images are available only for the BFNP, while only triennial aerial images are available for the rest of Bavaria, which presents a challenge in defining the causes of change.

When comparing the BFNP RapidEye data results and the digital aerial images interpretation, few differences stood out. Those differences recorded were attributed to manual digitization, in which the user will naturally delineate smooth borders rather than zigzag. Hence, the shape of the objects that represent changes will be estimated rather than exactly delineated. Previous studies (Heurich et al., 2010; Kautz et al., 2011) have discussed the consequences of manual digitizing, explaining that users tend to overestimate the magnitude of fallen trees. Moreover, results show that 8% of the object losses were detected solely using the RapidEye method, and only a few of these objects were mistakenly identified as losses. These errors were due to phenological differences from leaf-off to leaf-on, especially in the first period within deciduous stands, as this change increased the spectral reflectance of the red edge band. As a mark of its success, only 3% of the total losses were not detected by the RapidEye data. The lost objects were small, and were usually surrounded by healthy coniferous stands, deciduous stands, or laid within a shadow. It was therefore difficult to detect these objects by using the spectral information alone. Further to this, many of these losses were detectable only at the center of the damage, meanwhile detection of the

losses at the periphery was difficult. This can be explained by the complex structure of the forest and the shade at the periphery, as previously reported (Carvalho et al., 2001). Finally, though the results of the RapidEye data were not intended to entirely compensate for the results of the aerial images, RapidEye results achieved 97% of the results of aerial images. Furthermore, the cost of the RapidEye analysis was only 25% of the cost of the aerial image interpretation.

4.5.2 Forest tree species

4.5.2.1 Methods

The approach taken to identify forest tree species applied the use of 20 multi-seasonal RapidEye datasets, an approach developed in the Freising test site (Elatawneh et al., 2013, Publication 4 in Appendix). The approach was based on the "phenological fingerprint" concept, accounting for the long rotation period of forests which extends from 60 to 250 years. It was assumed that accumulating information over successive years would not corrupt the result, but would instead increase the reliability of the outcomes. The 20 analyzed datasets were acquired over three vegetation periods from the years 2009 to 2011, in order to identify 7 tree species. The primary research question was focused on tree species identification, with additional research questions pertaining to economic issues. Recall the investigated research questions, mentioned previously in section 1.2, as:

- How many datasets from various phenological phases are needed to obtain the most accurate results?

- How does using additional bands or indices influence tree species identification?

- Is there a phenological phase with high potential for identifying a specific tree species?

- Which phenological phase is the most promising to identify all tree species?

The workflow comprises first section 4.5.2.1.1, which includes the preparation of the phenological fingerprint – achieved by combining the phenological phases' attributes with the RapidEye dataset acquisition. Next, section 4.5.2.1.2 includes the cross validation method used for classification and validation of the RapidEye data. Finally, section 4.5.2.1.3 provides an overview of the strategy that was followed to analyze the RapidEye data in order in pursuit of answers to the aforementioned research questions.

4.5.2.1.1   Forest phenological fingerprint and RapidEye data acquisition

The phenological fingerprint principle is based on the spectral reflectance variation between tree species caused by the phenological phases timing, which will increase the separability among the tree species. The box plot in Figure 20 shows the phenological phases in the Freising test site, arranged in chronological ordered based on all phenological observations ranging from time periods of 3 to 51 years (see also Table 4).
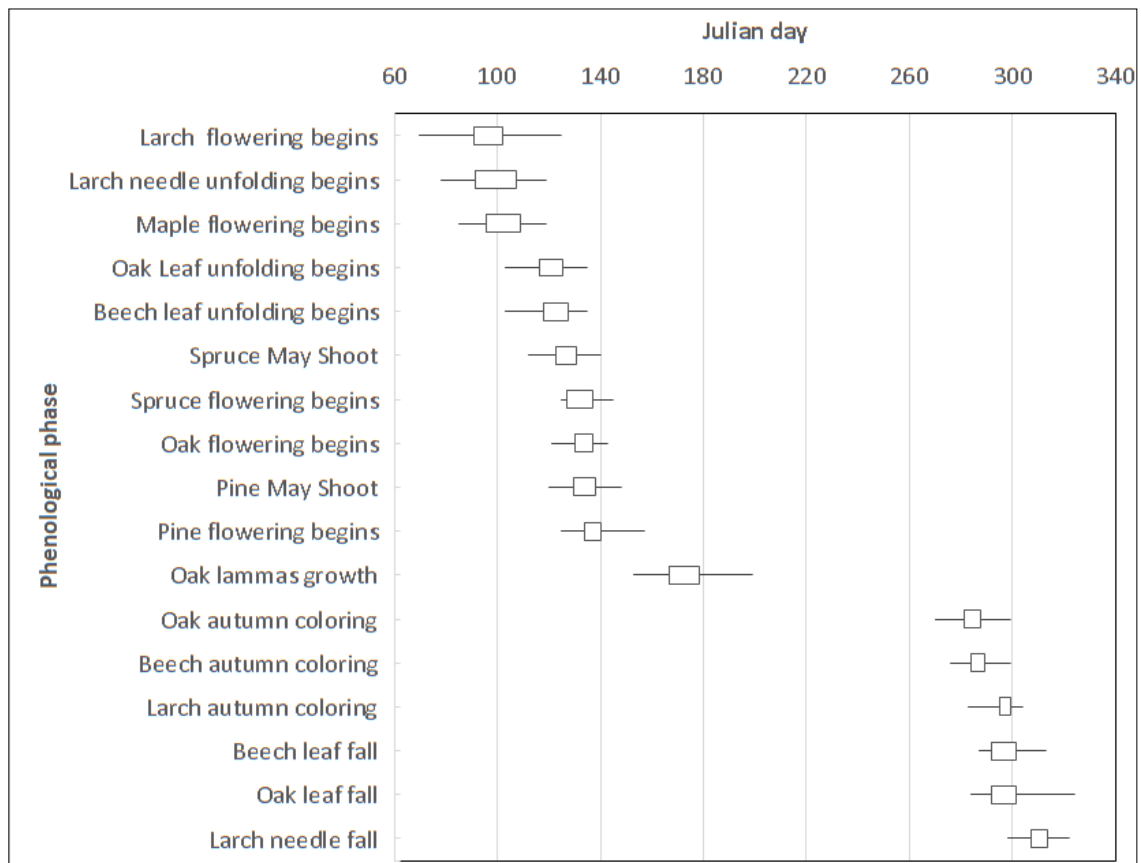
Figure 20: *Box plot showing the phenological phases' occurrence by the day of the year (Julian day) of the forest tree species at the Dürnast phenological station in Freising forest, based on all available observations (see **Table 4**)*

These historical phenological observations show that the phases' leaf / needle unfolding, May shooting and flowering usually occurred in the period from 100 to 140 of the Julian day (from early to late spring). Larch needles were observed to have a tendency to unfold first, followed by the oak about three weeks later, while the beech tends to unfold concurrently with the oak or a few days later. Although maple unfolding was not observed at the test site, maple tends to unfold together with the beech, around the end of April or the beginning of May (Schütt, 2006). This phenological state can therefore serve as an excellent indicator for separating larch, oak, beech and maple. For the coniferous species, the spruce May shoot tends to occur a week before the pine May shoot, similarly, spruce flowering tends to happen a week earlier than pine flowering. Uniquely, the oak

lammas growth, a second leaf unfolding, appears in early summer from mid-June until mid-July. This property can increase the chance of separating oak from other species.

Autumn coloring and leaf fall usually occurred in the period from 280 to 310 Julian day, or from mid- to late-autumn. Again, shifts in autumn coloring between oak, beech and larch can be very helpful tools in improving mapping. Based on personal observations, maple autumn coloring tends to take place first, followed by oak about two weeks later. While beech autumn coloring starts at the same time as oak or a few days later, and the larch about a week or two weeks later. With the passing of two more weeks, the oak and beech leaf fall begins, and the larch tends to starts losing its needles. All in all, the differences of phenological timing will result in variation in the pigmentation of the leaves between the various tree species, which can play an important role in supporting the phenological fingerprint concept.

These phenological observations can, however, shift from one year to another. To address this potential shift, observations from the individual years 2009, 2010, and 2011 where combined with the RapidEye data acquisition to better clarify the overlap between the phenology and the RapidEye data acquisition, (as seen in Figure 25 in page 94). Some of the phenological observations were not available for the years 2009, 2010 and 2011, including those for the larch, spruce and oak time of initial flowering, and the oak lammas growth. The chronological order of the single phenological phases was not found to change in these three years, except for the beech autumn coloring which tended to occur two weeks before oak autumn coloring in 2011. Such a shift in the beech autumn coloring is expected to improve the mapping of this species. Although twenty RapidEye datasets were available for this study, not all observations were acquired during the peak of the phenological phases. This is significant as the images acquired during the peak of the phenological phases are expected to achieve the best classification results.

4.5.2.1.2 Classification and validation using the cross validation method

Identifying tree species, the primary goal, was carried out using image classification. A successful classification requires a well-defined classification scheme and proper samples. Therefore, the selection of the tree species samples was supported by the inventory data and our field visits (Table 17). The sample selection was restricted to the brightest pixels of a collection of homogeneous pixels, which were identified to belong to pure tree species.

Table 17: Tree species identified in the Freising test site

ID	Tree Species	Binomial name	Species percent	# of samples
1	Norway spruce	*Picea abies (L.)*	73%	212
2	Douglas fir	*Pseudotsuga menziesii (M.F.)*	2%	32
3	Scots pine	*Pinus sylvestris (L.)*	4%	34
4	European larch Japanese larch	*Larix decidua (MILL.)* *Larix kaempferi*	5%	41
5	European beech	*Fagus sylvatica*	5%	153
6	European oak	*Quercus petraea (Mattuschka)*	3%	38
7	Sycamore maple	*Acer pseudoplatanus*	2%	36

The method of samples selection was adapted from previous studies, in which training samples were selected solely from sunlit crown areas, in order to select the spectra of tree species from very high spatial resolution data (Immitzer et al., 2012; Korpela et al., 2011). Sample selection within bright pixels can reduce the illumination variances among the same tree species that were caused by the shadow effect from the surroundings and the topography. To further minimize this effect, the Spectral Angle Mapper (SAM) was implemented to perform the classification, as it is less sensitive to illumination effects than other methods (Eckert and Kneubühler, 2004). Due to the absence of recent inventory data, the samples were used for training and validation by applying 10-fold Cross validation technique (Geisser, 1975; Stone, 1974; Waser et al., 2014). The 10-fold Cross validation partitioned the samples into 10 subsets, using each subset in turn as training samples for the classification, and the remaining data as validation points. The process was repeated 10 times, with the 10 results being combined to produce one validation result.

4.5.2.1.3 RapidEye data analysis strategy for tree species identification

The strategy of the RapidEye data analysis included two main aspects: the classification of each single dataset, and the classification of various combinations of the datasets. Investigation of the most promising phenological phases for tree species identification, and the potential of each

phenological phase to identify a specific tree species were based on the accuracy of the single dataset classification. The higher the achieved overall accuracy of a dataset acquired in a specific phenological phase, the more promising this phase for tree species identification. Similarly, the higher the user and producer accuracies of a specific tree species from data acquired in a phenological phase, the greater the potential this phase holds in identifying this specific tree species.

In order to investigate the number of dataset combinations that achieve the most accurate tree species identification, 20 RapidEye combinations were established from the RapidEye dataset. First, the result accuracy for each of the 20 RapidEye datasets was evaluated, and then 20 data combinations were established by choosing the best single-, two-, three-data, etc., until twenty-data combination. Each combination was established by stacking up all bands from the combined RapidEye data. After that, each combination of data was classified, and the results were assessed. The method also investigated the potential of using the newly introduced red edge band to improve the accuracy of tree species identification. Here, the same procedure and image combinations were implemented, but with the absence of the red edge band. Moreover, the influence of adding indices to the original dataset was investigated by applying the same procedure once more.

Additional indices beyond the NDVI index were developed and utilized, which was expected to emphasize the differences among the spectral reflectance of the tree species, due to the fact that the reflectance is often similar in many, but not all, bands. For this, slope difference indices were developed, as in Figure 21, because they represent the ratio of reflectance between the bands.
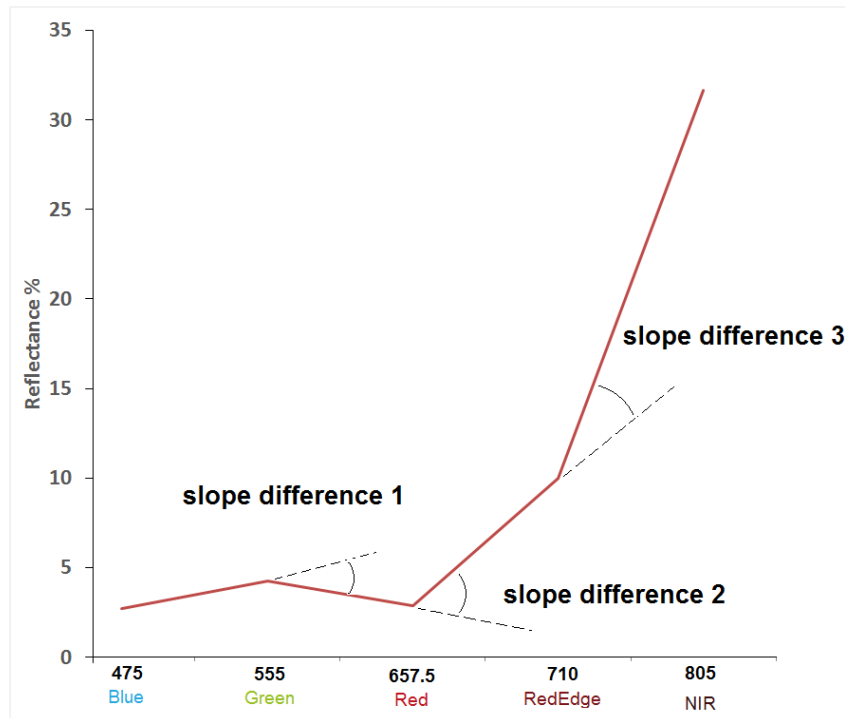
Figure 21: *Illustration of the slope difference indices developed in this study*

The developed slope indices are also expected to be less influenced by illumination variations, thus enhancing the species differentiation. Those indices were generated by calculating the difference in the slopes as shown in the following equations:

$$\text{Slope difference } 1 = \frac{(\rho \text{ Green} - \rho \text{ Blue})}{(\lambda \text{ Green} - \lambda \text{ Blue})} - \frac{(\rho \text{ Red} - \rho \text{ Green})}{(\lambda \text{ Red} - \lambda \text{ Green})}$$

$$\text{Slope difference } 2 = \frac{(\rho \text{ Red edge} - \rho \text{ Red})}{(\lambda \text{ Red edge} - \lambda \text{ Red})} - 2 \frac{(\rho \text{ Red} - \rho \text{ Green})}{(\lambda \text{ Red} - \lambda \text{ Green})}$$

$$\text{Slope difference } 3 = \frac{(\rho \text{ NIR} - \rho \text{ Red edge})}{(\lambda \text{ NIR} - \lambda \text{ Red edge})} - 0.5 \frac{(\rho \text{ Red edge} - \rho \text{ Red})}{(\lambda \text{ Red edge} - \lambda \text{ Red})}.$$

Where, the ρ represents the reflectance and the λ represent the central wavelength of the corresponding band. The indices were then enhanced by duplicating their values as illustrated in the equations. It is important to mention that these slope difference indices can be highly dependent on the quality of the radiometric correction.

4.5.2.2 Results

4.5.2.2.1 Results of single and combined use of RapidEye data

Results of single and combined RapidEye dataset classifications for tree species identification are presented in Table 18 and Figure 22. The results show that the increase in the amount of data used in the analysis increases the overall accuracy. However, the increase in the accuracy quickly improves at the beginning, then continues to improve at a decreasing rate. As Table 18 demonstrates, when the original bands and indices were used, one dataset achieved an overall accuracy of 72.8%, while seven dataset combinations achieved an accuracy of 84.0%, for an improved overall accuracy of about 11%. Using twenty dataset combinations achieved an overall accuracy of 86.3%, which shows that using thirteen additional datasets improves the overall accuracy by only about 2%.

Table 18: Overall accuracy of tree species identification with single and combined use of RapidEye data from different dates (see **Figure 22**)

Number of images	Image dates	Julian day	Season	Overall (one scene) accuracy %	Overall (image combinations) accuracy %		
					Original bands without red edge	Original bands	Original bands + indices
1	16.07.2011	197	Mid-summer	67.1	63.9	67.1	72.8
2	22.04.2010	112	Early spring	63.2	73.0	73.7	77.3
3	04.06.2011	155	Early summer	59.7	77.3	77.6	80.1
4	07.04.2011	97	Early spring	59.7	78.8	78.7	81.4
5	10.07.2011	191	Mid-summer	59.1	78.6	79.4	82.4
6	27.07.2009	208	Mid-summer	58.7	78.9	81.3	83.2
7	22.03.2011	81	Early spring	57.6	82.0	82.6	84.0
8	20.05.2009	140	Late spring	57.1	81.1	81.9	84.2
9	28.06.2011	179	Mid-summer	56.0	81.0	82.4	84.6
10	08.06.2010	159	Early summer	54.8	82.0	83.3	85.1
11	21.07.2010	202	Mid-summer	54.6	82.2	83.0	85.1
12	04.11.2011	308	Mid-autumn	53.8	83.5	83.9	85.9
13	22.10.2011	295	Mid-autumn	53.3	82.7	83.7	85.9
14	06.05.2011	126	Late spring	50.6	82.4	83.5	85.6
15	15.08.2010	227	Late summer	48.7	82.3	83.6	85.5
16	10.10.2010	283	early autumn	48.2	82.8	83.7	86.1
17	25.09.2011	268	early autumn	46.5	83.4	84.4	86.4
18	23.08.2011	235	Late summer	44.6	83.1	84.2	86.2
19	06.10.2011	279	early autumn	40.7	83.5	84.4	86.3
20	03.09.2011	246	Late summer	39.2	83.3	84.3	86.3

Similar results were also achieved when the original bands were used in the analysis, and also when the original bands (without the red edge band) were used. Nonetheless, it is not only the number of classified dataset that matters, but also the acquisition seasons of these datasets, as will be shown in the sections 4.5.2.2.2 and 4.5.2.2.3.
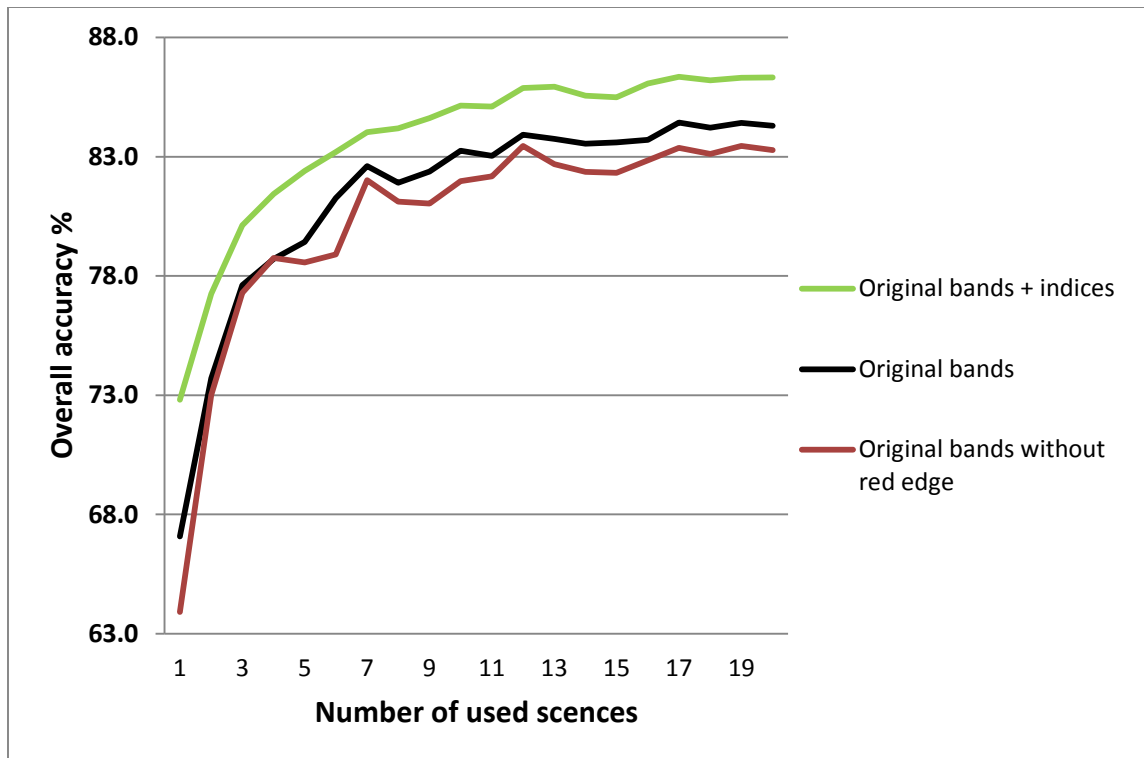
Figure 22: Overall accuracy of RapidEye data combination (see *Table 18*)

This investigation shows that the red edge has only a slight influence on the results, and the average improvement in the overall accuracy when the red edge band was used, was about 1%. Investigation of the influence of the utilized indices on the accuracy clearly demonstrates that indices improved the overall accuracy by about 4% when few combinations were used. Meanwhile, the average value of the improvement achieved by using the indices in the classification was about 2%.

For the investigation of the influences of the red edge band and the indices on the accuracy, it is interesting to review false-colored composite images from three multi-seasonal dates by using these indices and the red edge band presented in Figure 23. The images show high similarity among tree species in the forest, and very high dissimilarity among the crops in the surrounding fields.
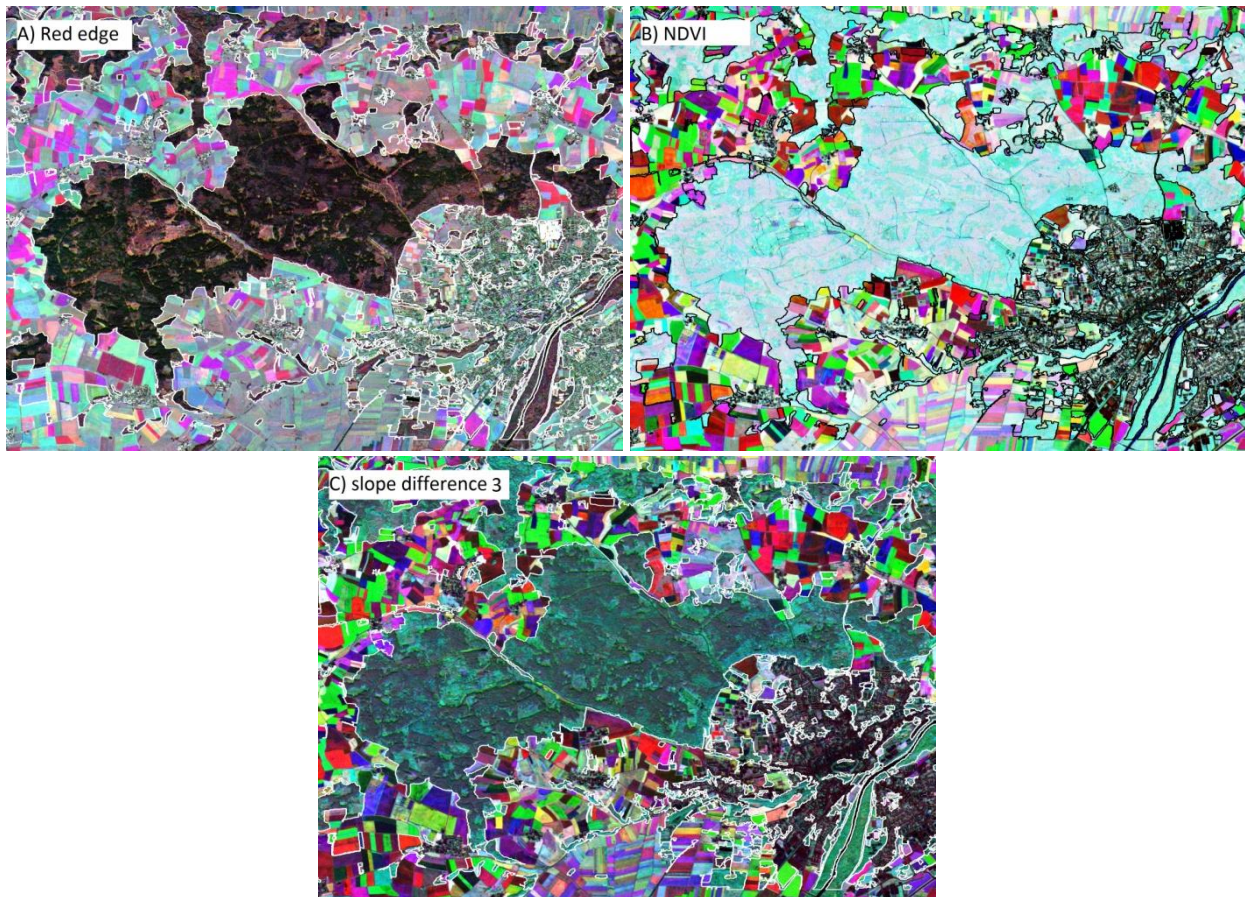
Figure 23: *False-colored composite images from three multi-seasonal dates 07 April, 23 August and 06 October 2011, by using a) red edge bands, b) NDVIs and c) slope difference 3 indices. They show very high dissimilarity between the crops more than that between the tree species in the forest*

The map in Figure 24 shows the distribution of the tree species identified in the Freising test site, using the best 17 data combinations. According to the field visits and the forest management maps from the forest administration in Bavaria, the results in the map describe very well the spatial distribution of the tree species in the forest. Generally, the map of tree species distribution was also similar to those from the latest inventory records from 2001, especially in the parts of the forest where no dramatic changes took palace. Unfortunately, no inventory data has been collected since 2001, and therefore it was not sensible to perform the accuracy assessment using the old inventory record.
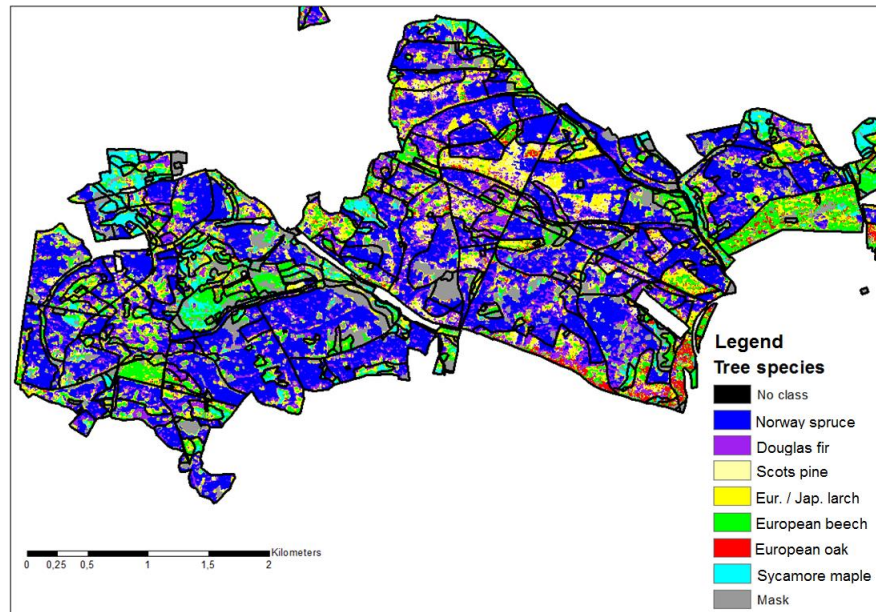
Figure 24: *Map of tree species distribution using 17 RapidEye data combination in the Freising test site*

Based on the accuracy assessment from the cross-validation procedure, Table 19 presents the confusion matrix of the result utilizing the best 17 data combinations.

Table 19: *Confusion matrix of the result of the cross validation analysis of the best 17 data combinations (original bands + Indices)*

Class.	Reference data							Sum	User Acc. %
	Spruce	Douglas	Pine	Larch	Oak	Beech	Maple		
Spruce	**1899**	9	0	0	0	0	0	1908	99.5
Douglas	46	**229**	0	0	0	19	0	294	77.9
Pine	2	12	**1033**	53	37	18	15	1170	88.3
Larch	3	1	56	**223**	17	37	12	349	63.9
Oak	20	2	55	41	**203**	2	19	342	59.4
Beech	28	9	16	7	3	**450**	0	513	87.7
Maple	11	3	76	22	16	4	**206**	338	61.0
Sum	2009	265	1236	346	276	530	252	**4914**	
Prod. Acc. %	94.5	86.4	83.6	64.5	73.6	84.9	81.8	Overall Acc. %	**86.4**

The user accuracy for the individual classes ranges from 59% to 99%, while the producer accuracy for the individual classes ranges from 64% to 94%. As can be seen, the individual accuracies for the classes spruce, Douglas fir, pine, beech and maple increased when the number of the analyzed RapidEye data increased. On the contrary, individual accuracies of larch and oak decreased when the multi-seasonal data were analyzed. There was also confusion between larch and oak, which was noticed in most of the results of the various data combinations. Although pine tree species determination was improved, there was still confusion between the pine with the larch, oak and maple classes, as presented in the results.

91

4.5.2.2.2 Potential phenological phases for specific tree species identification

Results of using the potential phenological phase to identify specific tree species based on the user and producer accuracy of each tree species RapidEye dataset are presented in Table 20. The user accuracies represent the percentage of tree species that were correctly identified and separated on a produced map. The producer accuracies represent the percentage of tree species on the ground that were correctly identified. Therefore, the higher the values of both user and producer accuracy of a specific tree species, the better the separability of this tree species from other species.

Table 20: Overall user (u) and producer (p) accuracy of each tree species using single RapidEye data. The highest (and close to the highest) accuracies of each tree species are shaded

	date	Spruce		Douglas		Pine		Larch		Oak		Beech		Maple	
		u	p	u	p	u	p	u	p	u	p	u	p	u	p
1	16.07.2011	83	79	37	35	60	56	44	61	83	79	32	31	31	44
2	22.04.2010	83	79	31	26	43	53	70	73	40	41	61	58	22	27
3	04.06.2011	76	75	42	37	54	48	58	58	23	31	58	59	47	51
4	07.04.2011	77	76	18	17	74	68	55	51	42	45	16	19	37	47
5	10.07.2011	76	77	33	34	41	40	68	67	30	32	52	46	34	41
6	27.07.2009	74	75	41	39	39	39	63	59	59	60	22	22	48	53
7	22.03.2011	73	75	37	37	62	59	22	28	58	57	45	38	41	42
8	20.05.2009	73	73	25	29	67	56	53	52	53	56	37	37	16	21
9	28.06.2011	69	72	24	20	56	52	39	41	48	49	58	56	41	47
10	08.06.2010	65	68	28	24	58	55	56	58	65	62	27	23	18	24
11	21.07.2010	71	68	25	24	36	37	55	56	49	52	52	48	36	44
12	04.11.2011	64	65	45	41	53	49	54	55	45	46	40	40	42	46
13	22.10.2011	74	72	16	14	40	46	35	33	58	61	28	26	39	45
14	06.05.2011	64	69	33	29	57	51	45	41	38	40	35	32	33	41
15	15.08.2010	60	62	31	28	54	48	34	33	50	51	49	47	12	16
16	10.10.2010	68	65	25	23	42	41	40	40	38	39	37	39	20	28
17	25.09.2011	66	67	41	42	42	40	16	18	12	13	44	36	28	32
18	23.08.2011	50	58	53	45	24	23	41	38	19	20	48	43	35	36
19	06.10.2011	58	58	42	40	25	25	9	10	30	27	38	33	8	13
20	03.09.2011	55	60	36	30	33	30	26	27	28	28	31	28	14	17

Based on the results outlined in Table 20, the data collection from 16 July 2011 took place about two weeks after the phenological phase of oak lammas growth, which has the potential to separate oak and spruce. Also, data collected on 22 April 2010, two weeks after the larch leaf unfolding, successfully separated spruce and larch while partially separating beech. Although data, from early summer, collected on 4 June 2011 was expected to shows limited potential in separating beech and maple, but in fact these data were the most successful at separating these two species. Data from 7 April 2011, during the deciduous leafless season, had the highest potential to separate the pine trees. Again, data from 10 July 2011 and 27 July 2009, collected after the oak lammas growth period, present the potential to separate larch and maple, respectively. Similarly, data from 28 June 2011, a period that follows the oak lammas growth period by a few days, showed potential for

separating the beech trees. Interestingly, results show that in general, data collected around the oak lammas growth phenological phase have more potential to identify oak than other phases. Finally, data collected on 23 August 2011 achieved the best identification for the Douglas fir.

4.5.2.2.3 Most promising periods for tree species identification

Results of the most promising phenological phases for tree species identification, based on the overall accuracy of each RapidEye dataset, can be obtained from Table 18. Figure 25 also serves as a visual illustration of the results, showing the Julian days of the phenological phases and of the RapidEye data acquisition combined with each RapidEye order, based on the overall accuracy of each. In general, results show that the most suitable acquisition time was found to be mid-summer, early spring, early summer and mid- / late-autumn, or, in other words, around the peak of the phenological phases, as expected.

As can be seen in autumn 2011, data collected after autumn coloring begins achieved much better results than those collected in late summer, two weeks prior. On the contrary, the most unsuitable time for acquisition for tree species identification seems to be late summer and early autumn. However, it is noticed that the results of data acquired during the promising periods also varied in their accuracy. Analysis in Figure 25 shows that data from 22 April 2010, which were collected around the beginning of oak leaf unfolding (two weeks after the larch needle unfolding has begun), achieved the second best accuracy. Similarly, the first and fifth best data were collected about four and three weeks, respectively, after the estimated oak lammas growth. The ninth best data were collected shortly after this phase. Also, the fourth best image from 07 April 2011 was acquired directly after the beginning of the larch needle unfolding.

Figure 25: *Julian day of the phenological observation and the single RapidEye data acquisition combined with the RapidEye order (in red, see* **Table 18**) *based on each single scene overall accuracy, in the Freising test site in the years 2009, 2010, and 2011*

94

4.5.2.3 Discussion

Investigations focused on tree species identification used twenty multispectral multi-seasonal RapidEye datasets. However, as was presented in Figure 23, tree species identification is a challenging task in comparison to other vegetation land cover, even when using multi-seasonal data. Ongoing investigations have yet to answer various economically important research questions related to forest tree species identification such as:

- How many datasets from various phenological phases are needed to obtain the most accurate results?

Results have shown that using the multi-seasonal RapidEye data increased the overall accuracy of tree species mapping. Interestingly, this result was sharply improved by using about seven datasets, and adding more datasets led to marginal improvements. Thus, the use of seven datasets in identifying tree species produced a similar success rate to that achieved using the entire dataset. Nevertheless, it should be noted that those seven datasets were among the best data because they were collected during phenological phases with high spectral variation between tree species, as will be discuss later in this section. Similar trends in overall accuracy improvements were also noticed when more aerial images were analyzed (Key et al., 2001). However, in this case the best achieved overall accuracy occurred when only 17 datasets were used, and not by using the entire dataset. It is important to note that increasing the amount of analyzed data can lead to a decrease in the accuracy, which is known in the literature as ''Hughes phenomenon'', as reported by (Hill et al., 2010; Key et al., 2001).

Previous studies have used multi-seasonal Landsat data (Wolter et al., 1995) and multi-seasonal ASTER and SPOT data, of similar characteristics to RapidEye data (Davranche et al., 2010; Stoffels et al., 2012). These studies did not investigate the number of datasets required to increase the temporal resolution, due to the limited number of scenes. Regardless of the forest condition, the implemented techniques, the number and types of tree species, and the assessment techniques used, multi-seasonal RapidEye data consistently demonstrate their high potential for tree species identification, when compared to sources used in previous studies. This leads to the following question:

- How does using additional bands or indices influence tree species identification?

Regarding the influence of using the red edge band and the indices on the accuracy, average improvements were about 1% and 4%, respectively. This 1% improvement was a result of using the red edge band, coming from its sensitivity to the spectra differences between the coniferous

and the deciduous tree groups. The red edge can be very sensitive to the spectra dissimilarity between the crops in the fields (Conrad et al., 2012). However, reduced sensitivity to the spectra differences between the tree species in the forest can be seen in Figure 23 A. Similarly, the indices, including the NDVI and the slope difference, show higher dissimilarity between the crops in the fields than between the tree species in the forest (Figure 23 B, C). As mentioned at the beginning of this section, tree species identification remains a challenging task for remote sensing.

It was found that using data from different growing or phenological seasons will increase the chance of separating tree species. This was revealed in the results of the multi-seasonal data combination analysis when compared to the single data analysis. The increase in the overall accuracy was due to the increase of the individual accuracies of spruce, Douglas fir, pine, and maple. Meanwhile, the individual accuracies of the larch and oak appeared to decrease, and were better identified using only one dataset from 22 April 2010 and 16 July 2011, respectively. The similarities amongst the two species along most phenological phases increased the confusion between them. However, this can be corrected using multi-seasonal data of phenological phases with high variation between oak and larch, to better distinguish between these species.

In terms of the phenological phase autumn coloring, in the year 2011 there were obvious differences between the species beech and oak (see Figure 25), and as a result, the confusion between these two species was minimal. The confusion between pine and the larch, oak and maple classes was reported because of the sparse pine stand structures, where pine stands are not typically dense, and consist of rejuvenation understory of mainly oak and maple, which influences the reflectance, thus increasing the confusion amongst these classes. This leads to the following question:

- Is there a phenological phase with high potential for identifying a specific tree species?

The results show that data collected during the phenological phases identified as most promising, also have the highest potential for separating specific tree species. Data from 16 July 2011, collected a few weeks after the oak lammas growth, has the highest potential to separate oak trees. This was because of the new oak leaves which had developed and were able to be detected. Indeed, most data collected shortly after that phenological phase had the highest potential to separate oaks. For spruce, separation was most successful on 16 July due to the low reflectance in red edge and NIR, and on 22 April due to the distinct overall low reflectance. Data collected on 22 April 2010, two weeks after larch unfolding started, had the highest potential to separate larch and beech, because larch was under leaf-on conditions while other deciduous species were leafless.

While beech was still leafless, explained by the associated undergrowth, a distinct and consistent signature was observed. Moreover, data from 4 June 2011 showed potential to separate beech and maple, however, the achieved accuracy was still low and confusion between beech and maple was still high. The reason for this was that the leaf unfolding phase for both species generally occurs simultaneously. Pine was best detected on 7 April 2011, when larch and deciduous species were all leafless. Again, this was because of the pine trees structure, which was not dense and mixed with its undergrowth consisting of many young oak and maple trees. Additionally, data from 10 July 2011 show high potential to identify larch due to the observed high reflectance in red edge and NIR. This can take place around the period of the highest concentration of chlorophyll in larch needles (Nakaji et al., 2006). Data from 27 July 2011 had the potential to separate maple trees, which can be explained by the higher reflectance in NIR of maple trees than that of deciduous species, especially beech. Although the data from late summer generally held little promise for tree species identification, these data showed potential to separate Douglas fir trees. This might be a result of the shoot extension which tends to last until mid-summer in response to moisture stress (Duryea and Landis, 1984).

In the end, it may be that the spectral variation among the tree species due to the phenological state during data collection is higher in spring and summer than that in autumn. This finding is critical and likely to be explained by several aspects, because the phenology does not fluctuate by species only, but also caused by photoperiodism, air temperature, soil moisture and temperature, and solar illumination (Key et al., 2001). Also, the spectral variations can occur for trees of the same species, within the same forest stand, in the same year (Hill et al., 2010) and between the different years (Figure 25). The next question posed is:

- Which phenological phase is the most promising to identify all tree species?

The most appropriate phenological seasons based on the single RapidEye data results were those in spring or early summer, the peak time for leaf unfolding and flowering phenological phases' activity. Conversely, the least appropriate times were late summer or early autumn because of the absence of most phenological activities. Data collected in mid-autumn achieved better results than the results achieved from late summer and early autumn data, because of autumn coloring and leaf fall phenological phases. This was achieved despite the fact that the mid-autumn datasets (collected on 22 October and 4 November 2011) had low solar elevation and low visibility.

An important finding was that the data collected around a specific phase in a season have more potential to lead to separation among tree species than other data collected in the same season. This

is explained by the maximized leaf-on and leaf-off situations between the tree species. For example, the second best data were collected on 22 April 2010, around the beginning of the oak leaf unfolding phase, and when oak, beech, and maple were still under leaf-off conditions, larch was already under leaf-on condition. Also, the first and fifth best data were collected a few weeks after the oak lammas growth, which increased the accuracy of oak, thus boosting the overall accuracy. Additionally, the fourth best image from 07 April 2011 was acquired directly after the beginning of the larch needle unfolding, when all deciduous species were still under leaf-off conditions, thus increasing the separability between the deciduous and coniferous species.

Contradictory results of the most appropriate season for data acquisition have been reported; some promote autumn (Schriever and Congalton, 1995; Wolter et al., 1995), while others state spring and autumn (Mickelson et al., 1998), and others report summer and autumn (Reese et al., 2002). However, these studies analyzed only one image from each season including spring, summer, and autumn. Therefore, the variations in their results can be explained by the success of data acquisition timing in the proper phenological phase, revealing the highest variations among the species. However, in the developed concept these differentiations are not a problem given the life span of the forest tree species. The results of the RapidEye data show that differentiating species is not only a matter of which season is better, but rather when the highest variation amongst phonological phases is observed across tree species. This key finding was delivered through the high frequency analysis of the RapidEye data, which enabled more frequent detection than was available from previous studies.

5   General discussion

Two satellite system technologies are investigated on the basis of their performances in providing user-defined parameters. The different design concepts may be summarized by 1) the high spectral resolution of the Hyperion sensor and 2) the ability to produce high temporal repetitions (2-3 days temporal resolution) with the RapidEye system. In terms of their limitations, while the Hyperion system yields a poor signal to noise ratio, despite 30 m pixel spatial resolution, the RapidEye system is limited to five spectral bands in the VIS and NIR region (silicon detector range). This section provides a summary of the discussion relating to the hyperspectral Hyperion data analysis, and the multi-seasonal multispectral analysis from RapidEye data. Following this, examination of the presented hypotheses are provided based on the dissection of the result.

Results of the forest cover, forest type, and tree species parameters extracted by the hyperspectral Hyperion data mostly revealed that OBIA outperformed the pixel-based techniques ANN and SAM. However, ANN was successful in achieving higher accuracy than OBIA for forest type extraction, as previously mentioned. The Hyperion data analysis allowed for the mapping of coniferous tree species, however, it was not possible to further separate the deciduous tree species. Low density of vegetation coverage was identified as a significant source of misinterpretations. This finding is due to the similar spectral responses of leaves and herbaceous ground vegetation and the mixed pixels of the 30 m spatial resolution of Hyperion. Additionally, the overall low energy response of the Hyperion sensor, which decreases the differences between the spectral reflectance of the different classes, reduced the accuracy. These reasons all lowered the training site accuracy, which then affected the results of the pixel-based analysis. Here, the OBIA results were the least affected since they depend also on membership functions.

Forest cover, forest type and gaps, forest monitoring, and tree species parameter extraction held a high potential to be successfully determined using the multi-seasonal multispectral RapidEye data. The primary success was the transferability of the developed methods in extracting forest cover, types, and gaps, and for monitoring the forest losses. The high repetition frequency of multi-seasonal RapidEye data assisted in applying a continuous monitoring of the forest cover, which in turn helped to avoid problems with clouds. Moreover, the multi-seasonal data precisely detected the phenological phases responsible for the best detection of tree species, and contributed to the concept of the "phenological fingerprint" approach. Spatial resolution of the RapidEye sensor was relatively appropriate for the parameter extraction, and the forest cover parameter was successfully extracted with high accuracy (between 94% and 98%). Method transferability showed that forest

types and gaps results were highly dependent on the topography and the forest structure of the test site. Forest types per stand corresponded appropriately to reality when describing the dominant type of each stand, which should be sufficient to meet foresters' stand-level management needs. The spectral information included in the RapidEye from various acquisitions dates shows slight differences because of the phenology as well as the data quality, which is affected by weather conditions and the solar angle during acquisition.

The hypotheses, mentioned in section 1.2, are examined in the following paragraph. The first hypothesis, tested based on the results of the extracted parameters for forest cover, forest types and forest tree species, using both the Hyperion and the RapidEye data, was:

H_1: Hyperspectral resolution outperforms multi-spectral high temporal resolution in determining forest parameters.

This hypothesis is to be refuted, for reasons based on each extracted parameter, as described below. The ***"forest cover"*** extracted by the Hyperion data achieved lower accuracy than that achieved by RapidEye data, and was more often mistaken for non-forest land cover classes. The relatively low spatial resolution (30 m) of the Hyperion data was the main reason for this result. The investigations into either system used a single dataset, and the assessments of the achieved results from either system were based on similar methodology. Moreover, the "***forest type"*** parameter was achieved with a higher accuracy using some single RapidEye datasets in the BFNP than using the Hyperion data, because of the higher spatial resolution of RapidEye data. This demonstrates that even with its high spectral resolution, the Hyperion data cannot compensate for its relatively low spatial resolution. Finally, the "***tree species"*** results clearly revealed that the multi-seasonal RapidEye data outperformed the Hyperion data. With the results of the RapidEye data, seven tree species, including both coniferous and deciduous species, were differentiated. Meanwhile, results of the Hyperion data only succeeded in separating two coniferous species, and could not separate the two deciduous species. Additionally, using multi-seasonal RapidEye data, further investigations into the phenological fingerprint concept were made possible, which proved to be essential for tree species identification. Hyperion single dataset therefore only has the potential to pick up on small parts of the phenological development of the species.

The second hypothesis, tested based on the results of the annual forest cover database of the three test sites in Bavaria, was:

H_2: The multi-seasonal RapidEye data evaluation approach does not meet the requirements for annual forest database updates.

This hypothesis was partly refuted, because the method developed was successful only in achieving annual updates of the forest tree cover. And RapidEye results could not achieve the same level of details which is usually achieved by aerial images interpretation. With the developed method, it was possible to monitor the forest cover continuously across the vegetation period. Using recently acquired RapidEye data, changes related to management practice at a scale of about 0.01 ha or 4 RapidEye pixels, or larger, could be detected with high precision. By accumulating the changes across the observation periods, the status of forest databases can be updated annually, more or less automatically for the parameter under investigation. Additionally, the multi-seasonal RapidEye data availability provided enough data to bypass the problem of partial cloud cover. All in all, the results of the forest cover update for all three test sites in Bavaria achieved overall accuracies of more than 96%. The method proved to be fast and cost effective. Under the same event, time and site conditions in the BFNP, approximately 97% of the results detected by the official aerial images survey were also detected using the RapidEye analysis. 8% of the losses were detected solely by RapidEye, the cost of the RapidEye analysis was only 25% of the cost of the aerial images analysis, and results were made available 9 weeks earlier.

The third and final hypothesis that was tested based on the result of the forest tree species identification in Freising test site using multi-seasonal RapidEye data was:

H_3: Applying the ''phenological fingerprint'' concept using the multi-seasonal RapidEye data does not improve the identification success of forest tree species significantly.

The hypothesis was refuted, as the ''phenological fingerprint'' concept proved to be essential for tree species identification. Investigations showed that a single dataset may improve specific tree species separability, while more datasets from various potential phenological phases are essential to increase the chance of successful tree species identification. Investigations have also revealed that there are specific seasons offering the highest potential for identification, primarily spring and early summer. This is contrary to the expected time frame of spring and autumn. Mid-autumn images still offered promise due to the coloring of leaves, which apparently achieved higher accuracy than acquisitions taken at the end of summer. Although mid-autumn data were expected to be more effective and significant in supporting species differentiation, low solar elevation, low visibility and non-perfect timing for data acquisition reduced their potential. Other explanations for this may be the special weathering conditions like storm events in autumn, defoliating all deciduous trees and prohibiting the differentiation based on autumn coloring. The results show that both seasonality and the timing of phenological phases (exhibiting maximum variation among tree species) are important factors in pursuit of species identification.

6 Conclusions and outlooks

This work investigated the potential of high spatial resolution (5 - 30 m) optical satellite data to application for forest parameter extraction. Hyperspectral Hyperion data were applied in a Mediterranean region, while multi-seasonal multispectral RapidEye data were applied in three Bavarian regions. Generally, the forest parameters were extractable from the hyperspectral Hyperion and multi-seasonal multispectral RapidEye data; however, based on the results some advantages and limitations were revealed.

6.1 Main conclusion

The main conclusion of this work is that the multi-seasonal multispectral RapidEye data show more potential for operational use than the hyperspectral Hyperion data when extracting forest parameters. This conclusion applies only to these high spatial resolution HSR satellites and can be supported by the following arguments relating to specific parameters:

- The forest cover parameter was extracted using single data collected from both systems. Spatial resolution was found to hold a greater influence on accuracy than the spectral resolution.

- The forest type parameter was extracted with single takes using RapidEye data, and, in some cases produced higher accuracies than when using Hyperion data. Results were based on topography and forest structure, and the low spatial resolution of the Hyperion sensor significantly affected the results.

- Forest tree cover databases can be annually updated using multi-seasonal RapidEye data, offering an operational continuous monitoring tool with a very high accuracy. Apparently, such benefits can not be offered with Hyperion data.

- Forest tree species were successfully separated, and the ''phenological fingerprint'' concept proved to be essential in separating tree species. All in all, the multi-season acquisition capability of RapidEye captures more data during various phenological phases, supporting tree species identification. The Hyperion dataset captures one phase of phenological development, and, although combined with rich spectral information, this did not lead to successful deciduous tree species separation.

The high spectral resolution of Hyperion data offers rich spectral information, which supports the successful extraction of forest parameters. However, the low spatial resolution of the Hyperion

sensor obscured this potential, at least in the highly structured Anapoli study site. Technically, the design of high spectral resolution sensor results in a low spatial resolution, to compensate for the low energy received by the narrow bands. Thus, the energy received at the Hyperion sensor was very weak, and it is expected to be weak for the next generation of hyperspectral sensors of similar characteristics, such as the German "EnMap" and the Italian "Spectra" as well. Conversely, the multi-seasonal RapidEye data successfully updated the annual forest cover database. In addition to that, the multi-seasonal data can contribute successfully to the ''phenological fingerprint'' concept, which is essential for the operational identification of tree species. This shows the potential of the next generation ''Sentinel'' ESA satellites, which have a revisit time of 6 days, along with the potential of the German hyperspectral satellite ''EnMap'' with a revisit time of 4 days, and can provide multi-seasonal data. Additionally, investigations into the "phenological fingerprint" at a target site, will assist in creating schedules for the most suitable timing of data acquisition.

Regarding the applied techniques, OBIA can be a strong tool for developing fast and transferable methods for forest cover mapping and monitoring. OBIA offers geometrical, logical, and spectral based features in addition to the integration of GIS data, which should contribute to achieving the forest cover definitions similar to what foresters expect. This can significantly contribute to forest cover mapping and monitoring, which are very important parameters, and yet are still not well documented at the regional level in many developing countries, or at the global level. On the other hand, the pixel-based technique is still necessary for tree species detection, especially the use of high spatial resolution data ($5 - 30$ m) to detect single tree crowns. The pixel-based technique was implemented here using SAM, however, other classifiers can be taken into consideration in the future such as support vector machine (SVM) or random forest (RF).

6.2 Economic aspects

Offering operational solutions for forest enterprises to make strategic / tactical decisions appears to be possible by utilizing HSR satellites data and taking into consideration system resolutions, area coverage and cost. However, the increase in any of the resolution types including spatial, spectral, radiometric and temporal resolution, will increase the cost. In this investigation, the multi-seasonal multispectral approach offered lower spectral resolution but higher spatial and temporal resolution than that of the mono-temporal hyperspectral approach. The cost of the multi-seasonal multispectral approach will remain more affordable than the hyperspectral approach, taking into consideration the limited coverage of the hyperspectral systems.

For the parameters forest cover and forest type, the spatial resolution of the RapidEye (5 m) was of key importance, especially in determining forest type. Meanwhile, the high spectral resolution of the Hyperion did not improve the results. Therefore, investments into the multispectral data of suitable spatial resolution (5 m or less) for these parameters should be considered as cost effective.

For the forest tree cover changes, the spatial resolution of the RapidEye data is sufficient, while the use of multi-seasonal data is necessary. Collecting data more frequently will increase the cost, but will offer an operational application for forest monitoring. This cost increase associated with the use of frequent multi-seasonal data is justified as when these data are collected at a suitable time, they will ensure the success of the ''phenological fingerprint'' concept. This approach is the only way to successfully offer operational tree species identification. Yet to consider the method of the tree species identification operational at broader scales, well defined clusters including the available tree species and their phenology, as well as training sites collection for each cluster, is still required.

6.3 Outlook and future development

The conclusions of this study can assist in improving future space remote sensing development for forest applications. There are three areas where investments can be made to potentially improve optical. These are:

1- Multi-date capability of the sensor

There is no single optimal time for data acquisition that is able to capture all the variations between tree species. This is due to the fact that for each specific tree species, distinguishing features appear at different dates. High spatial resolution hyperspectral data are limited in their ability to support tree species mapping if they are not collected during the proper phenological phase. Therefore, multi-seasonal data for tree species identification appears to be integral. Further research on this topic should focus on exploiting more phenological phases and multi-seasonal biochemical reflectance characteristics. Also, investigation into the phenological fingerprint concept for tree species identification in different Bavarian test sites should be conducted.

2- Few additional bands may be in short-wave infrared (SWIR)

In general, not all hyperspectral bands are suitable for analysis of forest parameters including tree species identification, while some additional bands (especially in the SWIR region of the spectrum) contribute to generating indices have the potential to increase accuracies. Additionally, increasing the spectral resolution of the hyperspectral data will decrease the spatial and radiometric

resolutions, which affects the results. Including the red edge additional band into analysis for tree species identification, had a tendency to increase the achieved accuracy. Therefore, development of new broad-band sensors with additional bands in the SWIR region or other regions sensitive to the tree species should therefore be considered.

3- Slight improvement in the spatial resolution

Forest management planning policies shape the forests of tomorrow, which are expected to become highly mixed and vertically structured. These forest types will form a challenge for the remote sensing of forest inventory. Even the 5 m spatial resolution demonstrated some difficulties in achieving appropriate accuracies of the forest type parameter, at least for the local / regional levels. The need to complement optical data with elements such as terrestrial data, and data from active sensors should be considered. Also, it would be worth investigating the fusion of the Hyperion data of 30 m spatial resolution with the RapidEye data of 5 m spatial resolution for forest parameter mapping. Improvements in the spatial resolution of the optical data is also recommended.

7   References

Anderson, J., Hardy, E., Roach, J., Witmer, R., 1976. A Land Use And Land Cover Classification System For Use With Remote Sensor Data. U.S. Geological Survey Professional Paper 964.

Baatz, M. & Schäpe, A., 2000: Multiresolution Segmentation – an optimization approach for high quality multi-scale image segmentation. In: Strobl, J. et al. (eds.): Angewandte Geographische Informationsverarbeitung XII. Wichmann, Heidelberg, pp. 12-23.

Bennett, B., 2001. What is a Forest? On the Vagueness of Certain Geographic Concepts. Topoi 20 (2), 189-201.

Berrichi, F., Singh, S., Agarwal, S., 2012. Tree Species Typing in Temperate Forests using Hyperspectral data of Hyperion EO-1 in western Himalayas, in: Jha, M.K. (Ed.), Proceedings of the 6th WSEAS International Conference on BUSINESS ADMINISTRATION (ICBA '12). Havard, Cambridge, USA, January 25 - 27, 2012, pp. 19–24.

Biging, G., Colby, D., Congalton, R., 1998. Sampling systems for change detection accuracy assessment, in: Lunetta, R.S.E.C. (Ed.), Remote sensing change detection. Environmental monitoring methods and applications. Ann Arbor Press, Chelsea, Mich.

Blaschke, T., 2005. Towards a framework for change detection based on image objects. Göttinger Geographische Abhandlungen 113, 1–9.

Blaschke, T., 2010. Object based image analysis for remote sensing. ISPRS Journal of Photogrammetry and Remote Sensing 65 (1), 2–16.

Blaschke, T., Hay, G.J., Kelly, M., Lang, S., Hofmann, P., Addink, E., Queiroz Feitosa, R., van der Meer, F., van der Werff, H., van Coillie, F., Tiede, D., 2014. Geographic Object-Based Image Analysis – Towards a new paradigm. ISPRS Journal of Photogrammetry and Remote Sensing 87 (0), 180–191.

Borry, F.C., Roover, B.P. de, Leysen, M.M., Wulf, R.R. de, Goossens, R.E., 1993. Evaluation of SPOT and TM data for forest stratification: a case study for small-size poplar stands: Geoscience and Remote Sensing, IEEE Transactions on. Geoscience and Remote Sensing, IEEE Transactions on 31 (2), 483–490.

Boyd, D., Danson, F., 2005. Satellite remote sensing of forest resources: three decades of research development. Progress in Physical Geography 29 (1), 1–26.

Bruzzone, L., Smits, P.C., Tilton, J.C., 2003. Foreword special issue on analysis of multitemporal remote sensing images: Geoscience and Remote Sensing, IEEE Transactions on. Geoscience and Remote Sensing, IEEE Transactions 41 (11), 2419–2422.

Buttler, K.P., 1991. Anleitung für die phänologischen Beobachter des Deutschen Wetterdienstes: (BAPH), 3rd ed. Vorschriften und Betriebsunterlagen 17. Deutscher Wetterdienst, Offenbach a.M, V, 155 S.

Campbell, J.B., 1996. Introduction to remote sensing, 2nd ed. Taylor & Francis, London, xxvii, 622.

Carlowitz, H.C.v., 1713, reprinted 2013. Sylvicultura oeconomica, oder, Hauswirthliche Nachricht und naturmässige Anweisung zur wilden Baum-Zucht. oekom, München, 550 pp.

Carpenter, G.A., Gopal, S., Macomber, S., Martens, S., Woodcock, C.E., Franklin, J., 1999. A Neural Network Method for Efficient Vegetation Mapping. Remote Sensing of Environment 70 (3), 326–338.

Carvalho, L.M.T., Fonseca, L.M.G., Murtagh, F., Clevers, J.G.P.W., 2001. Digital change detection with the aid of multiresolution wavelet analysis. International Journal of Remote Sensing 22 (18), 3871–3876.

Chen, G., Hay, G.J., Carvalho, L.M.T., Wulder, M.A., 2012. Object-based change detection. International Journal of Remote Sensing 33 (14), 4434–4457.

Congalton, R.G., Green, K., 1999. Assesssing the accuracy of remotely sensed data: Principles and practices. Mapping science. CRC/Lewis Publications, Boca Raton, 137 pp.

Conrad, C., Fritsch, S., Lex, S., Löw, F., Rücker, G., Schorcht, G., Sultanov, M., Lamers, J., 2012. Potenziale des Red Edge Kanals von RapidEye zur Unterscheidung und zum Monitoring landwirtschaftlicher Anbaufrüchte am Beispiel des usbekischen Bewässerungssystems Khorezm, in: Borg, E. (Ed.), Vom Algorithmus zum Produkt. Tagungsband zum 4. RESA-Workshop ; Neustrelitz, 21. - 22. März 2012, Orangerie Neustrelitz. GITO, Verl. für Industrielle Informationstechnik und Organisation, Berlin.

Coppin, P., Jonckheere, I., Nackaerts, K., Muys, B., Lambin, E., 2004. Review Article Digital change detection methods in ecosystem monitoring: a review. International Journal of Remote Sensing 25 (9), 1565–1596.

Davranche, A., Lefebvre, G., Poulin, B., 2010. Wetland monitoring using classification trees and SPOT-5 seasonal time series. Remote Sensing of Environment 114 (3), 552–562.

De Kok, R., Schneider, T., Baatz, M., Ammer, U., 1999. Object Based Image Analysis of High Resolution Data in the Alpine Forest Area. JOINT WS FOR ISPRS WG I/1, I/3 AND IV/4: SENSORS AND MAPPINHG FROM SPACE, 27–30.

Desclée, B., Bogaert, P., Defourny, P., 2006. Forest change detection by statistical object-based method. Remote Sensing of Environment 102 (1–2), 1–11.

Dorren, L.K.A., Maier, B., Seijmonsbergen, A.C., 2003. Improved Landsat-based forest mapping in steep mountainous terrain using object-based classification. Forest Ecology and Management 183 (1–3), 31–46.

Duryea, M.L., Landis, T.D., 1984. Forest nursery manual: Production of bareroot seedlings: (papers presented at the Bareroot nursery technology workshop; Corvallis - Ore., October 1982). Forestry sciences - FS 11. Nijhoff/Junk, The Hague a.o, X, 385.

Duveiller, G., Defourny, P., Desclée, B., Mayaux, P., 2008. Deforestation in Central Africa: Estimates at regional, national and landscape levels by advanced processing of systematically-distributed Landsat extracts. Earth Observations for Terrestrial Biodiversity and Ecosystems Special Issue 112 (5), 1969–1981.

Eckert, S., 2006. Acontribution to sustainable forest managment in Patagonia: Object oriented Classification and Forest Parameter Extraction based on ASTER and LandSat ETM+ Data. PhD, Zürich, Switzerland.

Eckert, S., Kneubühler, M., 2004. Application of Hyperion data to agricultural land classification and vegetation properties estimation in switzerland, in: Altan, O. (Ed.), Proceedings of the 20th ISPRS Congress (Geo-Imagery Bridging Continents), commission VII. Istanbul, Turkey, January 12 - 23, 2004, pp. 866-871.

References

Elatawneh, A., Kalaitzidis, C., Petropoulos, G.P., Schneider, T., 2012. Evaluation of diverse classification approaches for land use/cover mapping in a Mediterranean region utilizing Hyperion data: International Journal of Digital Earth. International Journal of Digital Earth, 1–23. Doi. 10.1080/17538947.2012.671378.

Elatawneh, A., Rappl, A., Rehush, N., Schneider, T., knoke, T., 2013. Forest tree species communities identification using multi phenological stages RapidEye data: case study in the forest of Freising, in: Borg, E. (Ed.), From the Basics to the Service. GITO, Verl. für Industrielle Informationstechnik und Organisation, Berlin, pp. 21–38.

Elatawneh, A., Wallner, A., Manakos, I., Schneider, T., Knoke, T., 2014. Forest Cover Database Updates Using Multi-Seasonal RapidEye Data—Storm Event Assessment in the Bavarian Forest National Park. Forests 5 (6), 1284–1303.

European Environmental Agency, 1995. CORINE land cover. http://www.eea.europa.eu/publications/COR0-landcover. Accessed 12 March 2014.

FAO, 2010. Global forest resources assessment. Food and Agriculture Organization of the United Nations.

Felbermeier, B., Hahn, A., Schneider, T., 2010. Study on user requirements for remote sensing applications in forestry, in: Wagner, W. (Ed.), 100 years ISPRS - advancing remote sensing science. ISPRS Technical Commission VII Symposium ; 1910 - 2010 centenary celebration Vienna, July 5 – 7, 2010. The international archives of photogrammetry, remote sensing and spatial information sciences 38,7. ISPRS, Vienna, pp. 210–212.

Foody, G.M., 2002. Status of land cover classification accuracy assessment. Remote Sensing of Environment 80 (1), 185–201.

Franklin, S.E., 2001. Remote sensing for sustainable forest management. Lewis, Boca Raton, Fla, 407 pp.

Gao, Y., Mas, J., Niemeyer, I., Marpu, P., Palacio, J. (Eds.), 2007. Object-based image analysis for mapping land-cover in a forest area.

Geisser, S., 1975. The Predictive Sample Reuse Method with Applications. Journal of the American Statistical Association 70 (350).

George, R., Padalia, H., Kushwaha, S.P.S., 2014. Forest tree species discrimination in western Himalaya using EO-1 Hyperion. International Journal of Applied Earth Observation and Geoinformation 28 (0), 140–149.

Goodenough, D.G., Dyk, A., Niemann, K.O., Pearlman, J.S., Hao Chen, Tian Han, Murdoch, M., West, C., 2003. Processing Hyperion and ALI for forest classification. Geoscience and Remote Sensing, IEEE Transactions on 41 (6), 1321–1331.

Hansen, P., Schjoerring, J., 2003. Reflectance measurement of canopy biomass and nitrogen status in wheat crops using normalized difference vegetation indices and partial least squares regression. Remote Sensing of Environment 86 (4), 542–553.

Heurich, M., 2001. Waldentwicklung im Bergwald nach Windwurf und Borkenkäferbefall. Nationalpark Bayerischer Wald / Hrsg.: Nationalparkverwaltung Bayerischer Wald. Bayerisches Staatsministerium für Landwirtschaft und Forsten 14. Nationalparkverwaltung Bayerischer Wald, Grafenau, 182 S.

Heurich, M., Neufanger, M., 2005. Die Wälder des Nationalparks Bayerischer Wald: Ergebnisse der Waldinventur 2002/2003 im geschichtlichen und waldökologischen Kontext. Nationalparkverwaltung Bayerischer Wald, Grafenau, 176 S.

Heurich, M., Ochs, T., Andresen, T., Schneider, T., 2010. Object-orientated image analysis for the semi-automatic detection of dead trees following a spruce bark beetle (Ips typographus) outbreak. European Journal of Forest Research 129 (3), 313–324.

Heylen, R., Parente, M., Gader, P., 2014. A Review of Nonlinear Hyperspectral Unmixing Methods. Selected Topics in Applied Earth Observations and Remote Sensing, IEEE Journal of 7 (6), 1844–1868.

Hill, R.A., Wilson, A.K., George, M., Hinsley, S.A., 2010. Mapping tree species in temperate deciduous woodland using time-series multi-spectral data. Applied Vegetation Science 13 (1), 86–99.

Holmgren, P., Thuresson, T., 1998. Satellite remote sensing for forestry planning—A review. Scandinavian Journal of Forest Research 13 (1-4), 90–110.

Hughes, G., 1968. On the mean accuracy of statistical pattern recognizers. IEEE Transactions on Information Theory 14 (1), 55–63.

Hussain, M., Chen, D., Cheng, A., Wei, H., Stanley, D., 2013. Change detection from remotely sensed images: From pixel-based to object-based approaches. ISPRS Journal of Photogrammetry and Remote Sensing 80 (0), 91–106.

Immitzer, M., Atzberger, C., Koukal, T., 2012. Tree Species Classification with Random Forest Using Very High Spatial Resolution 8-Band WorldView-2 Satellite Data. Remote Sensing 4 (9), 2661–2693.

Iordache, M.-D., Bioucas-Dias, J.M., Plaza, A., 2011. Sparse Unmixing of Hyperspectral Data. Geoscience and Remote Sensing, IEEE Transactions on 49 (6), 2014–2039.

Jensen, J.R., 1996. Introductory digital image processing: A remote sensing perspective, 2nd ed. Prentice Hall series in geographic information science. Prentice Hall, Upper Saddle River, N.J, xi, 316.

Kautz, M., Dworschak, K., Gruppe, A., Schopf, R., 2011. Quantifying spatio-temporal dispersion of bark beetle infestations in epidemic and non-epidemic conditions. Forest Ecology and Management 262 (4), 598–608.

Key, T., Warner, T.A., McGraw, J.B., Fajvan, M.A., 2001. A Comparison of Multispectral and Multitemporal Information in High Spatial Resolution Imagery for Classification of Individual Tree Species in a Temperate Hardwood Forest. Remote Sensing of Environment 75 (1), 100–112.

Knoke, T., 2012. Forstbetriebsplanung als Entscheidungshilfe. Ulmer, Stuttgart, 408 S.

Knoke, T., Hahn, A., Schneider, T., 2010. Linking Inventory and Forest Optimisation: Information and decision-making in forest management. European Journal of Forest Research 129 (5), 771-775.

Korpela, I., Heikkinen, V., Honkavaara, E., Rohrbach, F., Tokola, T., 2011. Variation and directional anisotropy of reflectance at the crown scale — Implications for tree species classification in digital aerial images. Remote Sensing of Environment 115 (8), 2062–2074.

Kruse, F.A., Lefkoff, A.B., Boardman, J.W., Heidebrecht, K.B., Shapiro, A.T., Barloon, P.J., Goetz, A.F.H., 1993. The spectral image processing system (SIPS)—interactive visualization and analysis of imaging spectrometer data: Airbone Imaging Spectrometry. Remote Sensing of Environment 44 (2–3), 145–163.

Lillesand, T.M., Kiefer, R.W., 2000. Remote sensing and image interpretation, 4th ed. John Wiley & Sons, New York, xii, 724.

Linke, J., Mcdermid G.J., Laskin D.N., Mclane A.J., Pape A., Cranston J., Hallbeyer M., Franklin S.E., 2009. A disturbance-inventory framework for flexible and reliable landscape monitoring. Photogrammetric Engineering & Remote Sensing 75 (8), 981–995.

Lu, D., Mausel, P., Brondízio, E., Moran, E., 2004. Change detection techniques. International Journal of Remote Sensing 25 (12), 2365–2401.

McDermid, G.J., Linke, J., Pape, A.D., Laskin, D.N., McLane, A.J., Franklin, S.E., 2008. Object-based approaches to change analysis and thematic map update: challenges and limitations. Canadian Journal of Remote Sensing 34 (5), 462–466.

McDermid, G.J., Pape, A., Chubey, M., Franklin, S. (Eds.), 2003. OBJECT ORIENTED ANALYSIS FOR CHANGE DETECTION, Montréal, Canada.

McRoberts, R.E., Tomppo, E.O., 2007. Remote sensing support for national forest inventories. ForestSAT Special Issue ForestSAT 2005 Conference "Operational tools in forestry using remote sensing techniques" 110 (4), 412–419.

Mickelson, J.R., Civco, D.L., Silander J. A., 1998. Delineating forest canopy species in the northeastern United States using multi-temporal TM imagery. Photogrammetric Engineering & Remote Sensing 64 (9), 891–904.

Nagendra, H., Lucas, R., Honrado, J.P., Jongman, R.H.G., Tarantino, C., Adamo, M., Mairota, P., 2013. Remote sensing for conservation monitoring: Assessing protected areas, habitat extent, habitat condition, species diversity, and threats. Biodiversity Monitoring 33 (0), 45–59.

Nakaji, T., Oguma, H., Fujinuma, Y., 2006. Seasonal changes in the relationship between photochemical reflectance index and photosynthetic light use efficiency of Japanese larch needles. International Journal of Remote Sensing 27 (3), 493–509.

Nelson, R.F., 1984. Classifying Northern Forests Using Thematic Mapper Simulator Data. Photogrammetric Engineering & Remote Sensing 50 (5), 607–617.

Pengra, B.W., Johnston, C.A., Loveland, T.R., 2007. Mapping an invasive plant, Phragmites australis, in coastal wetlands using the EO-1 Hyperion hyperspectral sensor. Remote Sensing of Environment 108 (1), 74–81.

Petropoulos, G.P., Arvanitis, K., Sigrimis, N., 2012a. Hyperion hyperspectral imagery analysis combined with machine learning classifiers for land use/cover mapping. Expert Systems with Applications 39 (3), 3800–3809.

Petropoulos, G.P., Kalaitzidis, C., Prasad Vadrevu, K., 2012b. Support vector machines and object-based classification for obtaining land-use/cover cartography from Hyperion hyperspectral imagery. Computers & Geosciences 41, 99–107.

Pignatti, S., Cavalli, R.M., Cuomo, V., Fusilli, L., Pascucci, S., Poscolieri, M., Santini, F., 2009. Evaluating Hyperion capability for land cover mapping in a fragmented ecosystem: Pollino National Park, Italy. Remote Sensing of Environment 113 (3), 622–634.

Pulla, P., Schuck, A., Johannes Verkerk, P., Lasserre, B., Marchetti. M., Green, T., 2013. Mapping the distribution of forest ownership in Europe: European Forest Institute, Technical Report 88.

RapidEye AG, 2012. Satellite Imagery Product Specifications. RapidEye AG. http://www.rapideye.com/upload/RE_Product_Specifications_ENG.pdf. Accessed 13 March 2013.

Rappl, A., Elatawneh, A., Thiele, A., Troycke, A., Schneider, T., Knoke, T., Hinz, S., 2012. Einsatz der Fernerkundungssysteme TerraSAR-X und RapidEye im Katastrophenmanagement von Windwurfereignissen, in: Informationstechnologie für eine nachhaltige Landbewirtschaftung. Fokus Forstwirtschaft ; Referate der 32. GIL-Jahrestagung, 29. Februar - 01. März 2012, Freising, Germany. Ges. für Informatik, Bonn, pp. 235–238.

Reese, H.M., Lillesand, T.M., Nagel, D.E., Stewart, J.S., Goldmann, R.A., Simmons, T.E., Chipman, J.W., Tessar, P.A., 2002. Statewide land cover derived from multiseasonal Landsat TM data: A retrospective of the WISCLAND project. Remote Sensing of Environment 82 (2–3), 224–237.

Salajanu, D., Olson C. E., 2001. The Significance of Spatial Resolution: Identifying Forest Cover from Satellite Data. Journal of Forestry 99 (6), 32–38.

Schneider, T., 2013. Methodenentwicklung zur Nutzung von Parametern aus Satellitendaten im Rahmen der forstlichen Betriebsplanung und des forstlichen Katastrophenmanagements: Acronym_ EUS-FH (Entscheidungs-Unterstützungs-System Forst-Holz); innovative Informationsprodukte durch synergetische Nutzung von RapidEye und TerraSAR-X Satellitendaten; Abschlussbericht zum 30.06.2013, Wissenschaftszentrum Weihenstephan für Ernährung, Landnutzung und Umwelt, Freising. Technische Informationsbibliothek u. Universitätsbibliothek, Hannover, 138 pp.

Schneider, T., Elatawneh, A., Rahlf, J., Kindu, M., Rappl, A., Thiele, A., Boldt, M., Hinz, S., 2013. Parameter Determination by RapidEye and TerraSAR-X Data: A Step Toward a Remote Sensing Based Inventory, Monitoring and Fast Reaction System on Forest Enterprise Level, in: Krisp, J.M., Meng, L., Pail, R., Stilla, U. (Eds.), Lecture Notes in Geoinformation and Cartography. Springer Berlin Heidelberg, Berlin, Heidelberg, pp. 81–107.

Schriever, J., Congalton, R., 1995. Evaluating Seasonal Variablity as an Aid to Cover-Type Mapping from Landsat Thematic Mapper Data in the Northwest. Photogrammetric Engineering & Remote Sensing 61 (3), 321–327.

Schütt, P., 2006. Enzyklopädie der Laubbäume: Die große Enzyklopädie mit über 800 Farbfotos unter Mitwirkung von 30 Experten, Sonderausg. ed. Nikol, Hamburg, XII, 642 S.

Shafri, H.Z.M., Suhaili, A., Mansor, S., 2007. The Performance of Maximum Likelihood, Spectral Angle Mapper, Neural Network and Decision Tree Classifiers in Hyperspectral Image Analysis. J. of Computer Science 3 (6), 419–423.

Singh, A., 1989. Review Article Digital change detection techniques using remotely-sensed data: International Journal of Remote Sensing. International Journal of Remote Sensing 10 (6), 989–1003.

Stehman, S.V., Czaplewski, R.L., 1998. Design and Analysis for Thematic Map Accuracy Assessment. Remote Sensing of Environment 64 (3), 331–344.

Stoffels, J., Mader, S., Hill, J., Werner, W., Ontrup, G., 2012. Satellite-based stand-wise forest cover type mapping using a spatially adaptive classification approach. European Journal of Forest Research 131 (4), 1071–1089.

Stone, M., 1974. Cross-Validatory Choice and Assessment of Statistical Predictions. Journal of the Royal Statistical Society. Series B (Methodological) 36 (2), 111–147.

References

Thenkabail, P.S., Enclona, E.A., Ashton, M.S., Legg, C., Dieu, M.J. de, 2004. Hyperion, IKONOS, ALI, and ETM+ sensors in the study of African rainforests. Remote Sensing of Environment 90 (1), 23–43.

Thiele, A., Boldt, M., HINZ, S., 2012. Automated detection of storm damage in forest areas by analyzing TerraSAR-X data, in: Geoscience and Remote Sensing Symposium (IGARSS), 2012 IEEE International : Geoscience and Remote Sensing Symposium (IGARSS), 2012 IEEE International : Geoscience and Remote Sensing Symposium (IGARSS), 2012 IEEE International, pp. 1672–1675.

Thomasson, l.A., Bennett, C.W., Jackson, B.D., Mailander, M.P., 1994. Differentiating Bottomland Tree Species with Multispectral Videography. Photogrammetric Engineering & Remote Sensing 60 (1), 55–59.

Townsend, P., Walsh, S., 2001. Remote sensing of forested wetlands: application of multitemporal and multispectral satellite imagery to determine plant community composition and structure in southeastern USA. Plant Ecology 157 (2), 129–149.

van Ardet, J., Wynne, R.I., 2001. Spectral Separability among Six Southern Tree Species. Photogrammetric Engineering & Remote Sensing 67 (12), 1367–1375.

Vohland, M., Stoffels, J., Hau, C., Schüler, G., 2007. Remote sensing techniques for forest parameter assessment: multispectral classification and linear spectral mixture analysis. Silva Fennica 41 (3), 441–456.

Walsh, S.J., 1980. Coniferous tree species mapping using LANDSAT data. Remote Sensing of Environment 9 (1), 11–26.

Walsh, S.J., McCleary, A.L., Mena, C.F., Shao, Y., Tuttle, J.P., González, A., Atkinson, R., 2008. QuickBird and Hyperion data analysis of an invasive plant species in the Galapagos Islands of Ecuador: Implications for control and land use management. Earth Observations for Terrestrial Biodiversity and Ecosystems Special Issue 112 (5), 1927–1941.

Walter, V., 2004. Object-based classification of remote sensing data for change detection. ISPRS Journal of Photogrammetry & Remote Sensing, special issue: Integration of Geodata and Imagery for Automated Refinement and Update of Spatial Databases. 58 (3–4), 225–238.

Wang, J., Chen, Y., He, T., Lv, C., Liu, A., 2010. Application of geographic image cognition approach in land type classification using Hyperion image: A case study in China. Supplement Issue on "Spatial Analysis-Modeling, Methodology and applications" 12, Supplement 2 (0), S212.

Wang, L., Silván-Cárdenas, J.L., Sousa, W.P., 2008. Neural Network Classification of Mangrove Species from Multi-seasonal Ikonos Imagery. Photogrammetric Engineering & Remote Sensing 74 (7), 921–927.

Waser, L., Küchler, M., Jütte, K., Stampfer, T., 2014. Evaluating the Potential of WorldView-2 Data to Classify Tree Species and Different Levels of Ash Mortality. Remote Sensing 6 (5), 4515–4545.

Willhauck, G., Schneider, T., De_Kok, R., Ammer, S., 2000. Comparison of object oriented classification techniques and standard image analysis for the use of change detection between SPOT multispectral satellite images and aerial photos, in: Schenk, T., Vosselman, G. (Ed.), International Archives of Photogrammetry and Remote Sensing. Vol. XXXIII, Part B3. Amsterdam, The Netherlands, July 16 - 23, 2000, pp. 35-42.

Wolter, P., Mladenoff D.J., Host G.E., Crow T.R, 1995. Improved forest classification in the northern Lake States using multi-temporal Landsat imagery. Photogrammetric Engineering & Remote Sensing 61 (9), 1129–1143.

Wulder, M.A., White, J.C., Coops, N.C., Butson, C.R., 2008. Multi-temporal analysis of high spatial resolution imagery for disturbance monitoring. Remote Sensing of Environment 112 (6), 2729–2740.

Zhou, W., Troy, A., Grove, M., 2008. Object-based Land Cover Classification and Change Analysis in the Baltimore Metropolitan Area Using Multitemporal High Resolution Remote Sensing Data. Sensors 8 (3), 1613–1636.

8 Appendix: Publications

8.1 Publication 1

Elatawneh A., Kalaitzidis C., Petropoulos G. P., Schneider T. 2012. Evaluation of diverse classification approaches for land use/cover mapping in a Mediterranean region utilizing Hyperion data. International Journal of Digital Earth. doi 10.1080/17538947.2012.671378

International Journal of Digital Earth

Evaluation of diverse classification approaches for land use/cover mapping in a Mediterranean region utilizing Hyperion data

Alata Elatawneh [a] [b], Chariton Kalaitzidis [b], George P. Petropoulos [c] & Thomas Schneider [a]

[a] Institute of Forest Management, Technische Universität München (TUM), 85354, Freising, Germany

[b] Department of Geoinformation in Environmental Management, Mediterranean Agronomic Institute of Chania (MAICh), Chania, 73100, Greece

[c] INFOCOSMOS, 13341, Athens, Greece

Available online: 29 Mar 2012

i First

PLEASE SCROLL DOWN FOR ARTICLE

demand, or costs or damages whatsoever or howsoever caused arising directly or indirectly in connection with or arising out of the use of this material.

Evaluation of diverse classification approaches for land use/cover mapping in a Mediterranean region utilizing Hyperion data

Alata Elatawneh[a,b], Chariton Kalaitzidis[b], George P. Petropoulos[c]* and Thomas Schneider[a]

[a]*Institute of Forest Management, Technische Universität München (TUM), 85354 Freising, Germany;* [b]*Department of Geoinformation in Environmental Management, Mediterranean Agronomic Institute of Chania (MAICh), Chania 73100, Greece;* [c]*INFOCOSMOS, 13341 Athens, Greece*

Information on Earth's land surface cover is commonly obtained through digital image analysis of data acquired from remote sensing sensors. In this study, we evaluated the use of diverse classification techniques in discriminating land use/cover types in a typical Mediterranean setting using Hyperion imagery. For this purpose, the spectral angle mapper (SAM), the object-based and the non-linear spectral unmixing based on artificial neural networks (ANNs) techniques were applied. A further objective had been to investigate the effect of two approaches for training sites selection in the SAM classification, namely of the pixel purity index (PPI) and of the direct selection of training points from the Hyperion imagery assisted by a QuickBird imagery and field-based training sites. Object-based classification outperformed the other techniques with an overall accuracy of 83%. Sub-pixel classification based on the ANN showed an overall accuracy of 52%, very close to that of SAM (48%). SAM applied using the training sites selected directly from the Hyperion imagery supported by the QuickBird image and the field visits returned an increase accuracy by 16%. Yet, all techniques appeared to suffer from the relatively low spatial resolution of the Hyperion imagery, which affected the spectral separation among the land use/cover classes.

Keywords: Hyperion; Earth's land use/cover mapping; digital image analysis; spectral angle mapper; sub-pixel classification; artificial neural networks; Greece

1. Introduction

Information on land use/cover (LULC) is very important in many natural resource applications. At local and regional scales, knowledge of both LULC forms a basic dimension of recourses available to any political unit (Kavzoglu and Colkesen 2009). Such thematic maps are also key inputs to environmental and land use planning at local, regional, and national levels. At a larger scale, LULC information is of key importance in delineating the broad patterns of climate and vegetation that form the environmental context for human activities. Furthermore, LULC maps are also a

valuable input in the development of conservation policies particularly so for environmentally or ecologically protected areas and the restoration of native habitats, as well as the monitoring of desertification and land degradation in regions such as Mediterranean (Castillejo-González *et al.* 2009).

Remote sensing has been a convenient source of data for LULC thematic mapping. A wide range of approaches have been developed for this purpose, with image classification being the most widely used (Mathur and Foody 2008). A recent overview of classification techniques used in remote sensing can be found in Lu and Weng (2007). Three main groups of classification approaches can be distinguished, namely: pixel-based, object-based, and sub-pixel techniques. Pixel-based techniques employ the reflective characteristics of the land surface items in order to perform a classification, by assigning pixels to land cover classes. Classifications using pixel-based techniques can be achieved by either supervised or unsupervised classification techniques. In object-based classification method, the basic processing units are image objects or segments, consisting of neighboring spectrally similar pixels and not just single pixels. On the other hand, sub-pixel classification techniques work at a pixel level and aim to separate the image pixel into surface material fractions (Small 2001, Plaza *et al.* 2005, 2009).

The recent evolution of remote sensing technology has resulted in the development of new multispectral, but also of hyperspectral remote sensing sensors. Hyperspectral sensors are capable of recording spectral information regarding land surface targets in numerous narrow continuous spectral bands. This allows these systems to use specific spectral information recorded by selective channels of the sensor accordingly to the characteristics of the specific problem under analysis (Galvao *et al.* 2005, Dalponte *et al.* 2009). A number of airborne and satellite hyperspectral remote sensing systems have been launched in the recent years. The Hyperion radiometer, onboard the Earth Observer-1 platform, placed in orbit in late November 2000 under NASA's New Millennium Program, is one of the most used satellite hyperspectral sensors. Hyperion is able to acquire spectral data at the reflective part of the spectrum at 242 spectral bands in total and at ground spatial resolution of 30 m. This sensor is regarded as the first 'real' space-borne hyperspectral sensor, offering the capability of frequent data acquisition of high spectral resolution from a satellite platform, at high spatial resolution.

Hyperion imagery has been the focus of LULC classification until today (Xu and Gong 2007, Pignatti *et al.* 2009, Wang *et al.* 2009, White *et al.* 2010). Different pixel-based classification algorithms have been combined with Hyperion data in various applications requiring image classification (Galvao *et al.* 2005, Wang *et al.* 2009). Various spectral unmixing classification techniques have also been combined with Hyperion data in land classification studies (e.g. Falcone and Gomez 2005, Fahimnejad *et al.* 2007). A few researchers have also evaluated the potential of the combined use of object-based classification with Hyperion (Eckert and Kneubühler 2002, Wang *et al.* 2009). Nevertheless, to our knowledge, not significant attention has been paid so far to the assessment of the combined use of Hyperion with advanced classification approaches, such as object-based classification, for LULC mapping (Walsh *et al.* 2008, Pignatti *et al.* 2009, Wang *et al.* 2010).

Understandably, being able to appreciate the extent to which different classification methods available today take advantage of the hyperspectral properties of

Hyperion imagery would be of great importance. This would be even more interesting if implemented over highly heterogeneous and topographically variable areas such as in Mediterranean landscapes, given also the relevance of LULC to desertification and land degradation (Castillejo-González *et al.* 2009).

In this context, the main objective of this study is to evaluate in a typical Mediterranean setting the combined use of Hyperion imagery with the spectral angle mapper (SAM) pixel-based, the object-based, and the non-linear unmixing classification techniques. A further objective is to investigate the effect of two approaches for training points selection in applying the SAM classifier to the Hyperion imagery, namely of pixel purity index (PPI) and of the direct selection of training points from the Hyperion imagery assisted by a QuickBird imagery and field-collected training sites.

2. Study area

The study area is located in the island of Crete in Greece, specifically in the south-eastern part of Chania prefecture (35°13′7″ Latitude and 24°5′5″ Longitude). The climate is typical Mediterranean, characterized by hot, dry summers and cool, wet winters. Elevation of the area ranges from sea level to 2200 m in the north and most of the surfaces have an inclination of at least 25 degrees, mostly with a south aspect. The vegetation formations in the study site, as in the Mediterranean areas, are a result of the lasting interaction between human and the environment. The main vegetation cover types are phryganic ecosystems, coniferous and broad-leaved forests, small-scale cultivations of various crops, few olive groves and vineyards and some Alpine vegetation at high elevations.

3. Datasets description

Earth Observer-1 Hyperion imagery over the studied region was obtained from the archive of the United States Geological Survey (USGS 2008). The imagery was acquired on 23rd May 2006 and was received as a full long scene (185-km strip) and at level 1 (L1R) processing, meaning that it was radiometrically but not geometrically corrected. In addition, a QuickBird very high resolution imagery acquired on 10th June 2003 and a Digital Elevation Model (DEM) had a spatial resolution of 20 m, both available from a previous study, were also used. The QuickBird imagery was already radiometrically and geometrically corrected, mapped to a cartographic projection with an absolute accuracy of 23 m.

The data samples collected through fieldworks were conducted in the same period of time of the Hyperion image acquisition on 16th, 17th, 21st, and 22nd March 2006 and 11th April 2006 and on 23rd May 2006. More field data were collected on 9th and 16th November 2007, 7th December 2007, 6th, 10th, 12th May 2008, and 31st October 2008. In addition, approximately 40 measurements of pure spectra of known vegetation types and land cover classes were collected during the field visits in the year 2006 using Hand Held spectrometer, and in the years 2007 and 2008 using an ASD FieldSpec® pro FR spectroradiometer (FieldSpec User's Guide 2000).

4   *A. Elatawneh* et al.

4. Methods

Land use/cover classification by applying different techniques was conducted for the study area using the acquired Hyperion imagery. An overview of the overall methodology followed is depicted in Figure 1.

4.1. Data pre-processing

Spectrum measurements in the field were collected in raw mode, coupled with measurements from a Spectralon panel to be used as a reference. Two main pre-processing steps were applied to the collected field spectra data, the conversion of the raw digital number (DN) data to reflectance, using the Spectralon reference measurements and the implementation of sensitivity drift elimination (FieldSpec User's Guide 2000). These spectra resulted from the pre-processing described earlier
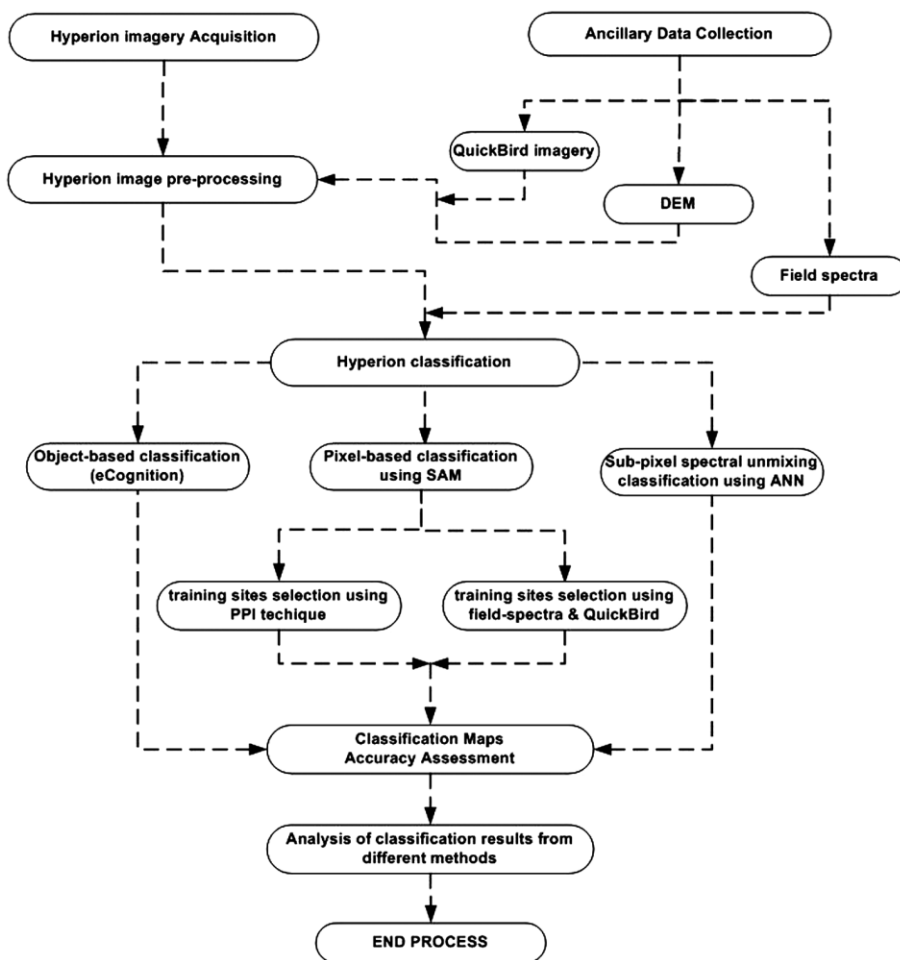
Figure 1. A flowchart summarizing the methodology followed in this study.

120

were subsequently used in the Hyperion pre-processing, specifically the Hyperion bands spectral polishing, as described next.

The first step in the Hyperion imagery pre-processing involved performing a linear interpolation of all the sensor detectors. The result was a 242-band image, with wavelengths representing the new common set of band centers, and averaged full-width at half-maximum values for each band. The next step involved the elimination of non-calibrated and the overlapping bands and performing a stripping correction to the Hyperion imagery. Atmospheric correction was then applied to the Hyperion imagery using FLAASH software (2006). FLAASH was developed by Spectral Sciences, Inc. with the cooperation of the Air Force Research Laboratory, and it is based on the Radiation Transport (RT) equation (Matthew *et al.* 2003). Following the atmospheric correction, spectral polishing was applied by applying a running average filter over nine adjacent channels, by using some of the field spectra, in order to reduce the spectral artifacts in the data (Beck 2003). This operation was also performed using the FLAASH module.

The geometric model used for orthorectification of the Hyperion image was based on the direct linear transformation (DLT) method (Imagine ERDAS 2001). The Nearest Neighbor resampling method was used along with the available DEM to perform the geometric correction, achieving a geometric accuracy of less than one Hyperion pixel (30 m). Subsequently, the resulting image was reduced to a subset of the study area, and a final pre-processing step, a minimum noise fraction (MNF) was applied in order to reduce the uncorrelated, or at most, locally spatially correlated noise, not addressed earlier by the spectral polishing approach. The MNF transformation handled the visible-near infrared (VNIR) and shortwave infrared (SWIR) data separately, since it was more efficient in managing the noise, due to its different structure in the two data sets (Datt *et al.* 2003). The Hyperion final data-set consisted of 157 bands, 49 in the VNIR and 108 in the SWIR regions. This was the data-set that was used for the image classification using the different classification approaches.

4.2. Hyperion classification

4.2.1. Hyperion pixel-based classification

The first step in performing the classification involved the definition of the classification scheme (Table 1). The classification key was developed based on the land cover map of Crete and the spectral seperability of the Hyperion data in the area. In order to create land cover map could be potentially derived from the Hyperion data in the area. Firstly unsupervised classifications (IsoData; K-Means) were implemented to the Hyperion data, whereas the IsoData performed better. Secondly the best result of the unsupervised IsoData classification was cross intersected with the available thematic maps and high resolution images of the area. By combing the CORINE land cover with the land cover map of the study area, the classification key is aligned to the classification scheme proposed by the EU for the Mediterranean (European Environmental Agency 1994).

Representative end-members of the different classes defined in the classification scheme were collected for the application of the SAM on the Hyperion imagery. Training points were collected directly on the Hyperion using two approaches. The

6   *A. Elatawneh* et al.

Table 1. Classification key which was used in the present study.

ID	Class	Class description (for more details see Section 4.2.1., 'Hyperion pixel-based classification')
1	Rocks	Large area of rocks cover mainly at high altitude and at the coastline
2	Cypress trees	*Cupressus sempervirens* in the forest
3	Pine trees	*Pinus brutia* in the forest
4	Cultivated field	Cultivated fields mainly vineyards
5	Phrygana	Low vegetation, mainly *Sarcopoterium spinosum*, *Phlomis fruticosa*, *Asphodelus albus*, *Urginea maritime*, *Coridothymus capitatus*
6	Sparse vegetation	Rarely conifers trees distributed over bare ground mainly south the village and near by the sea
7	Bare soil	Bare soil, some stones exist occasionally
8	Snow	Appears at high altitude
9	Alpine vegetation	Juniper trees at high altitude
10	Broadleaved trees	*Acer sempervirens, Quercus coccifera* in the forest
11	Olive groves	Olive plantations in Anopoli village
12	Sea	–

use of the PPI method and a method based on direct selection of well-defined training sites from the Hyperion imagery, assisted by the QuickBird imagery and field-collected training sites.

The PPI is computed by repeatedly projecting n-dimensional scatter plots on a random unit vector, where the function records the extreme pixels that reside at the edges of the vector unit (ENVI User's Guide 2008). Collection of image-based end-members was performed using the scatter-plots of MNF bands in combination with the PPI technique, a method that has also been applied previously with hyperspectral imagery (Falcone and Gomez 2005, Walsh *et al.* 2008). The PPI function was performed using only the MNF bands with the least noise, according to the MNF results (Section 4.1.), resulting in nine VNIR and the four SWIR bands. Two-dimensional scatter plots for the bands with the least noise were examined, to help identify the pure end-member pixels using this method. Examples of collected end-member spectra used to classify the Hyperion scene are presented in Figure 2.

In the second approach, end-members were obtained from Hyperion pixels representing homogenous areas, which were derived from the previously collected field training sites. In addition, the QuickBird imagery available for the region was also used in identifying the land cover fraction beneath one Hyperion pixel. Training sites were carefully determined and restricted to the most homogeneous regions with consistent land-cover. A total of 550 Hyperion pixels representing the classes defined in the classification key (Table 1) were identified as training data.

Pixel-based classification was performed on the Hyperion imagery using the SAM (Kruse *et al.* 1993) algorithm. SAM performs the classification based on the spectral similarity between image spectra and reference spectra. Reference spectra can be generally taken either from laboratory or field measurements or can be equally extracted directly from the remote sensing imagery: The method is based on the assumption that an observed reflectance spectrum is a vector in a multi-dimensional space, where the number of dimensions equals the number of spectral
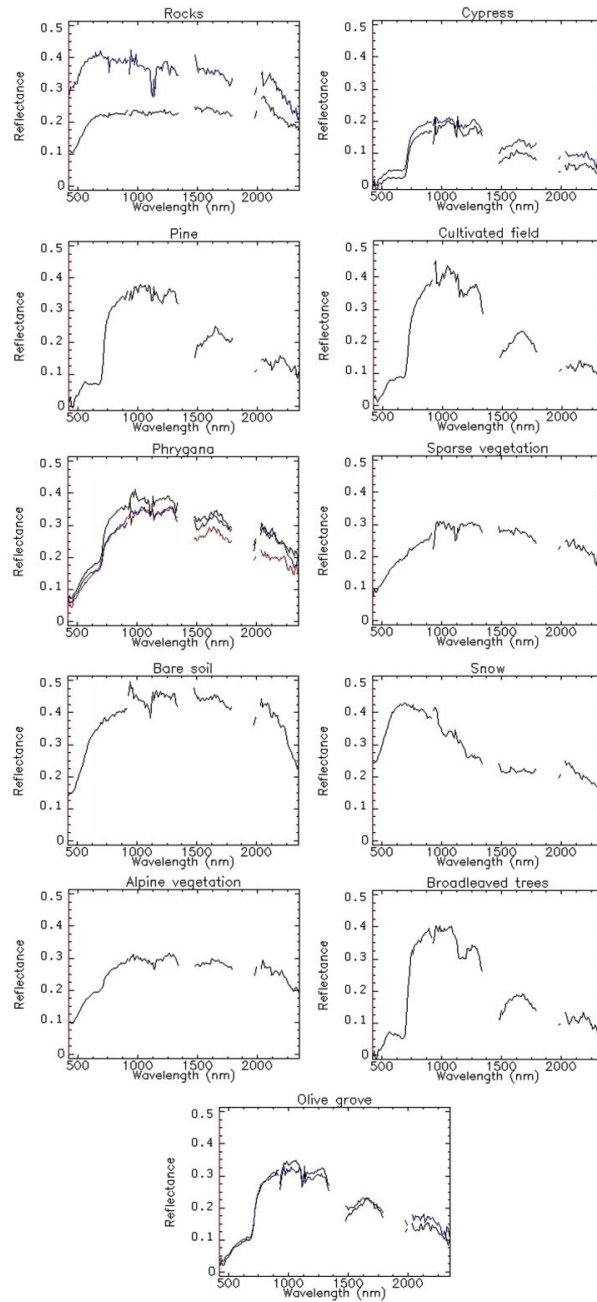
Figure 2. Examples of end-members' spectra for the classification key in our study.

8   *A. Elatawneh* et al.

bands. In SAM, spectral similarity is determined by calculating the angle between reference spectra and satellite imagery spectra to be classified treating them as vectors in n-dimensional space, where 'n' is equal to the number of spectral bands of the sensor. In an n-dimensional multispectral space, a pixel vector has both magnitude (length) and an angle measured with respect to the axes that defines the coordinate system of the space (ENVI User's Guide 2008). The angle (α) between two vectors is independent of their lengths. The angle between an unknown spectrum t to a reference spectrum r is computed by applying the following equation (e.g. Shrestha *et al.* 2005):

$$\alpha = \cos^{-1}\left(\frac{\vec{a} \bullet \vec{b}}{\|\vec{a}\| \bullet \|\vec{b}\|}\right), \tag{1}$$

which can be written as:

$$\cos^{-1}\left(\frac{\sum_{i=1}^{n} t_i r_i}{\left(\sum_{i=1}^{n} t_i^2\right)^{0.5}\left(\sum_{i=1}^{n} r_i^2\right)^{0.5}}\right), \tag{2}$$

The resulting value, computed in radians, is assigned to the corresponding pixel in the output SAM image. Small angles between the two spectrums indicate high similarity and wide angles indicate low similarity, whereas pixels with an angle larger than the tolerance level, the specified maximum angle threshold, are not classified (Kruse *et al.* 1993, Petropoulos *et al.* 2010). The threshold angle value is essentially expressing the maximum acceptable angle for the separation between the end-member spectrum vector and the pixel vector in n-dimensional space defined by the image (here the number of bands of each Hyperion image). Pixels with values higher than this threshold value are not classified.

In this study, SAM was implemented on the Hyperion imagery separately for the training sites collected by the two selection methods. This allowed the evaluation of the effect of training points selection method on the SAM-based Hyperion imagery classification accuracy. In both implementations, a training set of approximately 50 pixels per class was used. All 157 Hyperion bands were used in SAM implementation with a value of 0.11 radians set as the maximum thresholding value for all classes. This value was determined following numerous iterations of the method, using variable thresholds and evaluation of the results in terms of classification accuracy.

4.2.2. Hyperion object-based classification

In the object-based approach, image analysis consists of two main processing steps, namely segmentation and classification (Figure 3). Following segmentation, the resulting objects are intended to be used as primitive image segments, serving as information carriers and building blocks for further classification, assigned to certain classes according to their properties. Those include not just the spectral properties

International Journal of Digital Earth   9
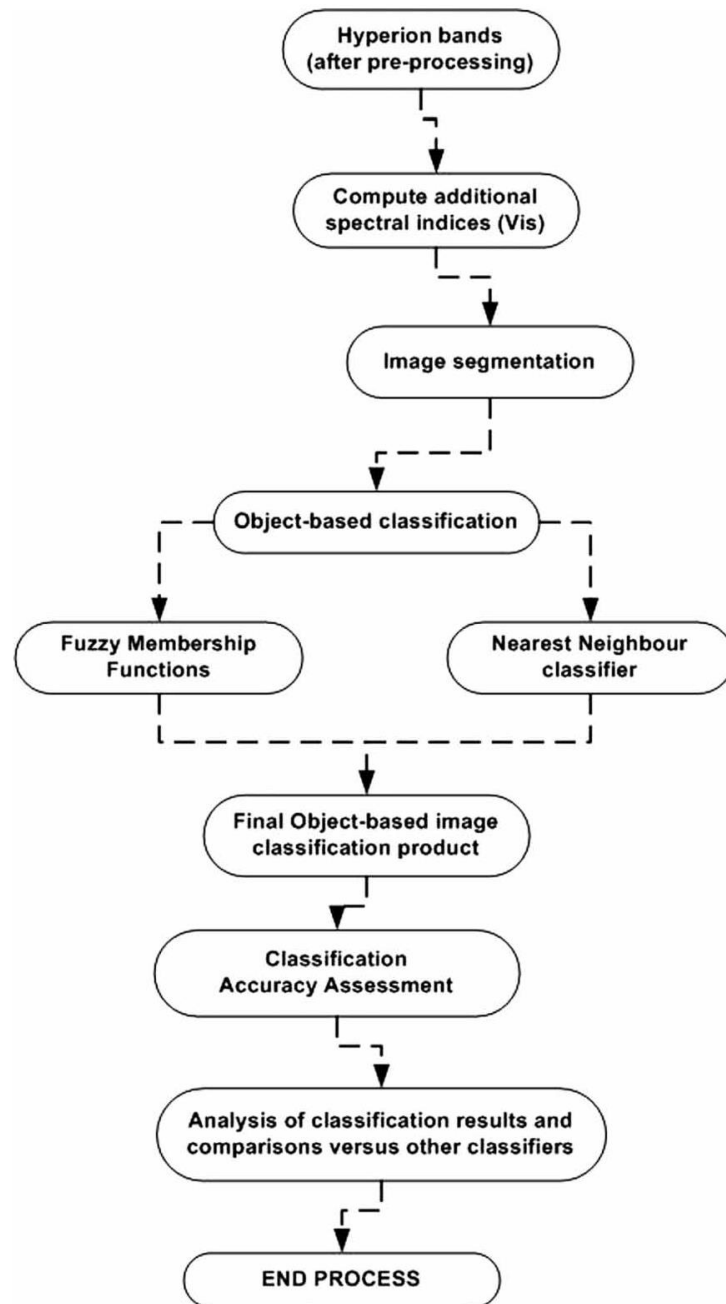
Figure 3. A flow diagram showing the object-based classification processing steps.

10 *A. Elatawneh* et al.

but also additional properties that describe the objects, such as mean value and standard deviation of shape descriptors, texture, spatial, and hierarchal neighbor-hood relations for the objects. The intention behind is always to create user-defined meaningful objects. Object-based classification was conducted in e-Cognition.

Pre-defined Hyperion bands were used in performing the Hyperion image segmentation. In addition, a range of Vegetation Indices (Thenkabail *et al.* 2000) were computed from the original Hyperion bands and included as additional layers in Hyperion image segmentation, in order to support the discrimination of the LULC classes included in our classification scheme. Initially many indices were computed and their use was examined in developing the object-based classification such as: Soil Adjusted Vegetation Index (SAVI), Normalized Difference Vegetation Index (NDVI), Blue-Green, Red-Green, NIR/Red, NIR-Red, $Band_{119}$ $Band_{133}$ (Rouse *et al.* 1974, Heute 1988). It is worth to mention here that various combination of the bands Blue (Bands 11, 12, 13), Green (Bands 18, 19, 20, 21), Red (Bands 28, 29, 30), and NIR (Bands, 55, 56, 57, 58) were used to formulate the pre-mentioned indices. Finally, a few only were eventually used based on how they assisted in better separating the LULC classes of our classification scheme, as a result of the differences in their properties. Those Vegetation Index's (VI's) included the NIR-Red ($Band_{56}$ $Band_{29}$), Blue-Green ($Band_{12}$ $Band_{20}$), Red-Green ($Band_{29}$ $Band_{20}$), as well as the NDVI. The NDVI was calculated using bands 56 and 29:

$$NDVI = \frac{Band_{56} - Band_{29}}{Band_{56} + Band_{29}}, \qquad (3)$$

Moreover, a simple difference between bands 119 and 133 in Short Wave Infra Red, at wavelength 1335 and 1476 nm, respectively, was introduced and normalized using the equation below and was subsequently added as an additional layer:

$$SWIR\_VI = \frac{Band_{119} - Band_{133}}{Band_{119} + Band_{133}}, \qquad (4)$$

These two bands were chosen in the SWIR region, at either ends of the first major water absorption feature, because they were the least noisy bands at either ends, where the slope between these two points was meant to be used. In addition, to the above indices, a new VI was introduced that was combing the NDVI and the SWIR_VI, which was expressed as:

$$NewVI = \frac{NDVI - SWIR\_VI}{NDVI + SWIR\_VI}, \qquad (5)$$

The computation of this new index from the combination of the two indices was based on the rationale that their joint use can assist in better discriminating the forest land cover from other land covers. For example, Gong *et al.* (2003) mentioned that VIs constructed with bands in SWIR and NIR produce higher correlation with leaf area index than those defined VIs that use red and NIR bands. This latter index was also used in the Hyperion image segmentation, because the segmentation process performed better when it was used, rather than when it was not.

In performing the image segmentation, apart from the specification of the layers that are included in the segmenting the image, other input parameters also required to be set. The first is the scale parameter, which is controlling the size of the objects,

generally defined empirically by a try and error approach. Here following also this approach, a value of 18 was used ensuring that the resulting objects were larger than single-pixels, but still representing homogenous areas. Other homogeneity criterion parameters were also set as follows: color 0.9, shape 0.1, smoothness 0.4, and compactness 0.6. The Hyperion bands 11, 33, 56, 110, and 191 and the additional layers NDVI, SWIR_VI, and New VI were given a weighting factor of 3, while the remaining Hyperion bands and layers were given a factor of 1. Hyperion bands with weighting of 3 were selected visually, based on high contrasts between the different land-cover types presented in the scene, and also based on the standard deviation values. The derivative image objects contained groups of homogenous pixels and in certain cases individual pixel objects were created.

Following the image segmentation, object-based classification was performed. To this end, the class hierarchy was created based on the same classification key used in the pixel-based classification (Table 1). The rule set developed for the classification of the objects resulted from the segmentation process employing fuzzy membership functions, feature thresholds and class-related features. Initially, all classes were identified from one segmentation level and subsequently certain classes were combined according to their spectral properties in the class hierarchy. The image was classified using both the nearest neighbor feature space classifier and membership functions. For the first method, the algorithm was trained with the definition of representative sample objects for each class. The membership functions were created for those classes that could be easily classified by using discrete membership functions. All functions were created according only to the spectral prosperities of the classes.

Classes such as 'sea' and 'snow' could be easily classified by using membership functions. The classes 'rocks' and 'bare soil' were classified also by using membership functions, but since the 'bare soil' class had a variety in its reflectance, two samples were taken and the Nearest Neighbor classifier was used. Similarly, the 'Phrygana' class was also classified using a membership function, but in order to prevent misclassification with the 'sparse vegetation' and 'alpine vegetation' classes, two samples were used with the Nearest Neighbor classifier. The 'alpine vegetation' class was classified using membership function that used the mean of the NDVI 'sparse vegetation,' which was also classified using a function and the 'not bare soil' and 'not rocks' functions. The 'cultivated field,' 'olive groves,' and 'broadleaved species' classes were classified by using membership functions. The 'broadleaved species' class was separated from the 'cultivated field' and 'olive grove' using the NDVI feature in a membership function in which it had a higher value for this feature. Finally the 'pine' and 'cypresses' classes were classified by using the new_VI feature which worked effectively in separating conifers trees from other species and vegetation cover, due to the combination of the NIR and SWIR bands in creating this VI.

4.2.3. Hyperion sub-pixel classification

The procedure used to determine the relative abundance of materials depicted in multispectral or hyperspectral remote sensing imagery based on the materials' spectral characteristics is called 'spectral unmixing' (Settle and Drake 1993, Adams *et al.* 1995). In spectral unmixing it is assumed that reflectance of each image pixel is a linear or a non-linear combination of the reflectance of each material

12   *A. Elatawneh* et al.

('end-member') present in any image pixel. In general, the number of end-members must be less than the number of spectral bands in order to apply this process. Also, all of the end-members present in the image should be employed (Kressler and Steinnocher 1996, Pu *et al.* 2008). The result of spectral unmixing is one image for each end-member, with pixel values between zero and one, representing the fraction of the original image attributed to the particular end-member. The results obtained by this method are generally highly dependent on the input end-members.

In this study, a sub-pixel classification through spectral non-linear unmixing algorithm employing an artificial neural network (ANN) method was applied since it has been more suitable for the discrimination of more than 10 classes (Carpenter *et al.* 1999). A logistic activation function was used. Eleven end-members that represent the classes excluding the sea class were extracted from well-defined training sites and sequentially used for the supervised classification, as well as being used initially for unmixing analysis as output nodes. The number of the nodes in the input layer was set equal to 157, which was the number of the Hyperion bands used in the classification. One hidden layer was used, as generally it has been shown that it provides satisfactory classification results (e.g. Mas and Flores 2008, Pu *et al.* 2008, Petropoulos *et al.* 2010). The training rate coefficient determined the magnitude of the adjustment of the weights, and a value of 0.3 was specified. A training momentum coefficient parameter value of 0.7 was specified and the training threshold contribution value of 0.9 was used. The training RMS exit criterion defines the RMS error value at which the training should stop and the parameter was set at a value of 0.1. The result of non linear unmixing of the Hyperion image using the ANN classifier was 11 images, in which each image was related to one class.

4.3. Hyperion classification accuracy assessment

Error matrices have been computed to control the classification process and to demonstrate the statistical classification success (Congalton and Green 1999). Sufficient samples must generally be acquired to be able to adequately represent confusion between classes and assess which classes are confused. It has been suggested that a minimum of 50 samples of each class to be included in the error matrix (Lillesand and Kiefer 1999). However, generally it is possible to calculate the number of samples per category depending on the target standard error and the presumed accuracy following equation (Crist and Deitner 2000):

$$n = \frac{p(1-p)}{s^2},\qquad(6)$$

where n is the sample size, p is the desired accuracy and s is the standard error. Applying Equation (6) with a presumed accuracy of 60% ($p = 0.6$) results in the most conservative estimate of sample size of about 30 samples per class needed to meet the criterion of a standard error of 9%. Herein, for validation purposes 170 sampling points were collected in total, based on the field visits conducted in our study region. Subsequently, evenly distributed random points were generated and added to the reference points group. Points of known reference, obtained based on the basis of our intensive fieldwork at the study area and the QuickBird imagery visual interpretation, were added to the sampling points (220 points). The combination of the

390 points were used for the accuracy assessment process. To ensure consistency in the comparisons, the same validation points were used to assess all LULC results from the implementation of the different classification techniques. Particularly for the case of the sub-pixel classification, intersection between the sampling points and 11 fraction maps was calculated for each map. The result was 11 tables in which each table illustrates the intersection for every sampling point with a percentage of the particular land cover class. Then the confusion matrix was formed by considering reference points occurring in the classified maps of percentage equal to or higher than 60% as confused points.

5. Results and discussion

5.1. Hyperion pixel-based classification

Accuracy assessment for Hyperion pixel-based classification using the SAM classifier and the PPI training sites selection technique, returned an overall classification accuracy and kappa coefficient of 32% and 0.24, respectively. These results suggested a generally poor agreement of the classification map derived with the reference data (Table 2, Figure 4). When the training sites obtained from the QuickBird imagery were used, both the overall accuracy and kappa increased to 48% and 0.41, respectively (Table 2, Figure 5). Confusion between all classes in the error matrix was also lower when training sets were selected using the latter method.

With regard to the accuracy of the individual classes, those were usually higher when the training sites were selected from the Hyperion using the QuickBird imagery and the training site, compared to when the PPI method was employed. When the PPI method was used in SAM, individual classes' accuracy ranged widely from 12% to 82%, while when the second training sites selection method employed, those varied between 13% and 100%. In both classifications, the highest class accuracy was observed in the 'snow' class, due to its characteristic reflectance response (Table 2). When the PPI method was used for training sites selection, the class with the lowest individual classification accuracy was the 'olive groves,' which was mostly confused with the 'phrygana' class. Spectral confusion between the two classes was most probably due to the scarce plantation pattern of the olives, resembling the density of phrygana bushes. When the field-based training sites assisted by QuickBird imagery were used in samples selection, the lowest accuracy was achieved for the 'sparse vegetation' class. The latter was attributed mainly to the frequent confusion with the 'phrygana' and 'alpine vegetation' classes. Notably, when training sites were identified the confusion between the 'sparse vegetation' with the 'bare soil' was reduced, in comparison with the training site selection with the PPI method, but also increased the confusion between the 'phrygana' and the 'alpine vegetation' classes (Table 2). The lower classification accuracy of the individual classes can also be partially attributed to the land cover characteristics that produced many mixed pixels, and hence similar spectral reflectance among many pixels located in different classes. Spectral variability between individual pixels belonging to one class is partly attributed to different inclination and aspect of the surface, when those pixels are scattered around the image.

The overall relatively low classification accuracy by the SAM can be partially attributed to the spectral characteristics of the classified classes, which lead to the

14

A. Elataweh et al.

Table 2. Classification results from the Hyperion classification using all classification techniques.

Classes	Rocks	Cypress	Pine	Cultivated	Phrygana	Sparse	Bare soil	Snow	Alpine vg.	Broad L.	Olive groves	Overall Accuracy
SAM techniques and the training sites selected using the pixel purity index (PPI) technique												
User	0.35	0.29	0.26	0.26	0.37	0.27	0.23	0.69	0.53	0.41	0.12	
Producer	0.35	0.24	0.21	0.22	0.50	0.31	0.26	0.82	0.42	0.36	0.14	
										Overall accuracy		32%
										Overall kappa		0.24
SAM classifier and training sites selected using QuickBird imagery and field-collected data												
User	0.55	0.35	0.94	0.70	0.48	0.13	0.39	1.00	0.37	0.53	0.36	
Producer	0.55	0.40	0.58	0.62	0.48	0.15	0.46	0.91	0.34	0.52	0.43	
										Overall accuracy		48%
										Overall kappa		0.41
Non-linear spectral unmixing classification												
User	0.80	0.71	0.70	0.89	0.38	1.00	0.41	0.65	0.30	0.79	0.32	
Producer	0.39	0.40	0.74	0.46	0.71	0.08	0.40	1.00	0.32	0.70	0.57	
										Overall accuracy		52%
										Overall kappa		0.46
Object-based classification												
User	0.94	0.90	0.97	0.73	0.80	0.80	0.81	0.92	0.97	0.71	0.71	
Producer	0.94	0.83	0.68	0.86	0.77	0.92	0.86	1.00	0.84	0.82	0.89	
										Overall accuracy		83%
										Overall kappa		0.81
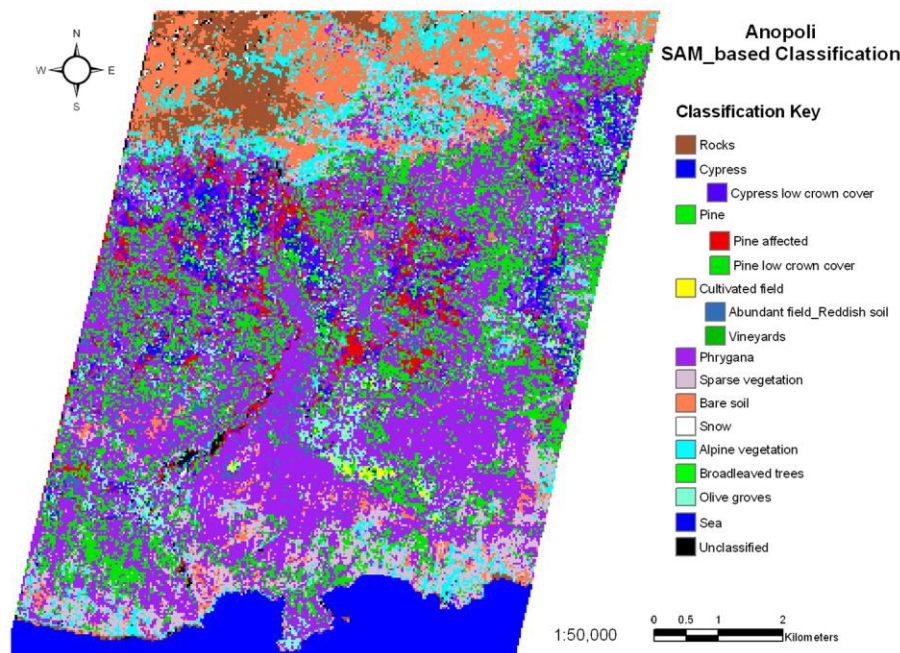
Figure 4. Hyperion pixel-based classification using training sites collected by the pixel purity index (PPI) technique.

similar spectral reflectance among many classes in the test region. This results to spectral confusion in pixels, leading potentially to classification errors for a spectral class by this method (Shrestha *et al.* 2005). The confusion between the 'phrygana' class and the 'sparse' and 'alpine' vegetation mostly occurred in the areas with less dense phryganic cover or where there were a lot of rocks amongst the phryganic vegetation. Similarly, most of the confusion between the 'broadleaved species' class and the conifers trees classes 'pine trees' and 'cypress trees' occurred in the areas where less dense broadleaved trees were found.

One of the main disadvantages of SAM is that it does not consider the sub-pixel value, which theoretically could significantly reduce possible mixing problems. The PPI method is a mathematical technique that depends on the values of bands with the least MNF, and also requires pure end-member spectra to be collected. Identification of 'pure' pixels, containing representative spectral signatures for a particular class, appears to be more efficient when visible interpretation of very high spatial resolution data are available, compared to the automated PPI method. The uncertainty behind the results of the PPI process appears to be more profound when a high degree of 'mixed' pixels is present in the Hyperion image.

Falcone and Gomez (2005) used the PPI technique to extract end-members from the Hyperion scene, using the SAM classifier for the classification of three impervious surfaces and reported high classification accuracy results. In their study, however, authors applied the PPI technique to collect 16 end-members representing diverse land cover types, mostly different vegetation types. More recently, Binal and

16   *A. Elatawneh* et al.
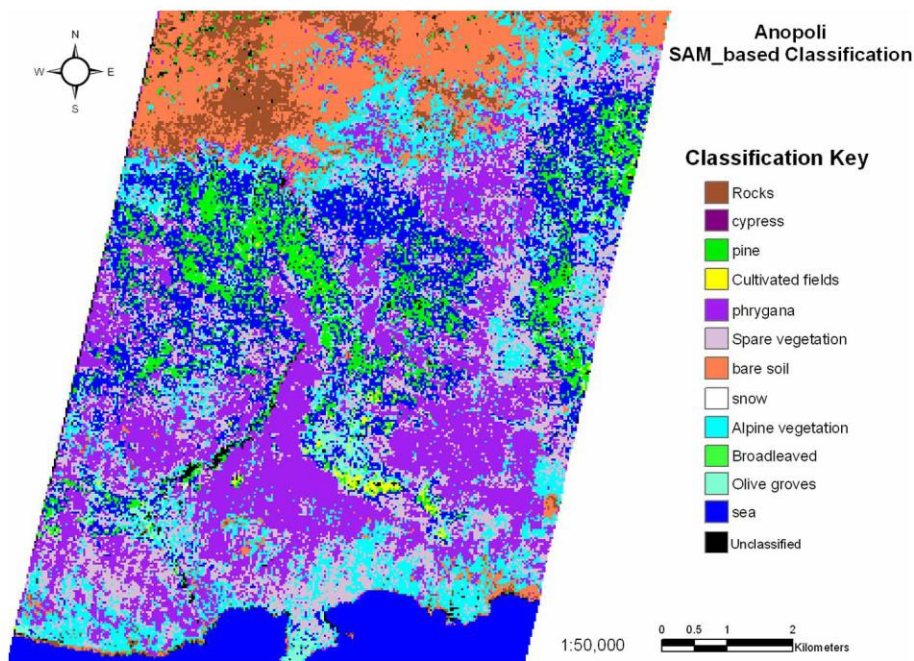
Figure 5. Hyperion pixel-based classification using training sites selected from Hyperion imagery assisted by the QuickBird imagery and field-collected spectra.

Krishnayya (2009) applied SAM with Hyperion imagery using the PPI technique for training sites selection for classifying tropical tree species in a region in India. Authors reported an overall classification accuracy of approximately 60%. The latter was attributed by the authors to the uniformity of the forest cover in the area, which was reducing the effect of within-pixel spectral variability present in more heterogeneous terrains.

5.2. *Hyperion non-linear spectral unmixing assessment*

Examples of the thematic LULC classes derived from the method implementation to the Hyperion imagery are illustrated in Figure 6. The overall classification accuracy of sub-pixel classification using the ANN algorithm was 52% (Table 2). Overall accuracies of individual classes ranged from 8% to 100% with the highest individual overall accuracy achieved in 'snow' class, and the lowest individual class accuracy was with the 'sparse vegetation,' due to the confusion with the 'phrygana,' 'alpine vegetation,' and 'olives grooves' classes. The most frequent confusion was observed between the 'phrygana' class with the 'cypresses,' 'sparse vegetation,' 'bare soil,' and 'alpine vegetation' classes, followed by confusion between 'olive groves' with 'cultivated fields,' 'phrygana,' and 'alpine vegetation' classes. Moreover, a noticeable confusion appeared to exist in the 'bare soil' and 'rocks' classes used. 'Alpine vegetation' and 'olive groves' classes were overestimated in comparison to the results returned for those classes by the implementation of the other classification
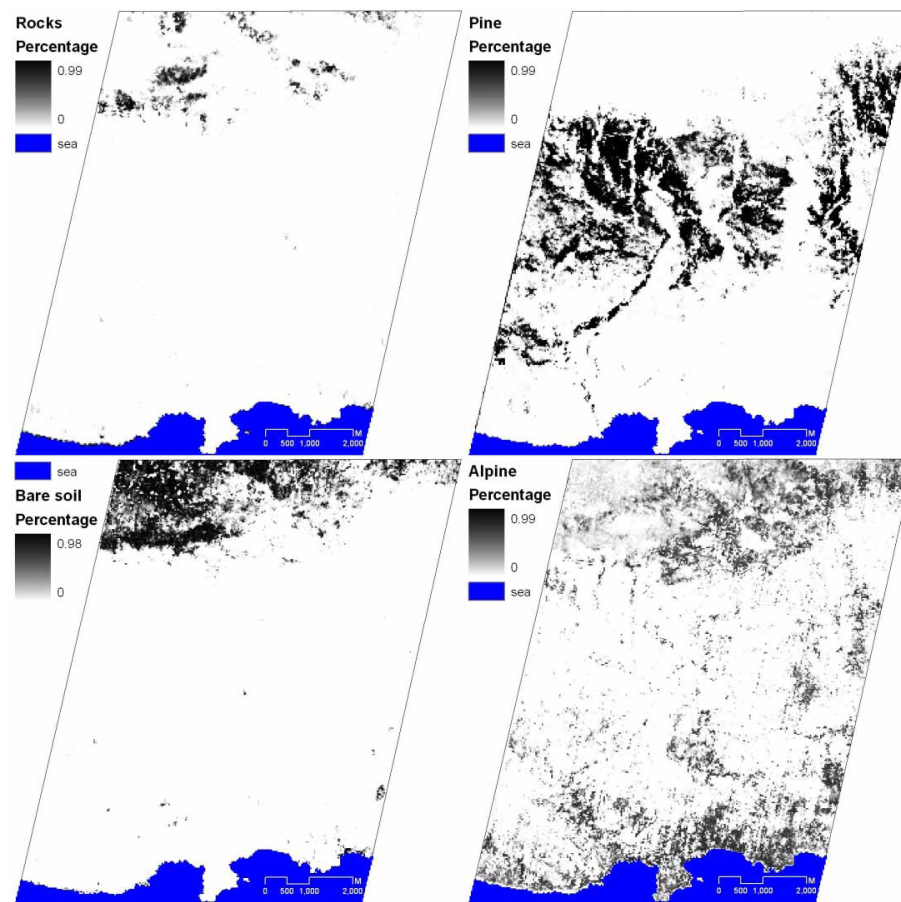
Figure 6. Abundance images result from the spectral unmixing based on Artificial Neural Network (ANN) analysis. Each of these images showed the percentage of that class estimated from the method, where darker gray tones express higher percentage, while the lighter tones a lower percentage.

techniques. A comparison with the SAM classification results (Table 2) reveals that similar misclassification occurred. However, classification results obtained from spectral unmixing are not directly comparable to those obtained by either pixel- or object-based classifications also applied herein. Other studies exploring the combined use of ANN classifier with Hyperion have also generally reported a decrease of the overall classification accuracy and classes' misclassification as a result of the training sites accuracy (Carpenter *et al.* 1999, Walsh *et al.* 2008). For example, Pignatti *et al.* (2009), using a linear unmixing classification approach, also demonstrated the ability of Hyperion imagery for discriminating land cover types in a highly complex natural ecosystem in Italy.

The higher overall classification accuracy of this method in comparison to the SAM results reported earlier is most likely due to the fact that this method is

18   *A. Elatawneh* et al.

assigning for each pixel values of the proportions of the end-members considered in the classification key. The latter results to diminishing possible spectral mixing effects between spectral similar classes, enhancing classification accuracy. A key advantage of spectral unmixing in comparison to pixel-based classifiers such as SAM, is that this provides more information regarding each class, in which the spatial extent of each class is described in a separate image, allowing to describe the cover density of each land cover class. What is more, the fraction images that are computed can be directly related to biophysical characteristics and thus, can potentially assist in improving classification accuracy (Lu *et al.* 2003). Specifically the incentive for using ANN in the spectral unmixing used in this study has been based on the fact that it has certain advantages in comparison to other techniques, since (1) it is able to learn complex patterns, allowing them to perform well, particularly when the feature space is complex and the source data has different statistical distributions, (2) it can easily adapt to different types of data and input structures facilitating synergistic studies, and (3) is able to perform supervised classification using less training data than the maximum probability (Dwivedi *et al.* 2004, Mas and Flores 2008).

5.3. Hyperion object-based classification

The object-based classification using the Hyperion imagery clearly outperformed both the SAM pixel-based and the spectral unmixing classification, returning an overall accuracy of 83% and a kappa coefficient of 0.81 (Table 2, Figure 7). Individual classes' overall accuracies ranged from 68% to 100%. Similar to the results from the previous classification techniques, highest classification accuracy was
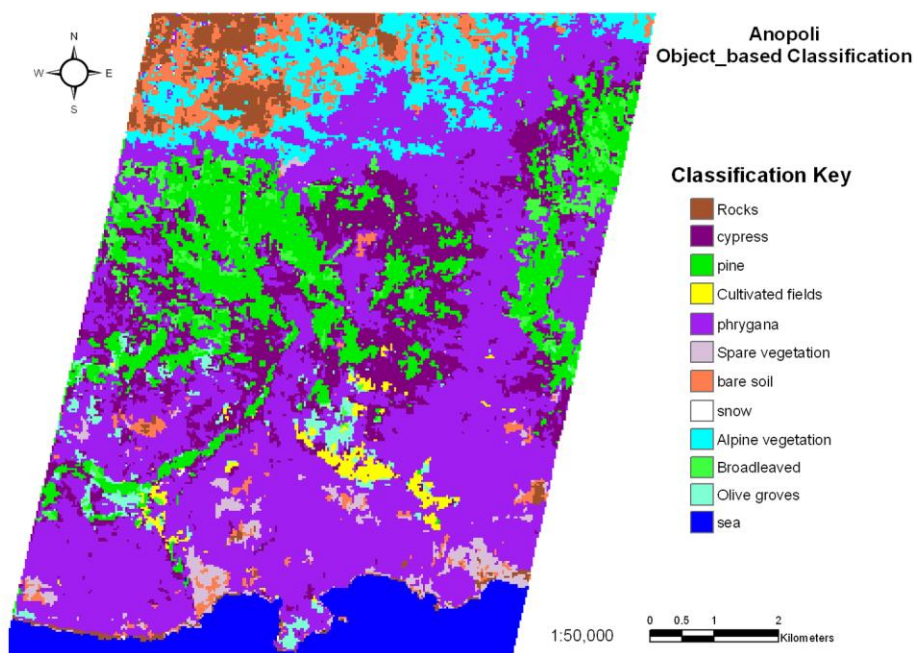

Figure 7. The Hyperion object-based classification for our study site.

134

achieved for 'snow' class, due to its distinct spectral response in comparison to that of the other classes included in our classification scheme. The 'alpine vegetation' was among the most accurately classified classes with 97% overall accuracy. The confusion in the 'alpine vegetation' class was reduced, in comparison to the pixel-based analyses, owing to the use of the membership functions in the classification process. The main confusion in 'pine trees' was with the 'broadleaved species' particularly in the areas with large and dense pine trees. In addition to the 'pine trees,' the 'rocks,' 'cypress trees,' 'snow,' and 'alpine vegetation' classes all had kappa coefficient values higher than 0.88, also representing good agreement with the reference data. The segmentation process that preceded the object-based classification which also included the use of different vegetation indices as additional segmentation layers significantly reduced the confusion among the classes, in comparison to the pixel-based classification results obtained earlier. However, slight misclassifications still occurred, particularly in the transition zones between classes. In many cases interspersed patches between two classes were misclassified as a third class, due to that segmentation delineated the object boundaries. This can be attributed largely to the spatial resolution of Hyperion in combination to the heterogeneity of the land cover in our study area. On the other hand, the confusion between the 'broadleaved species' and the 'cultivated field' classes was due to the membership function used to separate these two classes.

Our results are also in agreement with other studies comparing the performance of object-based classification versus pixel-based algorithms (including SAM), using however, multispectral imagery from sensors like QuickBird (Castillejo-González *et al.* 2009) and ASTER (Yan *et al.* 2006). Those studies have also reported object-based method producing higher overall classification accuracy than pixel-based methods. Wang *et al.* (2009) explored the potential use of object-based classification with Hyperion data for land cover mapping of a region in China, using eight classes in the classification key, reporting an overall accuracy of 88.3% and a kappa coefficient of 0.86.

All in all, the results showed that object-based classification combined with the Hyperion imagery generally provided the most accurate classification in comparison to all other techniques applied herein. Obviously, the segmentation process, combined with contextual information coming from image 'objects,' substantially assisted the achievement of high accuracy classification results, outperforming the other classification methods. Segmentation resulted in aggregating pixels into objects, which also helped reducing the pixels' variability and thus the 'salt and pepper effect,' which is often more pronounced in pixel-based classification (Yan *et al.* 2006). In object-based classification only adjacent spectrally similar pixels are combined into a single object due to the low spectral variance on one hand and the high variance with the neighboring objects on the other hand. Moreover, the scale, compactness and shape parameters play important role in determining which pixels and the number of those to be inherited in an object, hence producing more meaningful pattern and distribution of the LC classes. Various investigators have also underlined as a key advantage of the object-based over pixel-based classification, the fact that, in addition to the spectral information, additional information on image data (e.g. object size, object complexity, texture and spectral difference to neighboring objects) is available, allowing more accurate mapping and achieving higher classification accuracy (Benz *et al.* 2004, Fung *et al.* 2008).

20   *A. Elatawneh* et al.

6. Conclusions

The main objective of our study had been to evaluate the combined use of different land classification approaches with Hyperion hyperspectral imagery for performing LULC classification of a region representative of a typical Mediterranean landscape located in the island of Crete, in Greece. A further objective had been to investigate the potential added-value of the use of very high spatial resolution QuickBird imagery as well as of field-collected training samples for improving the LULC mapping from Hyperion imagery classification. LULC was derived from the Hyperion imagery using the SAM pixel-based technique, the object-based classification, and the non-linear spectral unmixing based on ANN methods.

Hyperion imagery combined with SAM and the PPI technique to collect training sites returned the lowest classification accuracy among all techniques (32%). When SAM was implemented selecting training sites directly from the Hyperion imagery with the assistance of the QuickBird imagery and the field-collected training samples, overall classification accuracy was somewhat improved (48%). Non-linear spectral unmixing classification applied using the ANN achieved a marginally higher overall accuracy of 52%. Object-based classification produced the highest overall accuracy of 83% in comparison to all other classification techniques applied herein. The latter was attributed to the combined effect of the contextual information of image 'objects' developed from the image segmentation, and the rich spectral information content of Hyperion imagery. Yet, all classification techniques applied herein appeared to suffer from the relatively low spatial and radiometric resolution of Hyperion, which also affected the spectral separation among the different LULC classes. However, the object-based technique was the least affected by these factors, mainly due to the segmentation process and the availability of object-related characteristics in addition to the spectral information. Finally, one could argue that the difference in time period of Hyperion data, QuickBird data, and ground spectral observation could be regarded as a major issue and may have caused some inaccuracies in the classification accuracies obtained. With regard to this, we would expect this factor could only have a small bearing as an error source, given that minimal changes would have been expected to have occurred in vegetation types phenology during this small period of time difference in the acquisition between the different datasets.

As our results have been based on a single Hyperion imagery analysis, those can be regarded as preliminary. Future work needs to be conducted in analogous and dissimilar implementation conditions that will allow deriving conclusive results as to the added value of Hyperion in LULC mapping when combined with advanced classification approaches, such as those used in our study. The latter, can be of particular importance from an operational perspective, as it can potentially allow obtaining efficiently, cost-effectively, and un-destructively accurate LULC cartography over large, often inaccessible otherwise regions.

given to the department facilities and the encouragement during the execution of the present study. In conclusion, authors are grateful to the anonymous reviewers for their very helpful and constructive feedback that substantially improved the originally submitted manuscript.

References

Adams, J.B., *et al.*, 1995. Classification of multispectral images based on fractions of endmembers: application to land-cover change in the Brazilian Amazon. *Remote Sensing of Environment*, 52, 137–154.

Beck, R. 2003. *EO-1 User guide*, v 2.3. Ohio: University of Cincinnati.

Benz, U., *et al.*, 2004. Multiresolution, object-oriented fuzzy analysis of remote sensing data for GIS-ready information. *ISPRS Journal of Photogrammetry and Remote Sensing*, 58, 239–258.

Binal, C. and Krishnayya, N.S.R., 2009. Classification of tropical trees growing in a sanctuary using Hyperion (EO-1) and SAM algorithm. *Current Science*, 96 (12), 1601–1607.

Carpenter, G.A., *et al.*, 1999. A neural network method for efficient vegetation mapping. *Remote Sensing of Environment*, 70, 326–338.

Castillejo-González, I.L., *et al.*, 2009. Object- and pixel-based analysis for mapping crops and their agro-environmental associated measures using QuickBird imagery. *Computers and Electronics in Agriculture*, 68, 207–215.

Congalton, R. and Green, K., 1999. *Assessing the accuracy of remotely sensed data: principles and practices* (p. 137). Boca Raton, FL: CRC/Lewis Press, 137.

Crist, P. and Deitner, R., 2000. *Assessing land cover map accuracy*. GAP Analysis Project Handbook. Moscow: University of Idaho.

Dalponte, M., *et al.*, 2009. The role of spectral resolution and classifiers complexity in the analysis of hyperspectral images of forest areas. *Remote Sensing of Environment*, 113, 2345–2355.

Datt, B., *et al.*, 2003. Preprocessing EO-1 Hyperion hyperspectral data to support the application of agricultural indexes. *IEEE Transactions on Geoscience and Remote Sensing*, 41, 1246–1259.

Dwivedi, R.S., Kandrika, S., and Ramana, K.V., 2004. Comparison of classifiers of remote-sensing data for land-use/land-cover mapping. *Current Science*, 86, 25–27.

Eckert, S. and Kneubühler, M., 2002. *Application of Hyperion data to agricultural land classification and vegetation properties estimation in Switzerland*. Switzerland: Remote Sensing Laboratories (RSL), University of Zürich.

ENVI User's Guide, 2008. *ENVI on-line software user's manual*. ITT Visual Information Solutions.

European Environmental Agency, 1994. CORINE land cover [online]. Available from: http://www.eea.europa.eu/publications/COR0-landcover. [Accessed 14 January 2012].

Fahimnejad, H., *et al.*, 2007. *Crop type classification by Hyperion data and unmixing algorithm*. Hyderabad, India: GIS development, Map World Forum.

Falcone, J.A. and Gomez, R. 2005. Mapping impervious surface type and sub-pixel abundance using Hyperion hyperspectral imagery. *Geocarto International*, 20 (4), 3–10.

FieldSpec® Pro User's Guide, 2000. USA. Analytical spectral Devices, Inc.

FLAASH Module User's Guide, 2006. ENVI, ITT Industries, Inc.

Fung, T., *et al.*, 2008. Analysis of green space in Chongqing and Nanjing, cities of China with ASTER images using object-oriented image classification and landscape metric analysis. *International Journal of Remote Sensing*, 29 (24), 7159–7180.

Galvao, L.S., Formaggio, A.R., and Tisot, D.A., 2005. Discrimination of sugarcane varieties in Southeastern Brazil with EO-1 Hyperion data. *Remote Sensing of Environment*, 94, 523–534.

Gong, P., *et al.*, 2003. Estimation of forest leaf area index using vegetation indices derived from Hyperion hyperspectral data. *IEEE Transactions on Geoscience and Remote Sensing*, 41, 1355–1362.

Heute, A.R., 1988. A soil-adjusted vegetation index (SAVI). *Remote Sensing of Environment*, 25, 295–309.

Imagine ERDAS, 2001. *User guide. ERDAS Inc.* Atlanta, GA, 339–370.

A. Elatawneh et al.

Kavzoglu, T. and Colkesen, I., 2009. A kernel functions analysis for support vector machines for land cover classification. *International Journal of Applied Earth Observation and Geoinformation*, 11, 352–359.

Kressler, F. and Steinnocher, K., 1996. Change detection in urban areas using satellite images and spectral mixture analysis. *International Archives of Photogrammetry and Remote Sensing*, XXXI (PartB7), 379–383.

Kruse, F.A., Lefkoff, B., and Dietz, J.B., 1993. Expert system-based mineral mapping in Northern Death Valley, California/Nevada, using the airborne visible/infrared imaging spectrometer (AVIRIS). *Remote Sensing of Environment*, 44 (2), 309–336.

Lillesand, T.M. and Kiefer, R.W., 1999. *Remote sensing and image interpretation*. 4th ed. USA: John Wiley & Sons, Inc, 592–597.

Lu, D. and Weng, Q., 2007. A survey of image classification methods and techniques for improving classification performance. *International Journal of Remote Sensing*, 28 (5), 823–870.

Lu, D., Moran, E., and Batistella, M., 2003. Linear mixture model applied to Amazonian vegetation classification. *Remote Sensing of Environment*, 87, 456–469.

Mas, J.F. and Flores, J.J., 2008. The application of artificial neural networks to the analysis of remotely sensed data. *International Journal of Remote Sensing*, 29, 617–663.

Mathur, A. and Foody, G.M., 2008. Crop classification by support vector machine with intelligently selected training data for an operational application. *International Journal of Remote Sensing*, 29 (8), 2227–2240.

Matthew, M.W., *et al.*, 2003. *Atmospheric correction of spectral imagery: evaluation of the FLAASH algorithm with AVIRIS data*. Orlando, FL: Algorithms and Technologies for Multispectral, Hyperspectral, and Ultraspectral Imagery IX. SPIE, 474–482.

Petropoulos, G., *et al.*, 2010. A comparison of spectral angle mapper and artificial neural network classifiers combined with Landsat TM imagery analysis for obtaining burnt area mapping. *Sensors*, 10, 1967–1985.

Pignatti, S., *et al.*, 2009. Evaluating Hyperion capability for land cover mapping in a fragmented ecosystem: Pollino National Park, Italy. *Remote Sensing of Environment*, 113, 622–634.

Plaza, J., *et al.*, 2005. *Automated generation of semi-labeled training samples for nonlinear neural network-based abundance estimation in hyperspectral data*. Seoul (S. Korea): IGARSS 2005, 1261–1264.

Plaza, A., *et al.*, 2009. Recent advances in techniques for hyperspectral image processing. *Remote Sensing of Environment*, 113, 110–122.

Pu, R., *et al.*, 2008. Spectral mixture analysis for mapping abundance of urban surface components from the Terra/ASTER data. *Remote Sensing of Environment*, 112, 939–954.

Rouse, J.W. Jr., *et al.*, 1974. Monitoring vegetation systems in the Great Plains with ERTS. *In*: *Third ERTS Symposium*, vol. 1, NASA SP-351, Washington, DC: U.S. Government Printing Office, 309–317.

Settle, J.J. and Drake, N.A., 1993. Linear mixing and the estimation of ground cover proportions. *International Journal of Remote Sensing*, 14, 1159–1177.

Shrestha, D.P., *et al.*, 2005. Analysis and classification of hyperspectral data for mapping land degradation: an application to southern Spain. *International Journal of Applied Earth Observation and Geoinformation*, 7, 85–96.

Small, C., 2001. Estimation of urban vegetation abundance by spectral mixture analysis. *International Journal of Remote Sensing*, , 1305, 22, 1334.

Thenkabail, P.S., Smith, R.B., and Pauw, E.D., 2000. Hyperspectral vegetation indices and their relationships with agricultural crop characteristics. *Remote Sensing of Environment*, 71, 158–182.

United States Geological Survey USGS, 2008. *EO1 User guide*. [online]. Available from: http://eo1.usgs.gov/userGuide/index.php?page=program [Accessed 14 January 2012].

Walsh, S.J., *et al.*, 2008. QuickBird and Hyperion data analysis of an invasive plant species in the Galapagos Islands of Ecuador: implications for control and land use management. *Remote Sensing of Environment*, 112, 1927–1941.

Wang, J., *et al.*, 2009. Application of geographic image cognition approach in land type classification using Hyperion imager: a case study in China. *International Journal of Applied Earth Observation and Geoinformation*, 12, 212–222.

Wang, Z., *et al.*, 2010. An automatic region-based image segmentation algorithm for remote sensing applications. *Environmental Modelling and Software*, 25, 1149–1165.

White, J.C., *et al.*, 2010. Characterising temperate forest structural and spectral diversity with Hyperion EO-1 data. *Remote Sensing of Environment*, 114, 1576–1589.

Xu, B. and Gong, P., 2007. Land-use/land-cover classification with multispectral and hyperspectral EO-1 data. *Photogrammetric Engineering & Remote Sensing*, 73 (8), 955–965.

Yan, G., *et al.*, 2006. Comparison of pixel-based and object-oriented image classification approaches – a case study in a coal fire area, Wuda, Inner Mongolia, China. *International Journal of Remote Sensing*, 27 (8), 4039–4055.

Copyright Clearance Center

RightsLink

Home | Account Info | Help | Live Chat

Taylor & Francis
Taylor & Francis Group

Title: Evaluation of diverse classification approaches for land use/cover mapping in a Mediterranean region utilizing Hyperion data

Author: Alata Elatawneh, Chariton Kalaitzidis, George P. Petropoulos, et al

Publication: International Journal of Digital Earth

Publisher: Taylor & Francis

Date: Mar 16, 2014

Copyright © 2014 Taylor & Francis

Logged in as:
Alata Elatawneh
Account #:
3000881941

LOGOUT

Thesis/Dissertation Reuse Request

Taylor & Francis is pleased to offer reuses of its content for a thesis or dissertation free of charge contingent on resubmission of permission request if work is published.

BACK | CLOSE WINDOW

Our Ref: LA/TJDE/P3237

05 March 2015

Dear Alata Elatawneh

Thank you for your correspondence requesting permission to reproduce the following material
from our Journal in your thesis and to be posted in the university's repository Technische
Universität München

Material Requested: Evaluation of diverse classification approaches for land use/cover mapping
in a Mediterranean region utilizing Hyperion data, Alata Elatawneh, Chariton Kalaitzidis, George
P. Petropoulos & Thomas Schneider published in International Journal of Digital Earth, Vol7:3,
pp194-216(2014)

We will be pleased to grant permission on the sole condition that you acknowledge the original
source of publication and insert a reference to the article on the Journals website:
http://www.tandfonline.com/

This is the **authors accepted manuscript** of an article published as the version of record
International Journal of Digital Earth © 05 Feb 2014
http://www.tandfonline.com/doi/full/10.1080/17538947.2012.671378

Please note that this license does not allow you to post our content on any third party websites or
repositories.

Thank you for your interest in our Journal.

Yours sincerely

Lee-Ann

8.2 Publication 2

Schneider T., Elatawneh A., Rahlf J., Kindu M., Rappl A., Thiele A., Boldt M., Hinz S. 2013 Parameter Determination by RapidEye and TerraSAR-X Data: A Step Toward a Remote Sensing Based Inventory, Monitoring and Fast Reaction System on Forest Enterprise Level; In: Krisp JM, Meng L, Pail R, Stilla U, eds. 2013. Lecture Notes in Geoinformation and Cartography. Berlin, Heidelberg: Springer Berlin Heidelberg, S. 81-107

Parameter Determination by RapidEye and TerraSAR-X Data: A Step Toward a Remote Sensing Based Inventory, Monitoring and Fast Reaction System on Forest Enterprise Level

Thomas Schneider, Alata Elatawneh, Johannes Rahlf, Mengistie Kindu, Adelheid Rappl, Antje Thiele, Markus Boldt and Stefan Hinz

Abstract State forest administrations in Central Europe have to adapt to future climatic and socioeconomic conditions. This results in new demands for up-to-date and precise forest information—especially with regard to the increase of forest damages by natural hazards. Remote Sensing techniques are appropriated for delivering information in support of such tasks. We present details of a research project that focuses on the demonstration of the potential of satellite data for forest management planning and disaster management. Integrated in the over-all concept of a decision support system (DSS) for the forest–wood chain (Entscheidungs-Unterstützungs-System Forst-Holz, EUS-FH), the frame conditions for a 'Remote Sensing based Inventory and Monitoring System' for the forest-wood chain are developed. Particular focus is on investigations towards synergistic and complementary use of the two German satellite systems RapidEye and Terra SAR-X. The comparison is done on base of the accuracy of parameter derivation with each of the systems. The results deliver a couple of arguments for combined multispectral and SAR data use for monitoring and fast response situations in case of sudden calamities. But it reveals as well that the references against the results should be compared and, at the end, which represents the data layers to be updated, do not always fit from both, the semantic meaning e.g., the definition of 'forest' to

T. Schneider (✉) · A. Elatawneh · J. Rahlf · M. Kindu
Institute of Forest Management (IFM), Technische Universität München (TUM),
Munich, Germany
e-mail: Tomi.Schneider@tum.de

A. Rappl
Bavarian State Institute of Forestry (LWF), Freising, Germany

A. Thiele · M. Boldt · S. Hinz
Karlsruhe Institute of Technology (KIT), Institute of Photogrammetry and Remote Sensing (IPF), Karlsruhe, Germany

81

cartographic differences, and the representation of object categories. Harmonisation of definitions and categories to be mapped is needed.

1 Introduction

Worldwide forest resources are affected by global change phenomena. In connection, Central Europe state forest administrations have to adapt to future climatic and socio-economic conditions. The Bavarian forest sector is faced with a situation where climate change effects seem to destabilize forest ecosystems, the socio-economic demands on the ressource "forest" are continuously increasing and budgets for managing forests are cut. Significant biotic and abiotic calamity frequency increases are attributed to climate change. More than 30 % of the annual workload of a forest enterprise in Bavaria is in response to such unpredictable events. The different functions of a forest are more and more understood as social benefits and claimed by the society in the sense of stakeholder rights. In addition, national and international reporting duties are to be fulfilled by the owners and/or governmental bodies. To cope with all these diverse tasks a decision support system (DSS) (Entscheidungs-Unterstützungs-System Forst-Holz, EUS-FH) was designed for the forest-wood chain. An assessment study performed to figure out the needs of forest practitioners in forest management resulted in a list of parameters. The highest relevance was assigned to the parameters forest area, gaps, forest border length, forest changes, tree species groups, stand/tree height, and forest densities. These parameters should be updated timely for a sound decision support system (Felbermeier et al. 2010).

Amongst others, a major trigger of the activities toward such a DSS is the improved quality of the new class of high-resolution satellite imagery. Hence, current research and development deals with the opportunities of a 'Remote Sensing based Inventory and Monitoring System' for the Bavarian forests. The concept is based on the idea of integrating existing data offered by official sources such as: the Bavarian Surveying and Geoinformation Administration (LVG), the Bavarian State Forest Administration and others along, with remote sensing data as the most actual information layer. The geodatabases provide the 'a-priori' information used for restricting the solutions of the image analysis process and the results are used to update these databases. The system should be able to steer management operations and especially to support management decisions at the strategical/tactical level of a forest enterprise. At the final stage, the information system should contribute to facilitate the diverse national and international reporting duties as well.

This general approach became possible due the improved capabilities of the new generation of high-resolution and fast-revisiting remote sensing satellite systems (e.g., RapidEye, WorldView-2, TerraSAR-X, Cosmo-SkyMed soon ESA's Sentinels). The presented research is funded by the Federal Ministry of Economics and Technology, within a program of the Space Agency of the German

Aerospace Center (DLR). The program aims to promote the synergistic use of optical and radar satellite data with special emphasis to the new German systems RapidEye (RE) and TerraSAR-X (TS-X). Taking into consideration the high revisit frequency and the large area covering capability of RE, an annual update of the forest databases for whole Bavaria is likely possible. The clouds and daytime independent operation ability of the TS-X system should help, especially in the calamity case to identify the affected areas. Such a fast response capability should allow starting preventive measures within a short time and such reducing the following damages and economic losses. Apart from these basic expectations, the determination accuracy of forest parameters with each of the systems is in the focus of the project. From multi-seasonal RE data, an improvement of tree species differentiation is expected. While the prospect of high spatial resolution TS-X data is an improvement in structure parameter determination such as heights, canopy roughness, border and gaps or even single tree detection. Within the present project stage, the under development system components should demonstrate the continuous data flow required for the future operational system.

2 Previous Work

Forest mapping by remote sensing is done from the global to the local scale. Systems, mapping scale and aims are different. Remote sensing as an operational tool is established on the global and the local scale. On global scale, particular parameters like the forest coverage and the derived variables such as: biomass, LAI, CO_2-sinks and radiation budget, etc. are of high interest. The target is either the small scale documentation of forested areas or the derivation of input variables for models; the scale is of 1:250.000 and less.

On local scale, very high resolution (VHR) systems are required. The data usage is primarily for orientation (orthophoto) and in support of management actions. Aerial photographs and since a couple of years LIDAR (Light Detection and Ranging) are the most frequently used systems, followed by Quick Bird type satellite data. Mapping scales in the range of 1:10.000 and larger are targeted.

In between, at the regional to continental level with typical mapping scales of 1:25.000–1:250.000, the implementation of remote sensing methods in operational applications is still missed, at least in Germany. The concept of the 3rd National Federal Forest Inventory 2011/12 for Germany is not considering remote sensing data as information source. Nevertheless, there are a couple of studies demonstrating the potential of using the high resolution data type, e.g., for continental mapping purposes (FIRS, Corine) but for national inventories (2nd National Forest Inventory of Germany) or FAO's AfriCover concept.

This section provides an overview on forest related information extraction concepts and methods. First, a brief overview about standard Bavarian State forest inventory concept is given, followed by optical and microwave based mapping methods.

2.1 Bavarian State Forest Inventory Concept

The Bavarian State forest administration inventory concept is based on a permanent regular sample point grid net. The inventories should provide an overview over the area managed by an enterprise. The envisaged update frequency is of about 10 years, an expansion up to 12–15 years is not a singularity. Each inventory point represents a forest area of 2–4 ha. The sample point area is differentiating an inner circle of 31,25 m^2, a mid-circle of 125 m^2 and an outer circle of 500 m^2. Inside the inner circle all trees with a diameter breast height (dbh) <11 cm are registered, in the mid circle trees with dbh between 11–29 cm and in the outer circle all trees with dbh >29 cm. At least the parameter tree species, dbh, tree height, crown closure, timber stock, stand structure are measured or registered and the regeneration is estimated (Anonymous 2001; Knoke et al. 2012)

Typically, one year after an inventory the forest operations for the next period are planned. For forest planning, orthophotos are used for steering the ground survey. The produced management maps display the established new stand borders, forest operations planned for the next period, forest functions and special treatment areas as well as single trees like standards, seed trees, clearing rests. Tree species share per stand, age, condition, etc., are mentioned in the tabular records and associated comments. Interim inventories for forest status assessment, wildlife damages, vegetation status assessments, etc., are performed supplementary.

2.2 Forest Mapping by Very High Resolution Systems

Traditionally, in Bavarian forest, aerial photographs are used in support of inventories, for management planning and monitoring. In most cases, aerial photographs are visually interpreted, in special cases by using 3D analyser for a map output (Rall and Martin 2002; Heurich 2006). In practice, orthophotos are mostly used for orientation and direct decision support in the field. Since a couple of years digital analytical work stations are used to extract forest relevant parameter for special cases like inventory and monitoring of Natura 2000 plots. As well as, for forest status assessment and mountain forest monitoring (Seitz et al. 2011; Waser et al. 2008). The LVG is covering the whole area of Bavaria with digital aerial photographs every three years.

Since about two decades, LIDAR systems are in the focus of forest research. LIDAR is the most accurate system in tree height and crown size determination. As full waveform system, a tomography like insight into forest canopies is possible, delivering information on the vertical structure of forests (Heurich 2006, Reitberger et al. 2008a, b). Recent research presented solutions for single tree identification even when crowns are interlaced (Reitberger et al., 2009). The 1 m, 2 m and 5 m grid digital terrain model (DTM) for Bavaria is based on LIDAR data. An update of that data base is not planned at present.

In the concept of the EUS-FH DSS, digital aerial photographs are used for base inventories of the Bavarian forests. Forest heights are derived by difference between the (VHR) LIDAR DTM and a digital surface model calculated from the digital aerial photographs of the LVG. VHR satellite data of the QuickBird type are not considered presently for forest parameter extraction by the Bavarian state forest administration.

2.3 Mapping by High Resolution Optical Systems

In general, high resolution optical systems means, the 5–30 m ground resolution category (e.g., Landsat type systems). The aims of forest related evaluations at this interim scale might be structured into: classification of forest cover (area), estimates of forest structure (tree species composition, age, height, etc.), forest change detection and forest growth simulations (management tool).

The trend in data analysis is toward parameters assessment. While typical classification results are strongly dependent on input data, classification method and operator experience, parameters may vary in accuracy of determination but the information is comparable. Further, a forest description on base of parameter is in line with forest management data and such facilitate modeling approaches like simulations of forest growth Pretzsch (2002) or calamity distribution dynamics (Kautz et al. 2011).

The pixel sizes of the high resolution category data type do not allow single tree detection and have always to be treated as mixed pixels. Fehlert (1984) by computer simulation and Kenneweg et al. (1991) by empirical experiments proved that in the range of the RapidEye ground resolution of 6,5 m a pixel wise classification must fail because of the mixed pixel problem. Object oriented analysis methods bypass this problem by using pixel aggregations as base objects for categorization (deKok et al. 1999; Schneider et al. 2000, Tiede et al. 2006, Eckert 2006). Already deKok et al. (1999) postulated, that for a monitoring system under Bavarian State Forest conditions it may be sufficient to rely on high resolution data to detect changes. Precondition is an established data and comparison base. Eckert (2006) demonstrated for a test site in Argentina with forests of similar complex structure like the ones we have to deal with in Mid-Europe, that high resolution data of different origin (Aster, Landsat) are appropriated to extract forest parameters with an acceptable accuracy for regional surveys. In Scandinavian countries, in Canada, etc. with extensive forest management systems the usage of high resolution data is standard.

In the present study, high resolution optical data are provided by Rapid Eye. The data are limited on the visible (VIS) and Near Infrared (NIR) spectral range, but firstly offer the option of multi-seasonal evaluations with a space operating system. The option of repeated observations under slightly changing appearances over the objects of interest is expected to bring advances in tree species identification and parameter determination.

2.4 Mapping by Microwave Systems

Synthetic Aperture Radar (SAR) remote sensing is an active imaging method based on microwave signals, which is—in contrast to optical remote sensing—independent of sun-illumination. Furthermore, the amplitude of the received signals is nearly free from atmospheric clutter (clouds, fog, etc.), so that SAR facilitates mapping tasks also under worse weather conditions. The high resolution of the new SAR satellite sensor generation (up to 1 m ground sampling distance) and the possibility of obtaining repeat and single-pass interferometric SAR (In-SAR) data from multiple images make this data attractive for the extraction of both radiometric and geometric/structural parameters. Hence, SAR data are commonly used for purposes of classification, elevation extraction, and change detection.

Approaches of classifying forest areas using SAR data utilizing the possibilities of SAR polarimetry are given in Sato and Koike (2003) and Lee et al. (2005). The combination of SAR image data with optical or hyperspectral image data and Lidar data are investigated in Volden et al. (1998), Zhang et al. (2008), Hilbert et al. (2010), and Ackermann et al. (2010). Other evaluations detecting forest areas treat the analysis of SAR texture (Kourgli and Belhadj-Aissa 2009). In Kirscht and Rinke (1998), a method of reconstructing the 2.5 dimensional structure of elevated objects (e.g., buildings and vegetation like trees and forest) is described by utilizing their radar shadow length in airborne SAR image data.

Lemp and Koch (2009), analyzed forest areas by using TerraSAR-X image data. They focused on the problem of separating forest from grassland, which show similar backscatter intensity and statistics dependent on surface roughness, incidence angle and look direction. Furthermore, they state that an interferometric evaluation is impossible since the TerraSAR-X data show high decorrelation in forest areas. Therefore, a combined analysis of multi-frequency data (e.g., L-band and X-band images) is recommended. This problem of InSAR and PolInSAR phase decorrelation in repeat-pass datasets was also stated by Koch (2010), whereby for example, single-pass interferometry, facilitated by the TanDEM-X mission, could solve this problem.

In De Zan et al. (2009) multi-baseline InSAR data of this new TanDEM-X mission were simulated to show the high potential for height extraction. Already with few interferograms promising results of extracting height profiles in vegetated areas were achieved. One further method extracting tree and forest heights is provided by SAR tomography, for example by using airborne data (Reigber and Moreira 2000) or an upcoming satellite mission (Cloude and Papathanassiou 2008).

In this study, we use first high resolution repeat-pass TerraSAR-X data alone.

3 Parameter Extraction from RE and TS-X Data

To consider various growth conditions the study covers different growth regions of Bavaria (Fig. 1).

Fig. 1 Test site locations across the growth zones of Bavaria

The focus of the paper is on image analysis. The aim is to show which kind of forest parameters are extractable from the electro-optical RE data and the microwave TS-X data respectively and which accuracies are retrievable with each of the systems (complementarities). Due to the fact that data take opportunities for the first observation period 2009 fit neither the time frames nor the areas, the present paper highlights solely examples demonstrating the approach. Accordingly, the image analysis starts by independently processing the multi-spectral and radar data.

Due to the high geometric and orbital accuracy and resolution of the data, the prospect in our case is an improvement in forest structure parameter determination like heights, canopy roughness, border and gaps or, in special cases, even single tree detection. Improvements in tree species identification are expected by the multi-seasonal imaging option of RE. The key in this case are the changes due to phenology. The expectations are toward fingerprint like profiles of tree species types.

The presented results have to be seen as the entrance step for tree species differentiation. Solely the assessment of the first set of the above listed parameters is addressed. Examples are shown for the assessment of the parameter forest area, border length, gaps and forest tree groups 'coniferous', 'broadleaved' and 'mixed' as well as for forest height estimations and change detection options. These parameters are controlled by the pixel size and may be considered as 'stable' or 'static', at least over the period of one season.

Table 1 Geodata provided by Bavarian State authorities used for verification

Geodata	Date	Producer
ATKIS-Basis-DLM (Amtlich-Topographisch Kartographisches Informations System, official topographic-cartographic information system)	2009	LVG
TN (Tatsächliche Nutzung, land use data)	2010	LVG
FÜK (Forstliche Übersichtskarte, forest overview map)	2009	LWF

3.1 Hypotheses

Hypothesis 1: Forest management relevant parameters are derivable from Rapid-Eye and TeraSAR-X data. The hypothesis is tested on base of multi-seasonal RapidEye and TerraSAR-X data from up to five test sites in different growth regions of Bavaria.

Hypothesis 2: The combination of both data sets improves the forest determination. Each of the sensors has specific advantages in parameter extraction. The hypothesis is tested by combining parameter derivable exclusively from each of the sensors in a synergistic manner.

Hypothesis 3: The complementarities of the two sensor concepts facilitate fast reactions in the disaster case. The hypothesis is tested in the frame of change detection studies by comparing the potential of detecting structural changes with both systems.

3.2 Data

3.2.1 Geodata

Geodata are provided by the Bavarian State Institute of Forestry (LWF), the Bavarian Surveying and Geoinformation Administration (LVG), and the Traun-steiner Stadtwald community forest administration. The data layers used for first verification purposes are listed in Table 1.

The ATKIS-Basis-DLM is a digitized land cover model based on the Bavarian topographic map 1:25.000 with an accuracy of $\pm$ 3 m (Katzur and Franke 2007). It has the same information about land cover use as the map TN, which is based on cadastral data and digital orthophotos. FÜK is a product of the LWF and shows the property pattern of state, private and municipal forests of Bavaria.

3.2.2 RapidEye Data

The RapidEye satellite constellation consists of five satellites carrying on-board the push broom sensor Jena Spaceborne Scanner JSS 56. Each sensor is capable of collecting image data in five distinct bands of the electromagnetic spectrum: Blue

Parameter Determination by RapidEye and TerraSAR-X Data   89

Table 2 RE images of the five test sites for five different phenological stages

Test site\phenology	2nd	3rd	4th	5th	1st
Traunstein er Stadtwald	17.05.2009	29.07.2009 01.08.2009	07.09.2009	23.09.2009[a]	11.05.2010
Bayerischer Wald	23.05.2009	01.08.2009 15.08.2009	01.09.2009	27.09.2009	
Freisinger Forst	20.05.2009	27.07.2009		22.09.2009[a]	22.04.2010
Oberammergau	20.05.2009	27.07.2009		20.10.2009[a]	29.04.2010
Iphofen/Steigerwald	17.06.2009		24.08.2009	23.09.2009[a]	19.04.2010

[a] images with large cloud coverage

(440--510 nm), Green (520–590 nm), Red 630–680 nm), Red-Edge (690–730 nm) and Near-Infrared (760–880 nm). The dynamic range is covering 12 Bit, the ground sampling distance 6,5 m, resampled to 5 m pixels. At 75 km swath width, this constellation offers large area coverage and a frequent revisit interval of 2–5 days.

Radiometric and geometric corrected level 3A data were ordered to cover each test site at least five times across the vegetation period from spring to autumn. The delivered data sets for the 2009 vegetation period are listed in Table 2. The second vegetation period to be analysed was planned for 2011.

3.2.3 TerraSAR-X Data

SAR data were provided by the German TerraSAR-X satellite system. Due to the daylight independence and the nearly all-weather capability of radar systems the acquisition chance depends more on system workload than on weather conditions. The test site specific image parameters are summarized in Table 3.

Hence, we focused first on the recording of repeat-pass images to allow InSAR analysis and second on a temporal overlap with the RapidEye acquisitions to support the fusion purpose. The SAR images are recorded in Spotlight Mode, in HH polarization, with a wavelength of 31 mm (X-Band). The incidence angle θ varies between 27 and 49 degree and the geometric slant range resolution is about 1.2 m. In addition to the 15 images of 2010, for change detection purpose, new acquisitions in 2011 and 2012 are planned.

3.3 Methods and Results

3.3.1 Pre-processing of RapidEye Data

The multi-seasonal image analysis to be performed with the RE datasets requires a precise georectification as well as an atmospheric correction at the highest possible level. The accuracy of the geometric correction of the images was checked, and most of the images were spatially matched together in each test site. However,

Table 3 Summary of test site specific TerraSAR-X image parameters

	First acquisition	Repeat-pass interval	θ	Orbit
Traunstein Stadtwald	20.05.2010	11 days (2 img.)	30°	Ascending
Bayerischer Wald	23.05.2010	11/22 days (4 img.)	42°/48°	De-/ascending
Freisinger Forst	30.05.2010	11 days (2 img.)	49°	Ascending
Oberammergau	02.06.2010	11 days (3 img.)	27°/33°	De-/ascending
Iphofen/Steigerwald	16.06.2010	11 days (4 img.)	33°	Ascending

some of the images that did not match were corrected by applying specific amount of shift in both direction (easting and northing). The final achieved RMSE is below 0.8 pixel. The atmospheric correction was applied for all images in each test site, by using ATCOR 3, implemented in PCI Geomatica 10.3.

3.3.2 Processing of RapidEye Data

To extract forest parameters from RE data an object-oriented analysis technique was employed using eCognition Developer 8 program of the Trimble Company (Baatz and Schäpe 2000, Schneider et al. 2000). Two levels of segmentation were created, the upper level to delineate the forest areas and the lower level to extract the tree species groups. For the upper level of segmentation, scale parameter of 60 was chosen, while for the shape and compactness parameters 0.3 and 0.2 respectively. For the lower level, the parameters were set to 15 for scale, 0.2 for shape and 0.6 for compactness. In addition, layer weights were set to 5 for the NIR, 3 for the red edge, green and blue bands, and 1 for the red band.

The second step is the classification of the created objects. The set of features for classification was selected by the help of the feature space optimization tool implemented in eCognition. The first step of the hierarchical classification rule set was to separate the urban areas and the water bodies, by analyzing the NDVI and NIR layers in the upper level. Then the forest areas were classified as described in the following subsection. Afterwards, the lower level was segmented and classified into deciduous, coniferous and mixed forest stands.

3.3.3 Parameter Extraction from RapidEye Data

Forest Boundaries (border length and area): Due to the different land use and ownership of Bavarian landscape, the task to delineate the forest boundaries is of great importance. Within the study we tried thatfore to figure out which phenological stage is best suited for a forest boundary determination and, second, which is the improvement by a multi-seasonal analysis. Forest masks were created for each study area from each mono-temporal dataset, as well as from the combination of all the images multi-seasonal analysis. For the extraction of the forest areas in the mono-temporal analysis the layer of brightness, NDVI and the ratios Blue/Green were selected. While in the multi-seasonal analysis the brightness and the ratios Green/Blue were used.

Parameter Determination by RapidEye and TerraSAR-X Data   91

Table 4 Error matrix of the RE multi-seasonal forest mask calculated with different GIS-layers of different administrations in Bavaria

Error matrix	Overall accuracy (%)	KHAT
ATKIS-Basis-DLM	94.69	0.89
TN	94.38	0.88
FÜK	91.35	0.82

Table 5 Overall accuracy of mono and multi-seasonal RE data takes evaluations for each parameter, subset Freising test site

Parameters	Overall accuracy			Multi-temporal (%)
	Mono-temporal seasons			
	22.04.2010 (%)	20.05.2009 (%)	27.07.2009 (%)	
Forest area	95.15	90.86	94.56	94.69
Gaps	98.82	97.92	98.48	99.11
Group of tree species	67.87	66.11	69.71	67.13

The first attempt to verify the evaluation success on base of the forest management maps was not successful. Forest management maps are produced to support production, are restricted on enterprise areas and differ in content, accuracy and actuality. Nevertheless, with regard to a future operational phase the result assessment should be performed on basis of official map sources. Maps with forest area layers are produced by different authorities. The maps finally used for these comparisons are listed in Table 4.

The result of the error matrix between ATKIS-Basis-DLM, TN and FÜK illustrate that the overall accuracy of ATKIS-Basis-DLM is the best, quite close followed by TN. Fig. 2 shows the comparison of RE forest masks [a, b, c] of different vegetation stages. The combined or multi-seasonal evaluation [d] delivered the most accurate forest mask [f]. A visual example of the fitting of the produced RE masks with the ATKIS-layer is shown in examples [e, f].

Extraction of Gaps: There are two forest gap types to be considered. Permanent unstocked areas e.g., wood storage and short term gaps due to clearance but calamities (storm throw, bark beetle attack, etc.). Especially the detection of the last category of gaps is of great importance for the DSS. The rule-sets developed for forest area determination have been expanded for a gap assignment rule (…surrounded by…). The evaluation of gap mapping success proved to be difficult. In general, there are no records on temporary gaps after clearings or disasters. Identification and delineation of gaps is such producing a new information layer. The results of the comparison against the ATKIS-Basis-DLM are displayed in Table 5.

Classification of Forest Types: The mono-temporal and multi-seasonal classification of the lower level of segmentation used the layers of Near-Infrared (NIR) and NDVI for the separation between the coniferous and deciduous tree stands. After first iteration, many objects were still unclassified due to the existence of the mixed stands in the area. Visually, most of these objects were identified as mixed
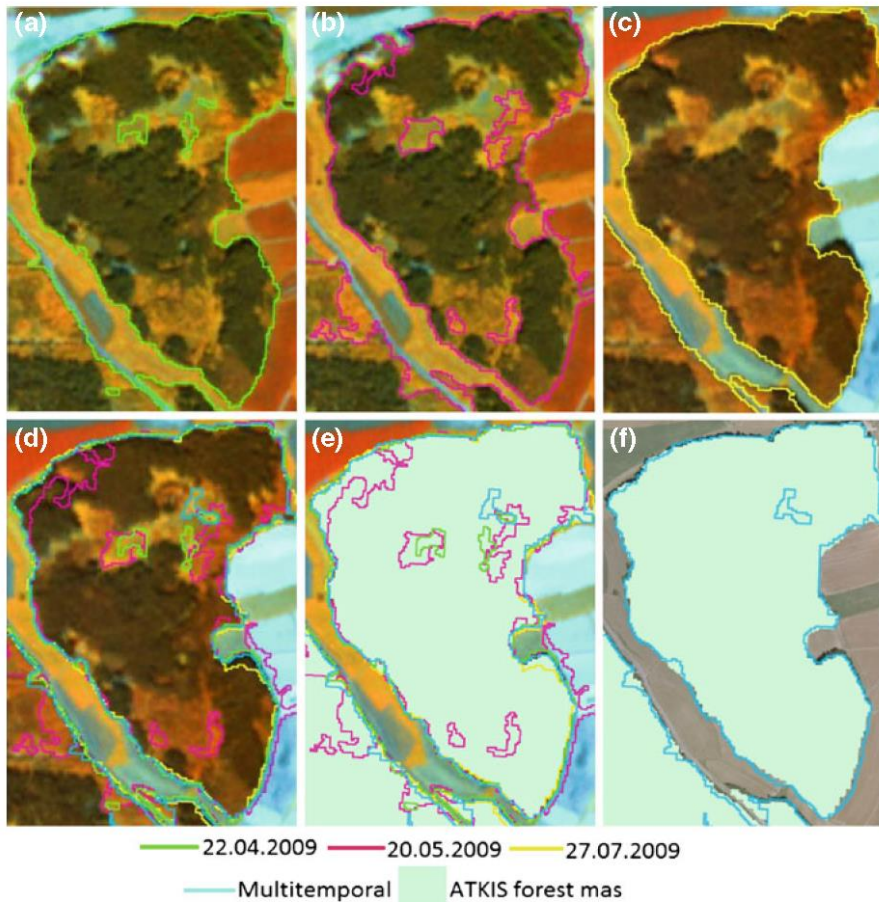
Fig. 2 Result of forest boundary extraction using RE image overlaid with mono and multi temporal extracted boundaries: forest boundaries from the images with date 22.04.2010 (**a**), 20.05.2009 (**b**), 27.07.2009 (**c**), RE image form 27.07.2009 overlaid with mono and multi temporal (**d**), RE image form 27.07.2009 overlaid with mono and multi temporal forest mask and ATKIS-Layer (**e**), orthophoto overlaid with multi temporal boundaries and ATKIS-Layer (**f**)

forest or shaded areas. Eventually the shaded areas in the forest were classified by using the NDVI layer value into mixed forest and streets in the forests that was later on excluded from the forest area Fig. 3a.

As post classification step, the forest type classifications were grouped within the state forest stands borders in GIS. Whereas, the classification result was tabulated within the state forest stands borders using 'tabulate area' function in zonal tool in Spatial Analyst Tools of ArcMap environment. The result was a detailed description for each stand. Figure 3b shows the percentage of the deciduous and coniferous trees within each stand.
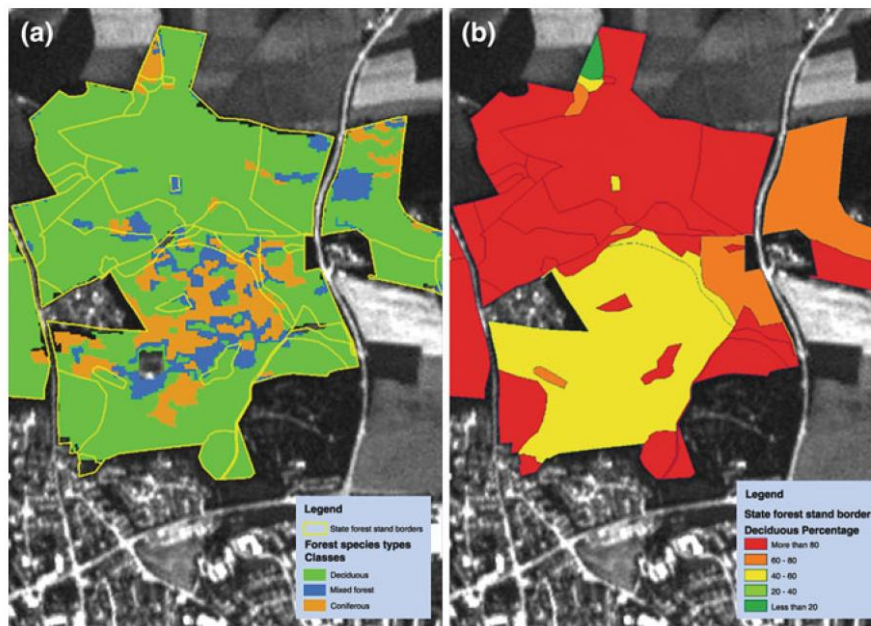
Fig. 3 Multi-temporal classification for the main tree species groups (**a**), and Forest stands with the percentage of deciduous trees in each stand according to the forest management records (**b**). Freising test site

The different group of tree species; coniferous, deciduous and mixed forest tree groups were classified and compared with the ATKIS-Basis-DLM in an error matrix.

3.3.4 Evaluation of Parameter Extraction Success

According to the results of the official GIS-layer assessment, the ATKIS-Basis-DLM forest layer was chosen for verifying the performance of the mono- to multi-seasonal forest mask and the accuracy of the parameter extraction (Table 4). For this task an error matrix (Lillesand et al. 2004) was generated with a point raster for the entire study area in Freising, with a point spacing of 50 m (total points 15928) (Straub et al. 2008). Table 5 gives an overview about the accuracy of the parameter determination for each mono and the multi temporal dataset.

The overall accuracy for the parameter forest area shows the highest agreement with the ATKIS-Basis-DLM forest layer for the image from the 22.04.2010 (Table 5). The generated multi-seasonal mask and the mask from the 27.07.2009 data show quite similar agreements. Only the mask from the 20.05.2009 data set shows a 4 % lower agreement. These results demonstrate that even a mono-temporal forest mask may be sufficient for forest non-forest delineation.

The overall accuracy in Table 5 for all images shows a good result of gap detection, especially the multi temporal dataset has an accuracy of 99.11 % with the gaps of the ATKIS-Basis-DLM. Again, the multi temporal layer includes all different vegetation spectral patterns, hence a more precise detection of the gaps is possible.

First results of group of tree species classification have an overall accuracy between 66.11 % and 69.71 %. The KHAT index (Congalton 1991) of the error matrix has a value between 0.44 and 0.50. Several factors have an influence on the classification for example different vegetation stages of the trees, training areas, quality of the images and especially the verification data. Therefore, a better result will be expected, if the comparison is done by inventory data.

3.3.5 TerraSAR-X Data Evaluation

In comparison to optical data analysis, our SAR image analysis takes advantage of the higher geometric resolution of the imagery and focuses in particular on structural parameters. In the following subsection, the geocoding procedure is described—the most important step for fusion and assessment. Subsequently, several approaches of automatic extraction of forest parameters are described and first results are shown.

3.3.6 Preprocessing of TerraSAR-X Data

The side looking SAR imaging principle leads to a projection of the recorded intensity values in slant range geometry. For this reason, the image position of an object is characterized, on one hand, by the azimuth position parallel to the flight track and, on the other hand, by the range position representing the distance between SAR sensor and object on ground. Due to this cylindrical geometry, the SAR signature of objects is different to optical images, which are generally taken in central perspective and/or parallel projection. Consequently, the appearance of elevated objects is very different; a displacement towards the sensor's nadir axis in SAR images and reversed in optical data (Thiele et al. 2006). Therefore, the requested fusion of the multi-sensor data, the assessment with GIS data, and the fusion of satellite images taken from ascending and descending orbits require a step of geocoding to achieve SAR information in world coordinate system. The correct geocoding, also called orthorectification, of a pixel in a SAR image can be determined based on the sensor carrier navigation data and the known distance between sensor and corresponding ground points. And hence, a good Digital Surface Model (DSM) including all elevated objects is required. Effects due to even small deviations of the navigation data from the true sensor position and missing height information in the elevation data are discussed in Thiele et al. (2006).

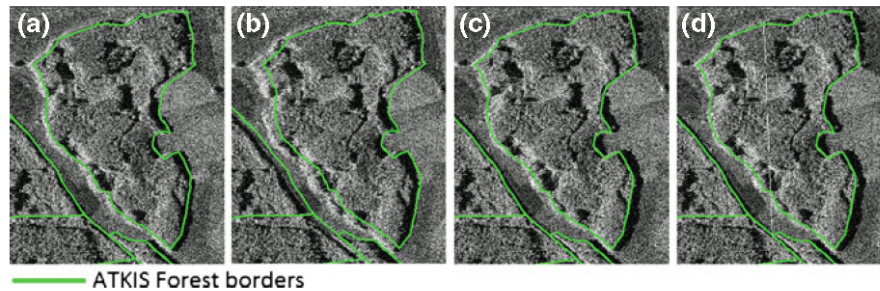Parameter Determination by RapidEye and TerraSAR-X Data   95

Fig. 4 Result of geocoding using mean terrain height from SAR header (a), SRTM heights (b), DGM5 (c), and DGM2 (d). Freising test area, subset

For this study, height models of different quality level are available, the "scene average height" extracted from the TSX metadata, SRTM data, a DGM5 and a DGM2 of the LVG. Additionally, high quality navigation data are delivered by DLR. The different results of geocoding overlaid with GIS information are shown in Fig. 4. As can be seen, the orthorectification results are reasonably good. For our purpose a high level of precision is requested, which can be better achieved by the use of the DGM5 and DGM2.

3.3.7 Processing of TerraSAR-X Data

For the subsequent parameter extraction depending on the workflow, slant range as well as ground range images are used. Radiometry based steps are done in slant range geometry to avoid interpolation effects, high level steps and assessment steps are accomplished in ground range geometry.

3.3.8 Parameter Extraction from TerraSAR-X Data

Extraction of Forest Boundaries: The signature of forest in the SAR images is characterized by rather high average magnitude values, which is mainly caused by volume scattering. Furthermore, side-looking geometry of the SAR system and the height of the trees lead to the layover (l) phenomenon appearing at objects facing towards the sensor and the shadow (s) phenomenon on object parts hidden for the sensor.

For automatic segmentation and classification of forest areas, we select two information layers, the magnitude and the local coefficient of variation (CoV). The CoV layer exploits SAR image statistics, which is dominated by the speckle effect—a multiplicative noise well known for all coherent imaging systems. In detail, the CoV is the ratio of standard deviation and mean intensity in a local neighbourhood $<I>$(Eq. 1).
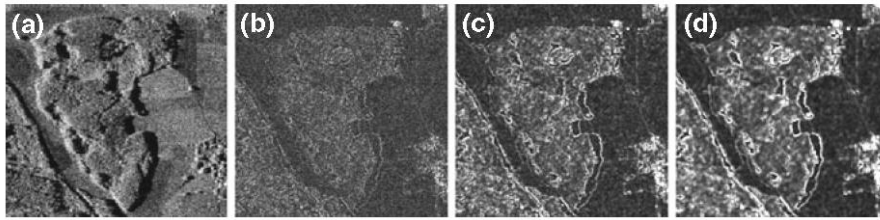
Fig. 5 Input layers of forest boundary extraction in a subset of the Freising test area: magnitude layer (**a**), CoV layer with window size 5 × 5 pixel (**b**), 9 × 9 pixel (**c**), and 13 × 13 pixel (**d**)

—— ATKIS Forest borders   ▇ Extracted Forest Boundaries

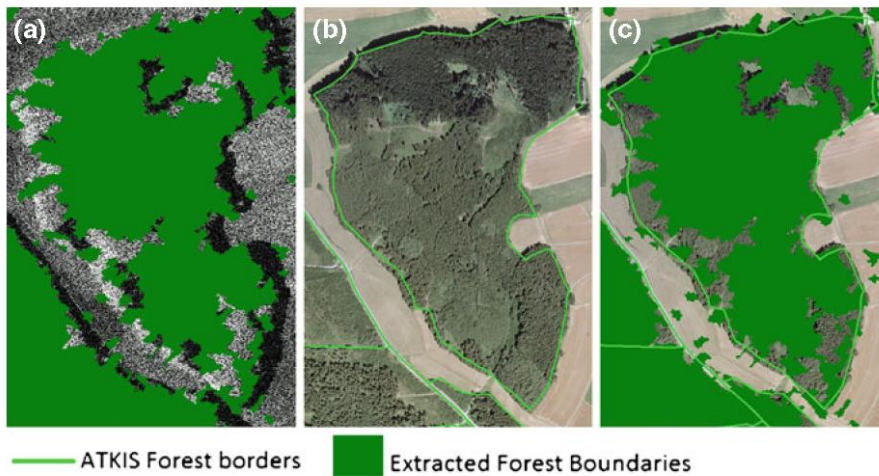**Fig. 6** Result of forest boundary extraction of a subset of the Freising test area: SAR magnitude image overlaid with extracted boundaries (**a**), orthophoto overlaid with ATKIS layer (**b**), and orthophoto overlaid with extracted boundaries and ATKIS layer (**c**)

$$CoV = \frac{\sigma}{\langle I \rangle} \qquad (1)$$

The local CoV is a good feature to distinguish between homogeneous and heterogeneous areas in SAR images with respect to the chosen window size (local neighbourhood). Different window sizes (see Fig. 5) are tested to differentiate between homogeneous vegetation (e.g., fields and grassland) and heterogeneous forest areas.

The results are given in Fig. 6 showing an overlay of orthophoto and GIS layer. The visual assessment shows a good overlap between SAR boundaries and ATKIS layer. Differences are visible in the level of detail, in the classification of enclosed grassland, and the misclassification of some Agricultural land. An improvement is expected by decreasing segmentation level, which is currently limited by image size.
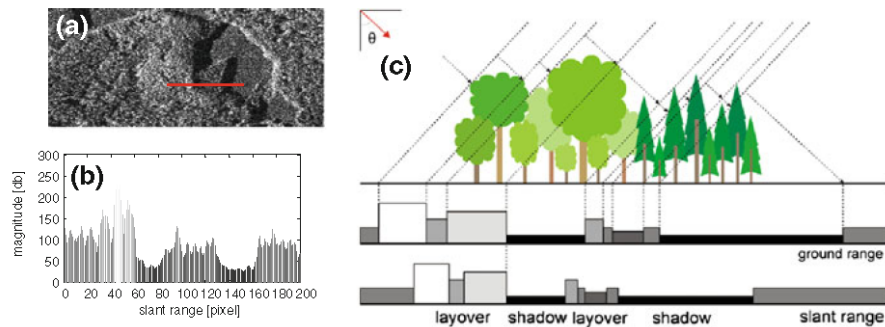
Fig. 7 Magnitude signature of deciduous trees and conifers and red marked slant range profile (**a**), slant range magnitude profile crossing deciduous trees and conifers (**b**), and scheme of backscattering situation for given profile (**c**). Bavarian Forest test area

Extraction of Forest Heights: The extraction of forest heights focused on the analysis of the already mentioned layover and shadow areas at forest borders. Similar to optical data, where the illumination by sun leads to the shadow, also the length of radar shadow s_{slant} contains information of object height. Furthermore, the length of the layover phenomenon (Bamler 2000) l_{slant} leads to a nearly similar relation between incidence angle θ and object height h (see Eq. 2), which allows in some cases a redundant estimation of the object height.

$$h = s_{\text{slant}} \cdot \cos \theta \qquad \text{and} \qquad h = \frac{l_{\text{slant}}}{\cos\theta} \qquad (2)$$

Next to the "simple" height estimation, more complex height relations can be analyzed due to growing situations visualized in Fig. 7. Deciduous trees in near range appear bright in the magnitude profile due to the high volume scattering. Behind them, a short shadow part can be observed caused by the height difference between deciduous trees and following conifers. Subsequently, the lower volume scattering of conifers leads to lower magnitude values in the slant range profile. The shadow area afterwards corresponds to the conifer height. With the assumption of nearly homogenous height distribution in small areas of same tree species, for this example the extraction of conifer and deciduous tree height is possible. Of course, competitive effects such as gaps, stands, clear-cut rests, or spurious shadow areas hamper height extraction by this method.

Besides this theoretical description of height extraction, our initial work focused on the comparison of layover and shadow measurements. Therefore, manual slant range measurements are accomplished in a forest area covered from ascending and descending orbit to achieve the mentioned redundant estimations. Furthermore, temporally correlated field measurements were realized. A magnitude image marked with the calculated tree heights is shown in Fig. 8. In Table 6, the estimated and the measured heights are listed.

The measurements based on the layover areas (*l*) show higher differences to the ground truth measurements than the ones based on shadow areas (*s*). In most

Fig. 8 SAR magnitude
image with marked locations
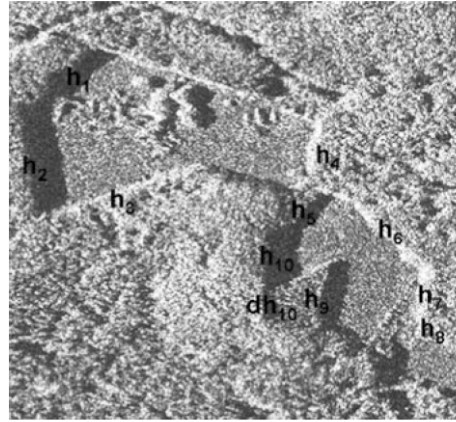of height estimation,
Bavarian Forest

Table 6 Summery of height
estimation by manual image
based and field measurements

Height	Descending orbit	Ascending orbit	Ground reference
h_1	25 m (l)	26 m (s)	appr. 30 m
h_2	27 m (l)	29 m (s)	aprx. 30 m
h_3	18 m (s)	–	aprx. 30 m
h_4	29 m (s)	27 m (l)	32.5 m
h_5	–	15 m (s)	20.5 m
h_6	13 m (s)	26 m (l)	21–32 m
h_7	29 m (s)	32 m (l)	30.5–32.5 m
h_8	13 m (s)	14 m (l)	15.5 m
h_9	15 m (s)	18 m (s)	20.4–24.6 m
h_{10}	25 m (l)	28 m (s)	30.5 m
dh_{10}	–	10 m (s)	–

cases, heights extracted from SAR images are underestimated, which can be
contributed to the partial penetration of the tree crowns at the very top. A rigorous
assessment between extracted and real measured height values is difficult. This is
due to spurious shadow areas in the SAR images and large height variations at the
real forest boundary. Nonetheless, the values of h_9, h_{10}, and dh_{10}, show that the
concept of combining relative heights (Fig. 7) fits quite well for this example. The
implementation of a semi-automated and fully automated approach for forest
height extraction is in process.

Estimation of Forest Density: In addition to the boundaries and the heights, the
forest density is also an important parameter to describe forest characteristics.
Forest density is related to stand **age** and **gap** occurrence. Next to the *CoV* layer,
also a shadow layer, an intermediate result of the forest boundary extraction, is
useful for this estimation. Especially, shadow areas enclosed from forest regions
are a measure of gappy forest areas. As older the forest as more gaps occur and as
rougher the surface appearance. Based on pyramid like changing of the segmen-
tation level, the discrimination between open space, glades, gaps and gappy
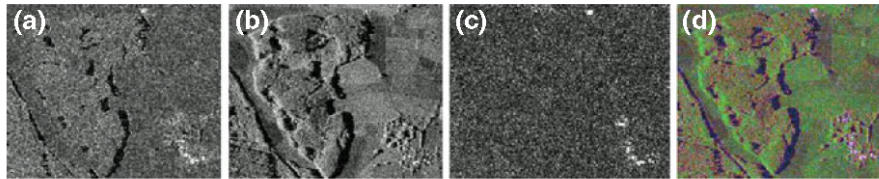
Fig. 9 Input layers of classification; coefficient of variation (**a**), SAR magnitude (**b**), interferometric coherence (**c**), result of CoVAmCoh layer stacking (**d**). Freising test area, subset

growth could be possible. Implementations toward density determinations for gap detection and age estimates are still in process.

Classification of Forest Types: The classification of different forest types is an additional task of this project. As first goal, discrimination into three classes—deciduous, conifer and mixed forest is envisioned. Therefore, three information layers are investigated, the *CoV*, the amplitude and the coherence. The local coherence *Coh* describes the correlation between two repeat-pass SAR images (S_1 and S_2), whereby high *Coh* values (~ 1) indicate coherent areas (e.g., urban area) and low Coh values (~ 0) independent signals due to high variation (e.g., vegetation).

$$Coh = \left| \frac{\langle S_1 \cdot S_2^* \rangle}{\sqrt{\langle S_1^2 \rangle \cdot \langle S_2^2 \rangle}} \right| \tag{3}$$

A reasonable way to visualize the contained information is the CoVAmCoh-Analysis presented in Schulz et al. (2009). The three input layers shown in Fig. 9 are arranged like RGB layers, with *CoV* as red, amplitude as green and *Coh* as blue layer.

The additive colour mixing emphasizes local features, for example, changes appear yellow, deciduous trees bright green, and fallow land blue. The eCognition software is a useful tool for multi-resolution segmentation. It is also useful for the fuzzy classification of the data based on suitable membership functions adapted to the three classes (deciduous, conifer and mixed forest).

4 Integration of RE and TS-X Evaluations

The integration of synergistic and complementarities options from both data types are considered of major importance for the DSS. Forest characterisation and change detection are presented as examples.

In Table 7 the ability of forest parameter determination of the two systems are weighted against the success of the most precise remote sensing method for this parameter. Solely, for the diameter at breast height (dbh), one if not the most important parameter in practice, no reference RS system is available, and a RS data based evaluation is not possible.

Table 7 Forest parameter determination accuracy at the local to regional scale from the RE and TS-X in comparison to competing Earth Observation systems. As reference the system with the best performance is given (+++)

RS system type/ parameter	RapidEye	TS-X	World View-2	Hyperspec. Scanner	Aerial photogr. (LVG)	LIDAR
Forest area	++	++	+++	++	+++	+++
Border length	++	++	+++	++	+++	+++
Stand height	–	+	+	±	++ (st)	+++
Gap	+	++	+++	++	+++	+++
Single tree	±	+	+	±	++	+++
Crown diameter	–	±	+	±	++	++
Dbh	–	–	–	–	–	±
Stand structure	+++	±	+++	+++	+++	+++
Conif./broadl.	+++	±	+++	+++	+++	+++
Broadl. species	++	–	++	+++	++	+
Conif. species	+	–	+	+++	++	++
Timber volume	±	±	+	+	++	+++
Age	±	±	+	+	++	+++
Repetition frequency	+++	+++	±	–	±	–
Data take restrictions	+	+++	+	+	+	+++
Area coverage	+++	++	±	–	+	–
Data evaluation costs	+++	+	±	+	++	+
Information costs	+++	+	±	++	++	+

+++—reference, ++—good, +—fairly good, ±—estimate, – not possible; dbh = diameter at breast height; data evaluation costs = work load for data analysis per unit area; Information costs = quality of information weighted against are coverage; st = stereoscopic analysis required; LVG = data of the regular Bavarian State survey; area coverage = annual is set as reference

The analysis of Table 7 lets us easily identify the synergy potential between TS-X and RE. While the advantages of RE are in species differentiation, area coverage and costs, TS-X is adding information on stand height, gap detection, single tree detection (in some cases) and has no data take restrictions in the emergency case.

The complementarities are given for the parameters area, border length and gap detection, all of them parameters describing static structure elements. The simultaneous data take and evaluation of that data during the development phase allow to determine the assessment accuracy and to use that information in case only one data set is available (disaster scenario).

With regard to change detection, the high repetition frequencies of the two systems are the key properties, allowing the immediate detection after occurrence. In case of TS-X repeat-pass data allows the detection of changes, e.g., by evaluating the already mentioned coherence, which is a measure initially introduced to assess the quality of the phase stability of an interferogram. Since coherence is a
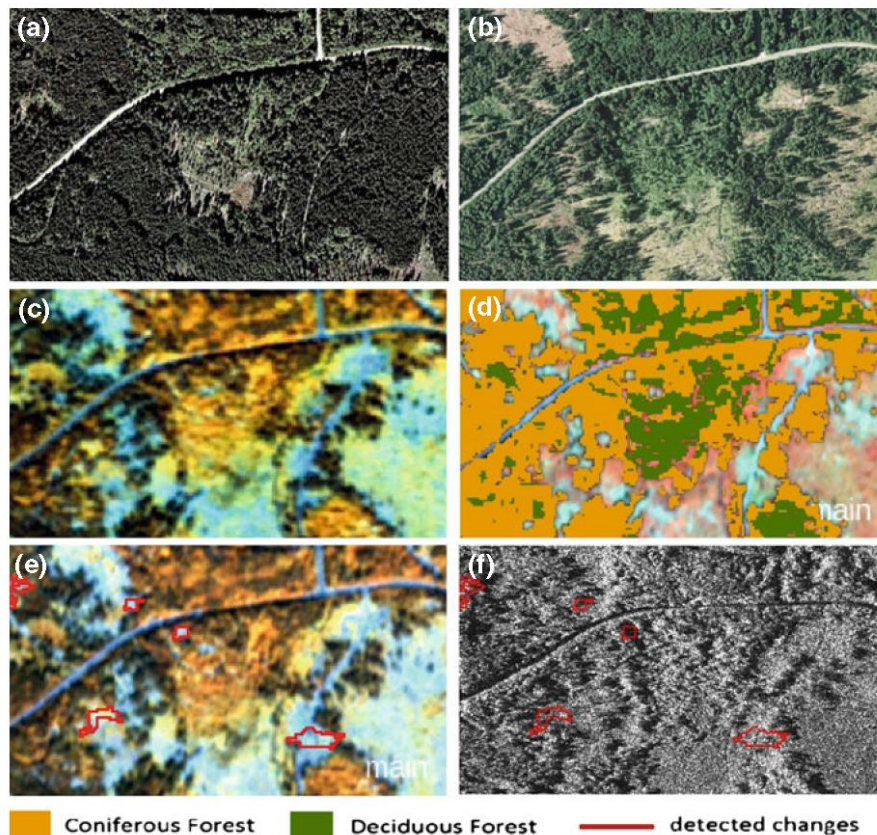
Coniferous Forest   **Deciduous Forest**   ——— **detected changes**

Fig. 10 Example of an information flow in the sense of the DSS for the forest–wood chain under development demonstrated for a subset of the Bavarian Forest test area. Aerial image from 2000 documenting the initial stage (**a**), aerial documenting damages after a storm event (**b**), RapidEye image May 2009 still reproducing the situation from 2001 (**c**), RapidEye image classification August 2009 (**d**), RapidEye image August 2009 with border line of changes compared to the situation in May (**e**), and TerraSAR-X proving no changes since August 2009 (**f**)

very sensitive measure (see Fig. 9c), considerable noise is expected making it necessary to rely on segment-based approaches for classification. A priori information seems essential.

For RE changes related to shifts in phenologic development are investigated with the aim of tree species differentiation (instable parameter behaviour). The static parameters area, gaps, border length, tree species group distribution, etc. are accessible from each data take.

Within the DSS for the forest wood chain, the advantages of both system types are combined. For establishing the data base, the information is extracted from both systems (synergy). In the fast response case, the complementarities of

163

information provision are used to get information about the event. The extracted information is cross checked with the established data base.

Figure 10 demonstrates the information flow within the DSS. Aerial photographs of the regular three year cycle of the Bavarian State survey are used to cross check and update existing forest data bases (10a). In the following winter season 2000/01 a storm event damaged large areas. According to the concepts of the DSS, satellite data should be analysed to decide whether a supplementary very high resolution data take is necessary for steering clearing measures. In our example from the Bavarian Forest test site, aerial photographs were taken in 2001 (10b) for bark beetle monitoring reasons. The damages of the storm throw from winter 2000/01 are still well displayed by the RE image from May 2009. The multi-seasonal classification is used to crosscheck and update the forest management records (c, d). Changes occurring between May and August 2009 are easily to be identified by an automatic change detection proceeding (e). Once the data base is regularly updated even in a fast response case under cloudy sky conditions the affected areas are detectable by SAR systems, in our example by TS-X (f).

5 Discussion

Despite that the presented results are stated as preliminary, it is possible to give some statements and to give an estimate of the success.

Hypothesis 1: *Forest management relevant parameters are derivable from Rapid Eye and TeraSAR-X data.* Hypothesis was tested on base of multi-seasonal RapidEye and TerraSAR-X data. It was examined in up to five test sites of different growth regions characteristics in Bavaria, and it is likely to be stated as confirmed. The parameter derivation success is not as high as in case of the reference systems for that parameter (Table 7). However, results are sufficient to support the aims of the envisaged DSS for the forest-wood chain. These findings are in line with the findings of deKok et al. (1999).

Hypothesis 2: *The combination of both data sets improves the forest determination.* The investigations confirmed the hypothesis validity. Specific advantages in parameter extraction using data from both sensors are contributing to a more precise determination of the forest characterisation. As shown in Table 7, especially in case of gap detection and height estimates, TS-X is delivering more accurate results than RE. While RE is contributing with a better stand structure description, at present confirmed solely at the tree species group level, but with a prospect of tree species differentiation. Nevertheless, because it was not possible to evaluate the data sets taken at the same period of time, this hypothesis needs to be further investigated before it is categorized as 'proved'.

Hypothesis 3: *The complementarities of the two sensor concepts facilitate fast reactions in the disaster case.* The concepts leading to hypothesis 3 assume that even small changes are detectable, once the data base is established and regularly updated by evaluating the same RS data type sets. Change detection is required,

either to compare the changes over years or in case of a clearly defined situation of a sudden event like a storm throw or a biotic calamity. In the concept of the DSS for the forest wood chain, such a calamity should be detectable by both sensor types. The microwave sensor can detect at any daytime or under any cloud coverage condition, while the optical sensor, which definitely requires clear sky conditions, is therefore not as flexible. On the other hand, systems like RE or later, ESA's Sentinel, are promising a high temporal repetition frequency and will be used to analyse the event further.

Whether the event was of a category that made it necessary to have a very high resolution imaging campaign is decided after crosschecking the classification results with the data base records. Once such an event is categorized as disastrous and the clearing urgency is high to very high, an additional data take with very high resolution systems like aerial photographs or LIDAR may be a cost efficient logistic option for steering the operations.

A data flow test confirming the hypothesis was performed with the presented change detection study at a test site in the Bavarian Forest (Fig. 10). A test case did not occurred during the reported period such the hypothesis cannot be finally confirmed.

Worth to be discussed are other findings of the study highlighting integration needs and bottlenecks of different nature affecting the success of the integration in the frame of the envisaged DSS. We will restrict the discussion on differences in recording the retrieved parameter and on pointing on the need of harmonisation of definitions.

In case of the tree species group differentiation task, forest management data bases are the only ones offering the required level of detail. Such data bases exist solely for forest areas with an administration, what applies on state forests, community forests and big private forest areas. One third of the Bavarian forests, about 800.000 ha belong to the 'small private forest' category and are covering areas not larger than 30 ha each. For such type of forests, the proposed system will be able to offer a consistent data base, of course not with that level of detail as for then the state forests with regular ground based inventories. However, even in case of the state forests and community forests with state of the art data bases the system under development will be of advantage. Such the records of the Bavarian State forest management data base are giving solely the percentage of forest tree species per stand, but not the position. The trend in forest planning is to larger and even larger stands and longer inventory cycles. The object based classification applied for this study is deciding per object. One object is defined by homogeneity criteria and is in general associated to a tree species type of comparable age. The percentage per stand is calculated by summing up the objects belonging to the respective stand. The position of each object is exactly known. This is a big advantage compared to the forest management records. Growth simulators are more and more used as planning instruments in forest management, allowing assessing different alternatives and their consequences. Especially growth simulators acting on base of competition models like SILVA (Pretzsch et al. 2002) will take advantage from this additional information in the future.

The need of harmonisation became already obvious at a very basic stage of the discussion: Which is the appropriated and generally accepted definition of 'forest', or, on the practical side, which 'official' forest layer should be used to compare the results? Even in the same county, in our case Bavaria, different authorities and administrations e.g., for forestry, nature conservation, the Bavarian State survey, etc., established their own data bases using different definitions for 'forest'. Following the most intuitive idea to use the forest management maps, the sources on which the decisions in forestry are based on, one must fail because the forest border is defined by the stem position. Remote sensing data derived results are crown projection controlled. For old growth broadleaved forest, this simple difference may introduce a positioning error for forest borderline determination of 10 m and more once that map is used as reference for validating RS derived results. Of course, this has consequences for forest area determination as well. Some other official sources like ATKIS do not consider the forest management road network. The dense Bavarian State forests road network must be subtracted before this data set is used as reference.

The discussion may be continued on different other topics. The study clearly reveals that there are many 'interface' problems to be solved until an operational solution may become possible. These problems do not directly touch the remote sensing and data evaluation context.

6 Conclusion and Outlook

The results presented above show the current state of implementation and are thus preliminary in some sense. The extracted parameters indicate the potential of Remote Sensing to support the forest-wood chain but their values should be considered as an initial feasibility test after putting together all the relevant imagery and geodata needed for the analysis. Nevertheless, it is possible to derive some conclusions about the concept itself and about the remote sensing data investigated as well.

The optical RapidEye data belong to the high (5–30 m), the SAR TerraSAR-X data are on the transition to the very high (0.5–5 m) spatial resolution class. Different to LIDAR or digital aerial photography techniques single tree observations are not possible. Exceptions are solitary trees or standards left for seed production or shading. After the presented first results we are far away from claiming a ready to use solution for practice, However, the results deliver a couple of arguments for the combined use of multispectral and SAR data for monitoring and fast response situations like sudden calamities.

The concept seems appropriate to deliver management relevant information useful for interim inventories. Such interim inventories are not intended to deliver all detailed information of a regular inventory cycle. However, they should help to give an overview about the main parameter, such as:

Parameter Determination by RapidEye and TerraSAR-X Data   105

- Tree species distribution (e.g., coniferous/broadleaved/mixed)
- Changes in area coverage (e.g., the conversion of stands after felling or as result of calamities)
- Management measures
- Information on stand structure parameters (e.g., number and position of standards, gaps and tree type mixture—single tree mixture, group wise)
- Information needed for the strategically/tactical planning level of a forest enterprise.

Most, if not all, of these information are retrievable more or less automatically from data sets like those offered by a combination of microwave and multispectral data. Again, not necessarily with a quality as that required for decision making, but surely with a sufficient accuracy for decision support and fast response actions!

In the context of global change phenomena, especially the observed increase of frequency and intensity of calamities, the presented combination of microwave and optical systems of the very high to high category seems well appropriated for fast reaction emergency systems all over the world. While the microwave system is delivering the first information about the extent of an event, without being hindered by clouds or daytime, the optical system will deliver the details needed for reconditioning logistics in forestry. A basic point in this context is an already existing GIS data base of the forests, allowing the fast assessment of the changes.

Still an open question is how to connect the results with existing concepts and especially the task of harmonisation of definitions hindering an integration of remote sensing derived information in practice.

References

Ackermann N, Thiel C, Borgeaud, M, Schmullius, C (2010) Potential of fusion of SAR and optical satellite imagery for biomass estimation in temperate forested areas. In: Proceedings of the ESA living planet symposium, Bergen, Norway

Anonymous (2001). Waldgesetz für Bayern. 25. August 1982 (BayRS 7902-1-L): Letzte Änderung 22. Juli 2005 (GVBI 2005, 313).Bayerisches Staatsministerium für Ernährung, Landwirtschaft und Forsten (StMELF), München

Baatz M, Schäpe A (2000). Multiresolution segmentation—an opotimization approach for high quality multi-scale image segmentation. In: Proceedings of the AGIT-symposium Salzburg 2000, Vol XII. Salzburg, pp 12–23

Bamler R (2000) Principles of synthetic aperture radar. Surv Geophys 21(2–3):147–157. doi:10.1023/A:1006790026612

Cloude S.R, Papathanassiou K.P (2008) Forest vertical structure estimation using coherence tomography. In: IEEE proceedings of geoscience and remote sensing symposium, pp 275–278

Congalton RG (1991) A review of assessing the accuracy of classifications of remotely sensed data. Remote Sens Environ 37:35–46

106   T. Schneider et al.

DeKok R, Schneider T, Baatz M, Ammer U (1999) Object based image analysis of high resolution data in the alpine forest area; In: Proceedings joint WSf ISPRS WG I/1, I/3 and IV/4: sensors and mapping from space 1999, Hannover, Sept 27–30

De Zan F, Papathanassiou K, Lee SK (2009) Tandem-L forest parameter performance analysis. In: Proceedings of international workshop on applications of polarimetry and polarimetric interferometry, Frascati, Italy, pp 1–6

Eckert. S. (2006): A contribution to sustainable forest management in patagonia—object-oriented classifiucation and parameter extraction based on ASTER and landsat ETM + data; Verlag des GeographischenInstituts der Uni. Zürich, Remote Sensing Series, Vol 45. pp S.154

Felbermeier T, Hahn A, Schneider T (2010) Study on user requirements for remote sensing applications in forestry. In: Proceedings of the ISPRS symposium TC VII, July 5–7, 2010, Vienna, Austria

Fehlert G-P (1984) Kalibrierung von MSS-Satellitenbilddaten zur Auswertung zeitlicher Reflexionsänderungen an Fichtenbeständen; DFVLR-FB 84–44

Heurich M (2006) Evaluierung und Entwicklung von Methoden zur automatisierten Erfassung von Waldstrukturen aus Daten flugzeuggetragener Fernerkundungssensoren. Forstliche Forschungsberichte München. 202/2006

Hilbert C, Schmullius C, Zink M (2010) Derivation of forest structure using satellite, multifrequent radar and lidar data in Thuringian Forest, Germany. In: Proceedings of silvilaser 2010, Freiburg, Germany

Katzur L, Franke W (2007) Qualitätssicherung bei der Bearbeitung der ATKIS®-Produkte. Vermessung Brandenburg, Heft 02:15–26

Kenneweg H, Förster B, Runkel M (1991) Diagnose und Erfassung von Waldschäden auf der Basis von Spektralsignaturen; In DLR Abschlußdokumentation—Untersuchung und Kartierung von Waldschäden mit Methoden derFernerkundung. Teil A, Oberpfaffenhofen

Kautz M, Dworschak K, Gruppe A, Schopf R (2011) Quantifying spatio-temporal dispersion of bark beetle infestations in epidemic and non-epidemic conditions. For Ecol Manag 262(2011):598–608

Kirscht M, Rinke C (1998) 3D reconstruction of buildings and vegetation from synthetic aperture radar (SAR) images. In: Proceedings of IAPR workshop on machine vision applications MVA''98, Makuhari, Chiba, Japan, pp 228–232

Knoke T, Schneider T, Hahn A, Griess VC, Rößiger J (2012) Forstbetriebsplanung als Entscheidungshilfe. Ulmer Verlag Stuttgart, p 408. ISBN 978-3-8001-7611-3

Koch B (2010) Status and future of laser scanning, synthetic aperture radar and hyperspectral remote sensing data for forest biomass assessment. ISPRS J Photogramm Remote Sens 65:581–590

Kourgli A, Belhadj-Aissa A (2009) SAR image classification using textural modelling. In: Proceedings of radar conference—surveillance for a safer world, Bordeaux, pp 1–6

Lee JS, Papathanassiou KP. Hajnsek I, Mette T, Grunes MR, Ainsworth T, Ferro-Famil L (2005) Applying polarimetric SAR interferometric data for forest classification. In: IEEE proceedings of geoscience and remote sensing symposium, Vol 7. Pp 4848–4851

Lemp D, Koch B (2009) Forest monitoring using TerraSAR-X data—evaluation of processing methods and first results. In: Proceedings of TerraSAR-X science meeting 2009

Lillesand T, Kiefer R, Chipman J (2004) Remote sensing and image interpretation. Wiley, New York, p 763. ISBN 13: 978-0471152279

Pretzsch H (2002): Application and evaluation of the growth simulator SILVA 2.2 for forest stands, forest estates and large regions. Forstwissenschaftliches Centralblatt 121(Suppl.1):28–51

Rall H, Martin K (2002) Luftbildauswertung zur Waldentwicklung im Nationalpark Bayerischer Wald 2001—Ein neues Verfahren und seine Ergebnisse zur Totholzkartierung. In: Berichte aus dem Nationalpark, Nationalparkverwaltung Bayerischer Wald 1 (2002)

Reigber A, Moreira A (2000) First demonstration of airborne SAR tomography using multibaseline L-band data(5). IEEE Trans Geosci Remote Sens 38(5):2142–2152. doi:10.1109/36.868873 (Part 1)

Parameter Determination by RapidEye and TerraSAR-X Data   107

Reitberger J, Schnörr CL, Heurich M, Krzystek P, Stilla U (2008a) Towards 3D mapping of forests: a comparative study with first/last pulse and full waveform LIDAR data; the international archives of the photogrammetry. Remote Sens Spat Inf Sci 37:1397–1403 (Part B8)

Reitberger J, Schnörr CL, Heurich M, Krzystek P, Stilla U (2008b) Analysis of full waveform LIDAR data for the classification of deciduous and coniferous trees. Int J Remote Sens—3D Remote Sens For 29(5):1239–1242. doi:10.1080/01431160701736448

Reitberger J, Schnörr CL, Krzystek P, Stilla U (2009) 3D segmentation of single trees exploiting full waveform LIDAR data. ISPRS J Photogramm Remote Sens 64:561–574. doi:10.1016/j.isprsjprs.2009.04.002

Sato M, Koike T (2003) Classification of tree types by polarimetric Pi-SAR. In: IEEE proceedings of geoscience and remote sensing symposium, Vol 1. Pp 431–433

Schulz K, Boldt M, Thiele A (2009) COVAMCOH-ANALYSIS: a method to improve the interpretation of high resolution repeat pass SAR images of urban areas. In: Proceedings of SPIE, remote sensing for environmental monitoring, GIS applications, and geology IX Vol. 7478:747805—747809 74780 doi: 10.1117/12.830441

Schneider T, de Kok R, Buck A, Manakos I (2000) Objektorientierte Bildanalyse—Paradigmawechsel in der thematischen Auswertung von Erdbeobachtungsdaten ? In: Lehrstuhl für Landnutzungsplanung und Naturschutz (2000): Landnutzungsplanung und Naturschutz. Aktuelle Forschungsberichte. Festschrift zur Emeritierung von Professor Dr. Ulrich Ammer. Freising, pp 234–258 ISBN 3-89685-564-6

Seitz R, Rappl A, Straub C, Troyke A (2011) Forstliche Fernerkundung an der LWF, AFZ-der Wald, 13/2011, pp 11–13

Straub C, Weinacker H., Koch B (2008) A fully automated procedure for delineation and classification of forest and non-forest vegetation based on fullwaveform laser scanner data. Int Arch Photogramm, Remote Sens Spat Inf Sci 37(8/11):1013–1019

Tiede D, Lang S, Hoffmann C (2006) Supervised and forest type-specific multi-scale segmentation for a one-level-representation of single trees. Int Arch Photogramm, Remote Sens Spat Inf Sci 36(4):C42 (Salzburg, Austria. http://www.commission4.isprs.org/obia06/)

Thiele A, Schulz K, Thoennessen U, Cadario E (2006) Orthorectification as Preliminary Step for the fusion of data from active and passive sensor systems. In: Proceedings of IEEE international conference on multisensor fusion and integration for intelligent systems, doi: 10.1109/MFI.2006.265629, pp 479–484

Volden E., Solberg AS, Huseby RB (1998) Forest classification using spectrometer and SAR Data. 1998 In: IEEE proceedings of feoscience and remote sensing symposium, Vol 5, pp 2732–2736

Waser LT, Ginzler C, Kuechler M, Baltsavias E (2008) Potential and limits of extraction of forest attributes by fusion of medium point density LiDAR data with ADS40 and RC30 images. In: SilviLaser 2008 8th international conference on LiDAR applications in forest assessment and inventory, Edinburgh, UK, Sept 18–19, 2008, pp 625–634

Zhang Z, Ni W, Fu A, Guo Z, Sun G, Wang D (2008) Estimation of forest structural parameters from Lidar and SAR data. Int Arch Photogramm, Remote Sens Spat Inf Sci 37:1121–1126 (part B8)

SPRINGER LICENSE
TERMS AND CONDITIONS

Jan 23, 2015

This is a License Agreement between alata Elatawneh ("You") and Springer ("Springer") provided by Copyright Clearance Center ("CCC"). The license consists of your order details, the terms and conditions provided by Springer, and the payment terms and conditions.

All payments must be made in full to CCC. For payment instructions, please see information listed at the bottom of this form.

License Number	3554800609489
License date	Jan 23, 2015
Licensed content publisher	Springer
Licensed content publication	Springer eBook
Licensed content title	Parameter Determination by RapidEye and TerraSAR-X Data: A Step Toward a Remote Sensing Based Inventory, Monitoring and Fast Reaction System on Forest Enterprise Level
Licensed content author	Thomas Schneider
Licensed content date	Jan 1, 2013
Type of Use	Thesis/Dissertation
Portion	Full text
Number of copies	100
Author of this Springer article	No
Order reference number	None
Title of your thesis / dissertation	thesis / dissertation Alata Elatawneh
Expected completion date	Jan 2015
Estimated size(pages)	230
Total	0.00 USD

Terms and Conditions

Introduction
The publisher for this copyrighted material is Springer Science + Business Media. By clicking "accept" in connection with completing this licensing transaction, you agree that the following terms and conditions apply to this transaction (along with the Billing and Payment terms and conditions established by Copyright Clearance Center, Inc. ("CCC"), at the time that you opened your Rightslink account and that are available at any time at http://myaccount.copyright.com).

Limited License
With reference to your request to reprint in your thesis material on which Springer Science and Business Media control the copyright, permission is granted, free of charge, for the use indicated in your enquiry.

Licenses are for one-time use only with a maximum distribution equal to the number that you identified in the licensing process.

This License includes use in an electronic form, provided its password protected or on the university's intranet or repository, including UMI (according to the definition at the Sherpa website: http://www.sherpa.ac.uk/romeo/). For any other electronic use, please contact Springer at (permissions.dordrecht@springer.com or permissions.heidelberg@springer.com).

The material can only be used for the purpose of defending your thesis limited to university-use only. If the thesis is going to be published, permission needs to be re-obtained (selecting "book/textbook" as the type of use).

Although Springer holds copyright to the material and is entitled to negotiate on rights, this license is only valid, subject to a courtesy information to the author (address is given with the article/chapter) and provided it concerns original material which does not carry references to other sources (if material in question appears with credit to another source, authorization from that source is required as well).

Permission free of charge on this occasion does not prejudice any rights we might have to charge for reproduction of our copyrighted material in the future.

Altering/Modifying Material: Not Permitted
You may not alter or modify the material in any manner. Abbreviations, additions, deletions and/or any other alterations shall be made only with prior written authorization of the author(s) and/or Springer Science + Business Media. (Please contact Springer at (permissions.dordrecht@springer.com or permissions.heidelberg@springer.com)

Reservation of Rights
Springer Science + Business Media reserves all rights not specifically granted in the combination of (i) the license details provided by you and accepted in the course of this licensing transaction, (ii) these terms and conditions and (iii) CCC's Billing and Payment terms and conditions.

Copyright Notice:Disclaimer
You must include the following copyright and permission notice in connection with any reproduction of the licensed material: "Springer and the original publisher /journal title, volume, year of publication, page, chapter/article title, name(s) of author(s), figure number(s), original copyright notice) is given to the publication in which the material was originally published, by adding; with kind permission from Springer Science and Business Media"

Warranties: None

Example 1: Springer Science + Business Media makes no representations or warranties with respect to the licensed material.

Example 2: Springer Science + Business Media makes no representations or warranties with respect to the licensed material and adopts on its own behalf the limitations and disclaimers established by CCC on its behalf in its Billing and Payment terms and conditions for this licensing transaction.

Indemnity
You hereby indemnify and agree to hold harmless Springer Science + Business Media and CCC, and their respective officers, directors, employees and agents, from and against any and all claims arising out of your use of the licensed material other than as specifically authorized pursuant to this license.

No Transfer of License
This license is personal to you and may not be sublicensed, assigned, or transferred by you to any other person without Springer Science + Business Media's written permission.

No Amendment Except in Writing
This license may not be amended except in a writing signed by both parties (or, in the case of Springer Science + Business Media, by CCC on Springer Science + Business Media's behalf).

Objection to Contrary Terms
Springer Science + Business Media hereby objects to any terms contained in any purchase order, acknowledgment, check endorsement or other writing prepared by you, which terms are inconsistent with these terms and conditions or CCC's Billing and Payment terms and conditions. These terms and conditions, together with CCC's Billing and Payment terms and conditions (which are incorporated herein), comprise the entire agreement between you and Springer Science + Business Media (and CCC) concerning this licensing transaction. In the event of any conflict between your obligations established by these terms and conditions and those established by CCC's Billing and Payment terms and conditions, these terms and conditions shall control.

Jurisdiction
All disputes that may arise in connection with this present License, or the breach thereof, shall be settled exclusively by arbitration, to be held in The Netherlands, in accordance with Dutch law, and to be conducted under the Rules of the 'Netherlands Arbitrage Instituut' (Netherlands Institute of Arbitration).*OR:*

All disputes that may arise in connection with this present License, or the breach thereof, shall be settled exclusively by arbitration, to be held in the Federal Republic of Germany, in accordance with German law.

Other terms and conditions:

v1.3

8.3 Publication 3

Elatawneh A., Wallner A., Manakos I., Schneider T., Knoke T. 2014. Forest Cover Database Updates Using Multi-Seasonal RapidEye Data—Storm Event Assessment in the Bavarian Forest National Park. Forests. 5: 1284-1303

Article

Forest Cover Database Updates Using Multi-Seasonal RapidEye Data—Storm Event Assessment in the Bavarian Forest National Park

Alata Elatawneh [1,*], Adelheid Wallner [1], Ioannis Manakos [2], Thomas Schneider [1] and Thomas Knoke [1]

[1] Institute of Forest Management, Center of Life and Food Sciences Weihenstephan,
  Technische Universität München, Hans-Carl-von-Carlowitz-Platz 2, Freising 85354, Germany;
  E-Mails: adelheid.wallner@tum.de (A.W.); tomi.schneider@tum.de (T.S.);
  knoke@forst.wzw.tum.de (T.K.)
[2] Information Technologies Institute, Centre for Research and Technology Hellas, Building A,
  6th km Harilaou-Thermi, P.O. Box 60361, Thessaloniki 57001, Greece; E-Mail: imanakos@iti.gr

* Author to whom correspondence should be addressed; E-Mail: alataaa@tum.de;
  Tel.: +49-8161-71-4272; Fax: +49-71-8161-4545.

Abstract: This study is a part of a research program that investigates the potential of RapidEye (RE) satellite data for timely updates of forest cover databases to reflect both regular management activities and sudden changes due to bark beetle and storms. Applied here in the Bavarian Forest National Park (BFNP) in southeastern Germany, this approach detected even small changes between two data takes, thus, facilitating documentation of regular management activities. In the case of a sudden event, forest cover databases also serve as a baseline for damage assessment. A storm event, which occurred on 13 July, 2011, provided the opportunity to assess the effectiveness of multi-seasonal RE data for rapid damage assessment. Images of sufficient quality (<20% cloud cover) acquired one day before the storm event were used as a baseline. Persistent cloud cover meant that the first "after event" image of sufficient quality was acquired six weeks later, on 22 August, 2011. Aerial images (AI) for the official damage assessment done by the BFNP administration were acquired on that same day. The RE analysis for damage assessment was completed two weeks after the post-event data take with an overall accuracy of 96% and a kappa coefficient of 0.86. In contrast, the official aerial image survey from the BFNP

was first released in late November, eleven weeks later. Comparison of the results from the two analyses showed a difference in the detected amount of forest cover loss of only 3%. The estimated cost of the RE approach was four times less than that of the standard digital AI procedure employed by the BFNP.

Keywords: forest cover monitoring; multi-seasonal; RapidEye; aerial images; storm damage

1. Introduction

In Central Europe, the most important natural disturbances in forests are storm events [1,2]. Disastrous events of, at least, "regional" dimensions have the potential to destabilize the timber market and trigger subsequent biotic calamities. Such event sequences occurred in 1991 and 1999 following the storms "Vivian/Wiebke" and "Lothar" in Southern and Southwestern Germany respectively. The most common biotic calamity following such a storm event is an extreme increase in propagation of the European spruce bark beetle (*Ips typographus* [L.]) [2–5]. Forest area depletion must be recorded and spatially located in order to delineate drivers, pressures, threats and impacts, and to issue warning signals and take mitigation actions wherever appropriate [6]. However, this requires baseline data on forest cover, generally acquired from forest management databases. Currently, forest management databases are available only for the state forests in Germany and for some community forests (less than 40% of the forests in Bavaria). The update cycles for these databases can be as long as 10 years. Increasing frequency and magnitude of disastrous events during recent decades has revealed the need for shorter update cycles for such databases. At present, in Bavaria, about 30 to 40% of the annual workload of a forest enterprise is in response to unpredictable hazardous events [7]. In order to prevent follow-on calamities like those described above, it is important to immediately clear affected areas, which in turn requires reliable information about the site, its accessibility, existing nearby facilities, availability of resources, and administration constraints on management of the affected area, such as restrictions which are meant to protect sites of cultural and natural importance.

To tackle some of these challenges, a Decision Support System (DSS) (Entscheidungs-Unterstützungs-System Forst-Holz, EUS-FH) project was designed for the forest-wood chain in Bavaria, which at the same time enables the fulfillment of both national and international reporting duties. EUS-FH contains a database-updating module that is based on remote sensing (RS) data [7]. This module, known as the "Remote Sensing-based Inventory and Monitoring System" (RS-IMS), is based on the idea of integrating existing data from official sources, such as the Bavarian Surveying and Geoinformation Administration (LVG), the Bavarian State Forest Administration, the Bavarian State Research Institute of Forestry, community forests, and National Parks like the Bavarian Forest National Park (BFNP) with RS data in order to update existing knowledge and to support trend analysis. The development of the EUS-FH was prompted by the launch of the German satellite systems TerraSAR-X (TS-X) and RapidEye (RE). The spatial resolutions of both systems fulfill the requirements of a 1:10,000 mapping scale [8], while the high acquisition frequency of two to three days [9] allows for operational and near real-time application of the data acquired.

Within the RS-IMS, special attention is given to detecting sudden canopy losses due to either natural or human-induced events. Using active sensors, changes due to both regular management and sudden events can be assessed within a short time, even under the cloud regime common in central Europe, where images with less than 20% cloud cover are rarely acquired. Recent studies, such as those by Rappl *et al.* [10], and Thiele *et al.* [11], have utilized data from the active sensor, TerraSAR-X, for the same area referenced in this study to assess the potential of these data for rapid mapping of windstorm events. However, these studies were more experimental than operational due to the small area coverage and high cost of the TerraSAR-X data.

A windstorm, which occurred between late night 13 July, 2011, and early morning 14 July, 2011, in the northern part of the BFNP, was the trigger for this study. A few months later, about 70,000 m^3 of timber was thrown down by the storm [12]. Thus, the conditions for a "regional" event were fulfilled. The processing chain within the 'Remote Sensing based Inventory and Monitoring System' (e.g., EUS-FH) is based on object-based change detection (OBCD) techniques, which have demonstrated advantages over pixel-based change detection techniques [13]. Chen *et al.* [14] classified OBCD methods into four groups: image-object, class-object, multitemporal-object, and hybrid change detection. The advantages and disadvantages of implementing these methods have been discussed in previous studies [15–17] in which hybrid methods performed better than others for forest change detection. OBCD has been used in several forest studies undertaken in the last decade to describe forest dynamics due to both biotic and abiotic disturbances. These studies have used Landsat [17–20] and SPOT images [15,16], as well as data from very high spatial resolution sensors, such as QuickBird and aerial images (AI) [4,21]. The topics addressed in these studies were as diverse as forest loss and disturbance monitoring, the potential and limitations of the techniques used, and the contribution of the results to further ecological analysis. However, while these studies utilized multi-annual images to perform annual updates of the forest status, they did not make use of multi-seasonal data, as was done in the study presented here. In addition, the problem of cloud presence was either avoided completely by working with cloud-free data [16], or the use of either more frequent optical data or data from active sensors to enhance the results where clouds exist was recommended [17]. In contrast, multiseasonal RE data (acquired every 45 days) are now available for the whole of Germany, according to the agreement between the German Federal Ministry of Economics and Technology (BMWi) and the RapidEye data provider.

In the study presented here, an innovative hybrid change detection technique was applied to multi-seasonal RE images to update an existing forest cover database. A new approach was developed to overcome the problem of partial cloud cover by using substitute data from subsequent data takes. This method was implemented on data from two different periods.

- The first period, between 19 April, 2011, and 22 June/12 July, 2011, helped to update the forest cover figures obtained from the most recent forest inventory for the area, which was done in order to document changes due to regular management practices.
- The second period, between 22 June/12 July, 2011 and 22 August, 2011, was after the above-mentioned storm event had occurred. This helped to demonstrate the evaluation chain for sudden catastrophic events by applying the same method.

The results of both periods were then compared to the results of the annual official AI survey from 2011, which was obtained from the BFNP. Finally, the costs of using each of the data sources and

associated methods were estimated and compared in order to assess their relative potential for operational use.

2. Experimental Section

2.1. Study Area

The study site is located in the northern part of the BFNP in southeastern Germany (49°03'53" N, 13°21'57" E) along the border with the Czech Republic (Figure 1). Together, the BFNP and the Šumava National Park in the southwestern part of the Czech Republic cover an area of 940 km^2 and form the most extensive protected forest in Central Europe. The BFNP is located in a mountainous region, with elevations ranging between 600 m and 1450 m. The BFNP was founded in 1970 as Germany's first national park with an area of 130 km^2. In 1997, the park was extended to include a total area of 240 km^2. Its landscape can be divided into three ecological zones—highlands, hillsides, and valleys. In each zone, different compositions of tree species are located. Based on inventory results from 2002 to 2003, Heurich and Neufanger [22] calculated the following tree species compositions for the dominant layer of the forest in each of these ecological zones: (a) In the highlands—90% Norway spruce (*Picea abies*), 2% beech (*Fagus sylvatica*), and 8% other broadleaf trees; (b) on hillsides—58% Norway spruce, 3% fir (*Abies alba*), 34% beech, and 5% other broadleaf trees; and (c) in the valleys—83% Norway spruce, 5% fir, 6% beech, and 6% other broadleaf trees. Thus, the main species in all of the ecological zones in the study area is Norway spruce, which is highly susceptible to damage due to calamities.

Figure 1. Location of the Bavarian Forest National Park.
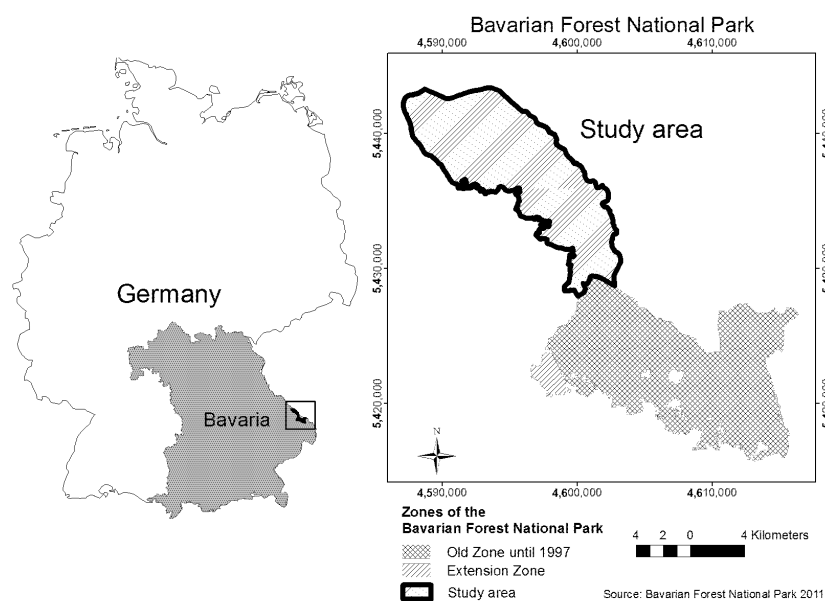
Severe disturbance cycles have been documented in the forest in the Bavarian Forest National Park (BFNP) since 1868 [23]. However, the frequency of disturbances has been increasing since 1983 and peaked at the beginning of the 1990s when about 17,000 m^3 of wood was affected [24]. As a reaction to the forest disease discussion, which began in the 1980s and was triggered by the aforementioned disturbance cycle in the BFNP, annual inventories using aerial photography have been performed since 1988 [4]. At present in the BFNP, in the case of an unpredictable event like storm break, fire, or biotic infestation, AI interpretation is always used to investigate the changes. The minimum mapping unit used in previous studies of this kind in the BFNP [4,5,25] has always been a patch of at least 5 trees. No reports have been issued describing the results of these analyses, but all changes have been documented in the annual updates. Despite the fact that automated approaches to change detection have been tested [4], visual interpretation is still considered the most reliable approach and is still officially used in the BFNP [25].

The philosophy of the BFNP administration allows no forest management activities in the core zone of the park. However, some small, private residential areas and agricultural fields still exist within the park boundaries. Bark beetle management is allowed within the park itself only in a small strip of 500–800 m along the boundaries of these areas and along the external boundaries of the park. A monitoring and management system has been established to observe calamity development and prevent further bark beetle breakouts in the extended zone.

2.2. Data Sets

2.2.1. RapidEye Data

RE data were the primary data used for this analysis. These data consist of five channels: one each in the blue, green, red, red edge, and near infrared regions of the spectrum. Typically, the data are collected at nadir, with a spatial resolution of 6.5 m (5 m resampled) and a swath width of 75 km. The data were ordered as level 3A products and provided by the RapidEye Science Archive (RESA) at the German Aerospace Center (DLR). Even at the nominal repetition time of the RE system of 2–3 days, only three scenes acquired during the period between April and October, 2011, fulfilled the maximum 20% cloud cover condition we set for this analysis; the first of these images was acquired on 19 April, 2011, the second on 22 August, and the third on 1 October. To cover the main growing season from May to July, two additional scenes, namely one from 22 June and one from 12 July, were combined to produce a dataset meeting the cloud coverage restrictions.

2.2.2. Ancillary Data

Reference data containing information about the losses in forest cover in the year 2011 were obtained from the BFNP administration and compared to the results of the data analysis performed here. Each year, flight campaigns are performed by the park administration to acquire color-infrared images (CIR), which are then used to update the databases of the BFNP [4]. Any changes in forest extent or condition are identified using visual image interpretation. For the analysis of changes that occurred in 2011, five change classes were defined, of which four described the effects of bark beetles, and one those of the storm. The change classes due to the bark beetle were referred to as standing

deadwood, groups of standing deadwood (max. 5 trees), cleared area of deadwood, and area of hand-debarked deadwood [25]. All of the classes described were delineated by hand using stereoscopic image interpretation. In 2011, the flight campaign was initiated by the storm event on 13 and 14 July, 2011. The first date after this event when cloud cover was sufficiently low to allow imaging was 22 August.

2.3. Methodology

2.3.1. Data Preprocessing and Preparation

The mapping accuracy of change detection using remote sensing systems is affected by the following factors: spatial scale, sensor viewing geometry, image geometric accuracy, and radiometric normalization [14]. All of the RE images used in this study were collected with the nominal 0° pointing geometry, resampled to 5 m pixels, and were ordered preprocessed to level 3A. The geometric accuracy of RE level 3A data ranges from less than one pixel to six pixels (5 m–30 m) [9]. The geometric accuracy of the data as acquired was examined and, when necessary, improved using co-registration to the available geo-databases, using ENVI 4.3. As is essential for multi-seasonal data evaluation, a combined atmospheric/topographic correction was performed using ATCOR 3 implemented in PCI Geomatica software. Thus, the resulting data set represents actual reflectance.

2.3.2. Detection of Forest Cover Loss

The basic concept of the method applied is to initially obtain change results using any of the various commonly used pixel-based change detection algorithms, and then apply the object-based technique to enhance the results [26]. In this way, the calculation time can be reduced by avoiding segmentation of the whole image, while at the same time allowing for automation of the process. The processing chain that was developed to aid in the annual update of forest databases compares any new data set with a previous one by applying a pixel-based technique, and a simple image-differencing algorithm ([27] and Figure 2). This algorithm computes the differences between the two images by subtracting the pixel values from the initial state image from those of the next state image. The closer the acquisition date of the later image data to a change event, the higher the spectral contrast and, thus, the better the ability to detect resulting changes. The result of this process is a difference image for each band of data representing the changes between the two state images, in which positive values identify pixels that became brighter, and negative values identify pixels with lower reflectance values Equation (1).

$$[\Delta x_{ij}^{k} = x_{ij}^{k}(t_2) - x_{ij}^{k}(t_1)]$$
(1)

where x_{ij}^{k} = the pixel value for band k; i and j are the x and y coordinates of each pixel; t_1 = the acquisition date of the initial state image; t_2 = the acquisition date of the second state image.

Equation (1) was solved for each RE band, as well as for a series of indices calculated from the raw band data, such as brightness, blue/green ratio, and NDVI. Afterwards, all resulting difference images were assessed visually. This evaluation of the huge windthrow area showed very clearly that the red edge band outperformed all other bands in quantifying the extent of the wind damage [28]. The results from the other bands and indices overestimated the losses in forest cover.

Figure 2. Overall methodology followed for the detection of loss in forest cover in the BFNP for the first period and second period.
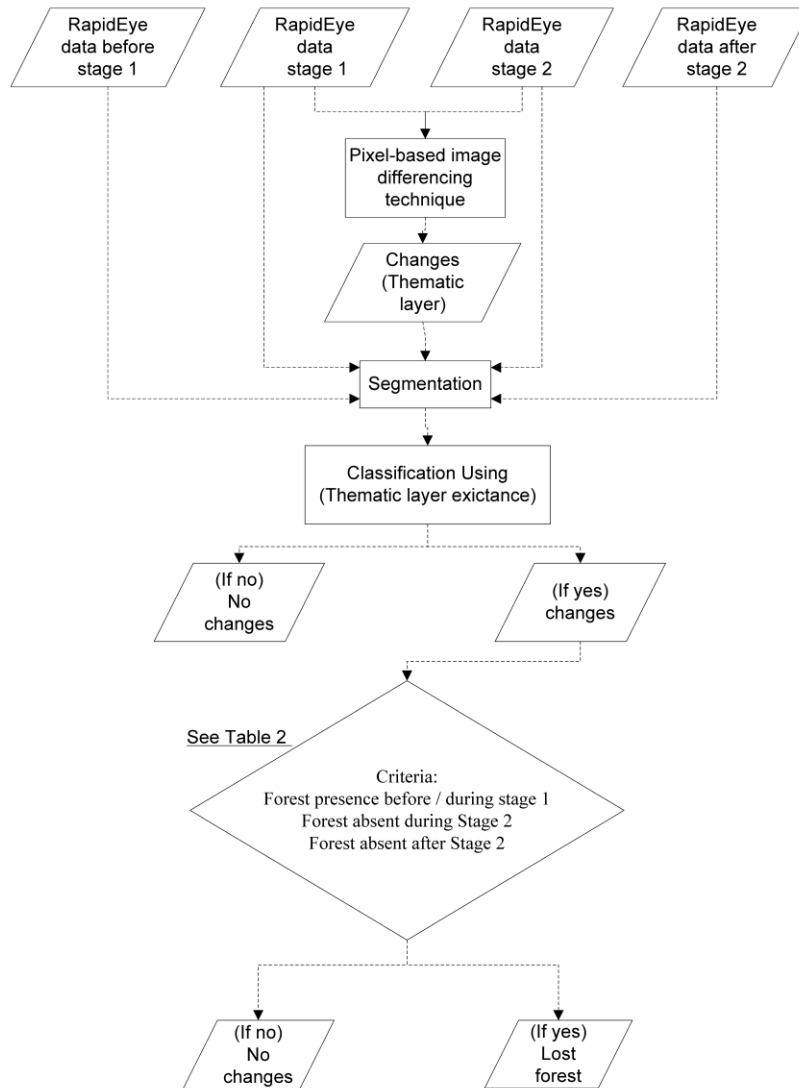
Losses in forest cover resulted in positive values, due to the increase of reflectance in all bands (except the green band) in the second stage image. Therefore, only areas with positive values were used for further analysis. This can be explained by the fact that forest has the lowest reflectance of any vegetative land cover, and, thus, any losses in forest cover will result in brighter reflectance values [29]. However, the areas with positive values in the initial result included not only areas of lost forest cover, but also areas where the changes in reflectance were due to clouds and their shadows, water bodies, and variations in phenology—especially in fields surrounding the forests. In the next step, a difference image representing all positive values was produced to be refined in the object-based environment.

For the object-based analysis (OBIA), eCognition software from Trimble (formerly Definiens) was used. A rule set, consisting of a batch of commands, was developed in eCognition for this study. The multi-resolution segmentation algorithm, which allows for the integration of a geo-database into the segmentation process and assigns weights to all bands, was used. In the segmentation process, the difference image that represents all detected positive values was used to create objects based on its borders. This was done to ensure that the exact extraction of the pixel-based change detection resulted in the formation of objects. Additionally, a few parameters, such as scale parameter, shape, and compactness, were estimated based on a trial and error iteration procedure (see Table 1). In the second part of the process, all objects were initially classified as "change" or "no change" based on the difference image representing positive values. The results were then refined in order to detect only the areas where forest cover was lost between the two data takes. To be assigned as lost forest, an object had to meet all of the following three criteria:

(I)   Existence of forest during the first stage (first data take) or before the first stage, as derived from additional RE data from previous image takes, in case of the presence of clouds during first data take.

(II)   Forest absence in the second stage (second data take).

(III) Forest absence after the second stage, in case of the presence of clouds during the second data take, also derived from later RE data takes.

Table 1. Multi-resolution segmentation parameters used in eCognition.

Parameter	First Period (April–June/July)	Second Period (June/July–August)
Scale	20	20
Shape	0.1	0.1
Compactness	0.9	0.9
Bands weights	All bands from April and August, the given weight was 1	All bands from April, August and October, the given weight was 1

The indices used to refine the results by these criteria are presented in Table 2. Criterion number one excluded all changes that occurred outside the forest area, such as changes due to water bodies or seasonal variations in plant phenology in nearby fields. Where clouds were present, criterion number one used also previous RapidEye data from before stage 1 to check the existence of the forest. Criterion number two examined whether the areas where the changes occurred were actually still forested in the second stage. If this was found to be the case, these changes were excluded from the forest change category and instead attributed to seasonal changes due to forest plant phenology. Where clouds were present in the second stage image, criterion number three safeguarded that the remaining changes did not belong to forest cover, by using subsequent RE data from after the second stage. After the application of all three criteria, objects that were still seen as changes in forest cover were assigned as lost forest.

Table 2. The indices used to create the three criteria used to extract the forest loss areas (see Figure 2).

Criterion	First Period (April–June/July)	Second Period (June/July–August)
Forest present before/during stage 1	Blue/Green ratio (April) Brightness (April) NDVI (April)	Blue/Green ratio (April) NDVI (April)
Forest absent during stage 2	Blue/Green ratio (June/July) NDVI (June/July)	Blue/Green ratio (August)
Forest absent after stage 2	Blue/Green ratio (August) NDVI (August)	NDVI (October)

2.3.3. Accuracy Assessment and Comparison with the Aerial Images Results

The change detection performance was assessed via an error matrix. Polygons were used as sampling units rather than points, as points tend to underestimate the accuracy of object-based results [30]. Each polygon was formed by centering a circle of 60 m in diameter on one corner of a $(350 \times 350 \text{ m}^2$ cell size) grid. This diameter was based on the average size of the objects formed during the change detection process. The reference values (change/no change) for these sampling units were assigned based on visual interpretation of the three RE scenes from April to October, additionally supported by interpretation of the aerial images from August. If any change was found within a polygon, it was assigned to the change category. Then, the agreement between the change detection results and the reference value was visually assessed for each polygon. In total, 849 polygons distributed systematically over the study area were used for the accuracy assessment. Out of this process, the overall user and producer accuracies, as well as the kappa coefficient were obtained [31,32]. This accuracy assessment process was carried out for the results from both the RE and the aerial images, and the results were compared to one another.

2.3.4. Cost Comparison between RapidEye Data and Aerial Images

For the cost calculation, it was assumed that reference data would already be available before the occurrence of a storm event and thus, only data from after the storm event need be acquired. Three main cost categories were taken into consideration: the price of the raw data, the cost of data pre-processing and data analysis. The raw data cost was calculated based on the number of images needed to cover the study area. At least a thousand aerial images of the resolution regularly used by the annual survey are necessary to cover this study area, at a cost of €18 per image, according to LVG. While only four RE images are enough to cover the same area, an additional four images were needed in this case to overcome the problem of cloud cover. Therefore, eight RE images were acquired, at a cost of €593 each. The costs for preprocessing and data analysis were calculated based on the working hours (WH) needed to complete them. An hourly rate of thirty-five Euros/hour (€35/h) was assumed, based on the average gross/hour of the actual public payment scheme in 2011 for workers with appropriate skills. Preprocessing steps included: Geometric correction, triangulation and atmospheric correction (only for RE data). The data analysis consisted of visual interpretation for the aerial images, and implementation of the hybrid method for the RE data, as described in this study.

3. Results

3.1. Solving the Problem of Cloud Cover

In order to determine the amount of forest cover lost using the multi-seasonal RapidEye data, the problem of cloud cover in the images had to be overcome. Figure 3 shows an example of how the method handled the problem of cloud presence during the second image acquisition period (from 22 June/12 July to 22 August). The results of the initial changes are presented in Figure 3 (left and middle), while Figure 3 (right) shows the final results for "lost forest" and the changes, which were excluded after refinement by application of the three criteria.

Figure 3. Example of how additional data from an additional Rapid Eye (RE) image were used to overcome the problem of the presence of clouds in two RE images used for change detection analysis. Initial analysis of the changes between an image from 22 June/12 July (**left**) and one from 22 August (**middle**) indicated differences, which were actually due to either clouds or lost forest. Additional data from the image from 1 October (**right**) facilitated the exclusion of those changes due to clouds and produced the final results showing the actual losses in forest cover, by implementing (1) first criterion; (2) second criterion; and (3) third criterion.
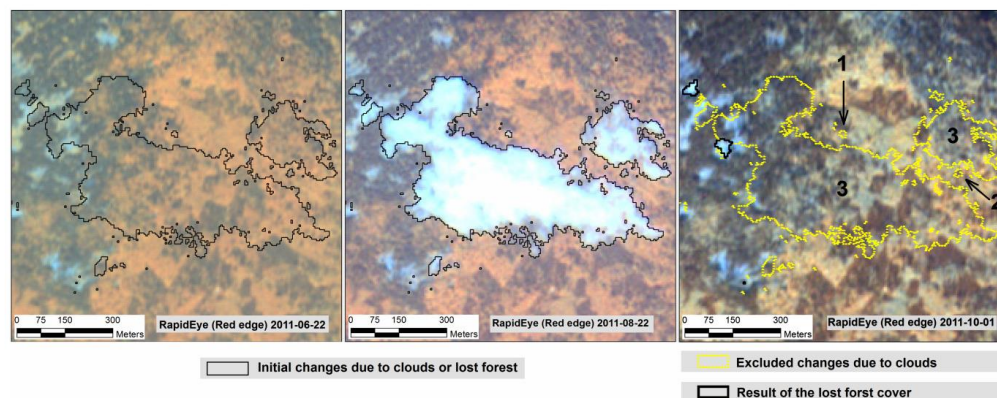
In this example, the first criterion excluded the objects that were not forest on 22 June, and the second criterion excluded the objects that were still forest on 22 August. However, few objects were actually excluded until the third criterion was implemented. The third criterion used the data collected on 1 October to exclude all objects still identified as forest. Thus, only the changes that represented an actual loss of forest cover remained.

3.2. RapidEye Analysis and Accuracy Assessment

The change detection result in Figure 4 shows the amount of forest cover lost during the first period from 19 April to 22 June/12 July. The polygons representing lost forest cover are shown overlaid on top of the two RapidEye images from April and June. As can be seen, the areas within the polygons appear to be darker in the April image than they do in the June image due to the loss of forest cover.

Such a visual comparison shows that the method being tested here achieved relatively accurate mapping of the losses. Most of these losses were probably due to management against bark beetle. Based on the analysis, an area of about 157 ha of forest cover were lost during this period. The change detection result in Figure 5 shows the amount of forest cover lost during the second period (from 22 June/12 July to 22 August). Visual comparison between the images from June and August shows that the result accurately delineated the losses in forest cover, most of which were due to the catastrophic wind storm that occurred in July. Based on this analysis, an estimated area of about 235 ha of forest cover was lost during the second period.

Figure 4. Example of some of the forest cover losses during the first period of analysis from 19 April to 22 June/12 July which were detected using RapidEye data.
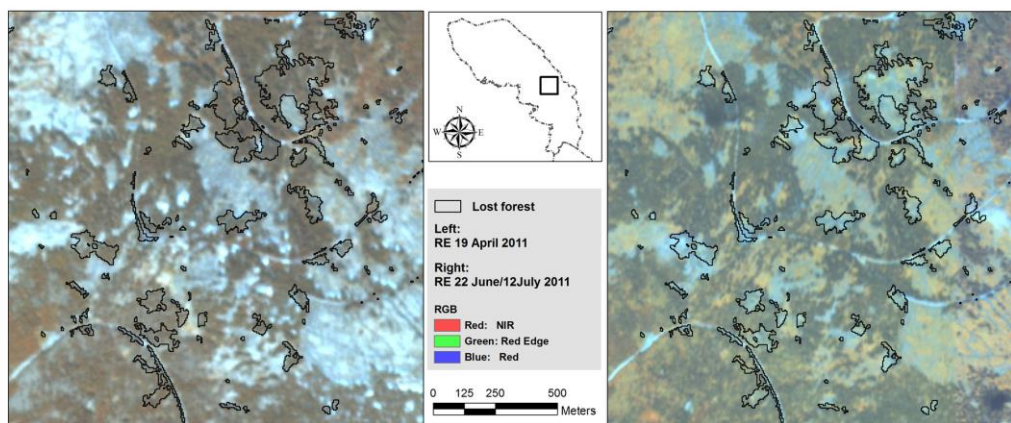
Figure 5. An example showing the forest cover losses during the second period of analysis from 22 June/12 July to 22 August detected using RapidEye data.
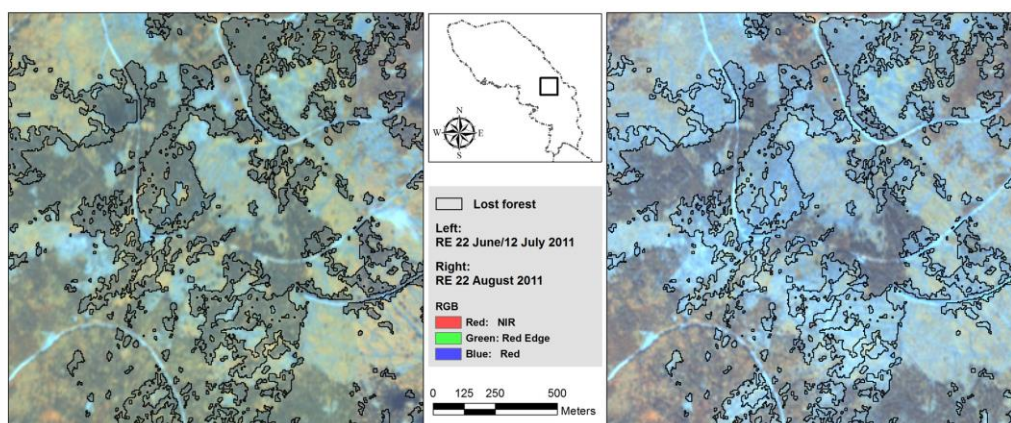
In total, an area of about 392 ha of forest cover was lost during the period from April to August (Figure 6—left). The statistics from the accuracy assessment are presented in Table 3. Overall, the change detection method used here returned satisfactory results in terms of identifying the amount of

forest cover lost, given a 5-m spatial resolution. With reference to the error matrix (Table 3), an overall accuracy of 96.7% and a kappa of 0.86 were achieved—a result which indicates a high level of agreement with the reference data.

Table 3. Error matrix for the change detection results using RapidEye data.

Change Detection RE	Reference		User's Accuracy %
	Change	No Change	
change	104	15	87.4
no change	13	717	98.2
producer's accuracy %	88.9	98.0	kappa 0.86
			overall accuracy 96.7%

The user and producer accuracies for the "lost forest" class were 87.4% and 88.9% respectively, indicating the overall success of the classification. In addition, the high producer's accuracy indicates a good degree of success in identifying most of the forest cover that was lost. However, a few losses were not detected and a few objects were mistakenly identified as losses when no actual loss had occurred. These errors were checked against the high-resolution aerial images as will be discussed later.

3.3. Accuracy Assessment of the Aerial Images

In order to assess the success of the results of the RapidEye data analysis in comparison to the results of the aerial image interpretation, the accuracy assessment of the aerial image was accomplished using the same method. The resulting forest cover losses, derived through on-screen digitizing of the aerial images, are shown in Figure 6 (right).

Figure 6. An example showing total forest cover losses during the period from 19 April to 22 August detected using (**left**) analysis of RapidEye data and (**right**) visual interpretation of aerial images.
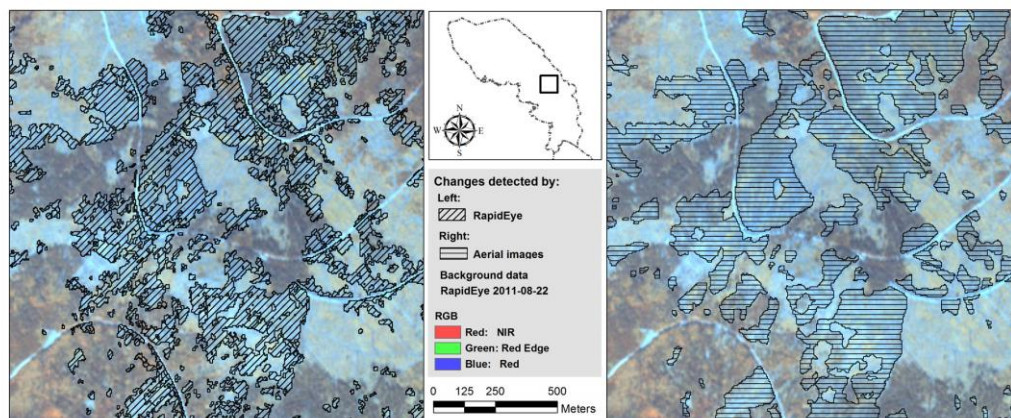
The accuracy assessment statistics are presented in Table 4. An overall accuracy of 98.1% and a kappa of 0.92, and user and producer accuracies for the "lost forest" class of 100.0% and 86.3%

respectively were achieved. A 100% user's accuracy is expected from a visual interpretation of aerial images. Based on aerial image interpretation, an area of about 373 ha of forest cover loss was estimated.

Table 4. Error matrix for the change detection results using Aerial images.

	Reference		
Change Detection AI	**Change**	**No Change**	**User's Accuracy %**
change	102	0	100.0
no change	16	733	97.9
producer's accuracy %	86.4	100.0	kappa 0.92
			overall accuracy 98.1%

3.4. Results and Cost Comparison between RapidEye and Aerial Images

The resulting maps of forest cover losses in the study area from both RapidEye data analysis and aerial images are presented in Figure 7. Statistics showing the level of agreement in hectares between the two results are depicted in Table 5. With reference to the intersection statistics, as observed, the agreement between the two results was found to be very high, and 361 hectares of forest loss were classified identically in both.

Figure 7. Example showing the forest cover losses that were detected only when using aerial image interpretation, those which were detected only when RapidEye data was used and those which were detected using both methods.
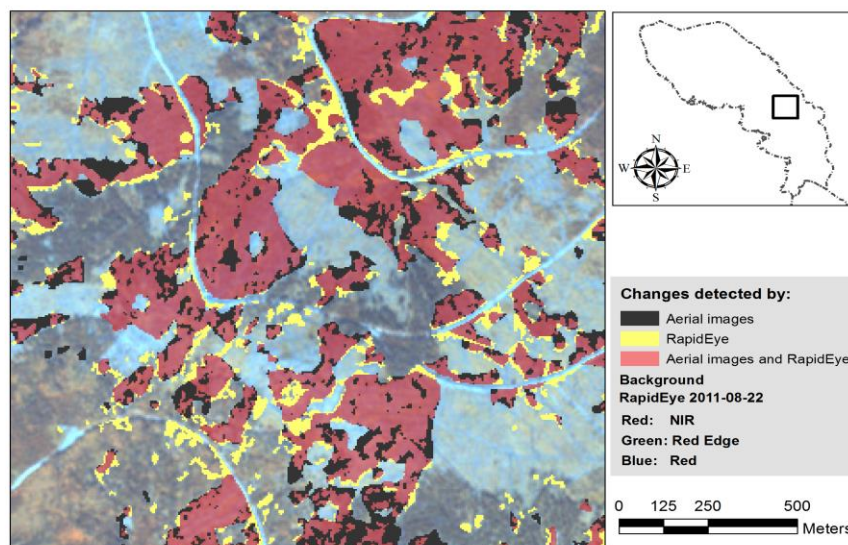
A comparison of the map produced from the analysis of the RapidEye images with the one produced using aerial image interpretation showed generally a very high similarity in the lost forest patch shape and spatial distribution. However, there were some differences between the two outcomes. Most of these differences were at the edges of patches and within the "lost forest", as seen in Figure 7.

The differences between the two results were quantified and analyzed. Then, they were separated into two groups—changes detected only using RapidEye (31 ha, or 8% of all losses) and changes detected only using aerial images (12 ha, or 3% of all losses) (Table 5).

Table 5. Calculated forest losses by data and method utilized.

Data Source	Total Area Detected in Hectares	Area Detected Only by a Specific Dataset in Hectares and (% of Total Area Detected Using This Method)
RapidEye	392	31 (8%)
Aerial images	373	12 (3%)
RapidEye and Aerial images	361	

Visual comparison of the changes detected solely by RapidEye data with the reference data shows clearly that these were actual changes in forest cover caused by either forest harvest or trees being thrown by the storm (Figure 8). However, an examination of the changes detected only by the aerial image analysis showed that some of these changes were not detectable using the RapidEye data, as will be discussed later.

Figure 8. Two examples showing objects classified as "lost forest" overlaid on a RapidEye image from 19 April (**left**), a RapidEye image from 22 August (**middle**), and aerial images from 22 August (**right**). In example A, forest cover losses that were detected solely by RapidEye images are shown. In example B, the aerial image on the right clearly shows the windthrown trees detected solely by the analysis using RapidEye data.
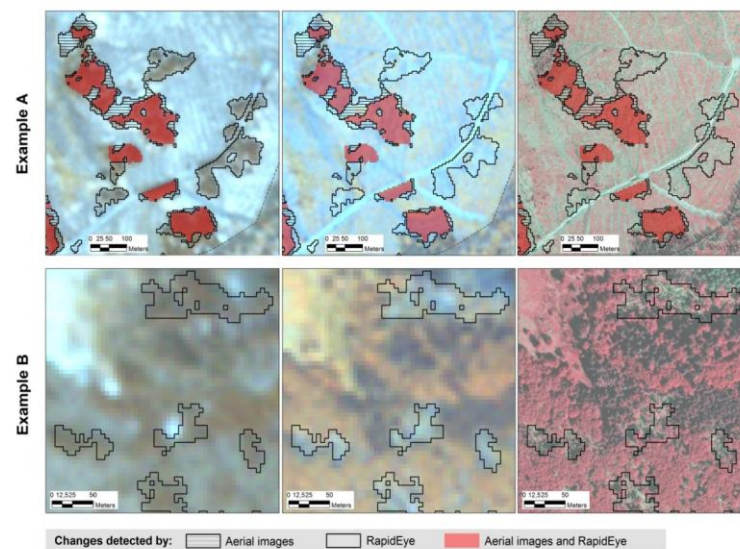
The costs of using RE and those associated with AI were estimated. The results of this comparison, presented in Table 6, show that implementing the RE methodology cost €5,660, while the visual

interpretation of the AI would have cost an estimated €22,200. This indicates that visual interpretation of AI would cost about four times as much as the method using RE data.

Table 6. Cost comparison of change analysis using RapidEye data and aerial images.

Category	RapidEye (Euros)	Aerial Images (Euros)
Raw data	(8 images × €593) = 4750	(1000 images × €18) = 18,000
Preprocessing	(10 WH × €35) = 350	(40 WH × €35) = 1400
Data analysis	(16 WH × €35) = 560	(80 WH × €35) = 2800
Total	5660	22,200

4. Discussion

Implementing this methodology using RapidEye data to detect changes in forest cover produced accurate results, and even small changes in forest cover were detected. The results were comparable to those produced using the official aerial images mapping provided by BFNP. The availability of multi-seasonal RapidEye data enabled the detection of forest losses over two periods of time within one year. This allowed for a better definition of the factors that caused the changes in forest cover. As an illustration, during the first period alone, from April to June/July, a substantial area of about 157 ha of forest cover was lost. This change was due solely to management undertaken as protection against the bark beetle, which indicates the aggressiveness of the calamity. In contrast to RE data, aerial images are only collected once a year in the special case of the BFNP and triennially in the rest of Bavaria. This means, it is not feasible to acquire such timely information from aerial images given the current image update frequency. Additionally, a predefined acquisition date is not possible for the aerial image survey. In the BFNP, the survey typically takes place at the end of the vegetation period. Another advantage, of using the multi-seasonal data, was its helpfulness in overcoming the problem of clouds. In contrast, using less frequently acquired optical data is usually a challenge due to cloud and haze presence [6,17].

The hybrid technique developed here employed multi-seasonal RapidEye data and provided rapid mapping of forest cover losses with up to 96% accuracy. Comparable results, depending on the resolution of the sensor, have been reported in the literature when object-based methods have been used for forest cover change detection using image datasets from sensors of high spatial resolutions. For example, Desclée *et al.* [16] implemented OBCD with SPOT data for forest change detection and achieved an overall accuracy of 93% and a kappa of 0.84. In addition, Duveiller *et al.* [17] estimated the deforestation in central Africa using Landsat data and OBCD with an overall accuracy of 91%. McDermid *et al.* [19] also used Landsat and OBCD in forest change detection and achieved an overall accuracy of 84% and a kappa of 0.69. Moreover, some studies which have utilized a hybrid method similar to that used here have achieved comparable results. In Canada, McDermid *et al.* [20] applied the hybrid method to Landsat data and reported an overall accuracy of 93% and a kappa of 0.889. Another study applied this method using a combination of SPOT data and aerial images and reported an overall accuracy of 94% [15]. However, none of these studies focused on sudden changes; but instead detected inter-annual changes over periods of three to 35 years. Additionally, they did not deal with the problem of cloud presence, but rather, recommended either using more frequently acquired optical data or active system observation.

As an alternative solution using data from satellite sources to map the same storm event addressed here, Rappl *et al.* [10] and Thiele *et al.* [11] demonstrated the use of data from the active satellite system, TerraSAR-X, to overcome the problem of clouds. This also allowed for rapid mapping of the remaining forest cover after the storm, and made comparison to pre-event forest cover estimates derived from RapidEye data or aerial images feasible. Although their results offered rapid estimation of the destruction, it was not possible to compare their results to ours, as there was no accuracy assessment conducted. In addition, the relatively small area of coverage and high cost of the TerraSAR-X data and aerial images remain an issue in using them more frequently, such as for operational use.

Technically, juxtaposing the performance of the RapidEye change detection performed here against that of the aerial images, some differences were detected. Some of these differences were due to the influence of the user in aerial image interpretation, who will naturally try, during manual digitization, to delineate objects that have smooth borders rather than zigzag ones. Moreover, in the manual digitization procedure, many small patches, which do not represent actual forest cover losses, were included in the "lost forest" class. The implications of manual delineation were discussed by Heurich *et al.* [4], and Kautz *et al.* [5], and can be explained by the minimum size of the unit of interest, which is a group of trees or even a stand, rather than a single tree. Our analysis of the differences between the AI interpretation and the RapidEye analysis showed that the RapidEye approach was able to detect solely many of the changes that occurred—about 8% of all losses. However, few objects of those 8% were mistakenly identified as losses, this was due to differences in phenology between April and June/July, and those objects were located mainly in deciduous stands. This can be explained by the increase in the spectral reflectance in the red edge bands in this period due to the change from leaf-off to leaf-on. Only 3% of all losses were not detected by RapidEye, and these were mainly due to the very small extent of these changes, such as only a few single trees, which had fallen within a healthy stand. Therefore, they were too fine to be detected using spectral information alone without actual visual interpretation of AI. Another reason these changes were not found is that they were located among the deciduous stands and shaded areas of the surrounding remaining trees; therefore they were difficult to detect using spectral properties alone. Also, it might be that a few of the changes detected in the AI interpretation occurred before April, 2011, and therefore, were not detectable in the RapidEye change analysis. However, some of these changes were still easily detectable at the center of the damages but not at the periphery. This was due to the complex structure at the periphery, which included thrown trees and healthy standing ones. Similar results were found using Landsat data and the hybrid method in Brazil [18], in which there were also a few objects which were mistakenly identified as losses, when in fact, no actual loss had occurred. The majority of these mistakenly identified losses were due to shaded areas among the tree crowns, especially in less dense forest stands.

From an operational point of view, the hybrid method implemented here allows flexibility and adaptability to a subsequent data set. This ensures continuous monitoring supported by the high temporal resolution of RapidEye data. Although the analysis of the RE data achieved fast and cost effective results, 3% of the changes detected in the official AI survey were not detected using the RE analysis. On the other hand, the RE data and analysis cost only 25% of that of the aerial image analysis. Even though, RE results cannot be expected to fully achieve the results possible using aerial images,

they can provide additional support for subjective and time-consuming visual interpretation of aerial images.

5. Conclusions

This study investigated the feasibility of updating forest cover databases in cases of both regular management activities and sudden events that cause changes in forest cover, such as bark beetle attacks and storm events, by means of RE satellite data. Overall, the five-meter spatial resolution of RapidEye data was suitable for performing detection of forest cover changes. Use of the RE data achieved rapid and cost-effective results that were comparable to those obtained from aerial image interpretation. The high temporal resolution of the RapidEye constellation was useful for the regular forest cover updates on a seasonal basis. This shows the potential of the new high temporal resolution satellites (e.g., Landsat 8 and Sentinels) for use in forest database updates. Hence, sudden changes may be detected in very short period, and addressed efficiently using appropriate management techniques. Local authorities and stakeholders may benefit from the outcomes of this study. The information generated is invaluable to decision makers in planning initial clean-up operations following forest disturbances due to storm events and biotic calamities, as well as in updating existing forest databases.

Although the work described here was restricted to forests in the BFNP, the motivation for the study arose from the *EUS-FH* project goal [7]. The study found that RE mapped 97% of the changes detected using AI interpretation at only 25% of the cost of AI interpretation. In addition, the annual AI survey is available only for the BFNP, while surveys are done only once every three years for the rest of Bavarian state. Moreover, multi-seasonal RE data (acquired every 45 days) are available for all of Germany. Thus, we conclude that the generalization of the methodology presented here to the project's other test areas distributed throughout Bavaria appears to be a must.

Author Contributions

The paper was written by Alata Elatawneh with a contribution by Ioannis Manakos. Additional data collection and preparation was done by Adelheid Wallner. The research approach was developed by Alata Elatawneh and Thomas Schneider. The research coordination and significant contribution to the discussion was done by Thomas Knoke.

Conflicts of Interest

The authors declare no conflict of interest.

References

1. Fischer, A.; Lindner, M.; Abs, C.; Lasch, P. Vegetation dynamics in central European forest ecosystems (near-natural as well as managed) after storm events. *Folia Geobot* **2002**, *37*, 17–32.
2. Wermelinger, B. Ecology and management of the spruce bark beetle *Ips typographus*—A review of recent research. *For. Ecol. Manag.* **2004**, *202*, 67–82.
3. Eriksson, M.; Pouttu, A.; Roininen, H. The influence of windthrow area and timber characteristics on colonization of wind-felled spruces by *Ips typographus* (L.). *For. Ecol. Manag.* **2005**, *216*, 105–116.
4. Heurich, M.; Ochs, T.; Andresen, T.; Schneider, T. Object-orientated image analysis for the semi-automatic detection of dead trees following a spruce bark beetle (*Ips typographus*) outbreak. *Eur. J. For. Res.* **2010**, *129*, 313–324.
5. Kautz, M.; Dworschak, K.; Gruppe, A.; Schopf, R. Quantifying spatio-temporal dispersion of bark beetle infestations in epidemic and non-epidemic conditions. *For. Ecol. Manag.* **2011**, *262*, 598–608.
6. Nagendra, H.; Lucas, R.; Honrado, J.P.; Jongman, R.H.G.; Tarantino, C.; Adamo, M.; Mairota, P. Remote sensing for conservation monitoring: Assessing protected areas, habitat extent, habitat condition, species diversity, and threats. *Biodivers. Monit.* **2013**, *33*, 45–59.
7. Schneider, T.; Elatawneh, A.; Rahlf, J.; Kindu, M.; Rappl, A.; Thiele, A.; Boldt, M.; Hinz, S. Parameter Determination by RapidEye and TerraSAR-X Data: A Step Toward a Remote Sensing Based Inventory, Monitoring and Fast Reaction System on Forest Enterprise Level. In *Lecture Notes in Geoinformation and Cartography*; Krisp, J.M., Meng, L., Pail, R., Stilla, U., Eds.; Springer Berlin Heidelberg: Berlin, Heidelberg, Germany, 2013; pp. 81–107.
8. De Kok, R.; Schneider, T.; Baatz, M.; Ammer, U. Object Based Image Analysis of High Resolution Data in the Alpine Forest Area. Presented at Joint Workshop for ISPRS WG I/1, I/3 AND IV/4, Sensors and Mappinhg from Space, Hanover, Germany, 27 September 1999; pp. 27–30.
9. RapidEye, AG. Satellite Imagery Product Specifications, 2012. Available online: http://www.rapideye.com/upload/RE_Product_Specifications_ENG.pdf (accessed on 13 March 2013).
10. Rappl, A.; Elatawneh, A.; Thiele, A.; Troycke, A.; Schneider, T.; Knoke, T.; Hinz, S. Einsatz der Fernerkundungssysteme TerraSAR-X und RapidEye im Katastrophenmanagement von Windwurfereignissen. In Informationstechnologie für eine nachhaltige Landbewirtschaftung, Fokus Forstwirtschaft, Referate der 32. GIL-Jahrestagung, Freising, Germany, 29 February–1 March 2012; Clasen, M., Ed.; Ges. für Informatik: Bonn, Germany, 2012; Volume 194, pp. 235–238.
11. Thiele, A.; Boldt, M.; Hinz, S. Automated Detection of Storm Damage in Forest Areas by Analyzing TerraSAR-X Data. In Proceedings of the 2012 IEEE International Geoscience and Remote Sensing Symposium (IGARSS), Munich, Germany, 22–27 July 2012; pp. 1672–1675.

12. Brunner: Sturmwürfe im Nationalpark Rasch Aufarbeiten 2012. Available online: http://www. forstpraxis.de/brunner-sturmwuerfe-nationalpark-rasch-aufarbeiten (accessed on 3 February 2012).

13. Hussain, M.; Chen, D.; Cheng, A.; Wei, H.; Stanley, D. Change detection from remotely sensed images: From pixel-based to object-based approaches. *ISPRS J. Photogramm. Remote Sens.* **2013**, *80*, 91–106.

14. Chen, G.; Hay, G.J.; Carvalho, L.M.T.; Wulder, M.A. Object-based change detection. *Int. J. Remote Sens.* **2012**, *33*, 4434–4457.

15. Willhauck, G.; Schneider, T.; De Kok, R.; Ammer, S. Comparison of Object Oriented Classification Techniques and Standard Image Analysis for the Use of Change Detection between SPOT Multispectral Satellite Images and Aerial Photos. In Proceedings of the XIX ISPRS Congress, Amsterdam, The Netherlands, 16–23 July 2000.

16. Desclée, B.; Bogaert, P.; Defourny, P. Forest change detection by statistical object-based method. *Remote Sens. Environ.* **2006**, *102*, 1–11.

17. Duveiller, G.; Defourny, P.; Desclée, B.; Mayaux, P. Deforestation in Central Africa: Estimates at regional, national and landscape levels by advanced processing of systematically-distributed Landsat extracts. *Earth Obs. Terr. Biodivers. Ecosyst. Spec. Issue* **2008**, *112*, 1969–1981.

18. Carvalho, L.M.T.; Fonseca, L.M.G.; Murtagh, F.; Clevers, J.G.P.W. Digital change detection with the aid of multiresolution wavelet analysis. *Int. J. Remote Sens.* **2001**, *22*, 3871–3876.

19. McDermid, G.J.; Pape, A.; Chubey, M.; Franklin, S. Object Oriented Analysis for Change Detection. In Proceedings of the 25th Canadian Symposium on Remote Sensing, Montréal, Canada, 14–17 October 2003.

20. McDermid, G.J.; Linke, J.; Pape, A.D.; Laskin, D.N.; McLane, A.J.; Franklin, S.E. Object-based approaches to change analysis and thematic map update: Challenges and limitations. *Can. J. Remote Sens.* **2008**, *34*, 462–466.

21. Wulder, M.A.; White, J.C.; Coops, N.C.; Butson, C.R. Multi-temporal analysis of high spatial resolution imagery for disturbance monitoring. *Remote Sens. Environ.* **2008**, *112*, 2729–2740.

22. Heurich, M.; Neufanger, M. *Die Wälder des Nationalparks Bayerischer Wald: Ergebnisse der Waldinventur 2002/2003 im geschichtlichen und waldökologischen Kontext*; Nationalparkverwaltung Bayerischer Wald: Grafenau, Germany, 2005.

23. Escherich, K. Die Forstinsekten Mitteleuropas ein Lehr-und Handbuch Band 2 Spezielle Teil Abt. In *1 Die Urinsekten, die Geradflügler, die Netzflügler und die Käfer. Systematik, Biologie, forstliches Verhalten und Bekämpfung*; P. Parey: Berlin, Germany, 1923.

24. Heurich, M. *Waldentwicklung im Bergwald nach Windwurf und Borkenkäferbefall*; Nationalparkverwaltung Bayerischer Wald: Grafenau, Germany, 2001.

25. Rall, H.; Martin, K. *Luftbildauswertung zur Waldentwicklung im Nationalpark Bayerischer Wald 2001*; Nationalparkverwaltung Bayerischer Wald: Grafenau, Germany, 2002.

26. Walter, V. Object-based classification of remote sensing data for change detection. *ISPRS J. Photogramm. Remote Sens.* **2004**, *58*, 225–238.

27. Singh, A. Review article digital change detection techniques using remotely-sensed data. *Int. J. Remote Sens.* **1989**, *10*, 989–1003.

28. Elatawneh, A.; Rappl, A.; Schneider, T.; knoke, T. A semi-automated method of forest cover losses detection using RapidEye images: A case study in the Bavarian forest National Park. Presented at Vom Algorithmus zum Produkt: Tagungsband zum 4. RESA-Workshop, Neustrelitz, Germany, 21–22 March 2012; Borg, E., Ed.; GITO, Verl. für Industrielle Informationstechnik und Organisation: Berlin, Germany, 2012; pp. 183–200.
29. Huang, C.; Song, K.; Kim, S.; Townshend, J.R.G.; Davis, P.; Masek, J.G.; Goward, S.N. Use of a dark object concept and support vector machines to automate forest cover change analysis. *Remote Sens. Environ.* **2008**, *112*, 970–985.
30. Biging, G.; Colby, D.; Congalton, R. Sampling Systems for Change Detection Accuracy Assessment. In *Remote Sensing Change Detection: Environmental Monitoring Methods and Applications*; Lunetta, R.S.E.C., Ed.; Ann Arbor Press: Chelsea, UK, 1998.
31. Congalton, R.G.; Green, K. *Assessing the Accuracy of Remotely Sensed Data: Principles and Practices*; CRC/Lewis Publications: Boca Raton, FL, USA, 1999.
32. Foody, G.M. Status of land cover classification accuracy assessment. *Remote Sens. Environ.* **2002**, *80*, 185–201.

8.4 Publication 4

Elatawneh A., Rappl A., Rehush N., Schneider T., Knoke T. 2013. Forest tree species identification using phenological stages and RapidEye data: a case study in the forest of Freising. In book: From the Basics to the Service, Editors: Erik Borg, Holger Daedelow, Ryan Johnson, Publisher: GITO Verlag, pp.21–38. ISBN: 978-3-95545-022-1

Forest tree species communities identification using multi phenological stages RapidEye data: case study in the forest of Freising

Elatawneh A.[1], Rappl A. [1,2] , Rehush N.[3], Schneider T.[1], Knoke T.[1]

[1]Institut of Forest Management, Technische Universität München (TUM)
[2] Bayerische Landesanstalt für Wald und Forstwirtschaft (LWF)
[3]Ukrainian National Forestry University (UNFU)

Tree species identification is a very important issue for forest management and planning. In the recent three decades, many studies have investigated this topic using multispectral multi-seasonal / temporal data. In this study we analyzed multi seasonal/temporal RapidEye images from twenty dates for the purpose of tree species classification. The main objective of this work was to investigate the effect of the temporal resolution on the accuracy, two specific aims were; i) to investigate the influence of the RedEdge band on the classification accuracy; ii) to investigate the influence of the indices on the accuracy. Spectral Angle Mapper (SAM) classifier and cross validation procedure were used for this purpose. The best overall accuracy achieved was about 86% that separated seven tree species (Three deciduous and four coniferous).increasing the temporal resolution has clearly improved the accuracy. Ranking the images according to their impact on the accuracy, using the first seven dates, has dramatically improved the accuracy, then the improvement slow down after the seventh date. Using the RedEdge bands has improved the overall accuracy with 1% to 4%, while using indices has additionally improved the overall accuracy with 2% to 4%.

1 Introduction

Forest management taking into the consideration the economic and the sustainable aspects requires persistent inventory for the forest conditions (Stoffels et al. 2012). Management planning and statistics assortment on enterprise level, as well as fulfillment of reporting duties on national and international level are based on such inventories. A frequent upgrade of ten years takes place for the national forest inventory In Germany, as well as for the Bavarian State owned forests. Typically a regular sample grid is established in field to collect databases attributes of various forest stand characteristics such as detailed species composition, age information, timber volume and further management-relevant features. However, such terrestrial inventories are cost-intensive and time-consuming.

In the recent decades multi-spectral Remote Sensing data appear as an attractive resource to complement and optimize forest inventories (Holmgren & Thuresson 1998, Vohland et al. 2007). The Remote Sensing based inventory has been focusing on 1) The forest (timber) type discrimination and 2) The estimation of biophysical and biochemical properties (Boyd &

1

Danson 2005, Holmgren & Thuresson 1998). It is of great value, to use such parameters as inputs for forest prognosis models, which offer an alternative solution for the forest management planning of the next 10 to 20 year period. Especially, single tree competition approaches like SILVA, used for management of Bavarian State Forest (Pretzsch et al. 2002), take advantage of tree species information.

Still, tree species identification is a challenging task for the Remote sensing community. Under Mid-European conditions tree species discrimination on base of high resolution (5-30m) multi- to hyperspectral data failed with mono-temporal approaches. However, the accuracy of these classifications can be enhanced using multi-seasonal data. This is because the classifications of multi-seasonal data sets detect the temporal change in the spectral response from different forest tree species types as a result of phenological activity (Boyd & Danson 2005).

Many studies, since early 1980s, have tried and used multi-seasonal multispectral data to benefit the phenology in order to enhance the tree species classification results. Sensors such as Landsat (Dorren et al. 2003; Franco-Lopez et al. 2001; Mickelson Jr. et al. 1998; Reese et al. 2002; Schriever & Congalton 1995; Townsend & Walsh 2001; Walsh 1980; Wolter 1995) SPOT (Davranche et al. 2010) and ASTER (Stoffels et al. 2012) have been used for this purpose. However, the previous studies have not focus on the evaluation of the increase of temporal resolution, due to the limited number of scenes. The data from the upcoming RapidEye satellite constellation with very high temporal resolution capability makes them potentially ideal to be tested and used for phenological monitoring (Stoffels et al. 2012).

In this study our main objective is to evaluate the increase of the temporal resolution on the tree species classification accuracy taking advantage from RapidEye time series. Two specific aims of this paper are 1) the evaluation of the Red Edge band influence on the result accuracy and 2) the evaluation of the indices influence on the accuracy.

2   Study Area and Materials

2.1 Study Area

The study area Kranzberger and Thalhausener Forest, in Freising (2178.9 ha) is located in the southern part of Bavaria close to the city of Freising (Figure 1). It covers the growth zone of the Bavarian Tertiary Hills, which is a high potential growing region for different tree species. The annually mean temperature is 7.5°C and the annual mean precipitation rate is 800 mm, with its maximum in summer time. The forest management of the study area belongs to the Bavarian State Forestry. The composition of the different tree species is shown in Table 2. Spruce is the main tree species and covers 60% of the area. The forest is managed with two different strategies. On the one hand pure stands of tree species with same age and on the other hand mixed stands with different layers of age.
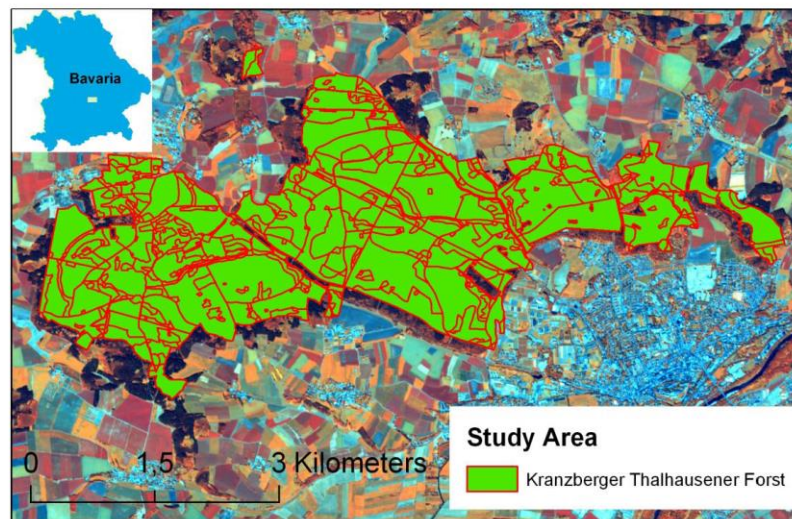
2

Figure 1: Freising forest study area in Bavaria, Germany.

2.2 Data set

2.2.1 Field observations

The field observation data used in this study to train and validate the tree species classification were collected in the field during the years 2010 and 2011. The tree species communities positions were recorded using hand held GPS, and by using digital aerial images (20 cm spatial resolution) from the year 2009. However, many observations were not representative and therefore, not taken into consideration. This is due to the invisibility of the tree crowns which don't reach the over story, this problem was also reported in few studies before (Key et al. 2001) and (Waser et al. 2011). At the end 546 points were considered for this study (Table 1).

Table 1: Tree species samples in the study area, species proportion of tree species is based on the terrestrial inventory from the Bavarian state forest from the year 2001:

Scientific name	Common name	Symbol	Number of samples	Species proportion
Picea abies (L.)	Norway Spruce	Fi	212	73 %
Pseudotsuga menziesii (M.F.)	Douglas fir	Do	32	2 %
Pinus sylvestris (L.)	Scots pine	Ki	34	4 %
Larix decidua (MILL.) Larix kaempferi	European Larch Japanese Larch	La	41	5 %
Fagus sylvatica	Beech	Bu	153	5 %
Quercus petraea (Mattuschka)	Oak	Ei	38	3 %
Acer pseudoplatanus	Maple	Ba	36	2 %

3

197

2.2.2 RapidEye images

A total of 20 RapidEye images of Level 3A were provided by RESA, over a period of 3 year, from may 2009 until November 2011. The images were at sensor radiometrically corrected and geometrically corrected as well. However, the geometric correction is not good enough, especially for the multi temporal image analysis, in which farther correction should be carried on.

Table 2: The RapidEye images were used in this study:

ID	Date time and sensor	ID	Date time and sensor
1	2009-05-20T110408_RE4	11	2011-06-04T110442_RE1
2	2009-07-27T105426_RE1	12	2011-06-28T110849_RE1
3	2010-04-22T105818_RE3	13	2011-07-10T111720_RE3
4	2010-06-08T110621_RE2	14	2011-07-16T110430_RE5
5	2010-07-21T110853_RE2	15	2011-08-23T112009_RE4
6	2010-08-15T111131_RE3	16	2011-09-03T111442_RE1
7	2010-10-10T110933_RE2	17	2011-09-25T111227_RE4
8	2011-03-22T110819_RE3	18	2011-10-06T110644_RE1
9	2011-04-07T110454_RE5	19	2011-10-22T112135_RE2
10	2011-05-06T111258_RE5	20	2011-11-04T111457_RE1

3 Methods

3.1 Data preprocessing

For all RapidEye images the geometric correction was improved, and shifts in both easting and northing directions were implemented if necessary. Moreover, Atmospheric correction was carried out for all images, using ATCOR 3 implemented in the PCI Geomatica 10.3 environment. ATCOR 3 algorithm uses the Digital Elevation Model (DEM) to consider the topographical effects on the spectral reflectance during the correction process, and eliminate the errors due to the topography. More and more, the visibility at the exact acquisition time for each image was also ordered from the Deutsche Wetter Dienst (DWD) and used in the correction.

3.2 Image analysis

Typically, the assumption is that the same tree species have similar reflectance at the same phenological stage. However, it's often that the illumination among the same tree species is different, due to the shadow effects from the surroundings and the topographical effects (even after the topographic correction). The Spectral Angle Mapper (SAM) (Kruse et al. 1993) was chosen to perform the classification because it is highly insensitive to illumination effects since it uses only the direction of the vector and not its length (Eckert & Kneubühler 2004, Elatawneh et al. 2012a). Additionally, to further minimize these effects, for selection of

4

samples we followed hints from Korpela et al. (2011)using Leica ADS40 very high resolution (VHR) data and Immitzer et al. (2012) using WorldView-2 data, which selected solely sunlit crown areas for picking the spectra of tree species to be used as training samples for classification. In our case the brightest pixel of a collective of homogeneous pixel identified to belong to a pure species tree group was selected as sample.

From our observation for the tree species reflectance we noticed that the reflectance is often similar in many band but not all of them. Therefore, angle indices are (Figure 2) will emphasize the differences among tree species, because they represent the reflectance ratios among the individual reflectance of the bands.
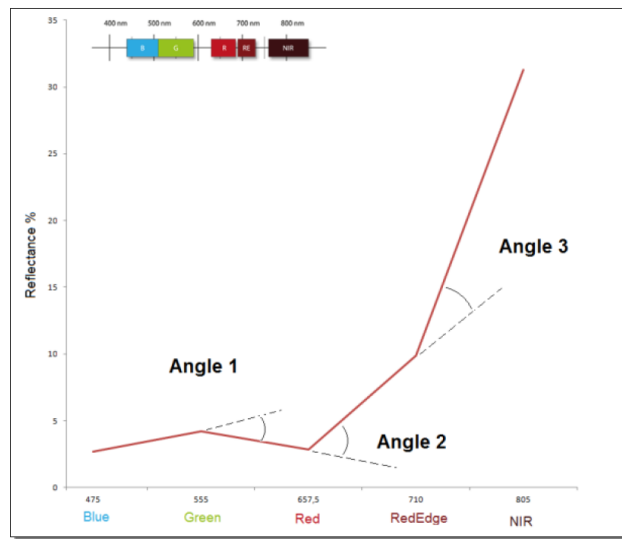
Figure 2: Angle indices illustration.

These indices are expected also to be less affected by the illumination variations and as a result will improve the classification accuracy. For the calculation of these indices we calculate the different in the slopes as explained in the following equations:

$$Angle\ 1 = 2\ \frac{(Red - Green)}{102} - \frac{(Green - Blue)}{80} \ldots \ldots \ldots \ldots equation\ 1$$

$$Angle\ 2 = \frac{(RedEdge - Red)}{52} - 2\ \frac{(Red - Green)}{102} \ldots \ldots \ldots \ldots equation\ 2$$

$$Angle\ 3 = \frac{(NIR - RedEdge)}{95} - 0.5\ \frac{(RedEdge - Red)}{52} \ldots \ldots \ldots \ldots equation\ 3$$

All indices were then enhanced by duplicating their values as seen in the equations. In addition to, the NDVI was also considered and added to these indices.

$$NDVI = \frac{(NIR - Red)}{NIR + Red} \ldots \ldots \ldots \ldots equation\ 4$$

5

3.3 K-fold cross validation

The K-fold Cross validation technique (Geisser 1975, Stone 1974) is a strategy that partitions the data randomly into a number of K-subsets, using each subset in turn as a training set for a model production and the remaining data as a validation set. Then, the process is repeated k-times, and the k results are either averaged or combined and produce one result. The advantage of using this strategy is that all dataset are used for both training and validation. For this study a 10-fold cross-validation strategy was used to carry out the classification.

3.4 Image combinations Selection and classification

To investigate the increase of the temporal resolution on the classification accuracy, 20 possible image combinations was selected. The first step was to evaluate the result accuracy for each of all 20 dates (using only the original bands). The classification and evaluation were carried out for each data using cross-validation strategy and Spectral Angle Mapper (SAM) classifier.

Once the accuracies were evaluated, the 20 image combinations were established by choosing the best single-, two-, three-dates, etc, until twenty-dates (table 3). Then each image combination was classified and the result was evaluated again using cross-validation strategy.

To investigate the RedEdge band influence on the classification, the same procedure and image combinations were implemented, but with excluding the RedEdge band. The procedure was implemented once more by adding the indices as additional band to evaluate the indices influence on the accuracy as well.

4   Results

The general trends as seen in Table 3 and Figure 3 illustrate that with the increase of the temporal resolution the overall accuracy also increase. However, this was the expected trend of the results, as the increase in the data will increase the accuracy. But on the other hand, it shows us that the trend in the increase is an inverse exponential function (IEF). On other words, the result improves dramatically at the beginning then it improves slightly. An important point here is revealed, which is satisfactory classification accuracy is achieved with less than the entire data set, about seven to eight data set.

The results of the bands combination selection show that the scenes from the spring or early phenological stage deliver in general better accuracy than scenes from the autumn. This is explained by the low solar angle during autumn thus the radiometric quality of these images was decreased. However, scenes from summer (e.g., first-, fifth-, and sixth-best images) were among the best scenes as well. The quality of these images was the best of all scenes. However, in this study it was not meant to investigate the effect of the quality on the achieved accuracy, and this point will not be discussed.

Regarding the effect of the RedEdge band on the accuracy, figure 3 shows clearly that using the RedEdge band has slightly improved the accuracy with about 1 %. However, it's noticeable that the RedEdge band does not improve the results using the image combinations

6

of best 2-, 3- or 4-dates, but on the other hand, with the increase of the image combination it produces better accuracy.

Table 3: Overall classification accuracy for the image combinations from different dates:

Number of images	Image Dates	Overall (one scene) Accuracy %	Overall (image combinations) Accuracy		
			All bands	4 bands without RE	All bands + Indices
1	2011-07-16T110430_RE5	67.07	67.07	63.92	72.81
2	2010-04-22T105818_RE3	63.15	73.71	73.02	77.25
3	2011-06-04T110442_RE1	59.73	77.61	77.29	80.12
4	2011-04-07T110454_RE5	59.67	78.71	78.75	81.44
5	2011-07-10T111720_RE3	59.14	79.43	78.57	82.40
6	2009-07-27T105426_RE1	58.65	81.26	78.90	83.19
7	2011-03-22T110819_RE3	57.61	82.60	82.01	84.03
8	2009-05-20T110408_RE4	57.06	81.91	81.12	84.19
9	2011-06-28T110849_RE1	56.04	82.38	81.03	84.62
10	2010-06-08T110621_RE2	54.76	83.25	81.97	85.14
11	2010-07-21T110853_RE2	54.62	83.03	82.17	85.10
12	2011-11-04T111457_RE1	53.79	83.92	83.46	85.88
13	2011-10-22T112135_RE2	53.30	83.74	82.68	85.94
14	2011-05-06T111258_RE5	50.57	83.54	82.36	85.55
15	2010-08-15T111131_RE3	48.72	83.60	82.32	85.49
16	2010-10-10T110933_RE2	48.15	83.70	82.84	86.06
17	2011-09-25T111227_RE4	46.48	84.43	83.37	**86.35**
18	2011-08-23T112009_RE4	44.57	84.21	83.11	86.20
19	2011-10-06T110644_RE1	40.74	**84.41**	**83.46**	86.30
20	2011-09-03T111442_RE1	39.21	84.29	83.27	86.32

Indices were developed for this study has clearly improved the accuracy. The average improvement in the accuracy using the first, second third and fourth best dates combinations was about 4%, then the rate of the improvement was slightly decrease to 2% for the last best combinations. However, using different or more indices could further improve the accuracy, but for the study the introduced indices has been only considered.

The confusion matrix of the best result achieved from 17 image combination is shown in Table 4. The producer accuracy for the individual classes ranges from about 64% to 94%. The highest accuracy was achieved for the spruce class 94.52%, where most of the classes achieved producer accuracy range between 82 and 86% namely Douglas fir, Pine, Beech and Maple classes. The least two accuracy values were about 64% and 74% for the classes Larch and Oak respectively. There was a highest amount of confusion with the Larch class was with both Pine and Oak classes, however, similarity in the reflectance of the Larch was noticed with these two classes in most of the phenological stages.

7
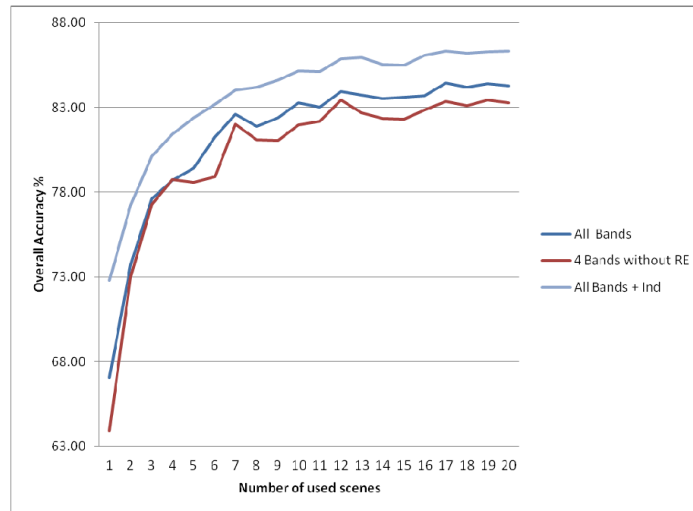
Figure 3: overall accuracy for date combinations (see also Table 3).

5 Discussions

This study attempted to classify seven tree species (four coniferous and three deciduous) in a typical mid-Europe forest area. Multi- seasonal/temporal RapidEye data (twenty scenes) have been used for the purpose of this study. We evaluated the increase of the temporal resolution on the accuracy of the classification. The results show that the temporal resolution has increased the accuracy, however, satisfactory classification accuracy was achieved using less than the entire images (about seven to eight images).

Table 4: Confusion matrix of the classification map using the best 17 dates (all bands + Indices):

	Reference data								
Class.	Spruce	Douglas	Pine	Larch	Oak	Beech	Maple	Sum	User Acc. %
Spruce	1899	9	0	0	0	0	0	1908	99.53
Douglas	46	229	0	0	0	19	0	294	77.89
Pine	2	12	1033	53	37	18	15	1170	88.29
Larch	3	1	56	223	17	37	12	349	63.90
Oak	20	2	55	41	203	2	19	342	59.36
Beech	28	9	16	7	3	450	0	513	87.72
Maple	11	3	76	22	16	4	206	338	60.95
Sum	2009	265	1236	346	276	530	252	4914	
Prod. Acc. %	94.52	86.42	83.58	64.45	73.55	84.91	81.75	Overall Acc. %	86.35

8

The effect of using the RedEdge band and indices was also evaluated in this work. The results show that using the RedEdge band has slightly improve the accuracy within the range of 1% to 4%, while using the indices has additionally improved the accuracy with 2% to more than 4% (see table 3).

The best overall accuracy of about 86% was achieved, using the best-17 image combination with indices and the RedEdge bands. However, some interesting points were not investigated here, (e.g.) to determine the best scenes (single and multiseasonal) for separating individual tree species classes. This is the advantage of an multiannual / multiseasonal approach as given by the investigated data set, compared to a multiseasonal approach with the ambition to update forest management databases on an annual basis, the integration of additional information from other sensor types, e.g. height information (Elatawneh et al. 2012b), etc.

6 Acknowledgments

7 Literature

Boyd D, Danson F. 2005. Satellite remote sensing of forest resources: three decades of research development. *prog phys geogr* 29 (1):1–26

Davranche A, Lefebvre G, Poulin B. 2010. Wetland monitoring using classification trees and SPOT-5 seasonal time series. *Remote Sensing of Environment* 114 (3):552–62

Dorren LKA, Maier B, Seijmonsbergen AC. 2003. Improved Landsat-based forest mapping in steep mountainous terrain using object-based classification. *Forest Ecology and Management* 183 (1–3):31–46

Eckert S, Kneubühler M, eds. 2004. *Application of hyperion data to agricultural land classification and vegetation properties estimation in switzerland*

Elatawneh A, Kalaitzidis C, Petropoulos GP, Schneider T. 2012a. Evaluation of diverse classification approaches for land use/cover mapping in a Mediterranean region utilizing Hyperion data. International Journal of Digital Earth. *International Journal of Digital Earth*:1–23

Elatawneh A, Tian J, Schneider T, Reinartz P. 2012b. Welche Aufl ösung wird für Aussagen auf Betriebsebene benötigt? Erkennen von Strukturveränderungen in heterogener Waldgebiete. *AFZ – Der Wald* (67):17–19

Franco-Lopez H, Ek AR, Bauer ME. 2001. Estimation and mapping of forest stand density, volume, and cover type using the k-nearest neighbors method. *Remote Sensing of Environment* 77 (3):251–74

Geisser S. 1975. The Predictive Sample Reuse Method with Applications. *Journal of the American Statistical Association* 70 (350)

Holmgren P, Thuresson T. 1998. Satellite remote sensing for forestry planning—A review. *Scandinavian Journal of Forest Research* 13 (1-4):90–110

9

Immitzer M, Atzberger C, Koukal T. 2012. Tree Species Classification with Random Forest Using Very High Spatial Resolution 8-Band WorldView-2 Satellite Data. *Remote Sensing* 4 (9):2661–93

Key T, Warner TA, McGraw JB, Fajvan MA. 2001. A Comparison of Multispectral and Multitemporal Information in High Spatial Resolution Imagery for Classification of Individual Tree Species in a Temperate Hardwood Forest. *Remote Sensing of Environment* 75 (1):100–12

Korpela I, Heikkinen V, Honkavaara E, Rohrbach F, Tokola T. 2011. Variation and directional anisotropy of reflectance at the crown scale — Implications for tree species classification in digital aerial images. *Remote Sensing of Environment* 115 (8):2062–74

Kruse FA, Lefkoff AB, Dietz JB. 1993. Expert system-based mineral mapping in northern death valley, California/Nevada, using the Airborne Visible/Infrared Imaging Spectrometer (AVIRIS). Airbone Imaging Spectrometry. *Remote Sensing of Environment* 44 (2–3):309–36

Mickelson Jr. J, Civco D, Silander Jr. J. 1998. Delineating forest canopy species in the northeastern United States using multi-temporal TM imagery. *Photogrammetric Engineering & Remote Sensing* 64 (9):891–904

Pretzsch H, Biber P, Ďurský J. 2002. The single tree-based stand simulator SILVA: construction, application and evaluation. National and Regional Climate Change Impact Assessments in the Forestry Sector. *Forest Ecology and Management* 162 (1):3–21

Reese HM, Lillesand TM, Nagel DE, Stewart JS, Goldmann RA, et al. 2002. Statewide land cover derived from multiseasonal Landsat TM data: A retrospective of the WISCLAND project. *Remote Sensing of Environment* 82 (2–3):224–37

Schriever J, Congalton R. 1995. Evaluating Seasonal Variablity as an Aid to Cover-Type Mapping from Landsat Thematic Mapper Data in the Northwest. *Photogrammetric Engineering & Remote Sensing* 61 (3):321–27

Stoffels J, Mader S, Hill J, Werner W, Ontrup G. 2012. Satellite-based stand-wise forest cover type mapping using a spatially adaptive classification approach. *Eur J Forest Res* 131 (4):1071–89

Stone M. 1974. Cross-Validatory Choice and Assessment of Statistical Predictions. *Journal of the Royal Statistical Society. Series B (Methodological)* 36 (2):111–47

Townsend P, Walsh S. 2001. Remote sensing of forested wetlands: application of multitemporal and multispectral satellite imagery to determine plant community composition and structure in southeastern USA. *Plant Ecology* 157 (2):129–49

Vohland M, Stoffels J, Hau C, Schüler G. 2007. Remote sensing techniques for forest parameter assessment: multispectral classification and linear spectral mixture analysis. *Silva Fennica* 41 (3):441–56

Walsh SJ. 1980. Coniferous tree species mapping using LANDSAT data. *Remote Sensing of Environment* 9 (1):11–26

Waser LT, Ginzler C, Kuechler M, Baltsavias E, Hurni L. 2011. Semi-automatic classification of tree species in different forest ecosystems by spectral and geometric variables derived from Airborne Digital Sensor (ADS40) and RC30 data. *Remote Sensing of Environment* 115 (1):76–85

Wolter PMDHGCT. 1995. Improved forest classification in the northern Lake States using multi-temporal Landsat imagery. *Photogrammetric Engineering & Remote Sensing* 61 (9):1129–43

10

An:

GITO mbH Verlag

Detmolder Str. 62

10715 Berlin

Abdruckgenehmigung

Geplante Publikation: Dissertation von Alata Elatawneh Technischen Universität München.

Quelle: Elatawneh A, Rappl A, Rehush N, Schneider T, knoke T. 2013. Forest tree species communities identification using multi phenological stages RapidEye data: case study in the forest of Freising. In From the Basics to the Service, ed. E Borg, pp. 21–38.

Es wird um Genehmigung zur Verwendung der o.g. Abbildung(en) für die Print- und Online Version des o.g. Buches gebeten.

Die Abdruckgenehmigung umfasst ein einfaches, räumlich und zeitlich unbeschränktes Recht der Speicherung, Vervielfältigung, Verbreitung, Weitergabe sowie öffentliche Wiedergabe und Zugänglichmachung der o.g. Abbildung(en)Dieses ist jedoch beschränkt auf die Nutzung in dem o.g. Buch in gedruckter oder elektronischer Form (z.B. online, innerhalb von Online-Paketen mit anderen Zeitschriften und Büchern, offline, mobil).

Selbstverständlich ist ein korrekter Quellenhinweis gewährleistet.

Beantragt von:

Alata Elatawneh
Ph.D. Candidate
Institute of Forest Management
Technische Universität München (TUM)
Hans-Carl-von-Carlowitz-Platz 2
85354 Freising
Germany

Genehmigt von:

GITO mbH Verlag
Detmolder Straße 62
10715 Berlin
Tel.: 030 / 41 93 83 64
Fax: 030 / 41 93 83 67
service@gito.de
www.gito.de

Ort, Datum, Unterschrift

Berlin, 26.01.2015

9 Danksagung